


Fall 12-2008

Investigation of the Interactions of Cationic Polyelectrolytes with Anionic Surfactants: Effects of Polymer, Surfactant and Solution Properties

Lisa Renee Huisinga
University of Southern Mississippi

Follow this and additional works at: <https://aquila.usm.edu/dissertations>

 Part of the [Materials Chemistry Commons](#), and the [Polymer Chemistry Commons](#)

Recommended Citation

Huisinga, Lisa Renee, "Investigation of the Interactions of Cationic Polyelectrolytes with Anionic Surfactants: Effects of Polymer, Surfactant and Solution Properties" (2008). *Dissertations*. 1144.
<https://aquila.usm.edu/dissertations/1144>

This Dissertation is brought to you for free and open access by The Aquila Digital Community. It has been accepted for inclusion in Dissertations by an authorized administrator of The Aquila Digital Community. For more information, please contact aquilastaff@usm.edu.

The University of Southern Mississippi

INVESTIGATION OF THE INTERACTIONS OF CATIONIC POLYELECTROLYTES
WITH ANIONIC SURFACTANTS: EFFECTS OF POLYMER, SURFACTANT AND
SOLUTION PROPERTIES

by

Lisa Renee Huisinga

Abstract of a Dissertation
Submitted to the Graduate Studies Office
of The University of Southern Mississippi
in Partial Fulfillment of the Requirements
for the Degree of Doctor of Philosophy

December 2008

COPYRIGHT BY
LISA RENEE HUISINGA

2008

The University of Southern Mississippi

INVESTIGATION OF THE INTERACTIONS OF CATIONIC POLYELECTROLYTES
WITH ANIONIC SURFACTANTS: EFFECTS OF POLYMER, SURFACTANT AND
SOLUTION PROPERTIES

by

Lisa Renee Huisinga

A Dissertation
Submitted to the Graduate Studies Office
of The University of Southern Mississippi
in Partial Fulfillment of the Requirements
for the Degree of Doctor of Philosophy

Approved:



December 2008

ABSTRACT

INVESTIGATION OF THE INTERACTIONS OF CATIONIC POLYELECTROLYTES WITH ANIONIC SURFACTANTS: EFFECTS OF POLYMER, SURFACTANT AND SOLUTION PROPERTIES

by Lisa Renee Huisinga

December 2008

The intent of this research is to explore and understand the effects that a range of polymer, surfactant and solution parameters have on the interaction of oppositely-charged polymers and surfactants. Cationic polysaccharides were chosen for this research because they are known to interact with anionic surfactants, and they offer a wide range of adjustable polymer properties, including molecular weight, charge substitution, and backbone structure. Cationic poly(vinylpyridinium hydrochloride) polymers were chosen for these studies because they provide the opportunity to explore the effects of charge position on the interaction of cationic polymers with anionic surfactants and how this influences the mechanism of interaction. The overall goal of this research is to define the effects of polymer and surfactant structural properties, and solution properties, on the interaction between cationic polymers and anionic surfactants, and the subsequent formation of coacervate in these systems.

The interaction of cationic polymers with varying properties with anionic surfactant was studied using conventional microscopic and macroscopic methodologies to probe the mechanism of interaction in these systems. Polyquaternium-10 systems interacted with anionic surfactant in accordance with the cooperative mechanism of

interaction and coacervate formation as described by Goddard. The mechanism of interaction between poly(vinylpyridinium hydrochloride) polymers and anionic surfactant was found to be dependent on the position of the cationic charge relative to the hydrophobic polymer backbone. Polymer-surfactant interaction with poly(4-vinylpyridinium hydrochloride) and anionic surfactant occurred via the site-specific cooperative mechanism of interaction. However, the interaction of poly(2-vinylpyridinium hydrochloride) with anionic surfactant exhibited characteristics of the site-specific cooperative interaction mechanism as well as the macroion-macroion interaction mechanism.

A high-throughput screening method was developed to facilitate systematic studies of the effects of polymer, surfactant and solution properties on the macroscopic property of coacervate formation. This method allowed rapid and reproducible preparation and analysis of multi-component systems and representation of the amount of coacervate and compositional range of coacervate formation in these systems in easily understood contour phase diagrams. In the cationic polysaccharide systems, the amount of coacervate and the compositional range of coacervate formation displayed a dependence on both the polymer charge density and molecular weight. Also, the polymer critical overlap concentration was observed to affect coacervate amount with higher coacervate formation observed above c^* .

Coacervate formation with the poly(vinylpyridinium hydrochloride) polymers was found to be dependent not only on the position of the cationic charge on the polymer, but also on the structure of the surfactant tail group. Coacervate formed initially with P4VP and P2VP and sodium capryl sulfonate and sodium xylene sulfonate was not stable

over 24 hours, however coacervate formed between these polymers and sodium dodecylbenzene sulfonate was stable over 24 hours. This indicates that a hydrophobic chain with sufficient length and/or an aromatic group is necessary to form thermodynamically stable coacervate.

The effect of salt in solution on polymer-surfactant interaction was studied with both classes of polymer. A dependence of coacervate amount and compositional range of coacervate formation on salt concentration was observed. The effect of salt was dependent on the degree of polymer charge substitution. The order of addition of polymer, surfactant, and salt also affected coacervate formation. This was consistent for both low and high molecular weight polymers, as well as low and high charge substituted polymers. Although an effect of addition order was observed in all systems, the specific effects differed depending on the polymer properties.

DEDICATION

To my parents for their unconditional love and support throughout my graduate career and in all aspects of my life. To my immediate and extended family and friends for keeping me in their thoughts and prayers. To my husband for his love, patience, guidance and support.

ACKNOWLEDGEMENTS

I would first like to thank my advisor, Dr. Robert Y. Lochhead, for his enthusiasm, support and guidance in my research and in achieving my career goals. I also wish to thank my committee members for the time and assistance they have provided throughout my graduate career: Dr. Charles Hoyle, Dr. Charles McCormick, Dr. Marek Urban, and Dr. Douglas Wicks.

I would like to acknowledge the Society of Cosmetic Chemists for their generous funding through the Graduate Research Fellowship and their support in my membership in their community. I would also like to thank the following companies for materials they have provided: Amerchol Corporation, Stepan Company, and Rhodia Incorporated. A special thank you is extended to Dr. Anthony Convertine and the McCormick research group for supplying the poly(vinylpyridine) polymers.

I extend a great deal of gratitude to Dr. Alicyn Rhoades who has been instrumental not only in regards to my research but also through support as an exceptional friend and confidante. I also extend a great deal of gratitude to Dr. Michael Fevola for volunteering his time and support in the final stages of my research and graduate career. I thank Marge Peffly and Dr. Eric Johnson for providing me the opportunity to experience research programs at Procter & Gamble, and giving me the freedom to experiment and gain instrumental experiences outside of my area of graduate research. I also thank Dr. Michael Fevola and Dr. Joseph LiBrizzi for the opportunity to experience research programs at Johnson & Johnson. I would like to thank Dr. Russell Walters, Dr. Michael Fevola, Dr. Alicyn Rhoades, Dr. David Rhoades, and Dr. Frank Sun

for their candid discussions on a variety of aspects of my research throughout my graduate career.

There are a number of other people without whom I could never have accomplished this research: Steve Selph and Dr. Chunyong Wu for support with high-throughput instrumentation, Dr. Sarah Morgan for assistance with statistical analyses, Dr. Lowell Kreeger and Dr. Hongwei Shen for characterization of the polyquaternium-10 polymer series, Dr. Anthony Convertine for assistance with polymer characterization, Shawn McConaughy and Dr. Russell Walters for assistance with rheological experimentation, Dr. Chris Rulison for surface tensiometry studies of polyquaternium-10/surfactant studies, Dr. Russell Walters for assistance with surface tensiometry experimentation, Adam Smith and Tim Cooper for assistance with static light scattering experimentation, and Dr. Brad Lokitz and Stacey Kirkland for assistance with dynamic light scattering experimentation. Lastly, I would like to thank the team of Lochhead Research group members without whom I would not have accomplished this research: Dr. Camille Sasik, Andrew Magenau, Kyle Price, Rahil Deepak, Christina Edwards, Tara Waller, Adarsh Maini, Sushila Rani, Anthony Hill, and Lauren Goodman.

TABLE OF CONTENTS

ABSTRACT.....	ii
DEDICATION.....	v
ACKNOWLEDGEMENTS.....	vi
LIST OF TABLES.....	x
LIST OF ILLUSTRATIONS.....	xi
CHAPTER	
I. GENERAL INTRODUCTION.....	1
II. OBJECTIVES AND NEED FOR RESEARCH.....	37
III. EXPERIMENTAL.....	40
Materials	
Methods	
IV. RESULTS AND DISCUSSION	
A. DEVELOPMENT AND VALIDATION OF A HIGH- THROUGHPUT SCREENING METHOD OF SAMPLE PREPARATION, ANALYSIS AND DATA REPRESENTATION IN POLYMER-SURFACTANT SYSTEMS.....	62
Method Development	
Method Validation	
Method Reproducibility	
B. INVESTIGATION OF CATIONIC HYDROXYETHYLCELLULOSE – ANIONIC SURFACTANT INTERACTIONS.....	88
Coacervate Physical Description	
Correlation with Traditional Systems	
Effect of Polymer Molecular Weight	
Detailed Investigation of Specific Systems	

C. CATIONIC POLYSACCHARIDE – ANIONIC SURFACTANT INTERACTIONS AS A FUNCTION OF POLYMER AND SURFACTANT PROPERTIES.....	127
Polymer Structural Effects	
Surfactant Structural Effects	
D. CATIONIC HYDROXYETHYLCELLULOSE – ANIONIC SURFACTANT INTERACTIONS IN THE PRESENCE OF SODIUM CHLORIDE.....	139
Effect of Addition Order	
Effect of Salt Concentration	
E. INVESTIGATION OF CATIONIC POLY(VINYLPYRIDINIUM HYDROCHLORIDE) – ANIONIC SURFACTANT INTERACTIONS	151
Polymer Solution Conformation	
Polymer-Surfactant Complex Formation	
Polymer-Surfactant Contour Phase Diagrams	
Salt Addition Studies	
V. CONCLUSIONS.....	199
VI. RECOMMENDATIONS FOR FUTURE RESEARCH.....	207
APPENDIX.....	209
REFERENCES.....	211

LIST OF TABLES

Table	
3-I.	PQ-10 series properties.....41
3-II.	Guar Hydroxypropyltrimonium Chloride series properties.....44
3-III.	Properties of cationic synthetic polymers.....45
4A-I.	Repetitive additions of surfactant (S) and polymer (P) solutions to centrifuge tubes using the liquid handler. The same probe tip was used for all additions of the respective materials.....65
4A-II.	Repetitive additions of surfactant (S) and polymer (P) solutions to centrifuge tubes using the liquid handler with an aspirate/dispense step prior to sample preparation. The same probe tip was used for all additions of the respective materials.....66
4A-III.	Absorbance readings of background components at 410 nm, 25 °C.....70
4B-I.	PQ-10 series properties.....101
4B-II.	High molecular weight polymer c^*102
4B-III.	Low molecular weight polymer c^*104
4C-I.	Guar hydroxypropyltrimonium chloride series properties.....131
4E-I.	P4VP and P2VP values for $[\eta]$, k' , and c^*159
4E-II.	pH readings of representative polymer-surfactant mixtures.....163

LIST OF ILLUSTRATIONS

Figure

1-1.	Schematic representation of the distribution of counterions around a polyelectrolyte.....	2
1-2.	Schematic representation of the electrical double layer in polyelectrolytes.....	3
1-3.	Schematic representation of the Dubin macroion-macroion coacervation mechanism. Darker shading represents increased micelle charge density.....	11
1-4.	Schematic representation of site-specific ion-ion coacervation mechanism.....	13
1-5.	Polyelectrolyte-surfactant interactions as a function of surfactant concentration.....	14
1-6.	Schematic representation of fluid-like coacervate phase.....	15
1-7.	Schematic representation of interactions between oppositely-charged surfactant and hydrophobically-modified polymer as a function of surfactant concentration.....	19
1-8.	Typical configurations of polyelectrolyte interactions with oppositely-charged macroions as a function of polymer chain stiffness, achieved through Monte Carlo simulations. Chain stiffness increases from (a) to (g).....	21
1-9.	Ternary phase diagram for mixtures of JR400-SDS in water.....	26
1-10.	Complete dynamic dual syringe method developed at NIST.....	29
1-11.	Validation of composition gradient formation using the dynamic dual syringe method.....	30
1-12.	Microfluidic devices designed for intricate mixing: (a) T-junction design and (b) ternary mixing design.....	31
1-13.	Microchannel reactor for controlled polymerization.....	32
1-14.	Sample clouding curve generated using a microfluidic temperature gradient device. Inset contains CCD images of the microfluidic channels where the blue regions are precipitant, pseudo-colored for clarity.....	33
1-15.	Sample vessel for creating 10 x 10 discrete arrays using liquid dispensing systems.....	34

1-16.	An example of a polymeric film array generated using ink-jet printing techniques.....	35
3-1.	Nominal chemical structure of Polyquaternium-10.....	40
3-2.	Molecular weight distributions of the PQ-10 polymer series.....	41
3-3.	Nominal chemical structure of Polyquaternium-67.....	42
3-4.	Nominal chemical structure of Guar Hydroxypropyltrimonium Chloride.....	43
3-5.	(a) P4VP, (b) P2VP, and (c) VBTAC chemical structures.....	45
3-6.	SLES chemical structure.....	46
3-7.	Surface tension as a function of SLES concentration.....	47
3-8.	ALES chemical structure.....	47
3-9.	Representative sodium alkyl sulfate chemical structure.....	48
3-10.	Surface tension as a function of SDBS concentration.....	49
3-11.	(a) SDBS, (b) SCS, and (c) SXS chemical structures.....	50
3-12.	PEG-12 chemical structure.....	50
3-13.	Beckman Coulter Biomek [®] FX Laboratory Automation Workstation.....	51
3-14.	Salt gradient profiles for PQ-10-SLES-NaCl investigations using the Salt Gradient method. The addition orders associated with each salt gradient are (a) polymer, surfactant, salt and salt, surfactant, polymer; (b) surfactant, polymer, salt and salt, polymer, surfactant; (c) polymer, salt, surfactant and surfactant, salt, polymer.....	54
3-15.	CMC determination in surfactant systems.....	55
3-16.	Zero-shear viscosity determination for polymers at multiple concentrations.....	56
3-17.	η_{sp} as a function of polymer concentration for c^* determination.....	57
3-18.	Zimm plot for low molecular weight P4VP obtained using static light scattering.....	60

4A-1. Ternary phase diagrams generated using multi-channel pipettes (PQ-10-ALES): (a) all samples investigated and (b) enlargement of the circled area.....	63
4A-2. Binary phase diagram of phase separation analyzed via visual observation (LR400-SLES).....	68
4A-3. Reproducibility in visual observation of phase separation analysis (LR400-SLES).....	69
4A-4. Absorbance scans of cationic polysaccharide-surfactant samples.....	71
4A-5. Absorbance scans of poly(vinylpyridinium hydrochloride)-surfactant samples.....	72
4A-6. Traditional ternary phase diagram for representation of polymer-surfactant interactions.....	73
4A-7. Discrete data points prepared and analyzed using high-throughput screening methods.....	76
4A-8. One and two phase regions and relative coacervate amounts based on discrete data points.....	77
4A-9. Binary contour phase diagram showing quantitative phase separation. Data obtained with the Tecan Safire UV-Visible spectrophotometer is represented by a color gradient.....	79
4A-10. Triangle mesh utilized by the DPlot software program to create the gradients between neighboring points of different absorbance units.....	80
4A-11. Traditional JR400-SDS phase diagram.....	81
4A-12. Comparison of one phase (square) and two phase (circle) regions of literature (closed symbols) and high-throughput (open symbols) phase diagrams for validation of the high-throughput screening method.....	82
4A-13. Validation of the quantitative phase separation method with a cationic polysaccharide-surfactant system (JR30M-SLES): (a) visual observation and (b) spectrophotometric analysis.....	83
4A-14. Validation of the quantitative phase separation method with a cationic synthetic polymer-surfactant system (VBTAC-SLES): (a) visual observation and (b) spectrophotometric analysis.....	84

4A-15. Reproducibility of high-throughput screening methods for a polysaccharide-surfactant system (JR400-SLES).....	86
4A-16. Reproducibility of high-throughput screening methods for a synthetic cationic polymer-surfactant system (P4VP-SDBS).....	87
4B-1. Photographic images of coacervate formed in cationic polysaccharide-anionic surfactant mixed systems at different compositions. Coacervate amount decreased from left to right, with no coacervate present at far right.....	88
4B-2. Solubility diagram of JR400 with sodium alkyl sulfates. Maximum precipitation lines are also shown for sodium alkyl sulfates with C ₈ , C ₁₀ , and C ₁₂ chain lengths.....	90
4B-3. Contour phase diagram of JR400 with SLES below 24 mM SLES. The 1:1 charge ratio is designated by the solid red line.....	92
4B-4. Contour phase diagram of JR30M with SLES below 24 mM SLES. The 1:1 charge ratio is designated by the solid red line.....	93
4B-5. Contour phase diagrams for (a) JR400 with SLES and (b) JR30M with SLES. Reproducibility diagrams for (c) JR400 with SLES and (d) JR30M with SLES.....	95
4B-6. Molar free energy of mixing as a function of polymer concentration for a miscible system.....	97
4B-7. Molar free energy of mixing as a function of polymer concentration for a phase-separated system.....	98
4B-8. Specific viscosity as a function of polymer concentration for JR30M and LR30M in DI water.....	102
4B-9. Specific viscosity as a function of polymer concentration for JR400, JR125 and LR400 in DI water.....	103
4B-10. Reduced viscosities of PQ-10 polymer series in DI water.....	105
4B-11. Contour phase diagrams of (a) JR125, (b) JR400, and (c) JR30M with SLES. Molecular weight increases from left to right.....	106
4B-12. Contour phase diagrams of (a) LR400 and (b) LR30M with SLES. Molecular weight increases from left to right.....	108

4B-13. Surface tension versus surfactant concentration data for 0.35 g/dL JR400 with SLES. — SLES; ♦ JR400-SLES mixture, Run 1; ● JR400-SLES mixture, Run 2.....	110
4B-14. Surface tension versus surfactant concentration data for 0.35 g/dL JR30M with SLES. — SLES; ♦ JR30M-SLES mixture, Run 1; ● JR30M-SLES mixture, Run 2.....	112
4B-15. Dynamic light scattering data for 0.35 g/dL JR400 – SLES mixtures.....	115
4B-16. Dynamic light scattering data for 0.35 g/dL JR30M with SLES.....	118
4B-17. Zero-shear viscosities of 0.35 g/dL JR400-SLES mixtures. Precipitation boundary; - - - CMC in the absence of polymer.....	120
4B-18. Zero-shear viscosities of 0.35 g/dL JR30M-SLES mixtures. Precipitation boundary; - - - CMC in the absence of polymer.....	121
4B-19. Data compilation for the 0.35 g/dL JR400 - SLES system.....	123
4B-20. Data compilation for the 0.35 g/dL JR30M - SLES system.....	125
4C-1. Contour phase diagrams of (a) LK, (b) LR400, and (c) JR125 with SLES. Charge substitution increases from left to right.....	128
4C-2. Contour phase diagrams of (a) LR30M and (b) JR30M with SLES. Charge substitution increases from left to right.....	129
4C-3. Relationship between polymer structural properties and coacervate formation for the PQ-10 series with SLES.....	130
4C-4. Relationship between polymer structural properties and coacervate formation for the cationic guar series with SLES: (a) C-1000, (b) Excel, (c) C-14S, and (d) C-17.....	132
4C-5. Contour phase diagrams for PQ-67 series with SLES: (a) SL-5, (b) SL-30, (c) SL-60, and (d) SL-100. The degree of hydrophobic substitution increases from left to right.....	134
4C-6. Contour phase diagrams of JR30M (a-c) and LR30M (d-f) with ammonium lauryl ether sulfates with increasing EO lengths from left to right.....	136
4C-7. Contour phase diagrams of JR30M with (a) ALES and (b) PEG-12/ALES premixed in a 2:1 ratio.....	137
4D-1. Contour phase diagrams for (a) LR400, (b) JR125, and (c) JR400 with	

SLES in the absence (left) and presence (right) of NaCl. The SLES-NaCl mixture contains a constant 30:1 ratio of SLES:NaCl.....	141
4D-2. Contour phase diagrams of (a) LR30M, (b) JR30M, and (c) JR400 with SLES in the absence of salt. c^* is represented by the red line.....	143
4D-3. PQ-10-SLES-NaCl contour phase diagrams: (a) LR30M, (b) JR30M, and (c) JR400 with (1) no salt and addition: (2) salt, polymer, surfactant; (3) polymer, salt, surfactant; (4) salt, surfactant, polymer; (5) surfactant, salt, polymer; (6) polymer, surfactant, salt; (7) surfactant, polymer, salt.....	144
4D-4. Contour phase diagrams of LR30M - SLES (a-c) and JR30M – SLES (d-f) with 0 mM, 43 mM, and 130 mM NaCl. NaCl concentration increases from left to right.....	147
4E-1. Zimm plot of low molecular weight P4VP in filtered HPLC grade water. A-E indicate concentrations of P4VP investigated (1.0, 4.9, 6.0, 8.0, 9.7 mg/mL). Blue dashed line follows curvature of the plot.....	152
4E-2. Zimm plot of low molecular weight P4VP in filtered HPLC grade water at low concentrations (A-C = 1.0, 4.9, 6.0mg/mL).....	153
4E-3. Zimm plot of low molecular weight P2VP in filtered HPLC grade water. A-D indicate concentrations of P2VP investigated (1.0, 2.0, 4.0, 6.0 mg/mL). Blue dashed line follows curvature of the plot.....	154
4E-4. Zimm plot of low molecular weight P2VP in filtered HPLC grade water at low concentrations (A-C = 1.0, 2.0, 4.0 mg/mL).....	154
4E-5. Surface tension as a function of concentration.....	155
4E-6. Relaxation time (τ) of 0.15 g/dL P4VP and P2VP.....	157
4E-7. Reduced viscosities of high and low molecular weight P4VP and P2VP in DI water at 25 °C.....	158
4E-8. Photographic images of coacervate formed in cationic poly(vinylpyridinium hydrochloride)-anionic surfactant mixed systems at different compositions: (a) P4VP-SDBS, high coacervate; (b) P4VP-SDBS, low coacervate; (c) P4VP-SDBS, no coacervate; (d) P2VP-SDBS, high coacervate; (e) P2VP-SDBS, no coacervate	161
4E-9. Surface tension as a function of concentration.....	164

4E-10. Surface tension as a function of surfactant concentration. ■ SDBS, ● 0.15 g/dL P4VP-SDBS, - 0.10 g/dL P4VP-SDBS, * 0.050 g/dL P4VP-SDBS.....	165
4E-11. Dynamic light scattering data for 0.15 g/dL P4VP – SDBS mixtures.....	168
4E-12. Apparent viscosities of 0.15 g/dL P4VP – SDBS mixtures. Precipitation boundary; --- CMC in the absence of polymer.....	170
4E-13. Surface tension as a function of concentration.....	171
4E-14. Dynamic light scattering data for 0.15 g/dL P2VP – SDBS mixtures.....	173
4E-15. Apparent viscosities of 0.15 g/dL P2VP – SDBS mixtures. Precipitation boundary; --- CMC in the absence of polymer.....	175
4E-16. Contour phase diagrams for P4VP-SDBS (a) initial analysis and (b) analysis after 24 hours.....	176
4E-17. Contour phase diagram of P4VP-SDBS. The 1:1 stoichiometric ratio is designated by the solid black line. Above the dashed white line coacervate amount was dependent on polymer and surfactant concentration.....	177
4E-18. Contour phase diagrams of P4VP-SDBS with P4VP molecular weights of (a) 9 000 g/mol and (b) 32 000 g/mol.....	179
4E-19. Zimm plot of high molecular weight P4VP in filtered HPLC grade water at all concentrations studied (1.0, 2.0, 4.0, 6.0, 8.0, 10.0 mg/mL).....	180
4E-20. Contour phase diagrams of P4VP-SCS (a) initial analysis and (b) analysis after 24 hours.....	181
4E-21. Contour phase diagrams of P4VP-SXS (a) initial analysis and (b) analysis after 24 hours.....	182
4E-22. Contour phase diagrams for P2VP-SDBS (a) initial analysis and (b) analysis after 24 hours.....	183
4E-23. Contour phase diagram of P2VP-SDBS. The 1:1 stoichiometric ratio is designated by the solid black line. Resolubilization is designated by the dotted black line.....	184
4E-24. Contour phase diagrams of P2VP-SDBS with P2VP molecular weights of (a) 6 000 g/mol and (b) 32 000 g/mol.....	186

4E-25. Zimm plot of high molecular weight P2VP in filtered HPLC grade water. A-D indicate concentrations of P2VP investigated (1.0, 2.0, 4.0, 6.0 mg/mL). Blue dashed line follows curvature of plot.....	187
4E-26. Zimm plot of low molecular weight P2VP in filtered HPLC grade water at low concentrations (A-C = 1.0, 2.0, 4.0 mg/mL).....	187
4E-27. Contour phase diagrams of P4VP-SCS (a) initial analysis and (b) analysis after 24 hours.....	188
4E-28. Contour phase diagrams of P2VP-SXS (a) initial analysis and (b) analysis after 24 hours.....	189
4E-29. Relaxation time (τ) of 0.15 g/dL P4VP and 0.15 g/dL P4VP with 0.05 g/dL NaCl.....	193
4E-30. Contour phase diagram of P4VP-SDBS in salt-free aqueous solution.....	195
4E-31. Contour phase diagrams of P4VP-SDBS in 8.6 mM NaCl solution, combined using the addition orders of (a) polymer, salt, surfactant and (b) surfactant, salt, polymer.....	196
AI-1. Relaxation time (τ) of 0.35 g/dL JR400 and 0.35 g/dL JR30M in aqueous solution.....	209

CHAPTER I

GENERAL INTRODUCTION

The mechanism of interaction and resulting complex formation between oppositely-charged polymer and surfactant has received considerable attention with both naturally-derived and synthetic polyelectrolyte-surfactant systems.¹⁻²³ Cationic polyelectrolytes are widely used in industrial applications because they have the ability to interact with negatively charged surfaces, and in some of these applications cationic polyelectrolyte is coupled with anionic surfactants. Some common industrial applications where these interactions are important include cosmetic products, paints and pharmaceuticals.¹⁷ To date, investigations of polymer-surfactant interactions have focused primarily on the dilute surfactant regime, however it is important to also understand these interactions in the semi-dilute and concentrated surfactant regimes.^{1-4, 6, 7, 22-30}

Polyelectrolytes

Polyelectrolytes are defined as macromolecules comprising monomeric units that contain ionizable groups and these charged groups are interconnected through chemical bonds.³¹ Depending on the nature of the ionizable groups these molecules can either be classified as strong or weak polyelectrolytes. Strong polyelectrolytes are those where the ionizable groups are permanently ionized, for example trimethylammonium substituted hydroxyethyl cellulose in which the ammonium group is quaternized. Weak polyelectrolytes are those for which the degree of ionization is controlled by dissociation, such as induction of ionization of the polymer through pH adjustment. Poly(methacrylic

acid) is an example of a weak anionic polyelectrolyte and poly(vinyl pyridine) is a weak cationic polyelectrolyte.³¹

The solubility of both types of polyelectrolytes in aqueous solution is governed by the electrical attractions between the polyelectrolyte and its oppositely-charged counterions. This attraction can be described similar to that of the Gibbs-Donnan effect, or the Donnan Equilibrium, which is the uneven distribution of charged species across two sides of a semi-permeable membrane.³²⁻³⁴ The uneven distribution is attributed to the presence of an existing charged species that is unable to pass through the membrane but that influences the motion of the charged molecules. Polyelectrolytes exist in the presence of their oppositely-charged counterions and in solution the counterions distribute unevenly, with the highest concentration near the polymer chain. The counterions are attracted to the chain through electrochemical potential (ϵ) but are driven into solution by effects of chemical potential (μ). This equilibrium is described schematically in Figure 1-1.

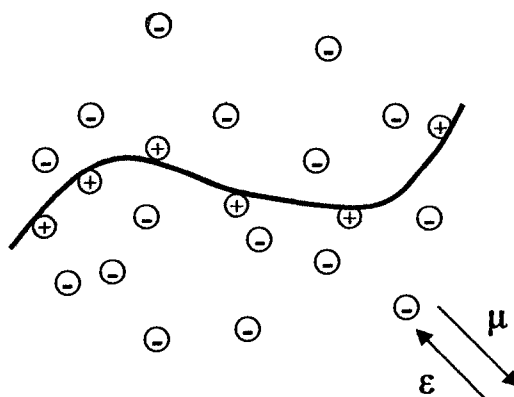


Figure 1-1. Schematic representation of the distribution of counterions around a polyelectrolyte.

Chemical potential drives counterions into solution because an increase in entropy of the system is produced. However, the electrochemical potential attracts the oppositely-charged counterions to the polyelectrolyte chain. As a result the counterions reside in a region that is determined by the equilibrium state between these opposing effects. This region can be described similarly to the electrical double layer in colloids. In the Gouy-Chapman-Stern model of the electrical double layer, two layers exist, the Stern layer and the diffuse layer (Figure 1-2).^{7, 35-39}

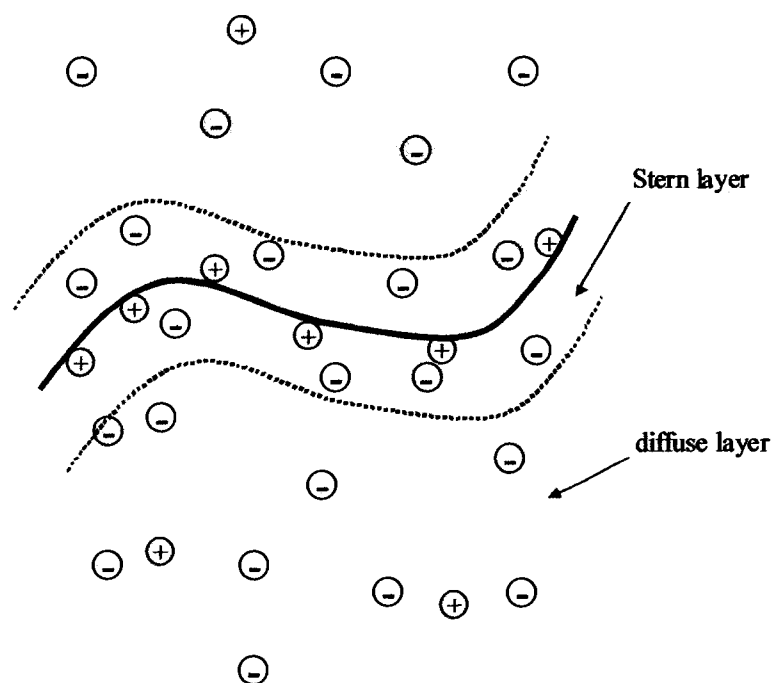


Figure 1-2. Schematic representation of the electrical double layer in polyelectrolytes.

The Stern layer is the inner layer where some counterions adsorb onto the charged surface. In the diffuse layer, the counterions are able to move in solution and the electrostatic attraction to the surface is in competition with Brownian motion. This results in a layer close to the charged surface that contains an excess of one type of ion.

This is similar to the polyelectrolyte-counterion associations described above. The formation of this electrical double layer region is important because the configurational entropy of the counterions makes a large contribution to the free energy of dissolution of the polyelectrolyte in water.⁸

The conformation of polyelectrolytes in solution is affected by the charges present along the polymer backbone. Electrostatic repulsions between the similarly-charged groups along the backbone occur when screening by counterions is not strong due to their location in the electrical double layer. These repulsions induce an expansion of the polyelectrolyte chain, which is typically described in terms of its persistence length.⁷ Persistence length (p) is a measure of the stiffness of the chain, determined by the energetic penalty to bend that chain. When persistence length is a significant fraction of the total contour length of the chain the polymer will be in a rod-like extended conformation. Conversely, when the contour length of the chain is large relative to the persistence length a flexible random coil conformation exists.^{7, 40} The Porod-Kratky wormlike chain model⁴¹ is useful for the intermediate stiffness regime between the flexible coil and the rod

$$\langle r^2 \rangle_0 / nl^2 = p/l - (p^2 / nl^2) [1 - \exp(-nl/p)] \quad \text{Equation 1-1.}$$

where n is the number of chain segments, l is the length of the segments, and $\langle r^2 \rangle_0$ is the end-to-end vector of the entire macromolecule and is given by

$$\langle r^2 \rangle_0 = Cnl^2 \quad \text{Equation 1-2.}$$

where C is a defined quantity known as the characteristic ratio which physically is the ratio of the actual dimensions of a chain in the fluid state to what they would have been if the chain had performed a truly random walk.⁷ This Porod-Kratky model is useful in

situations where interactions occur that cause a molecule to stiffen, such as an increase in linear charge density, because persistence length can be used as the relevant parameter to characterize the configurational change, as is the case for polyelectrolytes.⁷ In polyelectrolyte systems the persistence length is described by Equation 1-3, where P_{el} is used to differentiate its electrostatic character.

$$P_{el} = l_B / (4\kappa^2 b^2 \xi^2) \quad \text{Equation 1-3.}$$

The electrostatic persistence length involves several factors: the Bjerrum length

$l_B = e^2 / \epsilon kT$ is the separation at which the interaction between two electrostatic charges of magnitude e , in a solvent of dielectric constant ϵ , is comparable in magnitude to the energy kT ; κ^{-1} is the Debye screening length which is given by $\kappa^2 = 8\pi l_B c_s$, with c_s the monovalent salt concentration in solution; b is the distance between charges along the chain; ξ is a number between 0 and 1 that accounts for counterion condensation, discussed below.⁷ Equation 1-3 can be used in the Porod-Kratky model (Equation 1-1) to determine the polyelectrolyte configuration.

For stiff polymer chains, such as cationic polysaccharides, it is likely that discrete rods exist at low molecular weights because the contour length is low relative to the P_{el} and there are repulsions between cationic charges along the polymer chain.^{7, 8, 17, 40, 42, 43} At very high chain lengths, these polymers would be expected to form loose coils, however cationic repulsions along the backbone may alter this conformation.^{7, 40, 42, 43} For flexible polyelectrolytes, such as poly(vinylpyridines), a random coil solution conformation is common, with the actual conformation dictated by the repulsion of charged groups along the chain and the polymer concentration in solution.^{31, 44} For both polymer types, at high chain lengths and high polyelectrolyte concentrations, the

polymers will likely adopt a random coil conformation because the total contour length is higher than the P_{el} and mutual electrostatic screening of cationic repulsions along the polymer backbone occurs.^{7, 40, 45} This effect of chain length and concentration on polymer conformation is evidenced by the “polyelectrolyte effect”, where chain extension in very dilute solutions and coiling of the chains as concentration is increased occurs.³¹ This has been demonstrated, using poly(methacrylic acid) at high percent ionization, by a decrease in viscosity with an increase in concentration from 0.01 g/100mL to 0.1 g/100mL.³¹ Salt concentration and polymer charge density also influence polyelectrolyte conformation and from the Porod-Kratky model it is evident that P_{el} will decrease with an increase in salt concentration and will increase with increasing polymer charge density.⁷

An increase in persistence length is observed with an increase in the linear charge density of the polyelectrolyte; however, the degree of chain expansion due to increased charge density is limited by counterion condensation. Manning observed that if a polyelectrolyte possesses an ionic charge above a certain critical charge density, then sufficient counterions would condense on the polyelectrolyte chain to maintain the charge density at its critical level.⁴⁶⁻⁴⁹ Thus, all polyelectrolytes have a critical charge density above which chain expansion is not increased.

Polyelectrolyte chain expansion can affect the concentration at which polymer chains begin to overlap one another, known as the critical overlap concentration (c^*), which is the boundary between the dilute and semi-dilute polymer regimes. This concentration decreases with increasing molecular weight for any given polymer-solvent system.⁷ As discussed above, polyelectrolytes in solution are generally in an extended

conformation at low concentrations due to electrostatic repulsions between charged moieties along the polymer backbone or osmotic intrusion of water into the macromolecule.^{7, 50} The osmotic intrusion can be considered to be driven by the excess concentration of counterions within the intramolecular polymer domain compared to the lower concentration in the intermolecular aqueous phase.⁵¹ As polyelectrolyte concentration increases, mutual screening among the polyelectrolytes causes them to behave like neutral polymers and entanglements can occur.^{7, 43, 45, 52} Above c^* the average distance between segments of different polymer chains becomes important.⁷ This distance between segments, known as the correlation length between entanglements, decreases as the polymer concentration is increased.⁴⁵ The correlation length is also decreased and c^* is lowered in systems of hydrophobically-modified polymers, where hydrophobic interactions occur between water-soluble polymer chains due to self-association.^{53, 54}

Association Colloids

Surfactants are molecules characterized by their tendency to adsorb at surfaces and interfaces in order to lower the free energy of that interface.⁵⁵ Ionic surfactants contain a polar head group and a nonpolar, hydrophobic tail group.⁸ They are solubilized in water due to ion-dipole interactions between water molecules and the polar head group. However, interactions between water molecules are strong due to hydrogen bonding, forming a network structure,⁵⁶ and the introduction of a nonpolar group disturbs the water structure. Restructuring of water molecules around the nonpolar group is possible, however, this causes a loss in entropy and subsequent increase in the free

energy of the system.⁵⁵ To minimize the free energy of the solution, surfactant molecules are excluded from water, either migrating to the air-water interface or forming micelles in solution.^{8, 55} In both surface adsorption and micelle formation, the surfactant molecules orient so that the hydrophobic groups are directed away from the solvent. In micellization the hydrophobic groups cluster on the interior of the micelle, which imparts a loss of freedom of the surfactant molecules due to confinement in the micelle and electrostatic repulsions for anionic surfactants. These forces increase the free energy of the system and thus oppose micellization. Therefore, whether adsorption at the air-water interface or micelle formation is favored depends on the balance between the factors that promote or oppose micellization.^{8, 55}

At surfactant concentrations above the critical micelle concentration (CMC), micelles are present in solution. The head groups of anionic surfactants are similarly charged and repel each other, which imparts curvature to the associated surfactant structure. This curvature, or shape of association colloids varies depending on the effective size of the surfactant head group and/or tail group. This can be conceptually understood from a mathematical model that is based on the packing factor, P , (Equation 1-4), where v is the volume of the hydrophobic tail group, a is the cross-sectional area of the polar head group, and l_c is the length of the hydrophobic tail group.^{55, 57, 58}

$$P = \frac{v}{al_c} \quad \text{Equation 1-4.}$$

When $P < 1/3$, the molecule assumes a cone-shape, where the head group volume is much larger than the volume of the tail group and these cones are able to pack into spheres, producing spherical micelles whose structure is reinforced by electrostatic repulsions between the head groups and hydrophobic associations between the tail

groups. As P increases, the structures become less spherical, due to smaller head groups and/or bulkier tail groups. For ellipsoidal or cylindrical micelles, $1/3 < P < 1/2$.

Surfactants with a packing factor between $1/2$ and 1 form lyotropic liquid crystal structures. These liquid crystal structures are hexagonal, cubic, or lamellar, the former having a larger head group and smaller tail group than the latter.⁸

An increase in surfactant concentration also alters the size and shape of the micelle. As surfactant concentration increases micellar growth causes a transition from spherical to rod-like micelles. This occurs due to growth in one-dimension, where the hydrophobic core is similar in size to that of the spherical micelles but the linear length of the micelle can vary from less than 10 nm to many hundreds of nanometers.^{8, 59} The addition of ions to solution has been shown to increase micelle size and decrease micelle curvature as well. Additional ions, such as salt ions, cause the position of the Donnan Equilibrium to shift and favor a tightening of the electrical double layer with respect to the anionic head groups of the surfactant molecules, causing the anionic charge repulsions between neighboring molecules to be screened.⁶⁰ This change in the position of the Donnan Equilibrium at the micelle surface results in a reduction of the effective Bjerrum length and decrease the effective size of the ionic head group. The packing factor is inversely proportional to the effective size of the head group so screening of head group repulsions to decrease effective head group size affects the ionic micelle structure, causing formation of more ordered surfactant structures with higher P .^{7, 18, 19} Also, the addition of salt to aqueous solution induces increased structuring of the water molecules, which enhances hydrophobic associations between tail groups of surfactant molecules, contributing to micelle growth.⁸

Polymer-Surfactant Interactions

Mechanism of Interaction

The mechanism of complex formation has been explored for both oppositely-charged polyions, and oppositely-charged polyelectrolytes with surfactants in the dilute surfactant regime.^{5, 7, 18, 20, 61-64} The models developed for these interactions fall into one of two categories, either macroion-macroion interactions or site specific ion-ion interactions.^{5, 7, 18, 20, 61-64} Theoretical treatments of interactions between oppositely-charged polyions have been developed by Voorn and Overbeek, Veis and Aranyi, and Tainaka.⁶¹ The Voorn-Overbeek theory was developed to explain complex formation and phase separation between gelatin and acacia and describes a competition between electrical attractive forces and entropy effects, where the former tend to aggregate oppositely-charged polyions, while the latter disperse them. In this theory, a random coil configuration of the polymers in solution is assumed and the molecules interact on a macroscopic level such that water is able to be trapped.⁶¹ Trapping of water in the spaces between the two associated polyions creates a fluid separated phase called a coacervate. Site-specific interactions would lead to no trapping of water and precipitation or aggregation.⁶¹ A second theory of coacervate formation is the Veis-Aranyi theory, or the two-step "dilute phase aggregate model". The Voorn-Overbeek theory requires a sufficiently high charge density and/or molecular weight, but the Veis-Aranyi theory accommodates systems that do not meet this requirement. In the first step of this model, the oppositely-charged gelatins aggregate spontaneously due to electrostatic interactions, with formation of ion pairs. In the second step, the aggregates rearrange over time to increase configurational entropy. The Tainaka theory involves aggregate formation

similar to the Veis-Aranyi theory, but without specific ion pairing. These aggregates condense to form coacervate due to attractive forces between aggregates, dependent on a critical intermediate molecular weight and charge density.^{20, 61}

Dubin and coworkers²⁰ have presented a mechanism of coacervate formation between oppositely-charged polyelectrolyte and surfactant based on these polyion theories, particularly the Veis-Aranyi theory, using poly(diallyldimethylammonium chloride) (PDADMAC) and sodium dodecyl sulfate (SDS)/Triton X-100 (TX100) mixed micelles. They described the overall model as coacervation due to attractive forces between neutral aggregates which were formed by electrostatic interaction. In the Dubin model, a critical micelle charge density is required for complex formation and once this is reached, surfactant micelles bind to the polymer chain. A schematic representation of this mechanism presented by Wang and coworkers is shown in Figure 1-3.²⁰

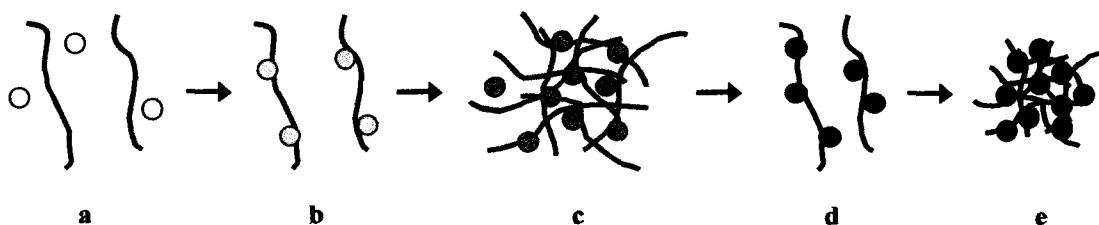


Figure 1-3. Schematic representation of the Dubin macroion-macroion coacervation mechanism. Darker shading represents increased micelle charge density.²⁰

Initial interactions occur between the polyion and surfactant micelles, described as macroion-macroion associations (Figure 1-3b). When electrical neutrality of the complex is reached, intrapolymer complexes aggregate into interpolymer complexes and coacervation occurs (Figure 1-3c). At higher micelle charge density intermicellar and intercomplex repulsion occurs and coacervation is absent (Figure 1-3d), but at very high

micelle charge density electrostatic interactions are so strong that tight binding occurs and precipitate is formed (Figure 1-3e). In summary, the Dubin model concludes that due to macroion-macroion interactions, the micelle charge density is the controlling factor in coacervate formation.²⁰

Contrary to the macroion-macroion coacervation mechanisms discussed above, some researchers have theorized mechanisms that involve site-specific ion-ion interactions, originally proposed by Goddard.^{5-7, 18} In these systems, complex formation is a cooperative process between electrostatic interactions and hydrophobic association/segregation.^{5-7, 18} The cooperative process is driven entropically by release of the counterions from both the surfactant and the polyelectrolyte into solution and enthalpically by binding of the polyelectrolyte ion to the surfactant ion (Figure 1-4a). The process is also driven both entropically and enthalpically by a strong driving force for the hydrophobic tail groups of bound surfactant molecules to reduce their hydrocarbon/water contact area resulting in association of these groups during binding to the polymer chain (Figure 1-4b).^{7, 18}

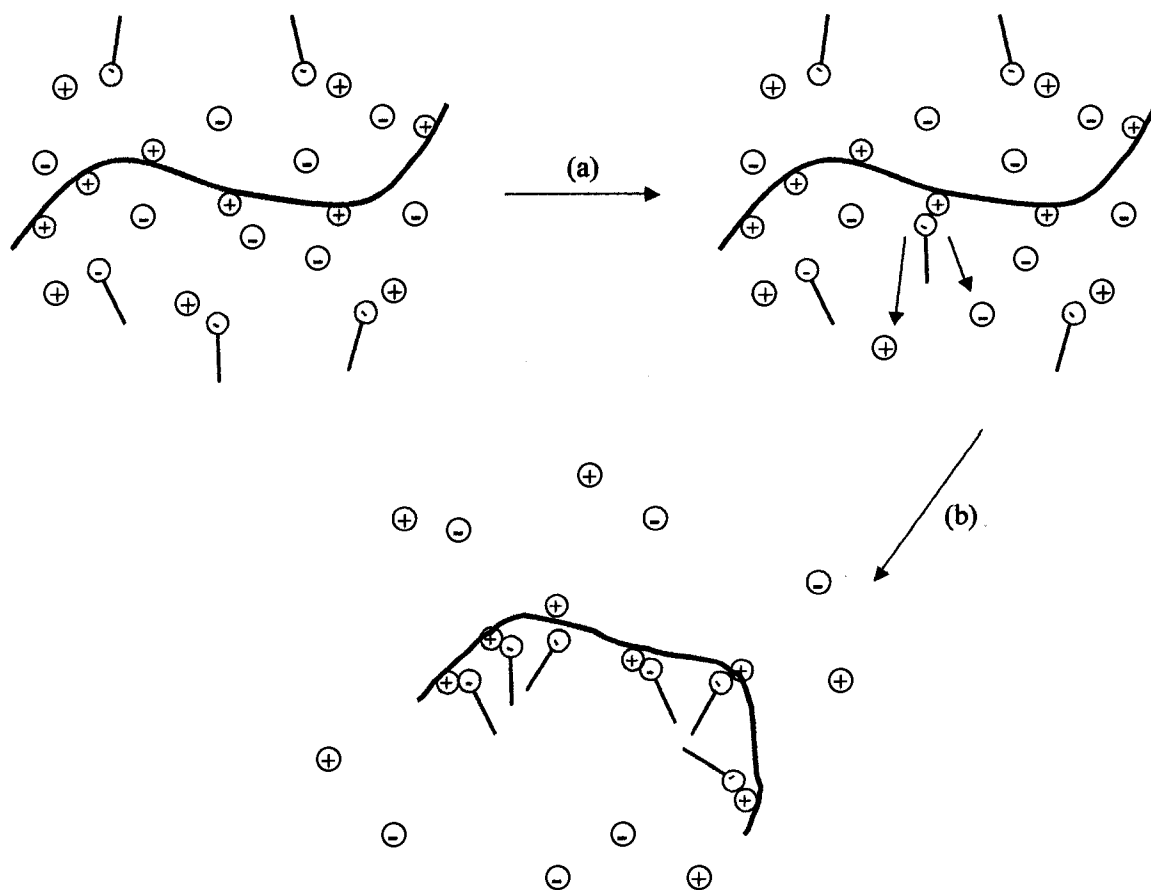


Figure 1-4. Schematic representation of site-specific ion-ion coacervation mechanism.

Using surface tension measurements with cationically-modified hydroxyethyl cellulose (Polymer JR) and SDS, Goddard and coworkers observed that complexation between oppositely charged polyelectrolyte and surfactant involves surfactant binding, phase separation and resolubilization, dependent on surfactant concentration. This is represented as three separate zones in Figure 1-5.^{5, 7, 65, 66}

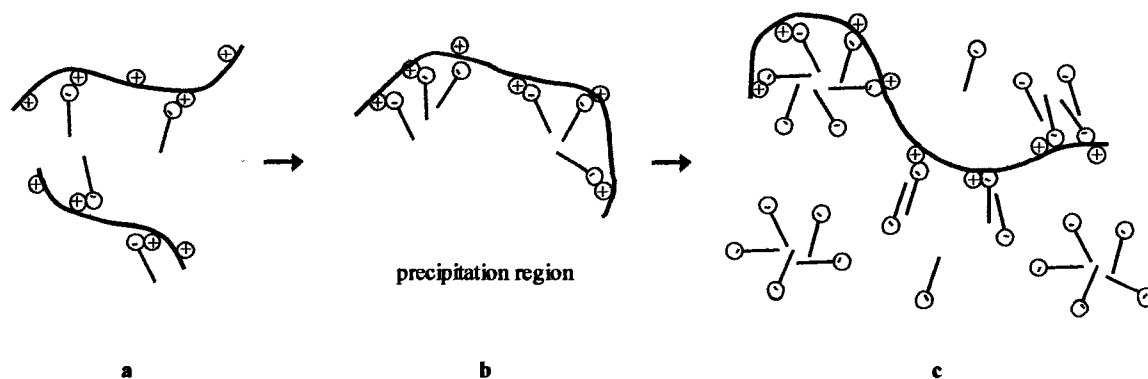


Figure 1-5. Polyelectrolyte-surfactant interactions as a function of surfactant concentration.

Interactions between oppositely-charged polymers and surfactants are strong due to their electrostatic attractions, thus the surfactant concentration required for these interactions to occur is much lower than the surfactant's normal CMC.¹⁸ Binding of surfactant molecules to the polyelectrolyte occurs at a surfactant concentration below CMC, known as the critical aggregation concentration (CAC).^{7, 16, 67-71} In the case of cationically-modified hydroxyethyl cellulose (HEC) with SDS, Ohbu and coworkers observed that the CAC was at $1/20^{\text{th}}$ of the CMC with 50 % of all cationic charges associated with a surfactant molecule at the CAC.^{7, 72} At these low surfactant concentrations, the polymer-surfactant complexes are soluble and the solution is single phase because the concentration of hydrophobic tails, now attached to the polyelectrolyte, is not high enough to promote aggregation. (Figure 1-5a). At intermediate surfactant concentrations, where there is a 1:1 charge balance between surfactant and polyelectrolyte, phase separation occurs (Figure 1-5b).⁷ At this point, the critical precipitation concentration (CPC), all charged units on the polymer are bound to a surfactant molecule head group.²¹ The hydrophobic tail groups of the bound surfactant

molecules aggregate to form micelle-like structures. Thus it is unable to interact strongly with water molecules and phase separation occurs, creating the fluid-like coacervate phase, described schematically in Figure 1-6.

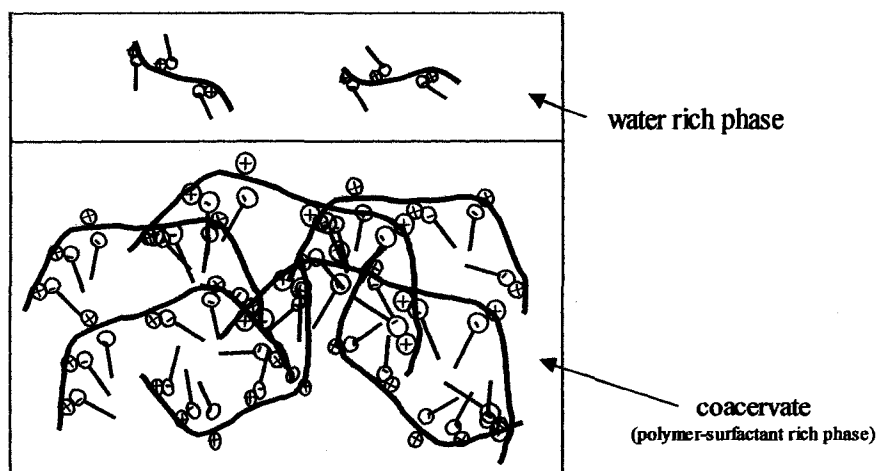


Figure 1-6. Schematic representation of fluid-like coacervate phase.

High surfactant concentrations are represented in Figure 1-5c. When the surfactant concentration sufficiently exceeds the 1:1 charge ratio, the excess surfactant molecules interact hydrophobically with the surfactant molecules that are bound to the polymer chain. This leaves the head group of the surfactant molecule exposed to ion-dipole interactions with water molecules, thus resolubilizing the polymer/surfactant complex through comicellization.^{7, 16, 72} The surfactant concentration at which this occurs is known as the critical resolubilization concentration (CRC).²¹ The CRC is dependent on the hydrophilic species of the surfactant and can be difficult to reach if the polyelectrolyte has a high charge density or if there are irregularities in the surfactant structure.^{7, 73}

Wang and Tam¹⁸ observed site-specific ion-ion interactions using isothermal titration calorimetry. With poly(acrylic acid) and dodecyltrimethylammonium bromide (DoTAB), they observed binding of individual surfactant molecules up to a critical surfactant concentration, at less than half the CMC of DoTAB, where an increase in ΔH_{app} indicated polymer-induced micellization of electrostatically-bound surfactant molecules. Saturation of the polymer with surfactant molecules and micellization of these bound surfactant molecules became complete at one-half the DoTAB CMC and free micelle formation was observed at a surfactant concentration near that of the CMC in the absence of polymer.¹⁸ Similar to Goddard and coworkers, Wang and Tam conclude that site-specific ion-ion interactions occur, where the initial attraction is due to electrostatic interactions and micellization is induced by the bound surfactant molecules.^{7, 18}

Polymer Property Effects

In both the macroion-macroion and the site-specific ion-ion interaction mechanisms of coacervation that have been presented in the literature, complex formation between polyelectrolyte and oppositely-charged surfactant is dependent on a variety of polymer and surfactant properties which impact the degree of surfactant binding, packing arrangements and conformation of each component.⁷ These properties include polymer molecular weight, charge density, structure, and flexibility and surfactant molecular architecture and micelle charge density.^{3, 7, 16, 19, 74} Both the Voorn-Overbeek and Tainaka coacervation theories show a dependence of coacervation on polymer molecular weight. In the former, a critically high molecular weight is required for coacervation to occur, while in the latter an increase in molecular weight provides a stronger attraction between the oppositely-charged components.⁶¹ Dubin and coworkers investigated

poly(sodium styrene sulfonate) (NaPSS) with DoTAB/TX100 mixed micelles and observed the onset of polymer-surfactant interaction at a lower DoTAB fraction with increased NaPSS molecular weight.^{14, 75} This was shown by Choi and Kim as well, with a lower CAC for high molecular weight poly(acrylic acid)-C_nTAB systems.^{14, 76} Dubin and coworkers have also investigated the effects of polymer molecular weight using PDADMAC-SDS/TX100 systems where little difference was observed for the coacervate complexes as molecular weight was increased; however in experiments involving a transition from intrapolymer to interpolymer complexes the molecular weight was important.^{14, 77} The polymer concentration required for this transition to occur was lowered with increased molecular weight and at low molecular weight no phase separation was observed.¹⁴ Chronakis and Alexandridis³ investigated the coacervation mechanism of low and high molecular weight cationic polysaccharides with various anionic surfactants and observed different types of interactions as a function of polymer molecular weight. For the high molecular weight system, they determined, using rheological methods, that the complexes formed with this polymer were polymer-dependent, or that the surfactant played a secondary role in complex formation. Coacervation in the low molecular weight systems displayed a dependence on the surfactant tail group architecture, indicating that this complexation was surfactant-dependent.³

The Voorn-Overbeek and Tainaka theories also predict a dependence of coacervation on polymer charge density, with a critically high charge density required in the former and stronger interactions at higher charge densities in the latter.⁶¹ Binding studies between oppositely-charged polymer and surfactant have demonstrated that the

attraction between these components is stronger with higher charge density polymers. This leads to a higher degree of binding and increased cooperativity in the coacervation process, and generally a higher number of bound surfactant molecules in the complexes formed.¹² Similar to molecular weight, higher charge density also lowers the CAC. Kogej and coworkers investigated the effects of increasing charge density of poly(acrylic acid) and poly(methacrylic acid) with *N*-cetylpyridinium chloride and *N*-dodecylpyridinium chloride and observed stronger interactions at higher charge densities. Also, at high charge densities, the bound surfactant molecules arranged into ordered structures upon micellization whereas with the low charge density systems, interaction and subsequent polymer-induced micellization occurred, but ordered structures were not formed.¹² A similar effect was observed by Chen and coworkers, where the charge density of ionene bromide polymers was varied by introducing different alkyl lengths into the polymer backbone. With low charge density polymer there was a large spacing between cationic charges and the surfactant tail groups were unable to pack into an organized structure. However, with the high charge density system (3,3-ionene bromide) the charges were close enough to one another that surfactant tail groups packed in a side-by-side organized array. The low charge density system exhibited resolubilization because comicellization was possible, however phase separation persisted in the high charge density system because comicellization was not favorable.² This effect of charge density on resolubilization has also been observed by Goddard and by Naderi and coworkers.^{7, 16}

Polyelectrolyte structure has also been shown to impact coacervate formation, particularly with respect to hydrophobic modification. Hydrophobic modification of

polyelectrolytes has been shown not only to affect polymer-surfactant interactions, but also to alter the mechanism of coacervate formation in regards to the surfactant binding process.¹⁶ In the absence of surfactant, hydrophobically-modified polymers self-associate intramolecularly and also intermolecularly, forming crosslink points (Figure 1-7a).⁷ These points of self-association can either be weakened or strengthened by interactions with surfactant molecules. Holmberg and coworkers⁸ have described interactions between hydrophobically-modified polymers and oppositely-charged surfactants, where the primary driving force is hydrophobic association between the hydrophobic moieties along the polymer backbone and the surfactant tail groups.^{7, 8} With increased surfactant concentration, micelles form around these hydrophobic moieties, connecting the polymer chains and inducing or enhancing crosslinking, which causes coacervate formation (Figure 1-7b).

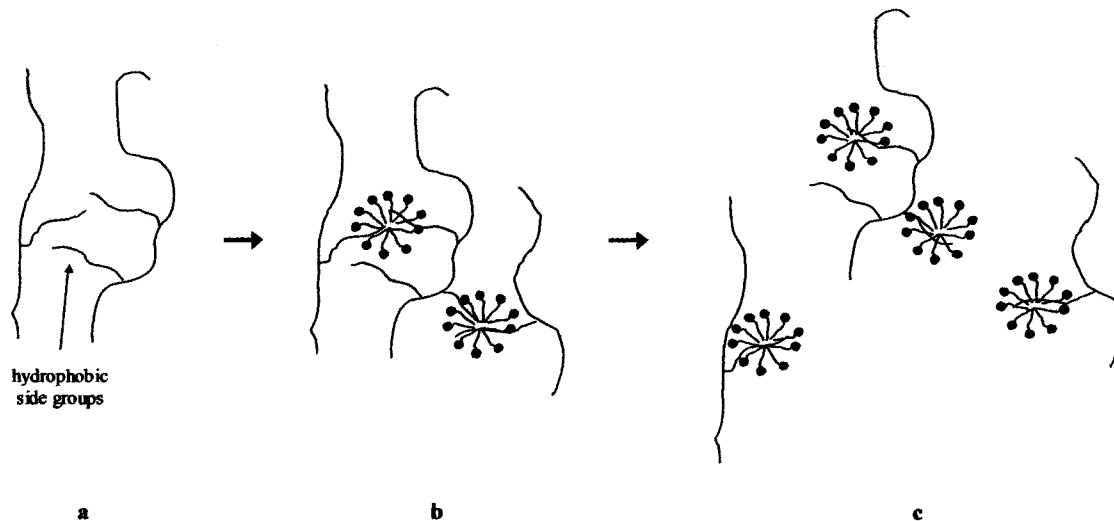


Figure 1-7. Schematic representation of interactions between hydrophobically-modified polymer and oppositely-charged surfactant as a function of surfactant concentration.⁸

As surfactant concentration is further increased a larger number of micelles are formed and the hydrophobic moieties are sequestered in individual micelles, disrupting micelle-

induced crosslinks and self-associations. This causes resolubilization of the coacervate (Figure 1-7c).⁸

The mechanism governing the onset of polymer-surfactant interaction with hydrophobically-modified polyelectrolytes was demonstrated by Smith and McCormick using hydrophobic terpolymers with cetyltrimethylammonium bromide (CTAB).²⁹ They observed that both electrostatic and hydrophobic interactions occurred in these systems, however hydrophobic groups along the polymer chain imparted a specificity to the interactions.^{7,29} Panmai and coworkers also observed that the presence of charged sites on hydrophobically-modified polyacrylamide enhanced interactions with the oppositely-charged CTAB⁵⁹, however binding occurred initially at very low surfactant concentrations with preferential binding at the hydrophobic groups along the polymer backbone.⁷ They also found, at very high surfactant concentrations after crosslink sites had been disrupted, the formation of rod-like micelles and subsequent bridging of neighboring rod-like micelles via hydrophobically-modified polymers.⁵⁹

Another structural aspect that has been shown to impact coacervate formation is the flexibility of the polymer backbone. Utilizing Monte Carlo simulations, Jonsson and Linse have demonstrated that the flexibility of the polyelectrolyte strongly affects binding of oppositely-charged macroions. Their investigations probed the degree of “wrapping” of the polymer chain around the macroion upon interactions as a function of chain stiffness (Figure 1-8).⁹

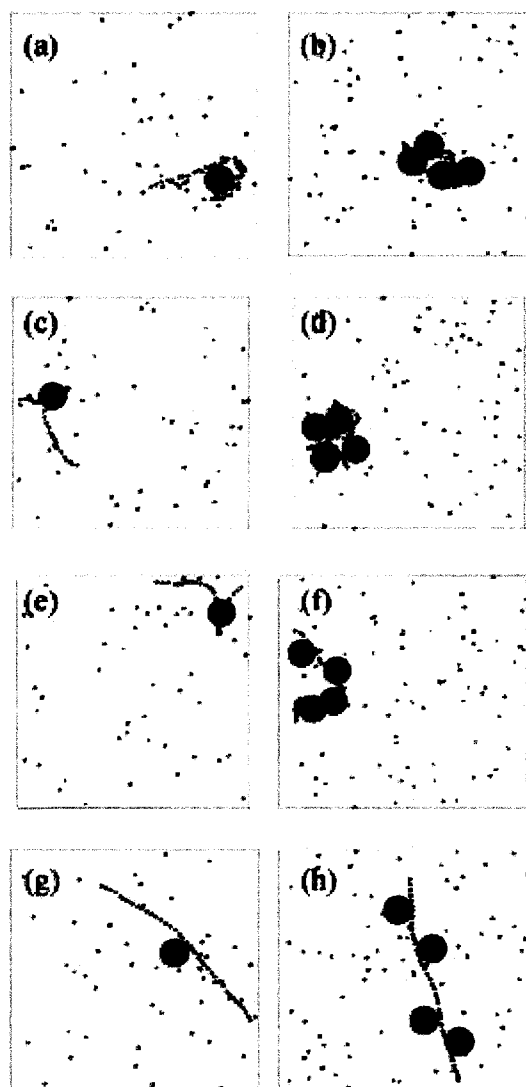


Figure 1-8. Typical configurations of polyelectrolyte interactions with oppositely-charged macroions as a function of polymer chain stiffness, achieved through Monte Carlo simulations. Chain stiffness increases from (a) to (g).⁹

From free energy calculations, the interaction of one surfactant macroion with the polymer chain becomes less favorable with an increase in chain stiffness. When one macroion is complexed to a flexible polymer chain, the polymer is able to wrap around the macroion so that many of the charged polymer segments are near the oppositely-charged macroion head groups (Figure 1-8a). However, stiff polymer chains remain straight even with macroion binding so that only a few of the charged polymer segments

are in contact with the macroion head groups (Figure 1-8g). The first few macroions complex strongest to the flexible polymer but once the complex is neutralized, binding of additional macroions to the stiff chain is stronger. The extended chain possesses more available area for additional macroions and electrostatic repulsions are lower because macroions are located farther from one another (Figure 1-8h). Addition of surfactant macroions to flexible polymer chains occurs with little additional extension of the polymer chain. Extension of the chain would result in an entropic loss so wrapping of the polymer chain around the additional macroions occurs and repulsions between bound macroions are screened so that the macroions are located close to one another (Figures 1-8b and 1-8d).⁹ The Monte Carlo studies provide insight into the effects of polymer flexibility with regards to the macroion-macroion interaction mechanism. With the flexible PDADMAC-SDS system, Li and coworkers experimentally observed the formation of a compact coacervate structure, similar to the Monte Carlo predictions. They attributed this conformation to minimization of conformational entropy loss during complex formation because random coil-like polymer conformations were maintained.¹⁵ Naderi and coworkers also investigated a flexible polymer system (poly{[2-(propionyloxy)ethyl] trimethylammonium chloride} (PCMA) with SDS and also observed a reduction in size of the polymer chain with the addition of surfactant.¹⁶ However, Guillot and coworkers investigated systems of sodium carboxymethylcellulose (NaCMC), a stiff polyelectrolyte, and observed that polymer size in the absence of surfactant was very similar to the complex size after the addition of surfactant.^{16, 78} This discrepancy in polymer collapse with the addition of surfactant was attributed to the

stiffer structure of NaCMC compared to PCMA, which is also in agreement with the Monte Carlo simulations.¹⁶

Surfactant property effects

Surfactant properties have been shown to affect coacervate formation, specifically surfactant structure and micelle charge density. Goddard and Hannan investigated polymer-surfactant interactions between cationically-modified HEC (JR400) and sodium alkyl sulfates of differing chain lengths, C₈, C₁₀, C₁₂, and C₁₄.⁷ They observed a line of maximum precipitation, at the 1:1 stoichiometric ratio, that terminated when the polymer concentration was lowered below a certain value. This polymer concentration increased with decreasing surfactant alkyl chain length, such that with increased surfactant alkyl chain lengths less polymer was required for coacervate formation.^{6,7} These researchers also investigated the effects of ethoxylation of the surfactant molecules on coacervate formation. The introduction of ethoxy (EO) groups into surfactant structures is known to influence surfactant micelle structure where the large tail group volume with increasing degree of ethoxylation lessens the desirability of hydrophobic chain packing.⁸ Goddard and Hannan observed that both monoethoxy and triethoxy n-dodecyl sulfates displayed interactions with JR400, as did 3EO and 7EO n-pentadecyl sulfates, although the longer alkyl chain sulfates required higher concentrations of surfactant for resolubilization. Thus they concluded that introducing irregularities, such as EO groups, into the surfactant structure can influence the resolubilization of coacervate.⁶

As mentioned previously, surfactant charge density effects were determined to affect coacervate formation. The surface charge of colloidal particles, such as surfactant micelles, is known to influence their adsorption characteristics.²¹ For oppositely-charged

polymers and surfactants, this property is of particular importance due to the ion-exchange interaction mechanism that contributes to polymer-surfactant interaction. Dubin and coworkers have extensively investigated the effect of micelle surface charge density on polymer-surfactant interactions.^{7, 14, 15, 79, 80} They have observed that above a critical micelle surface charge density complex formation occurs, with increasing coacervate formation as micelle surface charge density increases.⁸⁰

Solution property effects

Solution properties, such as component concentrations and the addition of salt, have also been shown to impact coacervate formation. As discussed previously, at high polyelectrolyte concentrations the polymers are more likely to adopt a random coil conformation due to mutual electrostatic screening of cationic repulsions among polymer chains, and this occurs at lower concentrations for polymers with longer chain lengths.^{7, 40, 45} Chain extension in very dilute solutions and coiling of the chains as concentration is increased is known as the “polyelectrolyte effect” and was demonstrated with poly(methacrylic acid) at high percent ionization.³¹ In regards to the binding process, the polymer concentration has been shown to affect the CAC. At low polymer concentrations, CAC is less than CMC, but as polymer concentration increases CAC also increases and finally at very high polymer concentrations the CAC is lowered again. This has been attributed to ionic strength effects of the solution.⁷ Leung and coworkers demonstrated the effects of polymer and surfactant concentration on coacervation specifically in the JR400-SDS system. Using 0.1 % JR400, a decrease in viscosity with increasing SDS concentration was observed, which they attributed to intramolecular complex formation. However, with 1.0 % JR400 the viscosity increased with surfactant

addition and produced a phase separation region. Just above the resolubilization zone, the viscosity dropped sharply, and was much lower than the viscosity of the polymer alone. At low surfactant concentration (0.1 % SDS) with 1% JR400 they observed pseudoplastic behavior of the polymer-surfactant solution. At a higher surfactant concentration (1.2 % SDS) rheopectic behavior was observed, which was attributed to shear-induced unwrapping of the polymer to provide a relatively extended polycation with an adsorbed bilayer of surfactant providing an overall negative net charge.¹³ Thus the formation of coacervate was strongly dependent on the polymer and surfactant concentrations in these systems.

The effect of surfactant concentration on complexation has also been explored. As was previously discussed, increasing surfactant concentration causes an increase in micelle size and eventually a transition from spherical to rod-like micelles to lyotropic liquid crystals.⁵⁹ Primarily, surfactant concentration effects have been investigated only at concentrations up to and slightly above the CMC. Utilizing fluorescence techniques, Ananthapadmanabhan and coworkers inferred that below the region of maximum precipitation hemi-micelles formed along the polymer backbone (systems of Polymer JR and SDS), but as surfactant concentration increased conventional micelle-type structures developed.¹ At very high surfactant concentrations, Panmai and coworkers found that bridging of neighboring rod-like micelles via hydrophobically-modified polymers occurred.⁵⁹ Svensson and coworkers investigated coacervation over a range of both polymer and surfactant concentrations using visual analysis. The resulting ternary phase diagram is shown in Figure 1-9.

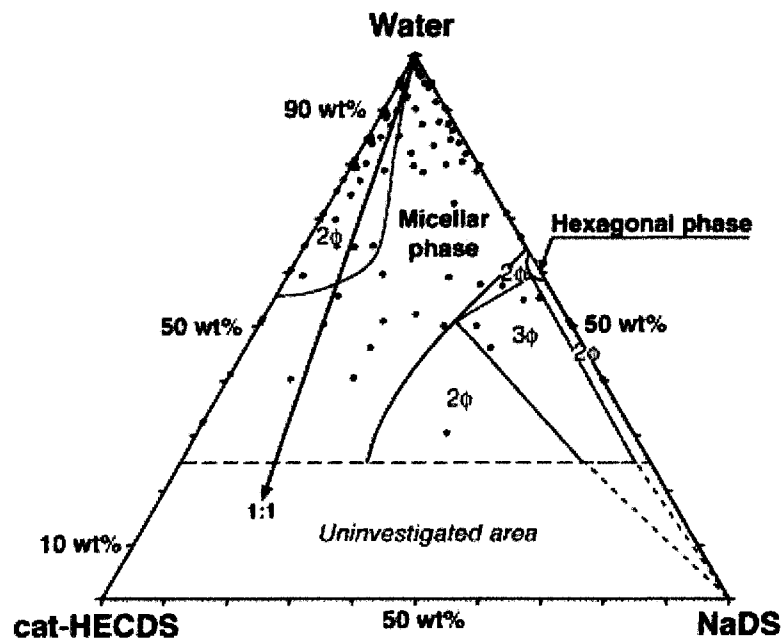


Figure 1-9. Ternary phase diagram for mixtures of JR400-SDS in water.¹⁷

At high surfactant concentrations multi-phase regions were observed and as this concentration decreased a transition to single-phase systems occurred. At low surfactant concentrations two-phase systems were again present. In the multi-phase regions at high surfactant concentration, the coacervate phase was isotropic and in the three-phase system SDS crystals with lamellar ordering were formed, determined using small-angle X-ray scattering (SAXS). In the two-phase region at low surfactant concentrations, no higher order structures were observed from SAXS analysis. Coacervation in this region was very near the 1:1 stoichiometric ratio as predicted by the Goddard coacervation mechanism. As polymer concentration decreased, this two-phase region also decreases. By examining mixtures of these systems over a wide range of concentrations, one is able to better visualize the effects of component composition on coacervate formation.

Many of the industrial applications described previously involve simple salts, which have the potential to affect interactions given the reliance of complex formation and resolubilization in these systems on electrostatic attractions.^{16, 19, 20} Generally accepted throughout the field, is the screening of electrostatic interactions by the addition of salt, which has resulted in both “coacervate suppression” and “coacervate enhancement”.^{7, 18-20} Coacervate suppression occurs via a decrease in binding of surfactant to polymer in the presence of salt and a subsequent decrease in coacervate formation. This interruption of electrostatic interactions between oppositely-charged polymer and surfactant has been observed by an increase in CAC for systems containing NaCl.²⁰ With the addition of CaCl₂, Chen and coworkers also observed a deviation from the 1:1 charge ratio for complex formation, with a greater deviation at increased salt concentrations.^{16, 81} In contrast to the above results, Guillemet and Piculell have indicated coacervate formation at lower surfactant concentrations in the presence of NaCl compared to the parent system. Thus, coacervate formation was enhanced by the addition of NaCl, which may be due to surfactant micelle growth with the addition of salt, as discussed previously.^{20, 82}

The occurrence of coacervate enhancement or coacervate suppression has been shown to depend on salt concentration. At low ionic strengths, the reduction of electrostatic interactions is predominant, where with the addition of salt, the critical aggregation concentration shifts to higher surfactant concentrations, but above CAC electrostatic interactions occur and micelle-like aggregates are found along the polymer chain.^{7, 19, 20} Resolubilization at high surfactant concentrations was also observed in these systems.²⁰ In systems with higher salt concentration, micelle formation becomes

dominant.^{7, 19} Wang and coworkers observed a decrease in CMC with the addition of NaBr demonstrating the promotion of micelle formation due to screening of head group repulsions. The interaction between polymer and surfactant in these systems was observed at surfactant concentrations where micelles existed in solution before introduction to polymer.¹⁹ Resolubilization of coacervate formed in the presence of NaCl was not observed for the PCMA-SDS systems explored by Naderi and coworkers and this was attributed salt screening of bound surfactant molecule repulsions between one another, restricting resolubilization.¹⁶ With these systems at very high NaCl concentrations Naderi and coworkers observed no coacervate formation, similar to observations of Wang and coworkers with PDADMAC-SDS/TX100 systems, where the NaCl concentration was high enough to completely screen electrostatic interactions.^{16, 20}

It is apparent from this previously published work that the effect of salt on polymer-surfactant interaction and subsequent coacervate formation shows no linear trends. Rather, it depends upon the balance of the effects of salt on polymer conformation, surfactant micelle structure and ion-ion binding between oppositely charged species, and these effects are dependent on the concentration of all components in solution. The lack of definite trends makes the investigation of an array of variables necessary to understand the effect of salt on polymer-surfactant systems, and high-throughput screening is a useful tool for investigating this vast number of systems.

High-Throughput Screening

The success of combinatorial and high-throughput screening methodologies in pharmaceutical research has triggered the introduction of these techniques to other

fields.⁸³ The field of polymer science is well suited to high-throughput screening and combinatorial methods due to the vast number of variables and parameters for investigation, including molecular weight, polydispersity, viscosity, and other application-specific parameters.⁸³ Schubert and coworkers have reported feasibility study findings that “combinatorial and high-throughput methods will represent an indispensable tool in the future of polymer research (although it most likely will not replace conventional techniques)”.⁸³ Recent high-throughput screening formulation method development has focused on the creation of compositional gradients and discrete libraries.⁸⁴⁻⁸⁷

Gradient Methods

Compositional gradients in films have been achieved at the National Institute for Standards and Technology (NIST) through a dynamic dual syringe system as well as with microfluidic systems.^{85, 86} Both of these systems offer advantages of thorough component mixing and facile isolation of the final compositions for analysis using traditionally based techniques. In the dynamic dual syringe method, component mixing, deposition and spreading is achieved (Figure 1-10).⁸⁶

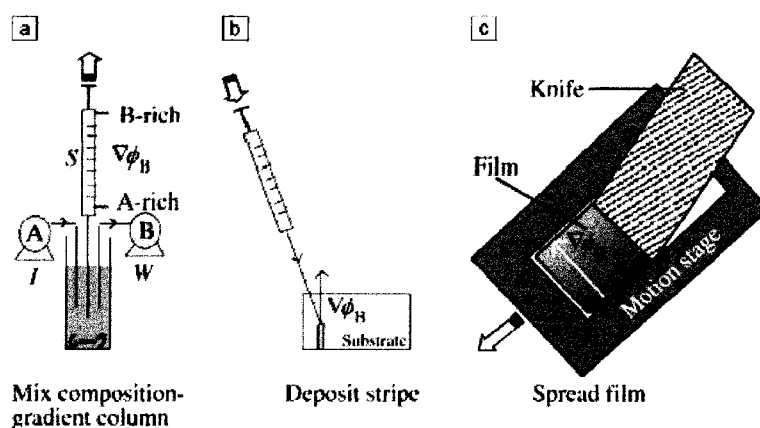


Figure 1-10. Complete dynamic dual syringe method developed at NIST.⁸⁶

In this technique, a vial is initially filled with pure component B. Component A is introduced gradually to the vial containing component B through rate-controlled syringes. As component A is being introduced, a third syringe is used to take aliquots from the vial. Over time, the controlled addition of component A causes a gradient of A in component B to form. This gradient is in turn transferred to the third syringe. After all of component A has been introduced to the vial, the contents of the third syringe are deposited on a substrate and spread into a thin film using a knife-edge coater. The films are then analyzed for the desired properties as a function of composition. This technique was validated using poly(caprolactide) (PDLA) and poly(caprolactone) (PCL) with the gradient film cast on a sapphire substrate. Fourier Transform Infrared Spectroscopy (FTIR) was employed at various positions along the gradient in order to determine mass fractions of each component at these points. PDLA absorbance increased as a function of film position, while PCL absorbance decreased, indicating the formation of a composition gradient along the film (Figure 1-11).⁸⁶

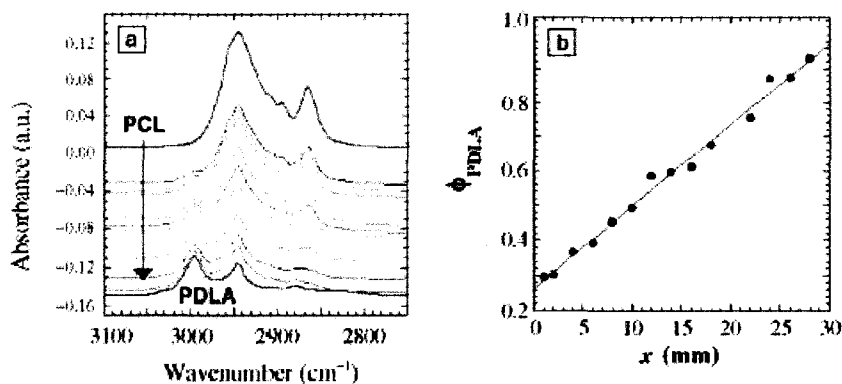


Figure 1-11. Validation of composition gradient formation using the dynamic dual syringe method.⁸⁶

In the microfluidic devices developed at NIST a gradient is generated by controlling the introduction rate of components and the geometry of the device. Microfluidics offers an added advantage of mixing and characterization *in situ*. To investigate the mixing capabilities of microfluidic devices, both T-junction and ternary designs have been developed (Figure 1-12).⁸⁵

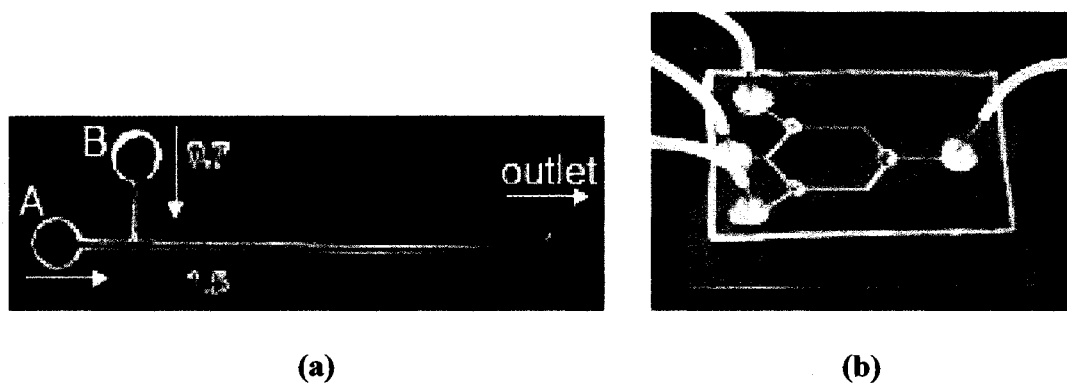


Figure 1-12. Microfluidic devices designed for intricate mixing: (a) T-junction design and (b) ternary mixing design.⁸⁵

To date, the compositional gradient capabilities of microfluidic devices have been investigated in terms of polymerization rather than formulation, where the devices act as microchannel reactors for controlled polymerizations (Figure 1-13).⁸⁵ By varying the flow rate or the rate of introduction of reactants, a continuous gradient of polymer properties is synthesized, such as a molecular weight gradient. The devices used for synthesis reactions are designed to provide an area for mixing and therefore may be adaptable to formulation techniques where rate of addition of one component is varied.

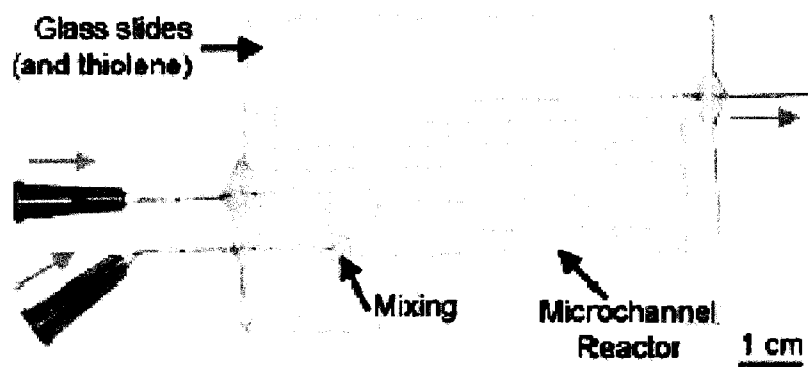


Figure 1-13. Microchannel reactor for controlled polymerization.⁸⁵

Bergbreiter and coworkers⁸⁸ have recently demonstrated a need for high-throughput screening in the determination of the lower critical solution temperature (LCST) for poly(N-alkylacrylamide) copolymers. Conventional techniques for LCST determination are time consuming which limits the ability to probe the structural effects of solvent and polymer on the LCST. The researchers developed a high-throughput screening technique that exploits the known effect of solution cloudiness that occurs at and above the LCST. By employing a light scattering detector and a temperature gradient microfluidic device they were able to determine the LCST by monitoring the change in scattering amount along the temperature gradient. An example of the results generated using this technique is shown in Figure 1-14.

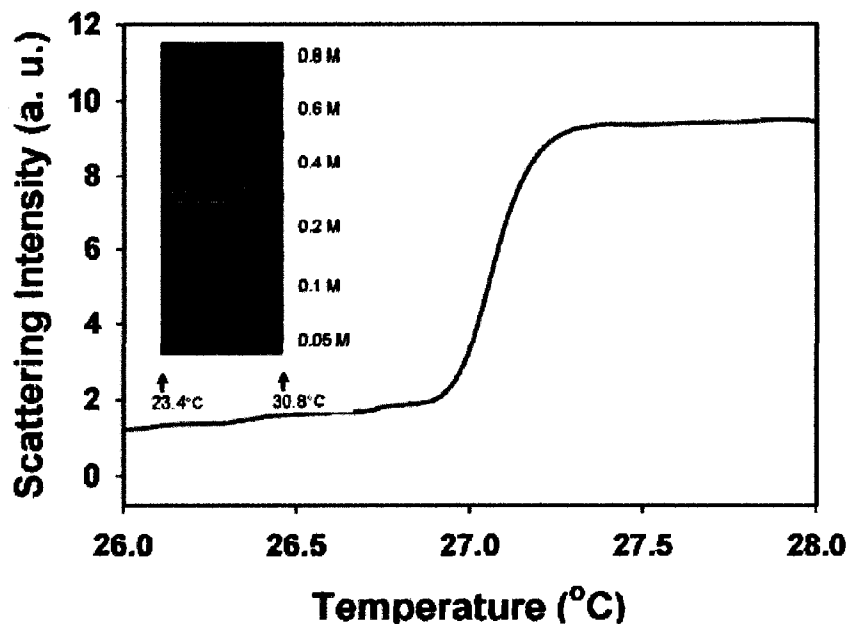


Figure 1-14. Sample clouding curve generated using a microfluidic temperature gradient device. Inset contains CCD images of the microfluidic channels where the blue regions are precipitant, pseudo-colored for clarity.⁸⁸

By utilizing this rapid screening technique they were able to probe structural effects of the solvent and polymer on LCST to enhance the understanding of the systems' behaviors.⁸⁸

Discrete Sample Methods

The major disadvantage of the compositional gradient techniques is the limited amount of materials that can be combined. To address this issue, researchers at NIST have also focused on the formation of discrete libraries. In their research, as well as other investigators, discrete libraries are formed using liquid dispensers for delivering materials onto either previously patterned surfaces or creating a pattern during dispensing.^{84, 89-91} Cabral has utilized tailored arrays created rapidly via photolithography techniques. In general, a 10 x 10 well array (2 mm x 2 mm) was used with varying wall heights, offering volume tailoring (Figure 1-15).⁸⁴

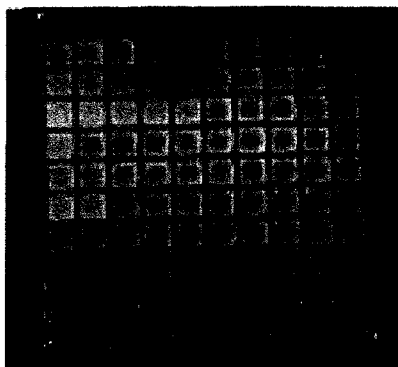


Figure 1-15. Sample vessel for creating 10 x 10 discrete arrays using liquid dispensing systems.⁸⁴

Dispensing the components into the arrays is accomplished via syringe pumps attached to an overhead actuator, with accuracy in both the volume dispensed and the position of the actuator over the well. This “tailor-made liquid dispenser” differs from commercially available liquid handlers in that it dispenses very small amounts of samples (0.1-1.0 μL). Similarly to the composition gradients, these tailored microwell arrays can be used in conjunction with traditionally based analysis techniques, such as combinatorial small angle X-ray scattering.⁸⁴

Schubert and coworkers have focused on development of ink-jet printing high-throughput techniques for use with polymeric systems.⁸⁹⁻⁹¹ Original work in this area focused on polymeric electronic devices where ink-jet printing has become a keystone technology. In brief, ink-jet printing of polymers is achieved by printing a library of individual dots or rectangles on a given substrate where the compositions are well-controlled (Figure 1-16).⁸⁹⁻⁹¹

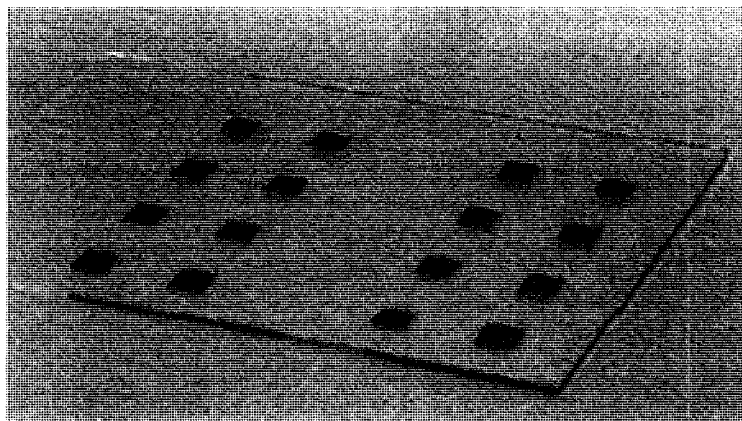


Figure 1-16. An example of a polymeric film array generated using ink-jet printing techniques.⁹⁰

The library shown in Figure 1-16 is one of the original examples of ink-jet printing as a method of polymer library generation.⁹⁰ There is a multitude of factors that need to be considered in employing this technique, including solution viscosity, nozzle deposition mechanism and solvent type.⁸⁹⁻⁹¹ In addition, the small sample size leads to rapid evaporation of solvent, leaving behind a film of the composition under investigation.⁸⁹⁻⁹¹ In a general sense, film formation is not a disadvantage but for the understanding of polymer-surfactant interactions it is desirable to investigate the system in the presence of its continuous phase, which is usually a volatile solvent such as water. This consideration eliminates Schubert's technique as a method to investigate compositional phase behavior that results from polymer-surfactant interaction.

The advantages of discrete library methods are that they offer the capabilities of preparing multiple component compositions and analysis via previously established methods. However, one significant drawback with the available discrete library methods is that the sample sizes are not large enough to ensure good sample mixing. Therefore,

their use is limited to components with low viscosities so that mixing is attained even at these small sample volumes. Taking into account these advantages and disadvantages from available high-throughput techniques a novel high-throughput screening technique that allows rapid investigation of polymer-surfactant systems in the liquid state was developed in this research (Chapter IV-A).

CHAPTER II

OBJECTIVES AND NEED FOR RESEARCH

The interaction between oppositely-charged polyelectrolyte and surfactant has been investigated in a variety of systems, including biological systems and naturally- and synthetically-derived polymers.⁷ Oppositely-charged polyelectrolyte and surfactant interact to form soluble complexes, as well as phase-separated complex coacervate, which has made them useful in many applications, including the food, toiletries, and pharmaceutical industries. A great deal of previous research has focused on understanding the interaction between polyelectrolyte and oppositely-charged surfactant on a microscopic level, which has generally focused on systems in dilute surfactant regimes near or slightly above the surfactant critical micelle concentration.¹⁻²³ The exploration of coacervation in the dilute surfactant regime has demonstrated that polymer-surfactant interactions are not governed by any one universal mechanism, but that multiple possible mechanisms exist and have been observed depending on the polymer-surfactant system.^{7,20} The properties of the polymer and surfactant components and of the solution have been shown to affect not only the mechanism of coacervate formation, but also the amount of coacervate formed and the compositions at which it is formed. An investigation of various possible parameters of these components over a wide range of concentrations would require an immense amount of time using conventional techniques. However, a broad ranging investigation is needed to unravel the apparently paradoxical mechanism of coacervate formation.

A fundamental understanding of the effects of polymer and surfactant structure, as well as solution properties, on the interaction between polymer and surfactant and the resulting coacervate formation over a wide surfactant concentration range is lacking. This fundamental understanding is critical for enhancement of the scientific understanding of these systems as well as for the practical design of polymer-surfactant systems for specific applications, which may range from enhanced deposition of polymer from solution to formation of stable complexes for targeted drug delivery.

This research aims to explore multiple polymer, surfactant and solution parameters that could potentially influence the interaction of oppositely-charged polymers and surfactants. The overall goal of this research is to define the effects of polymer and surfactant structural properties, and solution properties, on the interaction between cationic polymer and anionic surfactant, and the subsequent formation of coacervate in these systems. To achieve this goal, the interaction of cationic polymers with varying properties with anionic surfactant will be studied using conventional microscopic methodologies. In addition, polymer, surfactant and solution properties will be varied systematically and the macroscopic property of coacervate formation will be investigated using a novel high-throughput method.

The specific objectives of this research are to:

- Develop and validate a rapid and reproducible method capable of preparation of multi-component samples, analysis of these samples regarding formation of coacervate and representation of the immense amount of data for easy interpretation

- Examine the interaction of cationic HEC polymers and anionic surfactant to understand the mechanism of interaction as a function of molecular weight
- Perform a systematic study of the effect of polymer properties (molecular weight, charge substitution, and backbone structure) and surfactant properties (micelle charge density, tail group structure) on coacervate formation over a broad compositional range
- Thoroughly characterize the poly(vinylpyridinium hydrochloride) polymers to confirm the solution properties of these systems, enabling more accurate understanding of their interaction with surfactants
- Examine the interaction of cationic poly(vinylpyridinium hydrochloride) polymers and anionic surfactants to understand the mechanisms of interaction as a function of solution conformation and charge positioning along the polymer backbone
- Investigate the effects of solution properties (salt concentration, addition order) on coacervate formation over a broad compositional range and in multiple polymer-surfactant systems

CHAPTER III
EXPERIMENTAL

Materials

Cationic Polysaccharides

Cationically-modified cellulosic polymers, INCI name Polyquaternium-10 (PQ-10)⁹², were supplied by Amerchol Corporation, a division of The Dow Chemical Company and were used as received. These polymers are derivatives of hydroxyethylcellulose (HEC) modified via the addition of trimethylammonium substituted epoxides to create quaternary ammonium salts with a chloride counterion (Figure 3-1).⁹³ The average molar degree of ethoxylation along the HEC backbone is 2.5.

17, 94

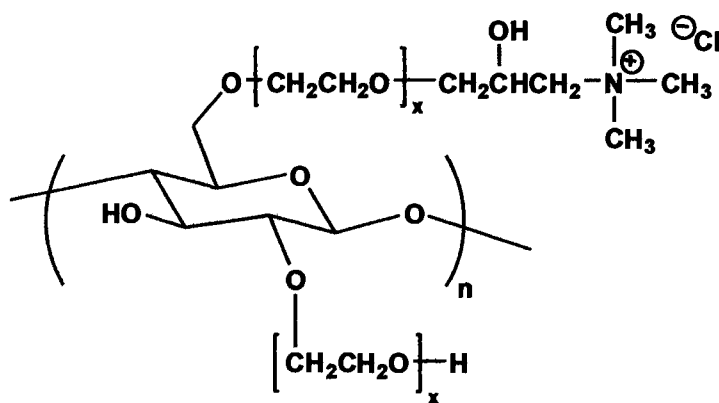


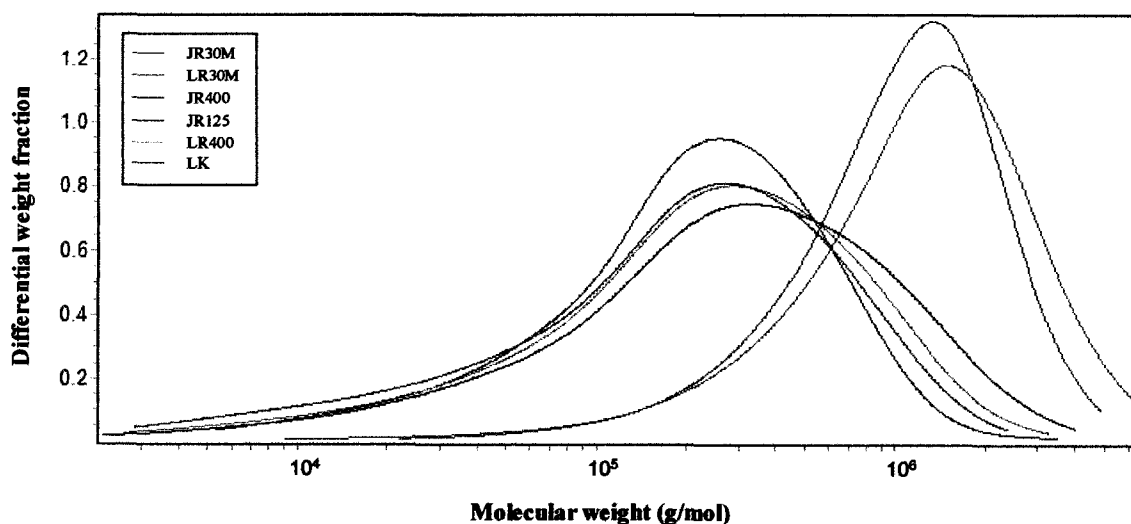
Figure 3-1. Nominal chemical structure of Polyquaternium-10.¹⁷

A series of PQ-10 polymers that differ in molecular weight and cationic charge substitution (CS) was studied (Table 3-I).

Table 3-I. PQ-10 series properties.

Polymer Name	M_w (10^3 g/mol)	M_w/M_n	% Nitrogen ⁹³	CS
LK	350	4.0	0.50	0.13
LR400	400	5.2	0.95	0.25
JR125	350	5.8	1.85	0.48
JR400	500	5.5	1.85	0.48
JR30M	1500	2.3	1.85	0.48
LR30M	1300	2.0	0.95	0.25

The values of molecular weight were determined using size exclusion chromatography (SEC) with multi-angle laser light scattering (MALLS) and differential refractive index detection, according to a previously published method.⁹⁵ An average dn/dc of 0.140 was used for all calculations. The molecular weight distribution was unimodal and broad for all PQ-10 polymers studied (Figure 3-2). The broad PDI observed with these systems may be due to heterogeneity of charge along and among the polymer chains, which is reasonable given the original cellulose molecular weight distribution and the subsequent derivitization and grafting processes.

**Figure 3-2.** Molecular weight distributions of the PQ-10 polymer series.

The CS is defined as the number of moles of nitrogen per mole anhydroglucose unit.⁹⁶

The percent nitrogen values were provided by Amerchol Corporation⁹³ and CS was determined using Equations 3-1 and 3-2

$$CS = \frac{N(mol)}{r.u.(mol)} = \frac{N(g)}{r.u.(mol)} \div N(g/mol) \quad \text{Equation 3-1.}$$

where $r.u.$ is the anhydroglucose repeat unit so that $r.u. (mol) = 1$, $N(g/mol) = 14$ g/mol,

and

$$\frac{N(g)}{r.u.(mol)} = \%N * \left(\frac{r.u.(mass)}{100} \right) \quad \text{Equation 3-2.}$$

where $r.u. (mass) = 366$ g/mol.

Hydrophobically-modified PQ-10 polymers, INCI name Polyquaternium-67 (PQ-67)⁹⁷, were supplied by Amerchol Corporation, a division of The Dow Chemical Company and were used as received. These polymers are derivatives of HEC modified via dimethyldodecyl ammonium substitution of the hydroxyethyl side chain to create quaternary ammonium salts with a chloride counterion (Figure 3-3).⁹³

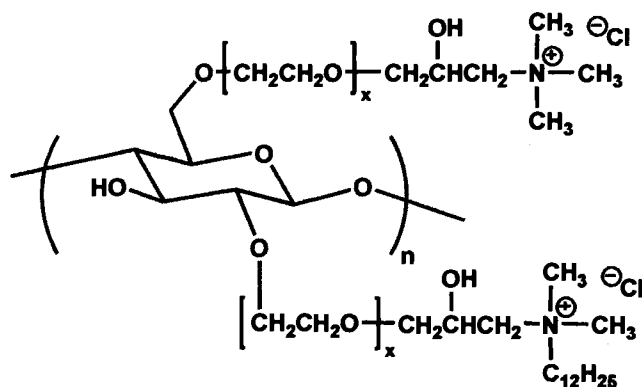


Figure 3-3. Nominal chemical structure of Polyquaternium-67.⁹⁷

A series of PQ-67 polymers was studied where all polymers have a molecular weight range of 200 000 to 800 000 g/mol and $CS = 0.25$.⁹⁷ The degree of hydrophobic

substitution is defined as the average number of moles of hydrophobic substituent per mole of the anhydroglucose repeat unit.⁹⁶ The degree of hydrophobic substitution (HS) differs for all polymers in the series ($HS_{SL-5} = 5 \times 10^{-4}$, $HS_{SL-60} = 5 \times 10^{-3}$, $HS_{SL-100} = 1 \times 10^{-2}$).^{96,97} The hydrophobic substitution for SL-30 was not reported, however it is known to be between that of SL-5 and SL-60.

Cationically-modified galactomannans, INCI name Guar

Hydroxypropyltrimonium Chloride (cationic guar)⁹⁸, were supplied by Rhodia Incorporated and were used as received. These polymers are derivatives of guar bean galactomannans, where a portion of the galactose units are cationically-modified with pendant quaternary ammonium salts with a chloride counterion (Figure 3-4).⁹⁹

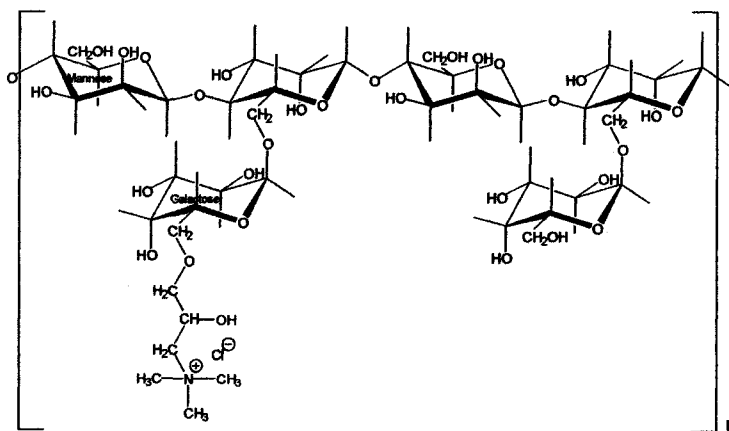


Figure 3-4. Nominal chemical structure of Guar Hydroxypropyltrimonium Chloride.

A series of cationic guar was studied and the properties are listed in Table 3-II.

Table 3-II. Guar Hydroxypropyltrimonium Chloride series properties.^{100, 101}

Polymer Name	M_w (10^3 g/mol)	CS
C-1000	1000	0.14
Excel	1500	0.14
C-14S	2000	0.14
C-17	2000	0.17

Synthetic Cationic Polymers

All cationic synthetic polymers were synthesized via reverse-addition fragmentation chain transfer (RAFT) polymerization by the McCormick Research Group at The University of Southern Mississippi, and donated for our studies. The details of the synthesis, purification, and characterization are reported by Convertine, *et. al.*¹⁰² The chain transfer agents used for poly(4-vinylpyridine) and poly(2-vinylpyridine) were 4-cyanopentanoic acid dithiobenzoate (CTP) and 2-dodecylsulfanylthiocarbonylsulfanyl-2-methyl propionic acid (DMP), respectively. Poly(*ar*-vinylbenzyltrimethylammonium chloride) (VBTAC) was also synthesized via RAFT with the CTP chain transfer agent. The polymers were used as received. Cationic charge was imparted on poly(2-vinylpyridine) and poly(4-vinylpyridine) using HCl to produce poly(2-vinylpyridinium hydrochloride) (P2VP) and poly(4-vinylpyridinium hydrochloride) (P4VP). The chemical structures of P4VP, P2VP, and VBTAC are shown in Figure 3-5.

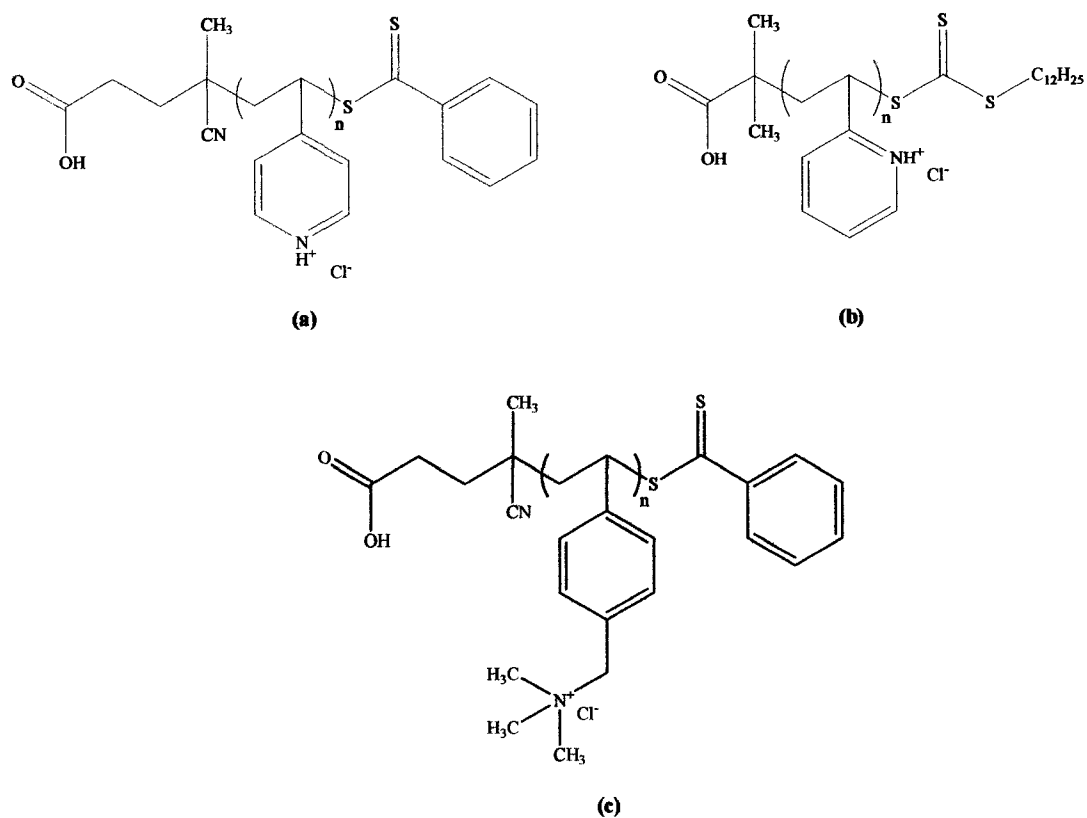


Figure 3-5. (a) P4VP, (b) P2VP, and (c) VBTAC chemical structures.

The properties of all cationic synthetic polymers studied are shown in Table 3-III.

Table 3-III. Properties of cationic synthetic polymers.

Polymer	M_n (g/mol)	PDI	Charge Density (% Ionization)
P4VP	9 000	1.2	86
P4VP	32 000	1.0	91
P2VP	6 000	1.2	85
P2VP	32 000	1.1	74
VBTAC	12 000	1.0	----

The values of M_n and PDI were determined using SEC according to a previously published method.¹⁰² The dn/dc values for P4VP and P2VP were 0.225 and 0.167 mL/g, respectively.¹⁰² Charge densities were controlled by pH adjustment using 1.0 N HCl. Percent ionization was calculated using Equation 3-3, where the apparent pK_a values of P4VP and P2VP are 4.0 and 3.5, respectively.¹⁰³

$$\% \text{ Ionization} = 100 / \left(1 + 10^{(pH - pK_a)} \right) \quad \text{Equation 3-3.}^{104}$$

VBTAC has a permanent quaternary ammonium cationic charge on each repeat unit.

Surfactants

Sodium lauryl ether sulfate (SLES) with an average of three ethylene oxide (EO) units per molecule and ammonium lauryl ether sulfates (ALES) with averages of three, twelve, and thirty EO units per molecule were supplied by Stepan Company and were used as received. The chemical structure of SLES is shown in Figures 3-6.

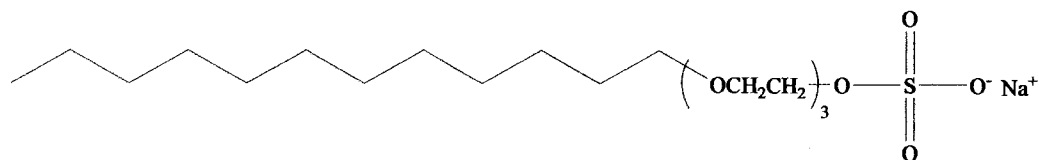


Figure 3-6. SLES chemical structure.

The critical micelle concentration (CMC) of SLES in water at 25°C was determined from surface tension (Figure 3-7).^{105, 106}

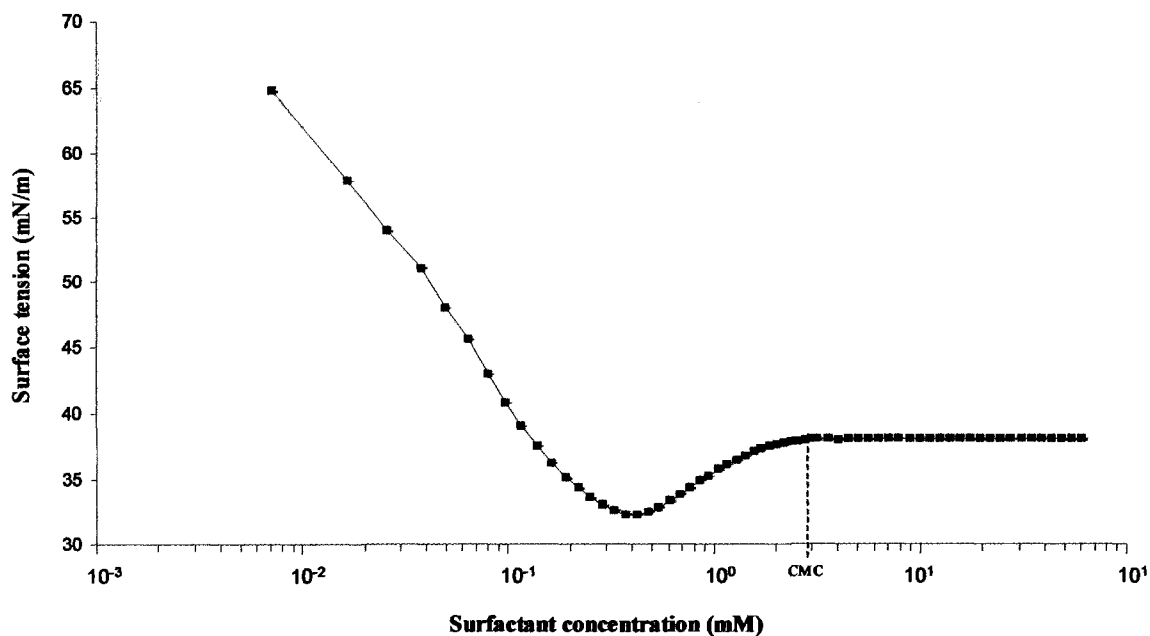


Figure 3-7. Surface tension as a function of SLES concentration.

The pre-CMC dip in the curve is likely due to impurities, and despite this the experimentally determined CMC of 3.0 mM is in good agreement with previously reported values.^{105, 106} Multiple runs were performed, exhibiting excellent reproducibility in the data.

The CMC values of ALES surfactants in water at 25°C were provided by the supplier (CMC_{3EO} = 0.41 mM, CMC_{12EO} = 0.14 mM, and CMC_{30EO} = 0.06 mM).¹⁰⁷⁻¹⁰⁹

The chemical structure of ALES is shown in Figure 3-8.

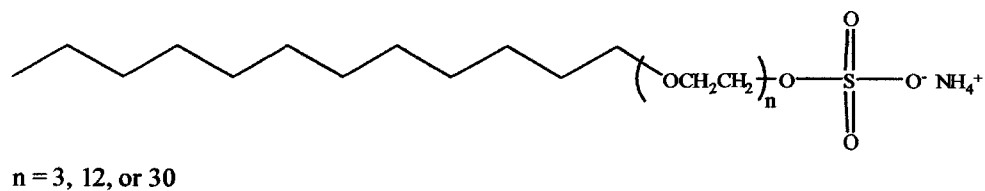


Figure 3-8. ALES chemical structure.

Sodium alkyl sulfates of differing linear chain lengths were obtained from Aldrich and used as received (sodium octyl sulfate (C_8S), sodium decyl sulfate ($C_{10}S$), sodium dodecyl sulfate ($C_{12}S$), and sodium tetradecyl sulfate ($C_{14}S$)). The CMC values in water were reported in previously published literature (C_8S : 140 mM (40°C), $C_{10}S$: 33 mM (40°C), $C_{12}S$: 8.6 mM (40°C); 8.2 mM (25°C), $C_{14}S$: 2.2 mM (40°C); 2.1 mM (25°C)). A representative chemical structure is shown in Figure 3-9.

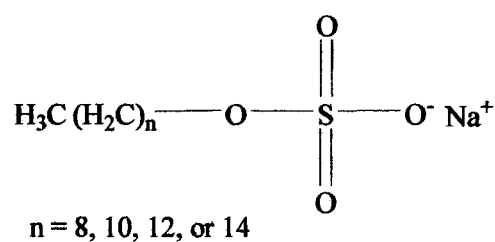


Figure 3-9. Representative sodium alkyl sulfate chemical structure.

Sodium dodecylbenzene sulfonate (SDBS) was supplied by Rhodia Incorporated and used as received. The CMC of SDBS in water at 25°C (2.4 mM) was determined from surface tension and is in agreement with previously reported values (Figure 3-10).¹⁰⁶

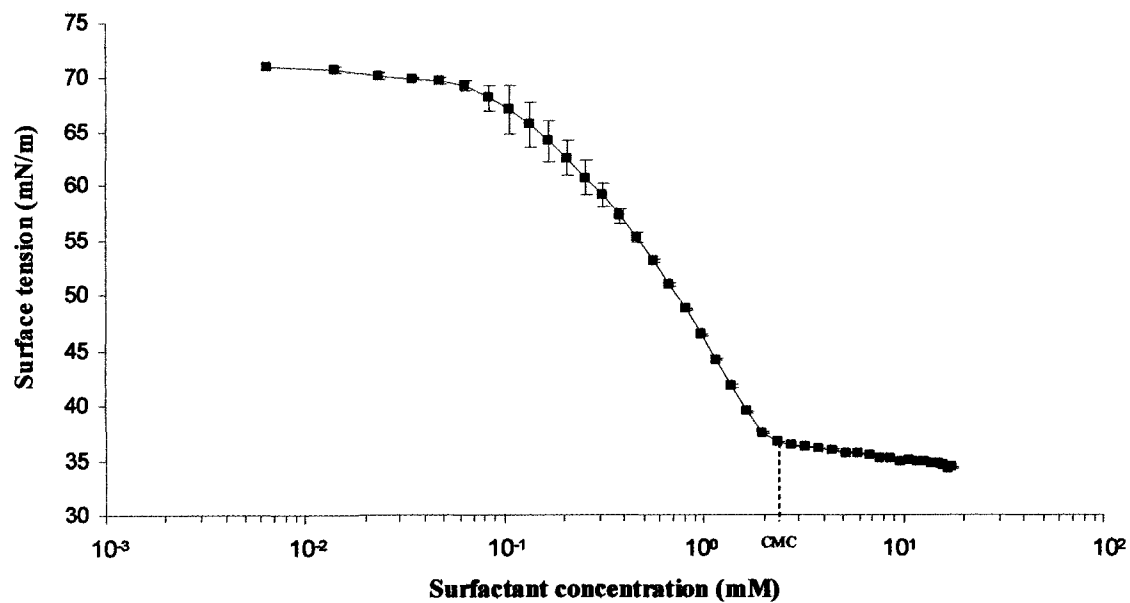


Figure 3-10. Surface tension as a function of SDBS concentration.

Sodium capryl sulfonate (SCS) and sodium xylene sulfonate (SXS) were supplied by Stepan Company and were used as received. The CMC of SCS was 48 mM.¹¹⁰ Sodium xylene sulfonate is highly water-soluble and does not form micelles. The chemical structures of SDBS, SCS, and SXS are shown in Figure 3-11.

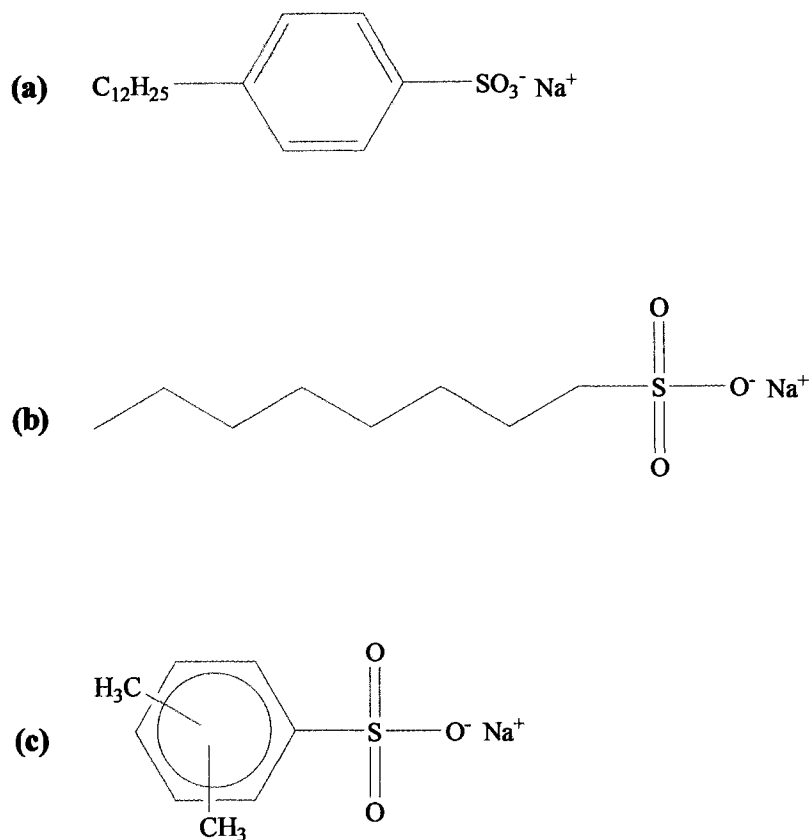


Figure 3-11. (a) SDBS, (b) SCS, and (c) SXS chemical structures.

Polyethylene glycol-12 laurate (PEG-12) was supplied by Stepan Company and was used as received. The chemical structure is shown in Figure 3-12.

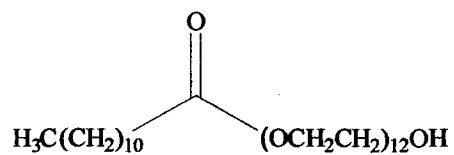


Figure 3-12. PEG-12 chemical structure.

Additional Materials

Sodium chloride (ACS reagent grade), citric acid (anhydrous, ACS reagent grade), and HPLC grade water were used as received from Fisher Scientific. Hydrochloric acid standard solution (0.99 *N*) and sodium hydroxide standard solution (1.0441 *N*) were used as received from Aldrich. Kathon™ CG Preservative (INCI name methylchloroisothiazolinone and methylisothiazolinone) was supplied by Rohm and Haas Company and was used as received. Deionized (DI) water was obtained from a Barnstead Nanopure (Barnstead International, Dubuque, IA) reverse-osmosis/filtration unit (resistivity = 18.0 MΩ).¹¹¹

Methods

High-Throughput Screening: Sample Preparation

High-throughput sample preparation was performed using a Beckman Coulter Biomek® FX Laboratory Automation Workstation (referred to herein as “liquid handler”) with a single-pod system and Span-8 configuration (Figure 3-13).

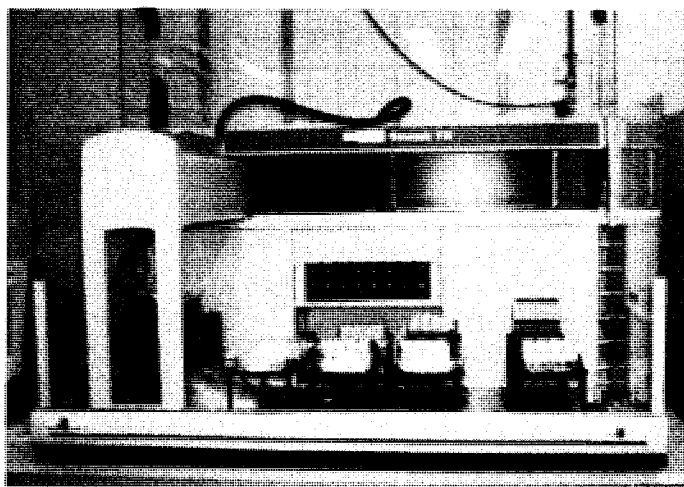


Figure 3-13. Beckman Coulter Biomek® FX Laboratory Automation Workstation.

To enhance accuracy, an aspirate/dispense step prior to dispensing into sample wells was utilized for all solutions. The sample vessels were Biotech Solutions 96-Well Multi-Tier™ Micro Plate systems (acrylonitrile-butadiene-styrene (ABS) plates with 0.5 mL glass flat bottom vials). For mixing and storage, 96-plug molded PTFE/silicone liners were used. All samples were prepared at room temperature.

Polymer Premix Solution Methods

The liquid handler requires all materials to be in the liquid form with a viscosity maximum of 100 mPa·s. All polymers were supplied as powders and surfactants were supplied as either powders or viscous liquids. Thus, premixed solutions (premixes) of all polymers and surfactants were made prior to their experimental use. All premixes were prepared with deionized (DI) water. Surfactant premixes were prepared by either dissolving the powder with mixing or diluting the viscous liquid. Polymer premix methods differed depending on the polymer type, as indicated below:

Cationic polysaccharide premix preparation method. The premix protocol for PQ-10 and PQ-67 was adapted from the protocol recommended by Amerchol Corporation.⁹³ Typical premixes were made at 0.5 % (w/w), with a total volume of 200 mL. DI water was heated to 45-50 °C in a glass jar and the polymer powder was added slowly to the heated water with constant agitation from a magnetic stirbar. Once a portion of polymer was added, all polymer was dissolved before subsequent additions to prevent hydrated gel formation. The jars were covered throughout the process to prevent loss due to evaporation. After all polymer was dissolved, the sample was allowed to cool to RT and 0.003 % (w/w) Kathon™ CG Preservative was added. Guar premixes were prepared using the same procedure as PQ-10 and PQ-67, with the addition of neat citric acid to

obtain pH ~6.5 before Kathon™ CG Preservative was added. This premix protocol was adapted from the protocol recommended by Rhodia Incorporated.¹⁰⁰

Poly(vinylpyridines) Premix Preparation Method. Typical premixes were made at 0.25 % (w/w) actives, with a total volume of 200 mL. A predetermined amount of hydrochloric acid (1.0 N) was added to DI water in a glass jar before polymer addition. pH adjustment of the water was performed to facilitate dissolution of poly(vinylpyridine). Polymer powder was then added slowly to the acidic water with constant agitation from a magnetic stirbar. Once a portion of polymer was added, all polymer was dissolved before subsequent additions to allow protonation, and thus solubilization, of the polymer. The jars were covered throughout the process to prevent loss due to evaporation. It was determined that an equilibrium pH was obtained after ~24 hours. Therefore, the pH was measured and recorded after at least 24 hours and this value was used to calculate the percent ionization.

Sample Mixing

Mixing of samples in the 96-well plates was performed after robotic addition of all materials via the liquid handler. The plates were sealed using PTFE/silicone liners as previously described. Mixing was accomplished using a Scientific Industries Vortex Genie 2 with a 96-well plate attachment. A mixing time of 30 s per 96-well plate was used.

Material Layering Methods

Two high-throughput layering techniques were used in studying the effects of salt and addition order in polymer-surfactant systems. In both methods the materials were added sequentially to the 96-well plate vials so that the first two materials were able to

mix via diffusion before the third was added, and the second and third materials were able to mix via diffusion before the entire plate was mixed to provide complete sample mixing. In the Constant Salt method the concentration of NaCl was the same in each composition investigated. In the Salt Gradient method the concentration of NaCl in each composition varied uniformly across the phase diagram and the concentrations were slightly dependent on addition order (Figure 3-14).

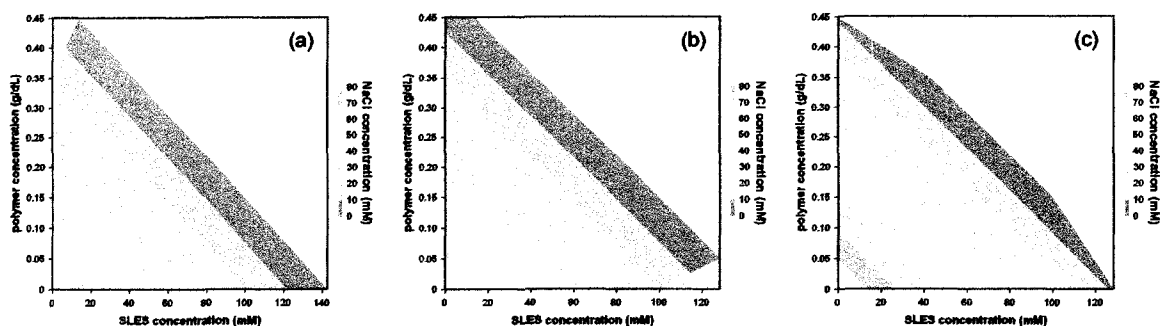


Figure 3-14. Salt gradient profiles for PQ-10-SLES-NaCl investigations using the Salt Gradient method. The addition orders associated with each salt gradient are (a) polymer, surfactant, salt and salt, surfactant, polymer; (b) surfactant, polymer, salt and salt, polymer, surfactant; (c) polymer, salt, surfactant and surfactant, salt, polymer.

High-Throughput Screening: UV-Visible Spectrophotometry

High-throughput UV-visible transmittance measurements were performed and absorbance values were calculated using a Tecan Safire™ Microplate Detection System. Absorbance scans were performed for new polymer-surfactant systems ($T = 25\text{ }^{\circ}\text{C}$) over a wavelength range of 230-1000 nm (10 nm step, 10 flashes per well, move time = 10 ms). For all samples, 410 nm was chosen as the appropriate wavelength for absorbance measurements (additional details provided in Chapter IV-A). For all samples transmittance was measured at a constant wavelength and temperature ($\lambda = 410\text{ nm}$, $T = 25\text{ }^{\circ}\text{C}$, 10 flashes per well) and absorbance values were calculated.

Surface Tensiometry

Surface tension measurements were performed at 25 °C using the Wilhelmy Plate method on either a Kruss K100 Processor Tensiometer (polysaccharide systems) or a Kruss K12 Processor Tensiometer (poly(vinylpyridinium hydrochloride) systems). Surfactant CMC was determined by successive dosing of a 50 000 mg/L surfactant solution (SLES) or an 8 000 mg/L surfactant solution (SDBS) into pure distilled water. A plot of surface tension (mN/m) versus surfactant concentration is generated, where CMC is defined as the surfactant concentration at the intersection of the lines from the linear concentration-dependent and concentration-independent regions (Figure 3-15).

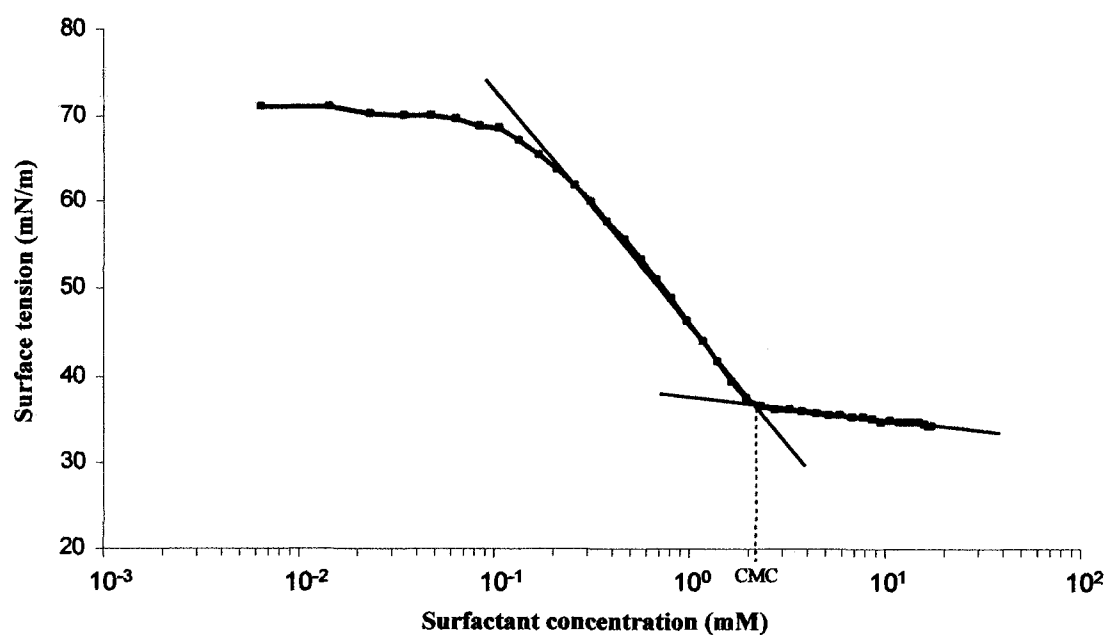


Figure 3-15. CMC determination in surfactant systems.

Surface tension was also measured for mixtures of polymer and surfactant and the surfactant concentration at the onset of interaction as well as the CMC in the presence of polymer were determined in a manner similar to Figure 3-15. For polysaccharide

systems, a solution of 50 000 mg/L surfactant was successively dosed into a 0.35 g/dL polymer solution. For poly(vinylpyridinium hydrochloride) systems, a solution of 8 000 mg/L surfactant was successively dosed into a 0.15 g/dL polymer solution. The polymer concentration was constant throughout all measurements.

Solution Viscometry

Zero-shear viscosities were measured for the PQ-10 polymers at multiple concentrations for determination of critical overlap concentration (c^*). Measurements were performed on a TA Instruments AR 2000 Rheometer using a standard-size double concentric cylinders geometry. A steady-state stress sweep was performed at 25 °C and zero-shear viscosity was determined by extrapolation of the plateau region to zero shear.¹¹² A representative plot of viscosity as a function of shear rate for multiple polymer concentrations is shown in Figure 3-16.

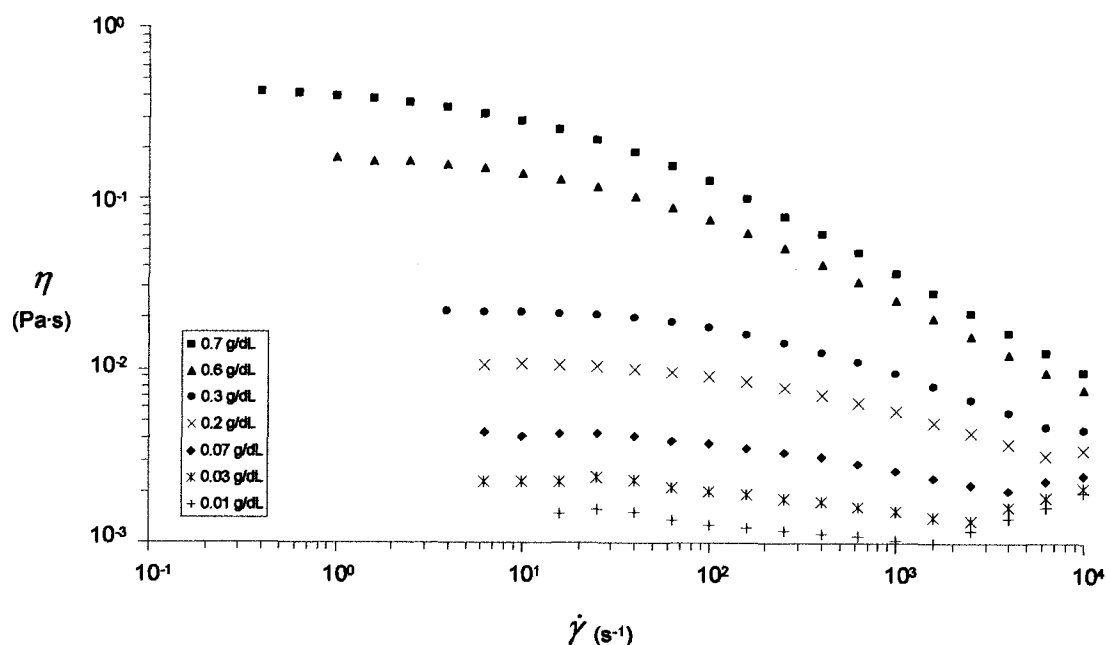


Figure 3-16. Zero-shear viscosity determination for polymers at multiple concentrations.

Zero-shear viscosities for cationic polysaccharide-anionic surfactant systems were determined using a Rheometric Scientific SR-5000 controlled-stress rheometer with a 25 mm cone and plate geometry. A steady-state stress sweep was performed at 25 °C and the Ellis model was used to fit the curve.

Apparent viscosities for the poly(vinylpyridinium hydrochloride) polymers and for mixtures of these polymers with anionic surfactant were measured using a Contraves LS-30 low shear rheometer with the 2T cup and bob geometry (5.96 s⁻¹, 25 °C).

Critical Overlap Concentration. For determination of c* the zero shear viscosity was determined for a range of polymer concentrations and a log-log plot of η_{sp} versus polymer concentration was generated, where c* is the polymer concentration at the intersection of two lines with slopes ~1.4 and ~3.4; ideally, for Gaussian chains below c* the viscosity should scale as 1.4 with respect to polymer concentration and above c* the viscosity should scale as 3.4 with respect to polymer concentration (Figure 3-17).⁸

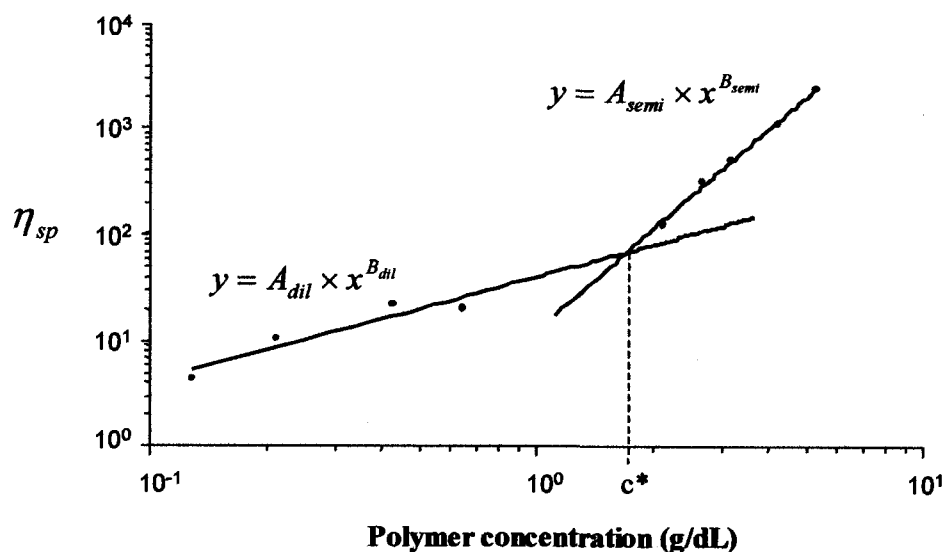


Figure 3-17. η_{sp} as a function of polymer concentration for c^* determination.

A power function was used to fit the curves and a numerical value of c^* (g/dL) was determined using Equation 3-4

$$c^* = 10^{((\log A_{dil} - \log A_{semi}) / (B_{semi} - B_{dil}))} \quad \text{Equation 3-4.}$$

where A_{dil} and A_{semi} are y-intercept values in the dilute and semi-dilute polymer concentration regions, respectively, and B_{dil} and B_{semi} are the slopes of the lines in the dilute and semi-dilute polymer concentration regions, respectively.

Dynamic Light Scattering

Dynamic light scattering (DLS) studies were performed using a Malvern Instruments Zetasizer Nano ZS, which has a particle size detection range of 0.6 nm to 6.0 μm . Particles are illuminated by a He-Ne laser (633 nm) and the scattering intensity is detected at a fixed 173° angle using a non-invasive backscattering technique.

Since particles in solution exhibit Brownian motion, small fluctuations in the scattering intensity are observed, which are manifested as an apparently random signal, which is in fact non-random, with smooth and continuous changes, over short time scales. This non-randomness is due to the physical confinement of these particles to a specific location, with limited movement, across these short time intervals. With the Zetasizer Nano ZS instrument, correlation statistics are applied to calculate the degree of non-randomness in this apparently random signal, generating a correlogram. The correlation expression is shown in Equation 3-5

$$G(\tau) = \frac{I(t_0)I(t_0 + \tau)}{I(t_\infty)^2} \quad \text{Equation 3-5.}$$

where $G(\tau)$ is the correlation coefficient, $I(t_0)$ is the initial scattering intensity, $I(t_0 + \tau)$ is the scattering intensity at some delay time, τ , and $I(t_\infty)$ is the scattering intensity at

infinite time. The correlation statistics are then fitted to an exponential algorithm, which embodies the diffusion coefficient (Equation 3-6)

$$G(\tau) = B + A^{-2q^2D\tau} \quad \text{Equation 3-6.}$$

where B is the amplitude of the correlogram, A is the baseline at infinite time, q is a known scattering vector, and D is the diffusion coefficient. The diffusion coefficient is then used to determine the radius of hydration (R_H) utilizing the Stokes-Einstein equation (Equation 3-7)

$$R_H = \frac{kT}{6\pi\eta D} \quad \text{Equation 3-7.}$$

where k is the Boltzmann constant, T is temperature, and η is the viscosity of the dispersant.¹¹³

The extraction of the R_H can be accomplished using either the cumulants single exponential decay or a multi-modal non-negative least squares approach. The former provides a Z -average size and a polydispersity index (PDI). The PDI is the distribution of particle size around the Z -average size and a high PDI is indicative of either a large distribution or a multi-modal system (PDI range from 0 to 1). If the PDI is high and multiple peaks are observed using the multi-modal analysis approach, then the confidence of the measurement lies with the radii of the multi-modal approach. Hydrodynamic sizes are presented as a % volume distribution, with an acceptable error in sizes of +/- 5 %, according to ISO standards.¹¹⁴

In our studies, premixes were prepared using HPLC grade water filtered through a 0.1 μm filter. Surfactant and polymer samples were filtered through 0.45 μm syringe filters prior to measurement. Size measurements were performed using either a low

volume disposable sizing cuvette or a disposable sizing cuvette. The sample settings were as follows: Dispersant: Water, 25 °C, viscosity = 0.8872 cP, RI = 1.33, with the dispersant viscosity used as the sample viscosity. For all systems, 3 runs were performed for each measurement at set run durations (polysaccharide systems: 420 s, poly(vinylpyridinium hydrochloride) systems: 200 s) and a total of 3 measurements were performed on each sample. Results were calculated using the Multiple Narrow Modes method to distinguish individual peaks.

Static Light Scattering

Polymer solutions were prepared using HPLC grade water filtered through a 0.02 μm filter as the solvent (the conformation of the polymer molecules upon interaction with surfactant was desired, thus no electrolytes were added to the solvent). MALLS was performed using a Wyatt DAWN[®] EOS 18-angle light scattering detector in batch mode. A syringe pump was used for precise sample injection. Using the multi-angle mode, multiple concentrations were analyzed and Zimm plots were generated for each polymer. A sample Zimm plot is shown in Figure 3-18.

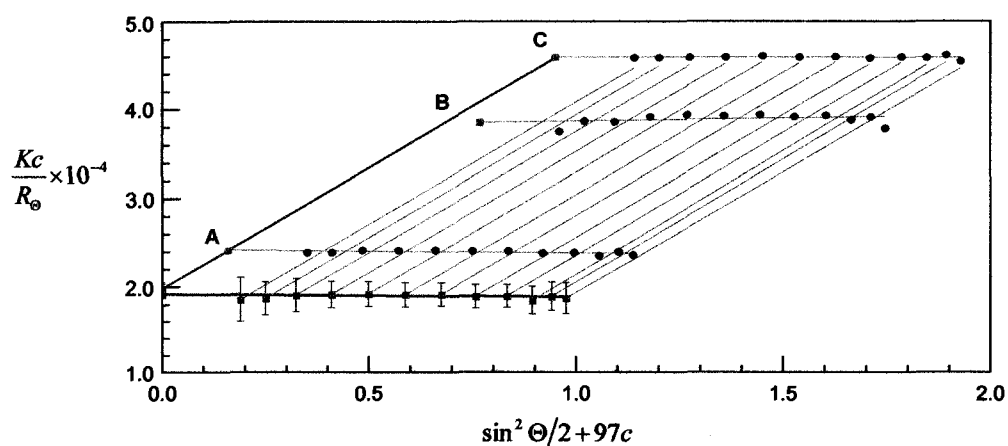


Figure 3-18. Zimm plot for low molecular weight P4VP obtained using static light scattering.¹¹⁵

The Zimm plot is defined by Equation 3-8

$$\frac{Kc}{R_{\Theta}} = \frac{1}{M_w} + \frac{2B(kc)}{k} \quad \text{Equation 3-8.}$$

where M_w is the weight-average molecular weight, B is the second virial coefficient, k is an arbitrary constant chosen to provide a spread of the data, and c is concentration. K is given by Equation 3-9

$$K = \frac{2\pi^2 n^2 \left(\frac{dn}{dc}\right)^2}{N_o \lambda^4} \quad \text{Equation 3-9.}$$

where n is the refractive index, N_o is Avogadro's number, and λ is the wavelength. In Equation 3-8, R_{Θ} is the Raleigh ratio and is given by Equation 3-10

$$R_{\Theta} = \frac{r^2 i_{\Theta}}{I_o (1 + \cos^2 \Theta)} \quad \text{Equation 3-10.}$$

where r is the distance between the detector and the oscillating dipole, i_{Θ} is the intensity at angle Θ , and I_o is the incident intensity. Extrapolation of the concentration, c , as $\Theta \rightarrow 0$ gives a line with $slope = 2B/k$ and from this line, the second virial coefficient was obtained. The second virial coefficient was used to determine polymer-solvent compatibility.¹¹⁶

CHAPTER IV-A

DEVELOPMENT AND VALIDATION OF A HIGH-THROUGHPUT SCREENING
METHOD OF SAMPLE PREPARATION, ANALYSIS AND DATA
REPRESENTATION IN POLYMER-SURFACTANT SYSTEMS

Method Development

Sample Preparation

In this research, the development of a novel high-throughput screening method was essential for investigating the large range of compositions inherent in generating a broad understanding of polymer-surfactant interactions. Primary efforts were directed towards preparing a large number of samples in a relatively short amount of time. Initially, Finnpiette® digital multi-channel pipettes from Thermo Electron Corporation, with both 8 and 12 channel heads, were employed for rapid sample preparation using a “by volume” method (versus traditional “by weight” methods). An experimental design where surfactant and polymer concentrations were varied systematically to obtain a wide range of compositions for analysis was developed. Before analysis, sample mixing was accomplished by inversion of the sample grid for 24 hours. Analysis of coacervate formation was performed through operator observation, where the amount of coacervate was classified as “large” or “small”. Traditional data visualization techniques of defining areas of one or two phases on ternary phase diagrams^{17, 20, 117} were employed (Figure 4A-1).

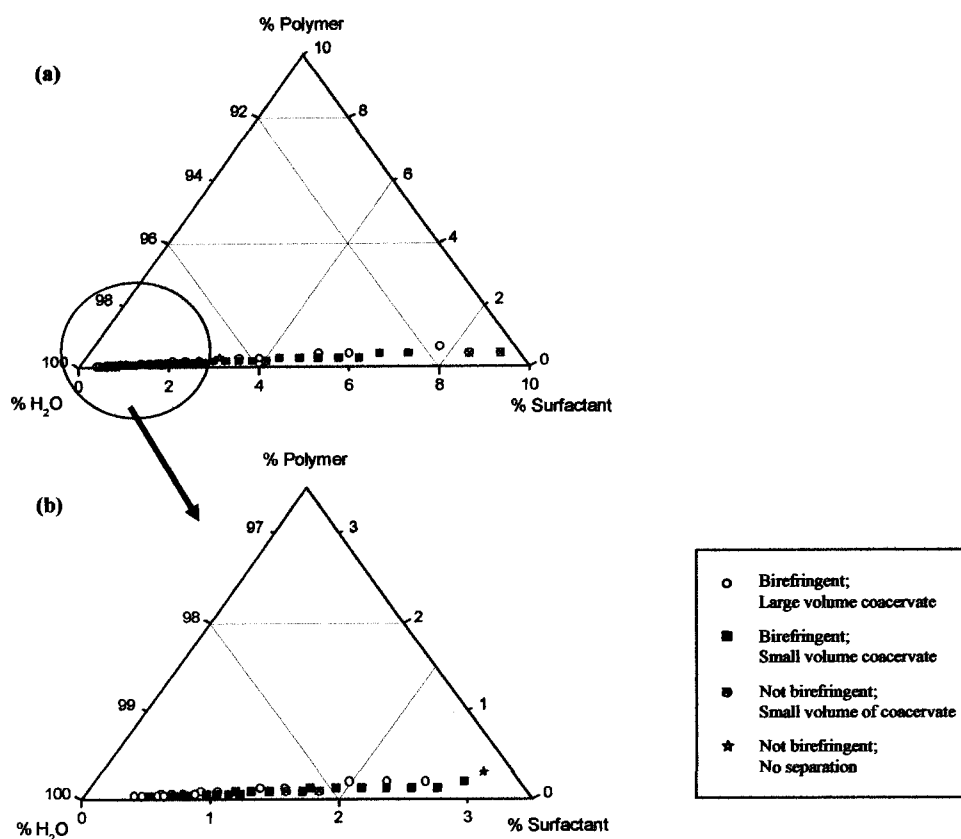


Figure 4A-1. Ternary phase diagrams generated using multi-channel pipettes (PQ-10-ALES): (a) all samples investigated and (b) enlargement of the circled area.

Although increased sample production was accomplished with the multi-channel pipettes and grid design method, there were significant drawbacks. Sample preparation was rapid, but manual operation was rate-limiting insofar as it did not allow the rapid generation of parallel libraries of compositions. Mixing techniques were also time consuming and were possibly subject to operator technique. Also, sample analysis was susceptible to inherent operator-operator error due to the subjective measurements of “large” and “small” amounts of coacervate. As can be seen in Figure 4A-1a, the phase diagram containing all compositions studied is narrow in scope despite the effort involved in generating the data. Presenting only the data at compositions below 3 %

surfactant (Figure 4A-1b) only slightly enhances the potential for interpretation of the diagram. Thus, the only advantage of the data representation technique was ease of recognition by those in the field.

Taking these drawbacks into consideration we explored other disciplines that routinely incorporate high-throughput screening into their research activities. Specifically, we turned to the pharmaceutical industry and investigated the potential use of automated liquid dispensing instrumentation. The chosen instrumentation was the Beckman Coulter Biomek[®] FX Laboratory Automation Workstation (liquid handler). The liquid handler offered many advantages over current and traditional techniques. Sample preparation is performed solely through the instrumentation, providing a completely “hands-off” sample preparation method. It also avoids the operator errors that are inherent in manual pipetting. One major drawback of this liquid handler system was its inability to deliver highly viscous materials and solids (viscosity maximum = 100 mPa·s), which limits the total compositional range to be studied. However, by making premixed solutions of our materials we overcame the viscosity limitation and investigated wide compositional ranges in short periods of time.

The second difficulty encountered with automated liquid handling arose from irreproducible wetting of the polyethylene pipette tips. This lessened the precision in the delivery of components to the sample vessel. This limitation was demonstrated by efforts to deliver 200 μ L of solution, where the same pipette tip was used for five repetitions. The results of the five successive aspirating/dispensing steps for both polymer and surfactant solutions are shown in Table 4A-I.

Table 4A-I. Repetitive additions of surfactant (S) and polymer (P) solutions to centrifuge tubes using the liquid handler. The same probe tip was used for all additions of the respective materials.

Sample	Tube (g)	Tube + Material (g)	Material Added (g)
S1	1.285	1.465	0.180
S2	1.257	1.456	0.199
S3	1.274	1.472	0.198
S4	1.238	1.434	0.196
S5	1.253	1.451	0.198
<i>Average of S1-S5</i>	<i>1.261</i>	<i>1.456</i>	<i>0.194 ± 0.008</i>
P1	1.279	1.452	0.173
P2	1.297	1.493	0.196
P3	1.246	1.442	0.196
P4	1.279	1.472	0.193
P5	1.227	1.424	0.197
<i>Average of P1-P5</i>	<i>1.266</i>	<i>1.467</i>	<i>0.191 ± 0.01</i>

Samples S1 and P1 were the first samples dispensed for the surfactant and polymer materials, respectively. The tip was used as received for these initial dispensings. A total volume of 180 μL and 173 μL was delivered for samples S1 and P1, respectively.

Samples S2-4 and P2-4 were the subsequent samples dispensed for the surfactant and polymer, respectively. The tip was not changed between dispensings so that the tip was coated by either surfactant or polymer for these subsequent dispensings. A total volume of ~ 199 μL and ~ 196 μL was delivered for each S2-4 sample and each P2-4 sample, respectively. Little variation occurred between the last four dispensings.

Aspirating 200 μL of the surfactant or polymer material (premix) into each pipette tip and then dispensing that volume into a waste container before any sample wells were filled was found to eliminate this source of irreproducibility (Table 4A-II).

Table 4A-II. Repetitive additions of surfactant (S) and polymer (P) solutions to centrifuge tubes using the liquid handler with an aspirate/dispense step prior to sample preparation. The same probe tip was used for all additions of the respective materials.

Sample	Tube (g)	Tube + Material (g)	Material Added (g)
S1	1.232	1.433	0.201
S2	1.291	1.495	0.204
S3	1.277	1.485	0.208
S4	1.226	1.430	0.204
S5	1.245	1.446	0.201
<i>Average of S1-S5</i>	<i>1.254</i>	<i>1.458</i>	<i>0.204 ± 0.003</i>
P1	1.247	1.461	0.214
P2	1.228	1.439	0.211
P3	1.295	1.512	0.217
P4	1.262	1.477	0.215
P5	1.239	1.453	0.214
<i>Average of P1-P5</i>	<i>1.254</i>	<i>1.468</i>	<i>0.214 ± 0.002</i>

This precision of the liquid handler method was increased with incorporation of the aspirate/dispense step, as verified by the decreased standard deviations of the samples in Table 4A-II compared to those in Table 4A-I. The statistical significance of the difference with incorporation of the aspirate/dispense step was evaluated using the t-test approach. The experimental t-value, t_0 , was calculated using Equation 4A-1

$$t_0 = \frac{A_2 - A_1}{\sqrt{MSE \left(\frac{1}{n_1} + \frac{1}{n_2} \right)}} \quad \text{Equation 4A-1.}^{118}$$

where A_2 and A_1 are average values for each data set, n_1 and n_2 are the number of runs in each data set, and MSE is the mean square error (Equation 4A-2)

$$MSE = \frac{\sum (n_r - 1)(S_r^2)}{\sum (n_r - 1)} \quad \text{Equation 4A-2.}^{118}$$

where S_r^2 is the square of the standard deviation. Using the values shown in Tables 4A-I and 4A-II, the difference between the standard deviations for the surfactant samples

without and with the incorporation of the aspirate/dispense step were determined to be statistically significant with a 95 % confidence interval, as were the standard deviations for the polymer samples.¹¹⁸ Thus, an aspirate/dispense step was incorporated for all sample preparation. The liquid handler was adopted as the sample preparation method for all subsequent polymer-surfactant interaction phase diagrams.

Phase Separation Analysis

It was important to develop a rapid and repeatable method for sample analysis that is compatible with samples prepared using the liquid handler. At the initial time of development, the common technique for sample analysis was visual observation of phase separation with classifications of one or more phases. In an effort to limit operator-to-operator error we chose 1.5 mL centrifuge tubes as the sample vessels, where volume markers on the centrifuge tubes were utilized to determine high, medium and low amounts of coacervate, with attempts to determine a percent coacervation based on the total volume of sample. These tubes were also compatible with the liquid handler. A representative diagram showing coacervate amount is shown in Figure 4A-2.

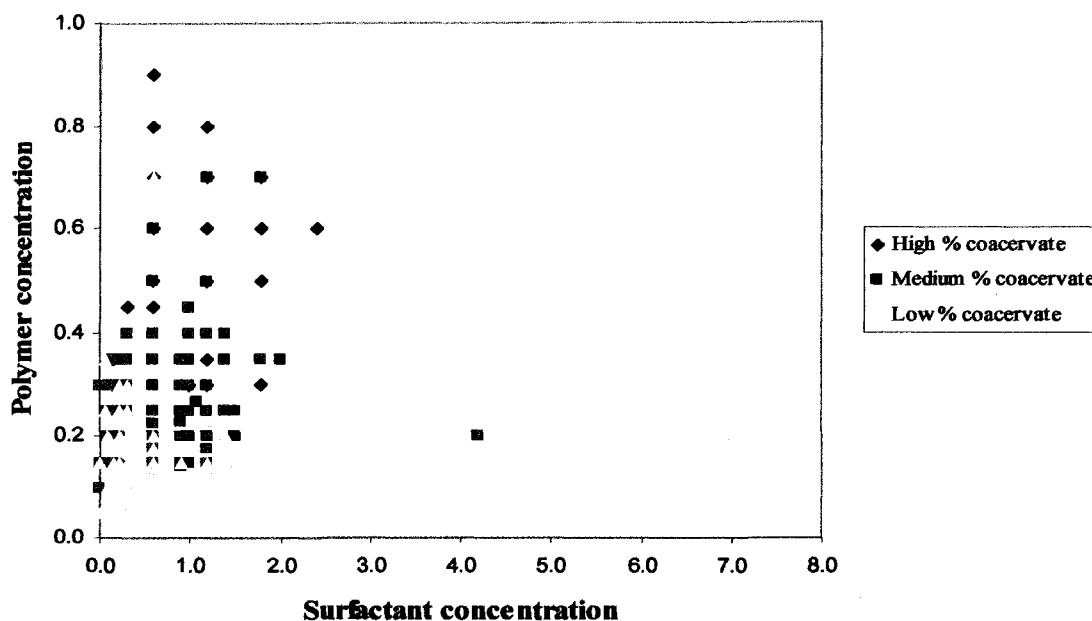


Figure 4A-2. Binary phase diagram of phase separation analyzed via visual observation (LR400-SLES).

From this diagram we observe the success of generation of a considerable amount of data in a reasonable time frame using the liquid handler for sample preparation. For example, the 120 discrete samples in Figure 4A-2 were generated in approximately 60 minutes. Centrifuging the samples after complete sample mixing via slow rotation increased the accuracy of visual measurements of phase separation, evidenced by moderately discrete regions of high, medium and low coacervate in Figure 4A-2. However, areas of significant overlap between low and medium coacervate amount were observed, demonstrating a need for more accurate and potentially quantitative analyses. Reproducibility measurements performed on data generated using this method further illustrates this point (Figure 4A-3).

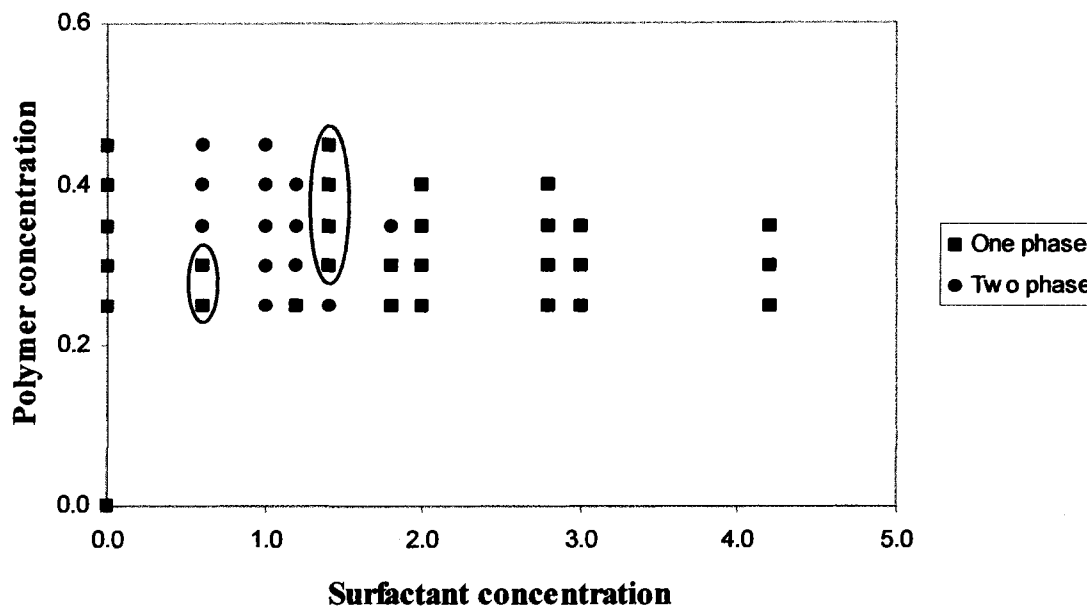


Figure 4A-3. Reproducibility in visual observation of phase separation analysis (LR400-SLES).

In Figure 4A-3 an original run and a repeat run are represented. Squares represent one phase regions and circles represent two phase regions in each run and points where one and two phase regions overlapped are circled. The reproducibility graph indicates that problems with repeatability existed using this method, but that the differences occurred in regions of transition from one to two phases might be expected because small changes in sample composition and/or environment could cause the system to traverse the phase boundary. This is discussed in more detail in Chapter IV-B.

Turbidity measurements are commonly utilized to detect coacervate formation and quantify coacervate amount in the dilute regime^{14, 16, 19, 20, 79, 119} so a high-throughput transmittance measurement was explored. In this method, 96-well plates are loaded into the Tecan Safire high-throughput UV-Visible spectrophotometric reader where a beam originates above the plate, passes through the sample, and exits through the bottom of the

well to a detector on the bottom of the reader. The amount of light transmitted is recorded and converted into an output reading of absorbance units.

Sample preparation on the liquid handler employed 96-well plates, which are compatible with the Tecan Safire UV-Visible spectrophotometer. The 96-well plates also have the advantage of mixing through a 96-well plate attachment on a Vortex Genie 2 (30 s per plate). The 96-well plates consist of 500 μL glass flat bottom well inserted into plastic plates with a slit along the bottom of each row of the plate so that the beam can pass through the well without interference from the plate. To determine whether normalization of each absorbance reading was necessary to account for solvent (water) and glass well absorbance, a study was performed with blank wells and wells containing only DI water at varying total volumes (Table 4A-III).

Table 4A-III. Absorbance readings of background components at 410 nm, 25 °C.

Background Component	Average Absorbance	Standard Deviation
glass wells	0.029	0.0050
150 μL DI water	0.068	0.015
300 μL DI water	0.040	0.0079

As will be discussed later, absorbance readings of 0.04 absorbance units are considered one phase systems so background readings of the glass wells (0.029 a.u.) and solvent (0.040 a.u.) are negligible with respect to characterization of polymer-surfactant interaction. Therefore, background normalizations were not performed.

In sample preparation with the liquid handler, the total volume of each sample was considered because the pathlength of each “cell” is dictated by the total sample volume. In order to compare absorbance reading between systems, the pathlength needed

to be held constant, as dictated by Beer's Law (Equation 4A-3), where A is absorbance, ϵ is molar absorptivity, b is pathlength, and c is concentration.

$$A = \epsilon bc \quad \text{Equation 4A-3.}$$

Pathlength effects were controlled by use of a constant sample volume (300 μL).

Absorbance scans were performed for each polymer-surfactant system to determine the appropriate wavelength for absorbance readings. A sample set from 96-well plates with different polymer-surfactant systems was chosen, consisting of 12-24 wells that visually exhibited high, medium, or no coacervation. These three levels of phase separation were investigated with a wavelength scan from 230-1000 nm to ensure that single phase systems were not exhibiting absorbance at the chosen wavelength and also to ensure that higher absorbance readings were obtained for high phase separation systems than medium phase separation systems. An example of three wavelength scans with these different separation amounts for a cationic polysaccharide-surfactant system is shown in Figure 4A-4.

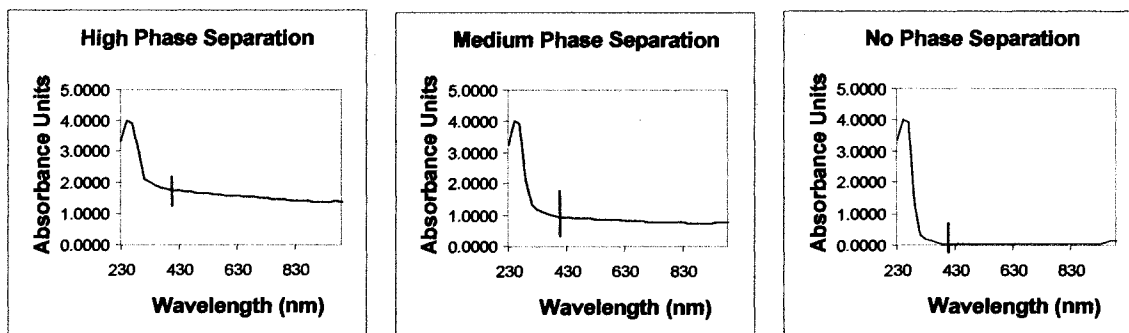


Figure 4A-4. Absorbance scans of cationic polysaccharide-surfactant samples.

An example of three wavelength scans with different separation amounts for a poly(vinylpyridinium hydrochloride)-surfactant system is shown in Figure 4A-5.

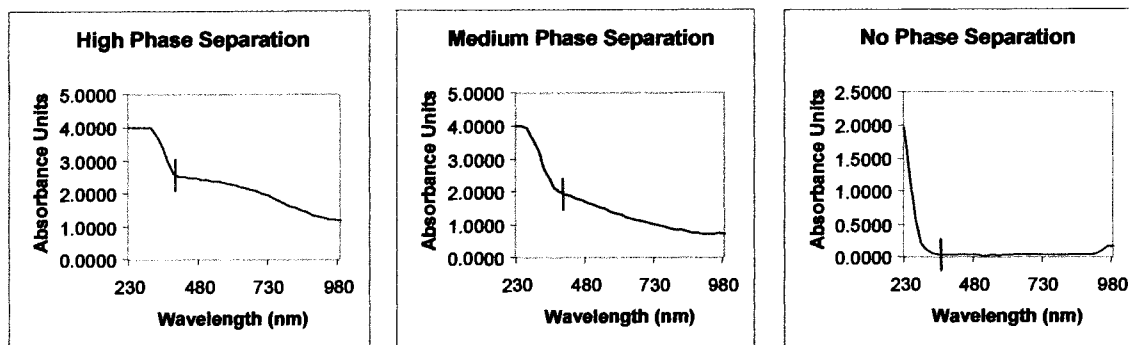


Figure 4A-5. Absorbance scans of poly(vinylpyridinium hydrochloride)-surfactant samples.

The most appropriate wavelength was chosen at a point on the curve with a low slope to avoid irreproducibility from sample to sample. Also, the known amounts of coacervation were taken into account, as described above. For both polymer systems, a low slope in all curves, as well as a higher absorbance reading for the high phase separation system versus the medium phase separation system, was observed at 410 nm, and the single phase system showed no absorbance at 410 nm. This wavelength was used for all subsequent UV-Visible spectrophotometric analyses.

Data Representation

Traditional methods of data representation focus primarily on ternary phase diagrams.^{7, 17} The phase boundaries in these diagrams can be accurately measured by separating the phases and precisely determining the composition of each phase. Each sample analyzed results in two (or three) points of a boundary in the phase diagram. Repeated analysis of many different phase-separated samples eventually produces enough points to define the phase boundaries by a “connect the dots” approach. This method is accurate, but laborious and too slow to offer practical, real-time guidance to investigators, especially as more components are added and the systems become more

complex.¹²⁰⁻¹²³ To expedite the process, investigators often characterize a limited number of samples and “guesstimate” the positions of the phase boundaries on the diagram.^{17, 20,}
¹¹⁷ This often leads to restricted diagrams with insufficient investigated points to clearly define the positions of the phase boundaries.^{6, 17} For example, Svensson and coworkers have investigated the interactions of polymer and surfactant in a water continuous phase using conventional techniques for ternary phase diagram generation.¹⁷ Their published ternary phase diagram is shown in Figure 4A-6.

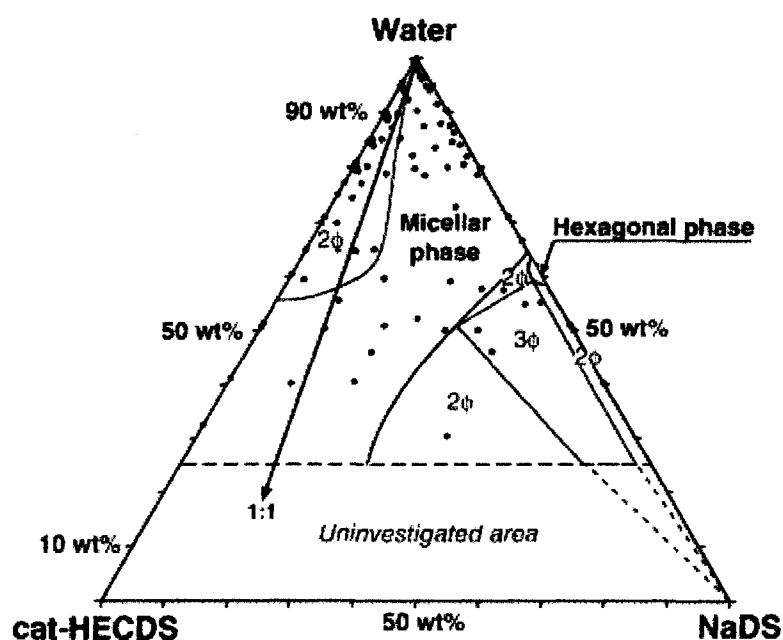


Figure 4A-6. Traditional ternary phase diagram for representation of polymer-surfactant interactions.¹⁷

To generate this traditional phase diagram, samples were prepared and stored for a number of weeks before analysis, attempting to reach thermodynamic equilibrium. The number of phases present was determined visually for all compositions, and the structures

were identified sample by sample, using small-angle X-ray diffraction.¹⁷ Because of these labor-intensive methods, development of a single phase diagram is tremendously time consuming. In addition, a small number of points are actually investigated which can mask elucidation of trends and could lead to theoretical misunderstanding based on artifacts. Also, with only a few data points and laborious phase diagram generation, it is difficult to develop a holistic understanding as a function of property variation and therefore difficult to truly gain a “big picture” understanding of how the polymer and surfactant are interacting.

The high-throughput screening methods that were developed in this research offer the opportunity to rapidly generate and characterize a sufficient number of samples to definitively show the location of the phases and their boundaries in a phase diagram. Therefore, we have the advantage of constructing phase diagrams with more detail and better accuracy than the “guesstimate” approach. However, we do not chemically analyze the samples and, as a consequence, our current methods do not lend themselves to the determination of tie lines or precise chemical compositions of points on the phase boundaries. With these advantages and limitations in mind, it became clear that we would have to devise a new way to represent our pseudo-phase diagrams in a manner that:

- emphasized the detailed accuracy for the position of phase boundaries and semi-quantitative accuracy with respect to the amount of the separated phase (coacervate)

- distinguished our results from those of the extremely accurate traditional methods by clearly illustrating that our diagrams did not contain tie lines or information on chemical composition of the phases
- could be adapted to image analysis to enable comparisons between different pseudo-phase diagrams. This aspect considers a future in which an enormous number of pseudo-phase diagrams would be available for comparison, and mining of the data by computer would be preferable to human visual scrutiny

In simple polymer-surfactant interaction studies there are only three components (polymer, surfactant, and water) and their phase behavior can be presented using either binary or ternary phase diagrams. Conventionally, phase diagrams for oppositely-charged polyelectrolyte and ionic surfactants have been depicted as binary phase diagrams^{6, 7}, and in this work we continued this tradition.

The first iteration of binary phase diagrams was presented in Figure 4A-2. Utilizing color-coding, areas of low, medium, and high phase separation were clearly delineated. However, as discussed, there were areas of overlapping points so the new data representation method must be capable of indicating areas of overlap in addition to distinguishing between areas of no, low, medium and high phase separation. With the implementation of quantitative coacervate amount analysis using the UV-Visible spectrophotometer, the new data representation method was required to allow straightforward visualization of compositions exhibiting distinct coacervate amounts.

The software program DPlot was used to create binary phase diagrams with components plotted as a function of absorbance: surfactant (x-axis), polymer (y-axis),

absorbance units (z-axis, color gradient). Each point on the graph contains a discrete concentration of surfactant and a discrete concentration of polymer. It is understood that water makes up the balance of the composition to 100 % (w/v). A sample diagram showing the discrete compositions that were investigated is shown in Figure 4A-7.

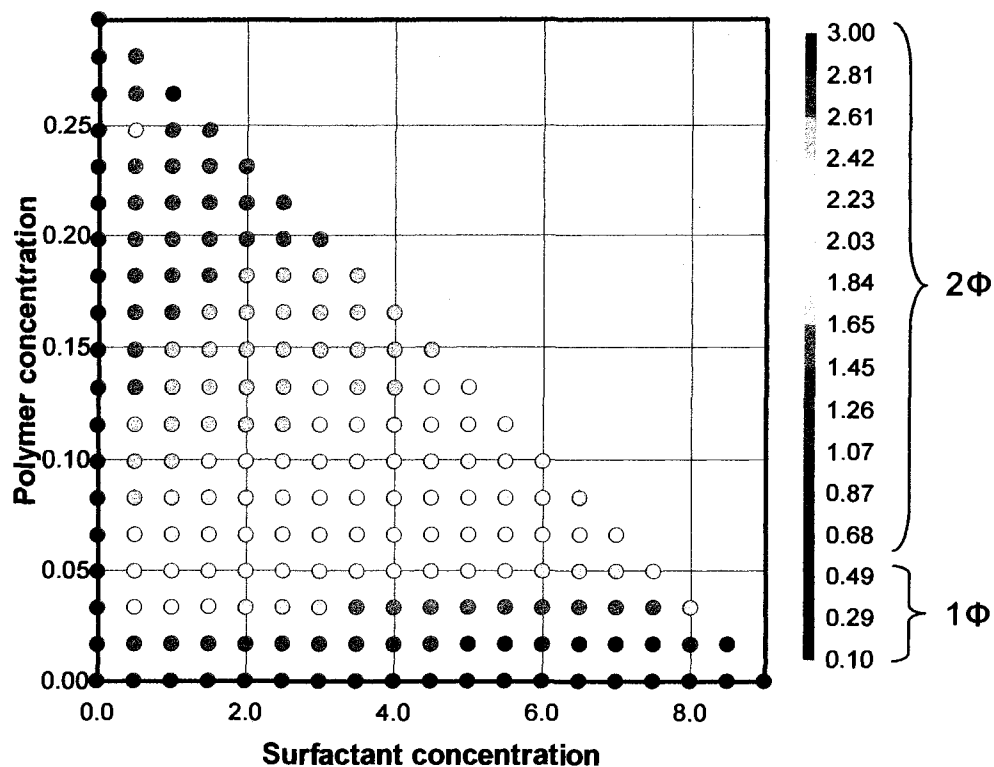


Figure 4-7. Discrete data points prepared and analyzed using high-throughput screening methods.

A “connect the dots” approach could be applied to this binary diagram, as is traditionally done. Typically, designations of one or two phase regions are made (Figure 4A-6); however the high-throughput screening analysis method has the added advantage of quantitatively determining coacervate amount, and by using a contour function these regions can be clearly delineated (Figure 4A-8).

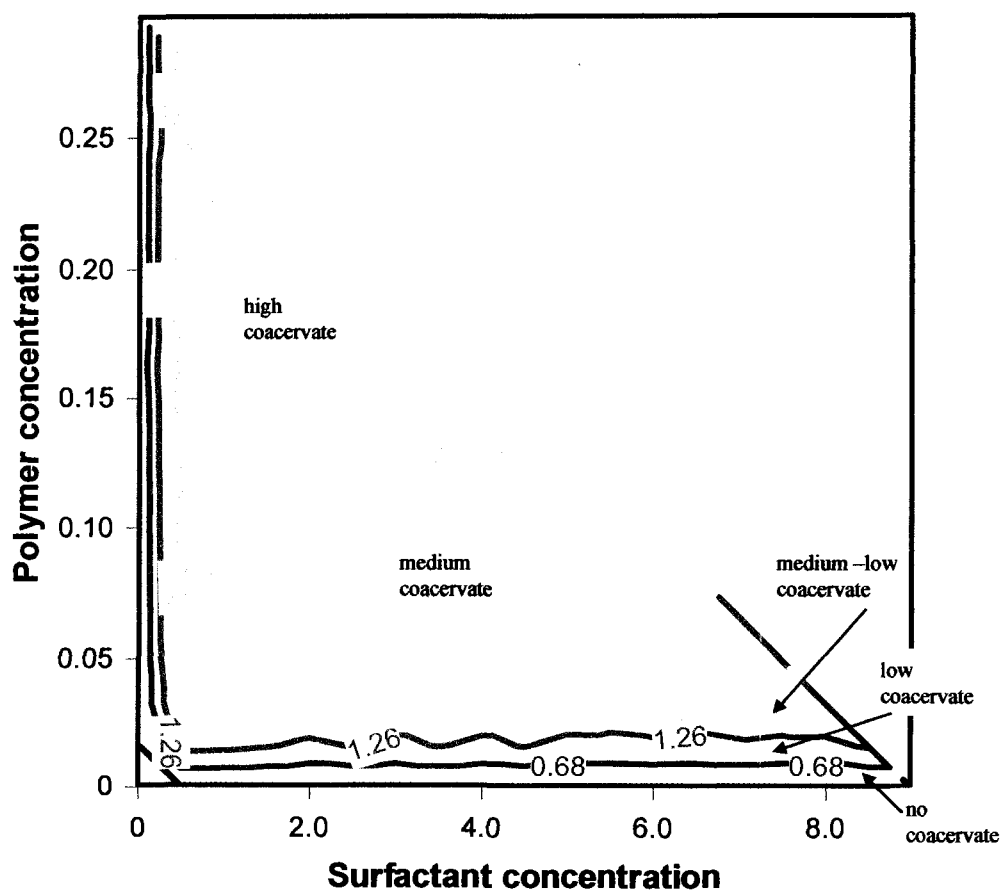


Figure 4A-8. One and two phase regions and relative coacervate amounts based on discrete data points.

The mapping of regions of phase separation and the relative amount of coacervate in each region (Figure 4A-8) provided a phase diagram with more distinct boundaries than traditional diagrams due to analysis via UV-Visible spectrophotometry. Although this type of diagram is related to traditional phase diagrams, it was also desirable to develop a phase diagram format in which phase separation patterns could be quickly recognized and visually compared. This is necessary to rapidly analyze the large amounts of data that can be generated using high-throughput screening methodologies.

A color gradient offers a way to depict and visualize coacervate amounts that emphasizes the accuracy of the high-throughput screening methods, but also distinguishes our diagrams from those of extremely accurate traditional methods. This was accomplished by converting the discrete data points (Figure 4A-7) into a 2-dimensional surface plot where the absorbance unit data along the z-axis was represented by a color gradient, similar to a topographic contour map. In this color gradient, blue areas indicate one phase systems (i.e., no visible coacervate formation). The gradient represents an increase in coacervate amount up to the red areas, which represent the highest amount of coacervate formed for the class of polymers under investigation. Intermediate values are shown by intermediate colors in the spectrum, viz green, yellow, and orange in that order. An example of this data representation is shown in Figure 4A-9. The description of the color gradient in terms of coacervate amount is also provided in Figure 4A-9.

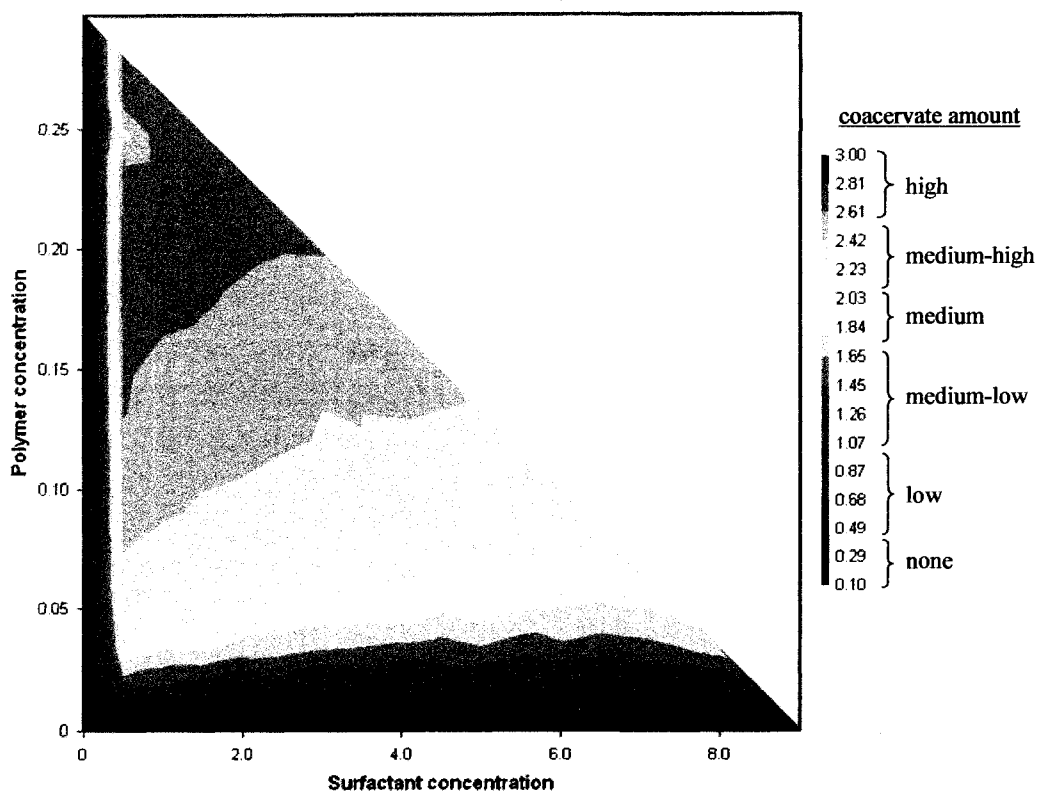


Figure 4A-9. Binary contour phase diagram showing quantitative phase separation. Data obtained with the Tecan Safire UV-Visible spectrophotometer is represented by a color gradient.

A brief discussion of the method through which DPlot software generates the contour phase diagram is necessary. When data is entered as input into the DPlot program the points exist as the corners of a triangle grid design and through a mesh procedure, the software averages the z-axis values at the three corners of the triangle creating the color contour diagram from these meshes (Figure 4A-10).

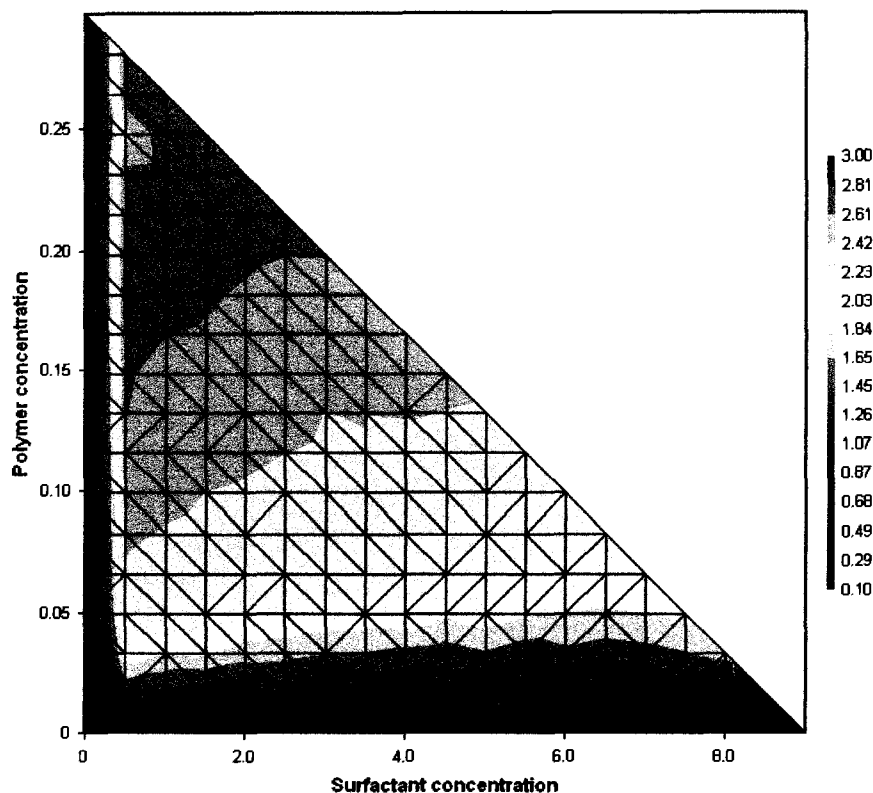


Figure 4A-10. Triangle mesh utilized by the DPlot software program to create the gradients between neighboring points of different absorbance units.

This mesh is important because it can indicate a gradient phenomenon between points where in reality the gradient may not be as distinct. An example of this can be found along the y-axis in Figure 4A-10, where two points of the triangle (0.5, 0.28) and (0.5, 0.26) are high absorbance (red) and one point (0, 0.28) is low absorbance (blue).

However, recognition of this can actually increase the amount of learning that is gleaned from a phase diagram. In the situation described above, the gradient formed as a result of the mesh procedure shows that in the samples with no surfactant, one phase exists, however, with an increase of surfactant to 0.5 %, large amounts of coacervate are formed.

Thus polymer-surfactant interactions occurring below 0.5 % surfactant could be identified as systems to investigate in more detail.

Method Validation

Initial validation of the high-throughput screening method was performed by visual comparison of phase separation in samples prepared using the liquid handler to samples prepared using traditional methods.⁶ Validation of the high-throughput screening method was performed with JR400 and four sodium alkyl sulfates, C₈, C₁₀, C₁₂, and C₁₄. For discussion purposes, the JR400-SDS system was chosen to represent this validation work. The original diagram from the work of Goddard and Hannan is shown in Figure 4A-11.

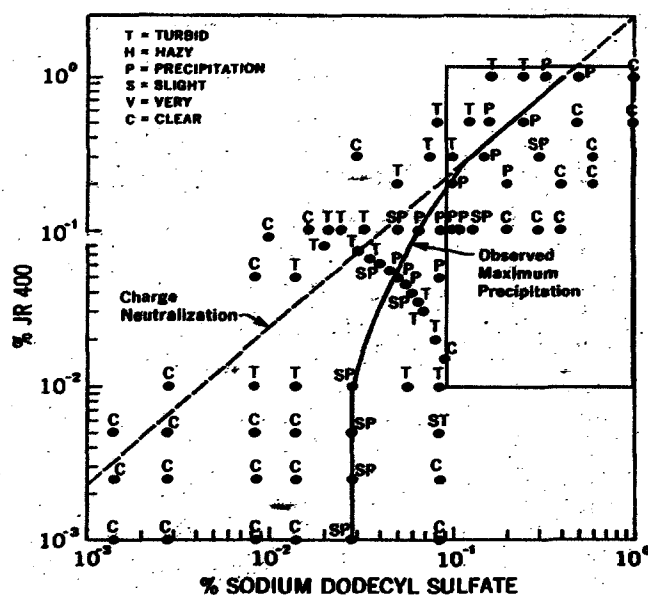


Figure 4A-11. Traditional JR400-SDS phase diagram.⁶

For comparison between the high-throughput screening data and the literature phase diagram (Figure 4A-11), the boxed region of Goddard and Hannan's phase diagram was

investigated. Given the subjectivity in phase separation terminology from the literature study (e.g. turbid vs. hazy)⁶ we have chosen to describe points as simply two phase or one phase. The observations from the literature and from high-throughput screening are summarized in Figure 4A-12.

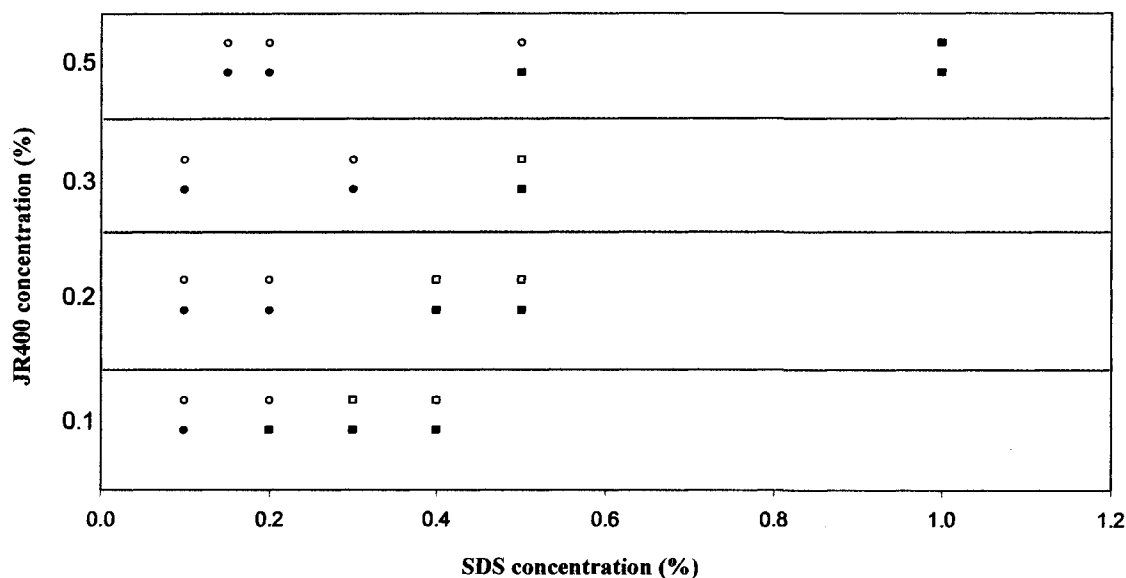


Figure 4A-12. Comparison of one phase (square) and two phase (circle) regions of literature (closed symbols) and high-throughput (open symbols) phase diagrams for validation of the high-throughput screening method.⁶

Of the points compared in Figure 4A-12 only two points did not show reproducibility between methods which can be expected given the subjectivity of the analysis. This good agreement with a classic phase diagram was validation that our sample preparation method was appropriate.

We found no literature reports for the use of UV-Visible spectrophotometry to quantitatively determine the presence and amount of coacervate. Therefore, the complete high-throughput screening method was validated against visual observation methods. Samples were prepared using the liquid handler and then analyzed via UV-Visible

spectrophotometry. After UV-Visible spectrophotometric analysis, visual observations were made and the amount of coacervate was estimated. The results for a representative cationic polysaccharide-surfactant system are shown in Figure 4A-13.

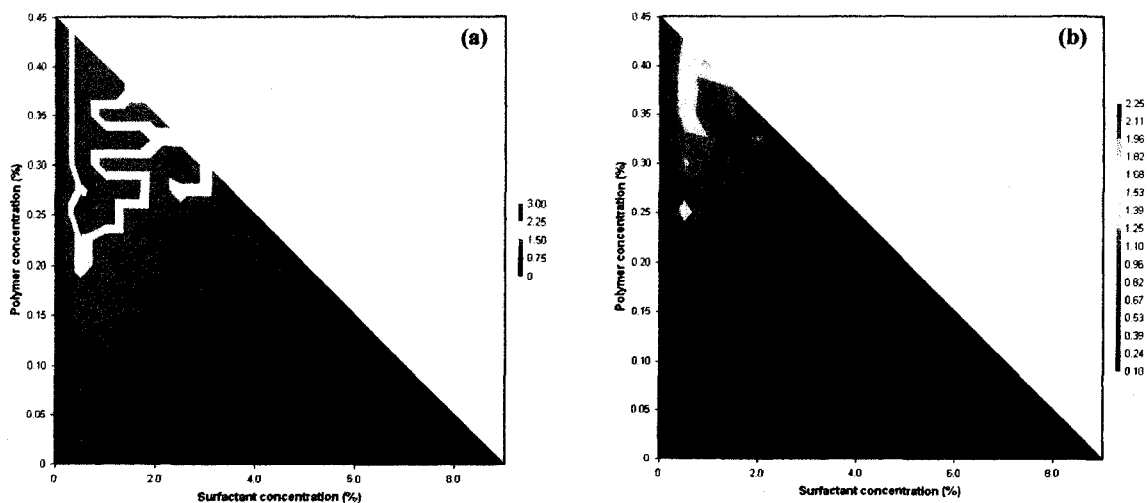


Figure 4A-13. Validation of the quantitative phase separation method with a cationic polysaccharide-surfactant system (JR30M-SLES): (a) visual observation and (b) spectrophotometric analysis.

Figure 4A-13 shows two views of the same cationic polysaccharide-anionic surfactant system. Coacervate amounts in Figure 4A-13a were determined using visual observation and ranked as high, medium, low, or no phase separation. Samples in Figure 4A-13b were analyzed using UV-Visible spectrophotometry, as previously described. In both plots the overall shape of the phase separation area is similar and the areas of high, medium, low and no coacervation are comparable. Additionally, the sensitivity of analysis with UV-Visible spectrophotometer is greater.

There were visible differences in the nature of the coacervate formed from different polymer systems, therefore validation of the quantitative analysis technique was also performed for synthetic cationic polymer-surfactant systems (Figure 4A-14).

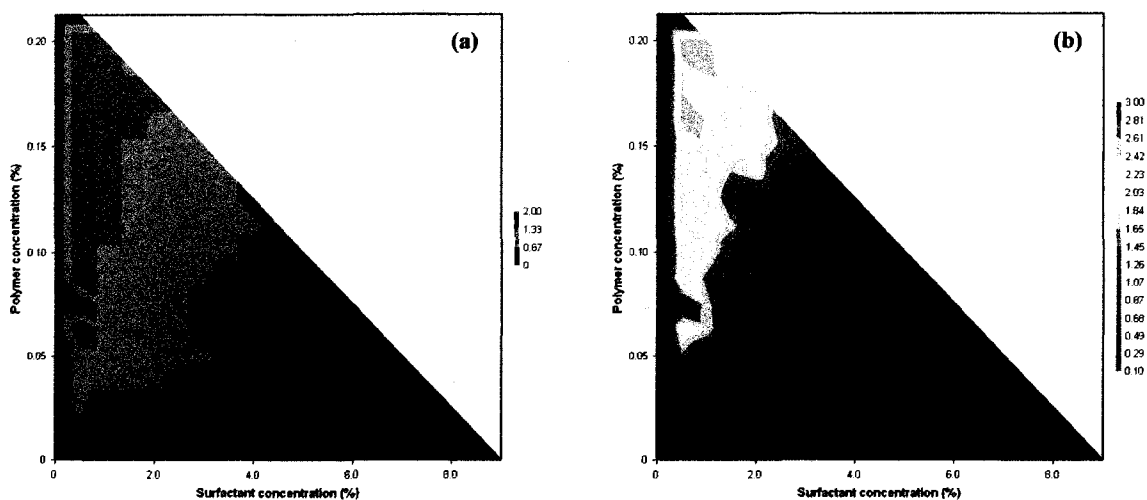


Figure 4A-14. Validation of the quantitative phase separation method with a cationic synthetic polymer-surfactant system (VBTAC-SLES): (a) visual observation and (b) spectrophotometric analysis.

The results in Figure 4A-14 further indicate the agreement between visual observation and quantitative analysis and the increased sensitivity and advantage of using the UV-Visible spectrophotometric method over conventional visual observation techniques for quantitative coacervate analysis.

Method Reproducibility

Reproducibility is an important consideration with high-throughput screening. With such high volume data generation it is imperative that the data produced is reproducible so that artifacts do not distort the results. Since this was a novel coacervate screening method, it was important to ascertain the reproducibility of these phase

diagrams. Reproducibility analyses were conducted for every system studied and the reproducibility was reported in color-coded diagrams that mirrored the coacervate amount phase diagrams. The compositional ranges of interest and the programs utilized for sample preparation evolved as the project proceeded and, as a result, the methods used for reproducibility determination with polysaccharides differed slightly from those used for poly(vinylpyridinium hydrochlorides).

Polysaccharides

For the polysaccharide systems, repeat compositions were incorporated into the same 96-well plate so that some compositions had two or more repetitions. For compositions with only two repetitions, the absolute value of the difference between the absorbance readings was calculated. For compositions having more than two repetitions the standard deviation of absorbance readings was determined. The results of these calculations were plotted as a function of the composition. The degree of difference between repetitions as a function of the total range of absorbance readings was presented via color coding, where all compositions in green were reproducible within 20 % of the absorbance range and all compositions in red varied more than 20 %. Typical reproducibility for the polysaccharide method is shown in Figure 4A-15, where Figure 4A-15a is the coacervate amount phase diagram and Figure 4A-15b is the corresponding reproducibility diagram.

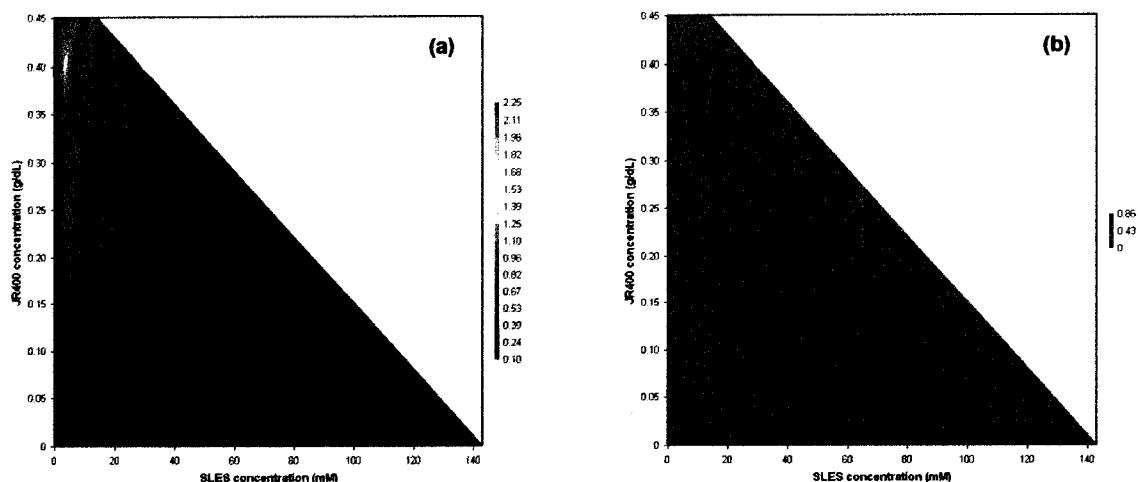


Figure 4A-15. Reproducibility of high-throughput screening methods for a cationic polysaccharide-surfactant system (JR400-SLES).

Poly(vinylpyridinium hydrochlorides)

For the poly(vinylpyridinium hydrochloride) systems, repeat compositions were not incorporated into the same 96-well plate, but a complete duplicate experiment was performed so that all compositions have two repetitions. For all compositions the absolute value of the difference between the two absorbance readings was calculated and the results of this calculation were plotted as a function of the composition. Data representation was performed in the manner described above. Typical reproducibility for this method is shown in Figure 4A-16.

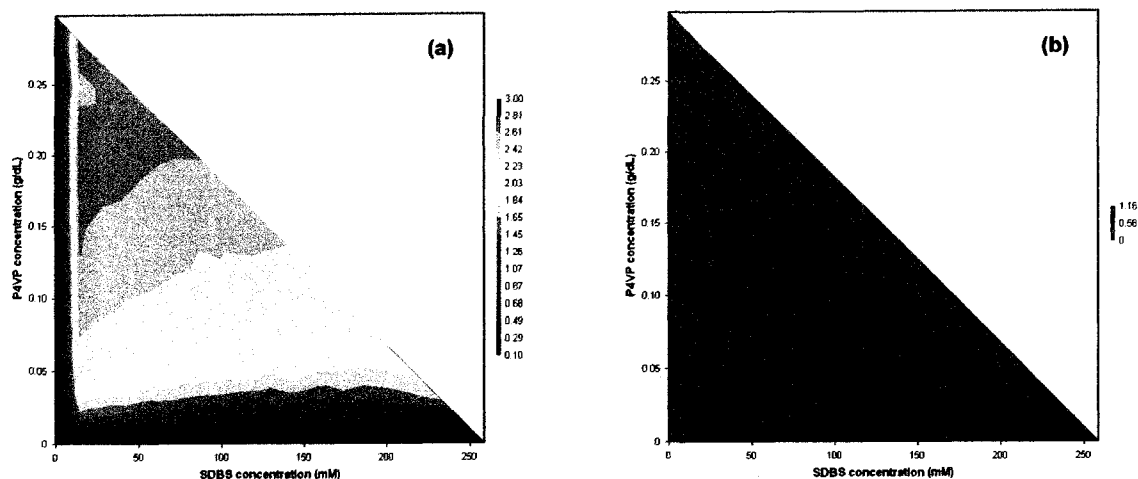


Figure 4A-16. Reproducibility of high-throughput screening methods for a synthetic cationic polymer-surfactant system (P4VP-SDBS).

For screening purposes, we accepted that reproducibility within 20 % was adequate to quantify the coacervate phase behavior across the composition diagram, and almost all of the systems showed good reproducibility at this level.¹²⁴

In summary, a high-throughput screening method capable of rapid and repeatable sample preparation, analysis and data representation has been developed. Using a liquid handling system for sample preparation we are able to produce ~400 samples in 60 minutes, including a complete repeat set of data to ensure reproducibility. Those 400 samples are analyzed rapidly using a high-throughput UV-Visible spectrophotometer to determine a quantitative amount of phase separation. The data is represented using contour mapping on a binary phase diagram which presents the results in a manner that is easily interpreted and understood, where trends can be rapidly discerned as a function of sample composition and as a function of polymer or surfactant properties by comparing and contrasting individual contour phase diagrams.

CHAPTER IV-B

INVESTIGATION OF CATIONIC HYDROXYETHYLCELLULOSE – ANIONIC SURFACTANT INTERACTIONS

Coacervate Physical Description

The separated phase observed with polymer-surfactant systems of opposite charge is commonly referred to as a complex coacervate, which is rich in polymer and surfactant and contains some water. For cationic polysaccharide-anionic surfactant systems, visual observation of this separated phase showed it to be a gel-like coagulum. Photographic images of representative samples are shown in Figure 4B-1.

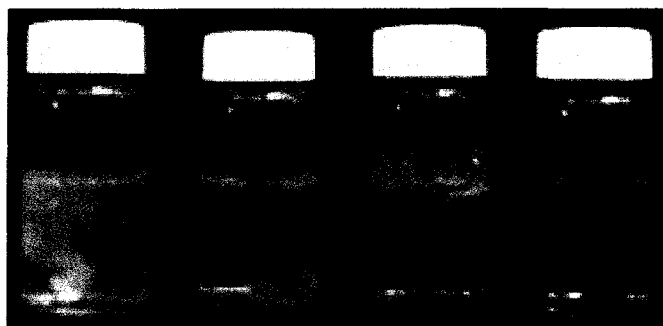


Figure 4B-1. Photographic images of coacervate formed in cationic polysaccharide-anionic surfactant mixed systems at different compositions. Coacervate amount decreased from left to right, with no coacervate present at far right.

The first two samples in Figure 4B-1 were formed using the JR30M-SLES system and the last two samples were formed using the JR400-SLES system. It was apparent from visual observation that the macroscopic coacervate properties were similar across these systems.

Correlation with Traditional Systems

Interaction of oppositely-charged polymer and surfactant has been extensively studied in the dilute surfactant regime, and a general mechanism of coacervate formation has been demonstrated by Goddard and others.^{7, 8, 18} Polymer-surfactant complexes are formed only above a critical concentration of surfactant, called the critical aggregation concentration (CAC). Above this concentration, according to Goddard, site-specific interactions occur between anionic surfactant molecules and cationic sites along the polymer backbone. As surfactant concentration increases, additional interactions occur until a concentration is reached where the polymer-surfactant complex (coacervate) phase separates from the aqueous solution. Further increase in surfactant concentration to the vicinity of the critical micelle concentration (CMC) of the system can result in solubilization of the coacervate, to produce a macroscopically single-phase system. At a 1:1 charge equivalence ratio of surfactant and polyelectrolyte, maximum phase separation usually occurs, and this phase separation can persist at all surfactant concentrations for this charge ratio, as was demonstrated by Goddard and Hannan (Figure 4B-2)^{6, 7}

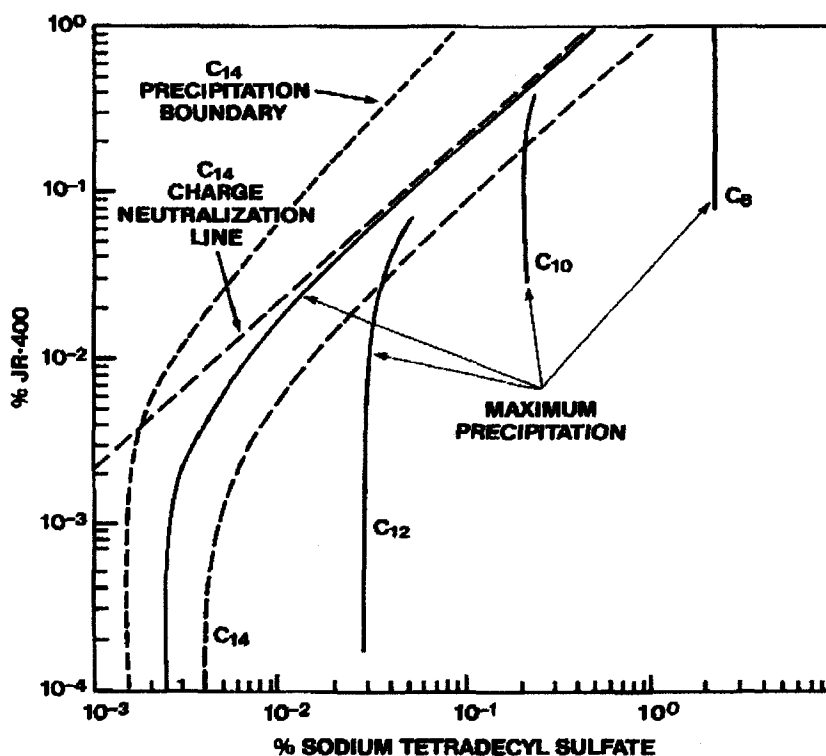


Figure 4B-2. Solubility diagram of JR400 with sodium alkyl sulfates. Maximum precipitation lines are also shown for sodium alkyl sulfates with C₈, C₁₀, and C₁₂ chain lengths.⁷

Goddard and Hannan also observed phase separation proximal to the 1:1 charge equivalence lines, designated in Figure 4B-2 as the precipitation boundary.^{6,7} When the polymer fraction was lowered below a certain concentration, maximum precipitation was no longer observed along the 1:1 charge equivalence line, and instead the phase boundary extended over a much broader range of polymer concentrations below the 1:1 charge ratio. With JR400 and sodium dodecyl sulfate (SDS), the polymer concentration below which 1:1 charge equivalence effects terminated was ~ 0.07 g/dL and the constant surfactant concentration where this occurred was ~ 0.70 mM.⁶ For reference, the CMC of pure SDS is 8.3 mM.^{105, 106}

JR400 was also investigated in our research, however the primary anionic surfactant studied was sodium lauryl ether sulfate (SLES), as opposed to the more commonly investigated sodium dodecyl sulfate (SDS). SLES is better suited to these studies than SDS because many of the techniques used require solutions that remain in liquid-form at room temperature. The Krafft point of SDS is $38\text{ }^{\circ}\text{C}$ ¹⁰⁶, which is higher than room temperature. Thus, SDS has the potential to separate into crystalline phases during sample preparation and analysis, which could lead to confusing results. The Krafft point of SLES is $< 0\text{ }^{\circ}\text{C}$ ¹²⁵ so phase separation at room temperature is not problematic. In addition, SLES is often the primary surfactant used in commercial cleansing formulations.

The long alkyl chain of SLES was expected to promote hydrophobic interactions between bound surfactant molecules, in a manner similar to proposed models with SDS, causing coacervate formation.⁷ The contour phase diagram for the JR400-SLES system generated using our high-throughput screening method is shown in Figure 4B-3.

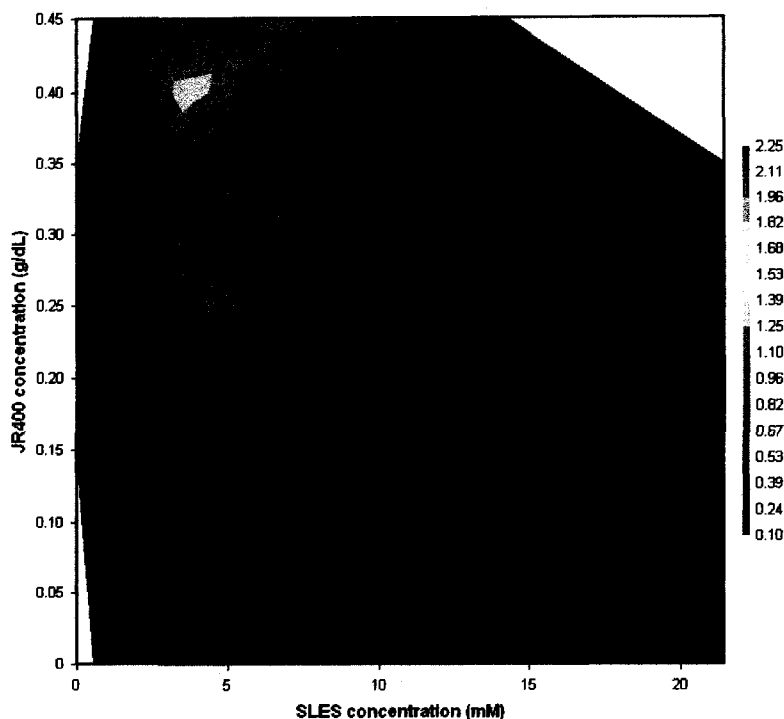


Figure 4B-3. Contour phase diagram of JR400 with SLES below 24 mM SLES. The 1:1 charge ratio is designated by the solid red line.

Examining the compositional range that was investigated for JR400-SDS by Goddard and Hannan (Figure 4B-2), we observed that phase separation in the JR400-SLES system, generated using high-throughput screening, was consistent with the SDS system investigated using traditional techniques. For JR400-SLES, maximum coacervation occurred near the 1:1 stoichiometric ratio, which is in agreement with the region of maximum coacervation in Goddard's phase diagram. Also in agreement with Goddard's phase diagram was the deviation of maximum coacervate formation from the 1:1 stoichiometric ratio at a certain polymer concentration. For the JR400-SLES system, this deviation occurred at ~ 0.2 g/dL JR400 and coacervation was observed over a range of JR400 concentrations extending below 0.2 g/dL, and at a constant surfactant

concentration of 4.8 mM SLES. For reference, the CMC of SLES was determined to be 3.0 mM (*vide infra*).

JR30M was also investigated with SLES. JR30M has the same charge substitution (CS) as JR400 but has a greater molecular weight (measured as 1 500 000 g/mol and 500 000 g/mol, respectively). The contour phase diagram for the JR30M-SLES system investigated over the compositional range studied by Goddard and Hannan is shown in Figure 4B-4.

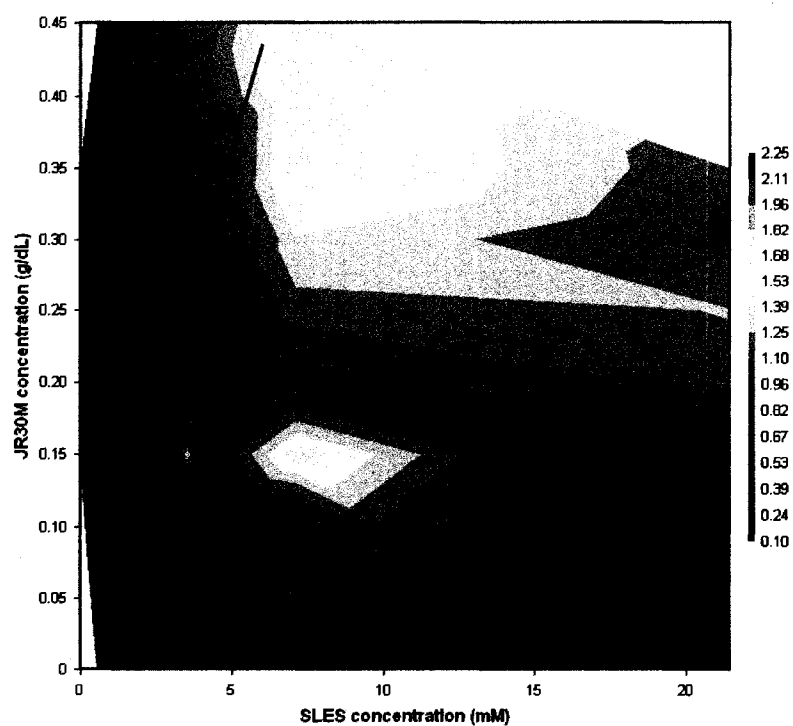


Figure 4B-4. Contour phase diagram of JR30M with SLES below 24 mM SLES. The 1:1 charge ratio is designated by the solid red line.

The most noticeable aspect of this phase diagram is the increased range of compositions exhibiting phase separation with the higher molecular weight polymer. The JR30M-

SLES system exhibited maximum phase separation near the 1:1 stoichiometric ratio. Deviation of maximum separation from the 1:1 stoichiometric ratio occurred in this system at ~ 0.25 g/dL JR30M. Below 0.25 g/dL JR30M, coacervation occurred at a constant surfactant concentration range, between 4.8 and 19 mM SLES. These properties are in agreement with the trends of coacervation observed in Goddard's phase diagram and the JR400-SLES phase diagram, but the compositional range of coacervate formation is much broader.

Effect of Polymer Molecular Weight

Phase Diagrams

Although both the JR400-SLES and JR30M-SLES systems exhibited coacervate formation in agreement with Goddard's systems, the amount of coacervate formed and the compositions at which it formed were markedly different for the different systems. The amount of coacervate produced with JR30M was much greater and occurred over a much wider compositional range than that of JR400. Using the high-throughput screening technique, these systems were explored at higher surfactant concentrations. The contour phase diagram and the corresponding reproducibility diagram for the JR400-SLES system and the JR30M-SLES system are shown in Figure 4B-5.

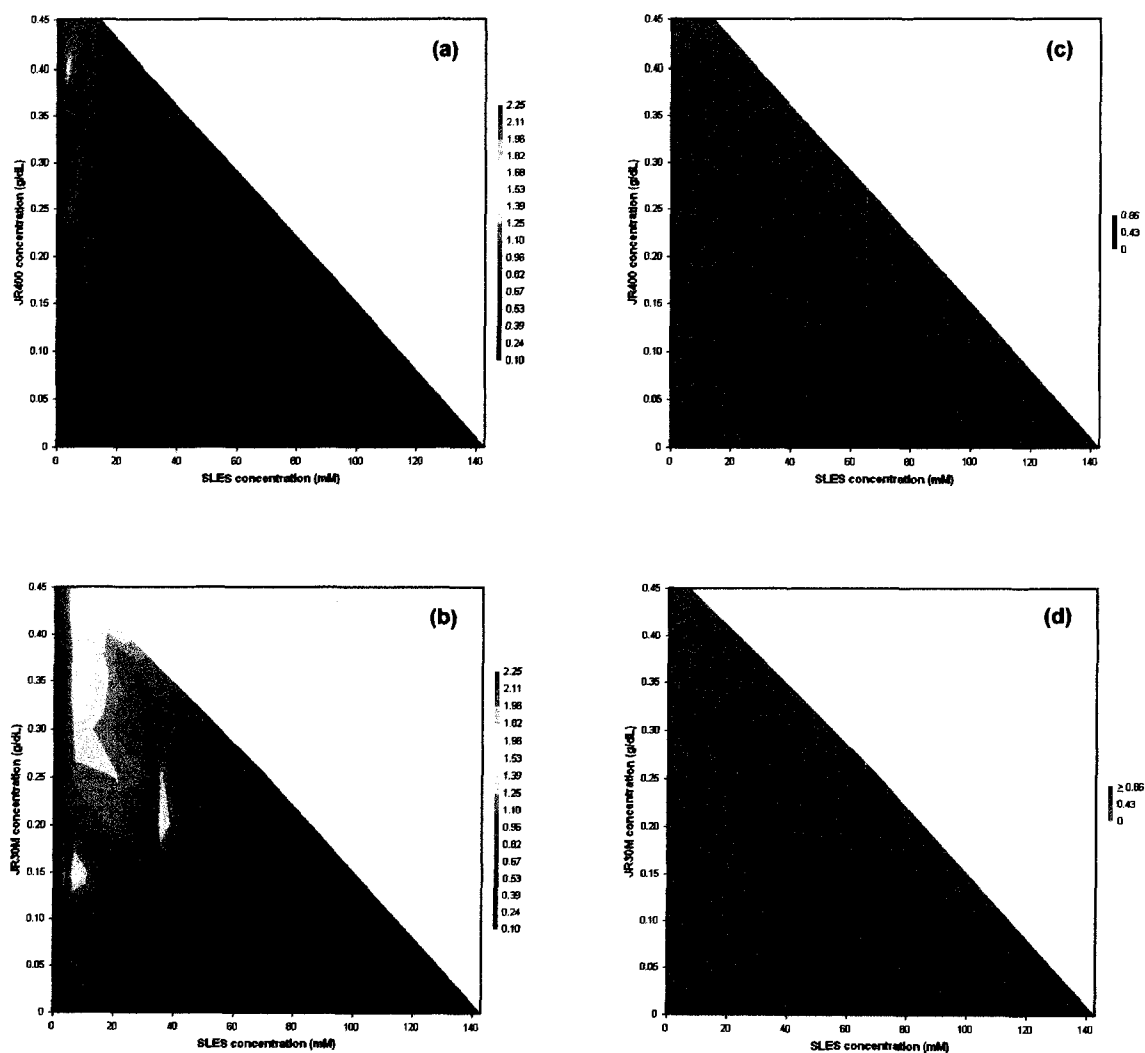


Figure 4B-5. Contour phase diagrams for (a) JR400 with SLES and (b) JR30M with SLES. Reproducibility diagrams for (c) JR400 with SLES and (d) JR30M with SLES.

The reproducibility phase diagrams for both polymer-surfactant systems indicate compositions where the presence of a one or two-phase system was not repeatable. Much of the irreproducibility was found in compositional regions between one and two phase systems. For instance, in the JR30M-SLES system, two-phase systems were consistently present at high polymer concentration and one-phase systems were consistently present at low polymer concentration. At intermediate polymer concentrations, between 0.05–0.3

g/dL polymer, irreproducibility was observed. It is reasonable to attribute this lack of reproducibility to entrapment within the spinodal region, which is a fundamental consideration in polymer solubility.

The concept of spinodal entrapment can be understood by considering the free energy of mixing (ΔG_{mix}) as a function of polymer composition. The thermodynamics of polymer solubility are classically described by the Flory-Huggins equation^{51, 126}

$$\frac{\Delta G_{mix}}{RT} = n_1 \ln \phi_1 + n_2 \ln \phi_2 + \chi n_1 \phi_2 \quad \text{Equation 4B-1.}$$

where n_1 is the mole fraction of solvent, ϕ_1 is the volume fraction of solvent, n_2 is the mole fraction of polymer, ϕ_2 is the volume fraction of polymer, and χ is the Flory-Huggins interaction parameter. The first two terms on the right-hand side describe the combinatorial entropy of mixing, and this will always be favorable to molecular mixing of the polymer and the solvent. In the original conceptual thinking of Flory-Huggins theory, the third term arises only from the enthalpy of mixing, and the polymer and solvent are completely miscible over the entire composition range if^{51, 126-128}

$$\chi < 0.5 \left(1 + (V_2/V_1)^{-1/2} \right)^2$$

where V_1 is the molar volume of the solvent and V_2 is the molar volume of the polymer. This equation predicts that the solubility of a polymer will decrease with an increase in the molar volume of the polymer, and hence its molecular weight, and that a polymer and solvent should be completely miscible if the value of the Flory-Huggins interaction parameter, χ , is less than 0.5.

The simple Flory-Huggins theory has several drawbacks which limit its applicability to systems of polyelectrolyte and oppositely charged surfactant, including

the variation of χ with concentration and temperature, the complications in extending χ to multicomponent systems, and the necessity for modification of χ to include terms for molecular orientation and specific binding such as interactions between oppositely charged ions.¹²⁷ However, the consideration of ΔG_{mix} can assist us in broad conceptual understanding of the phase behavior in our polymer-surfactant systems.

A one-phase homogeneous polymer solution occurs when

$$\frac{\partial^2 \Delta G_{mix}^m}{\partial \phi_2^2} > 0$$

for all compositions between two polymer volume fractions ϕ_2^α and ϕ_2^β . For example, in Figure 4B-6 a one phase system is present at all compositions below the curve, or all polymer volume fractions.

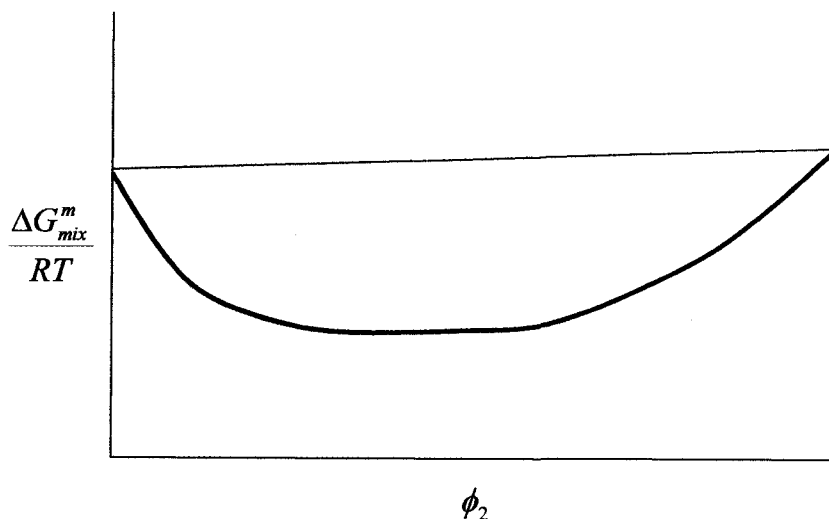


Figure 4B-6. Molar free energy of mixing as a function of polymer concentration for a miscible system.

In this system, the energetics of miscibility are more favorable than the energetics of phase separation so miscibility occurs for all compositions.

In a system where phase separation occurs over some compositional range the free energy curve exhibits multiple minima (Figure 4B-7).

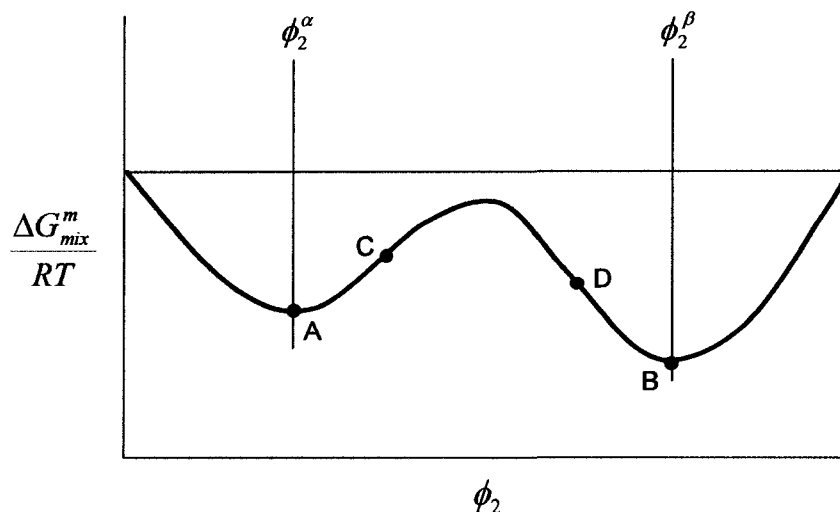


Figure 4B-7. Molar free energy of mixing as a function of polymer concentration for a phase-separated system.

In the regions to the left of point A and right of point B

$$\frac{\partial^2 \Delta G_{mix}^m}{\partial \phi_2^2} > 0$$

so a one-phase homogeneous system exists, as described above. Between points C and D

$$\frac{\partial^2 \Delta G_{mix}^m}{\partial \phi_2^2} < 0$$

and a phase separated condition is more energetically favored. The two separate phases in this region do not mix and thus one phase grows at the expense of the other. The points where the slope is changing from positive to negative, the inflection points, are observed when

$$\frac{\partial^2 \Delta G_{mix}^m}{\partial \phi_2^2} = 0$$

and are represented by points C and D. These inflection points are called spinodals and the regions between the spinodals and the free energy minima (regions A→C and B→D) are metastable regions known as spinodal regions. According to Fick's second law, the diffusion of a polymer into solution is described by

$$D = \phi_2 M_2 \left(\frac{\partial \mu_2}{\partial \phi_2} \right)_{T,P} \quad \text{Equation 4B-2.}$$

where D is the diffusion coefficient of the polymer, M_2 is the polymer mobility, and

μ_2 is the chemical potential of the polymer. Fick's second law states that D is

proportional to $\frac{\partial \mu_2}{\partial \phi_2}$ and since, at the inflection point the second derivative goes through

a maximum turning point,

$$\frac{\partial \mu_2}{\partial \phi_2} = \frac{\partial^2 \Delta G_{mix}^m}{\partial \phi_2^2} = 0$$

That is, at the spinodals $D = 0$. In the region between the spinodals (between points C and D), diffusion-driven phase separation is favored and spontaneous separation into two phases usually occurs. In the metastable spinodal regions, between the free energy minima and the spinodal, the molecules have to diffuse 'uphill' against the chemical potential and phase separation is thermodynamically disfavored.

Entrapment within a spinodal region is especially pertinent to systems exhibiting complex coacervation between oppositely-charged polymer and surfactant. Slow diffusion is expected for the polymer and surfactant in a spinodally-entrapped gel due to the surfactant's capability of hydrophobic self-assembly which would be expected to

slow the diffusional motion of the relatively stiff polymer. This “gelation” would be expected to trap the system in a pseudo-equilibrium state for an indeterminate time depending upon random diffusional fluctuations. Thus, irreproducibility of phase separation would be expected adjacent to the two-phase region and that was what was observed in our phase diagrams for JR400-SLES and JR30M-SLES. The points occurring in the spinodal region (represented in red in Figure 4B-5c-d) were, therefore, not considered as representative of thermodynamically equilibrated biphasic regions in the contour phase diagrams.

In the JR400-SLES contour phase diagram (Figure 4B-5a), it was observed that maximum coacervate formation occurred below 24 mM SLES and above 0.2 g/dL JR400; in the JR30M-SLES contour phase diagram (Figure 4B-5b), maximum coacervate formation was observed below 48 mM SLES and above 0.1 g/dL JR30M and the compositional range of coacervate formation persisted into much more concentrated surfactant regimes. The CS of both polymers is the same and therefore this effect must be due to the higher polymer molecular weight of JR30M.

Critical Overlap Concentration

Chronakis and Alexandridis investigated the coacervation mechanism of JR400 and JR30M with different anionic surfactants and proposed that chain entanglements and crosslink points formed through bound aggregates were important to coacervate formation for the high molecular weight JR30M polymer.³ These studies, performed in the dilute surfactant regime, indicate that polymer entanglement could be an important factor in coacervate formation. In order to probe the importance of chain entanglement in our systems, the c^* was determined for the series of cationic HECs presented in Chapter

III. A summary of the polymer molecular weights and charge substitutions for this PQ-10 series is shown in Table 4B-I.

Table 4B-I. PQ-10 series properties.⁹³

Polymer	M_w (10^3 g/mol)	M_w/M_n	% Nitrogen	CS
LR400	400	5.2	0.95	0.25
JR125	350	5.8	1.85	0.48
JR400	500	5.5	1.85	0.48
JR30M	1500	2.3	1.85	0.48
LR30M	1300	2.0	0.95	0.25

As described in Chapter III, the polymer specific viscosity (η_{sp}) in salt-free solution was plotted as a function of polymer concentration on a log-log scale. The linear regions of the dilute and semi-dilute regimes were fit to the power law equation given in Equation 4B-3, where A is the pre-exponential factor, c is polymer concentration, and b is the scaling exponent.

$$\eta_{sp} = A \cdot c^b \quad \text{Equation 4B-3.}$$

Critical overlap concentration is given by the intersection of the two lines from the dilute and semi-dilute regimes and was calculated using Equation 3-4. The plot of η_{sp} versus concentration for the high molecular weight polymers JR30M and LR30M is shown in Figure 4B-8.

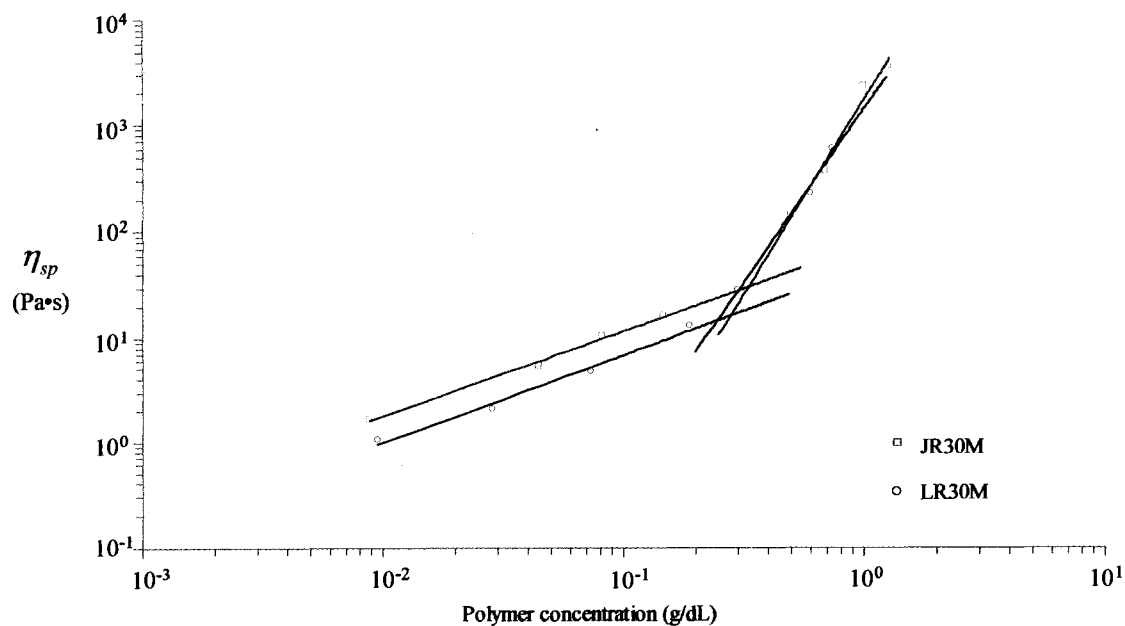


Figure 4B-8. Specific viscosity as a function of polymer concentration for JR30M and LR30M in DI water.

The calculated c^* and scaling exponents from the dilute and semi-dilute regimes for these polymers are summarized in Table 4B-II.

Table 4B-II. High molecular weight polymer c^* .

Polymer	M_w (10^3 g/mol)	CS	c^* (g/dL)	b (dilute)	b (semi-dilute)
JR30M	1500	0.48	0.3	0.8	3.6
LR30M	1300	0.25	0.25	0.8	3.3

Theoretically, for non-interacting Gaussian chains in dilute solution the specific viscosity should scale as a power of 1.4 with concentration, and for non-interacting overlapping chains in semi-dilute solution the specific viscosity should scale as a power of approximately 3.4. The b scaling values for both JR30M and LR30M in the dilute regime were less than 1.4, which can be attributed to the polyelectrolyte effect, which

causes an increase in viscosity at very low polymer concentrations. The values of 0.8 are similar to that observed by Candau and coworkers ($b = 0.65$) for polyelectrolyte below c^* .¹²⁹ In the semi-dilute regime, both polymers displayed a scaling exponent near the theoretical value for non-interacting Gaussian chains. This indicates that the cationic charges have little effect on intermolecular interactions in this region. The c^* values were similar for both polymers, but slightly lower for the lower charge substituted LR30M. This is likely due to enhanced intermolecular repulsion with higher CS of JR30M requiring a slightly higher polymer concentration for entanglement to occur.

The plot of η_{sp} versus concentration for the lower molecular weight polymers in the PQ-10 series, JR400, JR125 and LR400, is shown in Figure 4B-9.

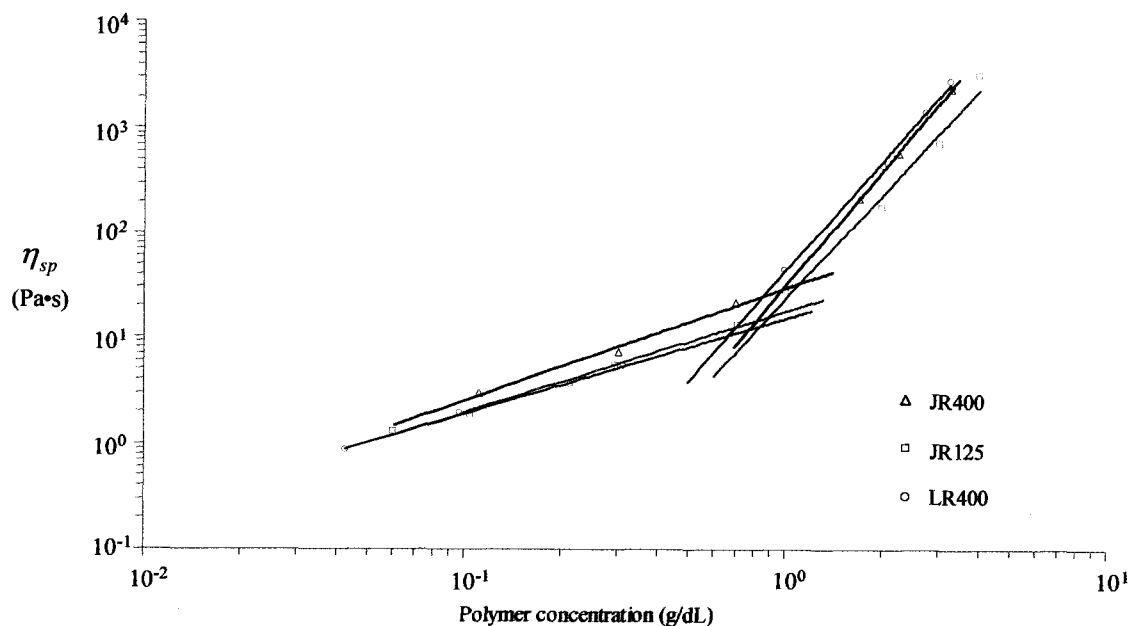


Figure 4B-9. Specific viscosity as a function of polymer concentration for JR400, JR125 and LR400 in DI water.

The calculated c^* and scaling exponents from the dilute and semi-dilute regimes for these polymers are summarized in Table 4B-III.

Table 4B-III. Low molecular weight polymer c^* .

Polymer	M_w (10^3 g/mol)	CS	c^* (g/dL)	b (dilute)	b (semi-dilute)
LR400	400	0.25	0.7	0.9	3.5
JR125	350	0.48	0.9	1.0	3.3
JR400	500	0.48	1.0	1.1	3.7

The b scaling values for the lower molecular weight JR400, JR125 and LR400 polymers were also less than 1.4, which is attributed to the polyelectrolyte effect. In the semi-dilute regime, all polymers displayed a scaling exponent near the theoretical value for non-interacting Gaussian chains, indicating that the cationic charges have little effect on intermolecular interactions in this region. This consistency in scaling factors with the high molecular weight systems is reasonable because the CS range is the same. The c^* values for these lower molecular weight polymers were all significantly higher than their high molecular weight counterparts, which is again reasonable given the known effects of molecular weight on c^* . Low CS LR400 had the lowest c^* of this group, which is likely due to a lower degree of intermolecular electrostatic repulsions with low CS. The c^* values of JR400 and JR125 were essentially the same, indicating that for this class of polyelectrolytes a molecular weight difference of 150×10^3 g/mol has little effect on chain entanglement, possibly due to the relative stiffness of the polymer backbone or the polydispersity of the systems.

The interaction between polymer chains can be described by the relationship between c^* and $\frac{1}{[\eta]}$, where if $c^* < \frac{1}{[\eta]}$ then attractive forces are present and if $c^* > \frac{1}{[\eta]}$ repulsive forces are present. These comparisons were attempted for the salt-free PQ-10 systems, however due to the polyelectrolyte effect in dilute solution a negative slope was obtained (Figure 4B-10), making extrapolation to determine $[\eta]$ impractical.

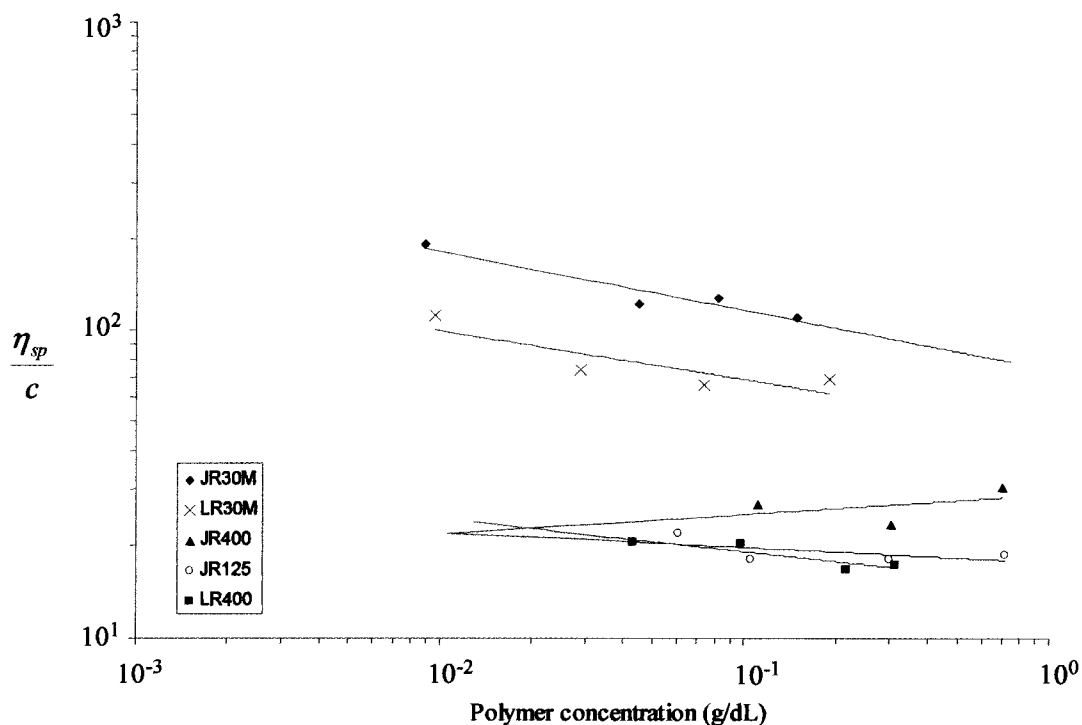


Figure 4B-10. Reduced viscosities of PQ-10 polymer series in DI water.

The c^* values were considered in analysis of the data from the high-throughput and more detailed studies and were determined to affect coacervate formation. The contour phase diagrams for JR125, JR400, and JR30M with SLES are shown in Figure 4B-11, with a red line indicating the critical overlap concentration of the polyelectrolyte, if applicable. The molecular weights were 350 000, 500 000, and 1 500 000 g/mol, respectively, and the CS was 0.48 for each polymer.

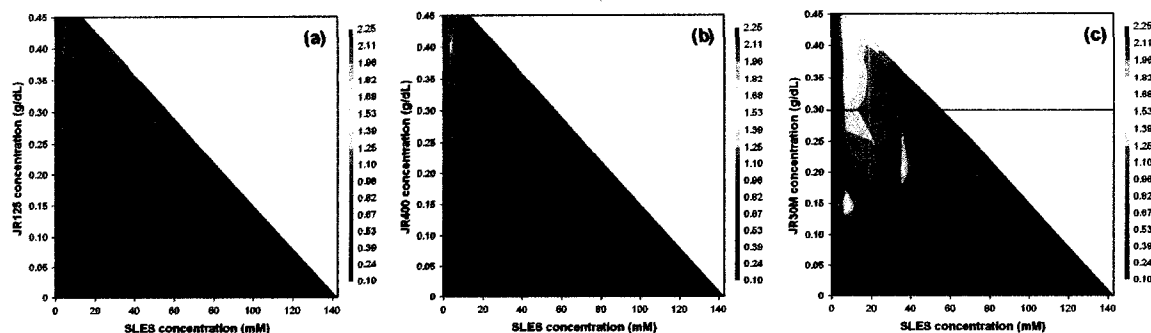


Figure 4B-11. Contour phase diagrams of (a) JR125, (b) JR400, and (c) JR30M with SLES. Molecular weight increases from left to right.

For all systems in Figure 4B-11, the pattern of coacervation as a function of surfactant concentration followed the general principles of coacervation, where phase separation was observed at low surfactant concentrations and as the amount of surfactant increased solubilization occurred, providing a one-phase system at high surfactant concentrations. The phase separation in the JR125-SLES and JR400-SLES systems occurs below c^* and maximum phase separation occurs in the region near the surfactant CMC (3.0 mM). For the JR30M-SLES system, the same behavior was observed, except in this system additional regions of coacervate were found above the polymer c^* and at higher surfactant concentrations.

Theoretically, polymers will separate from solution at theta conditions and under these conditions it is generally accepted that the mesh size becomes equal to the Kuhn length. Goddard and Hannan attributed phase separation in similar polymer-surfactant systems to the attachment of hydrophobes to the hydrophilic polymer chain, where the bound surfactant tail groups are likely to form hydrophobic associations. This would promote a decrease in mesh size that is consistent with phase separation in the PQ-10-

SLES systems. A decrease in mesh size would decrease the configurational and conformational entropy of the polymer molecules. Since ΔG_{mix} is governed by

$$\Delta G_{mix} = \Delta H_{mix} - T\Delta S_{mix} \quad \text{Equation 4B-4.}$$

the free energy of mixing will be less favorable and a two phase system is more likely with a decrease in entropy of the polymer molecules. This was observed in all high CS PQ-10-SLES systems, where phase separation occurred below the polymer c^* . We also observed an effect of c^* on coacervate amount, where above c^* in the JR30M-SLES system a greater amount of coacervate was formed, which can be attributed to a decrease in mesh size due to an enhancement of the polymer entangled network with the addition of anionic surfactant.

The effect of molecular weight was also studied at low charge substitution (CS = 0.25) using LR400 and LR30M (400 000 and 1 300 000 g/mol, respectively). The contour phase diagrams for these two polymers with SLES are shown in Figure 4B-12, with a red line indicating the c^* of the polyelectrolyte, if applicable.

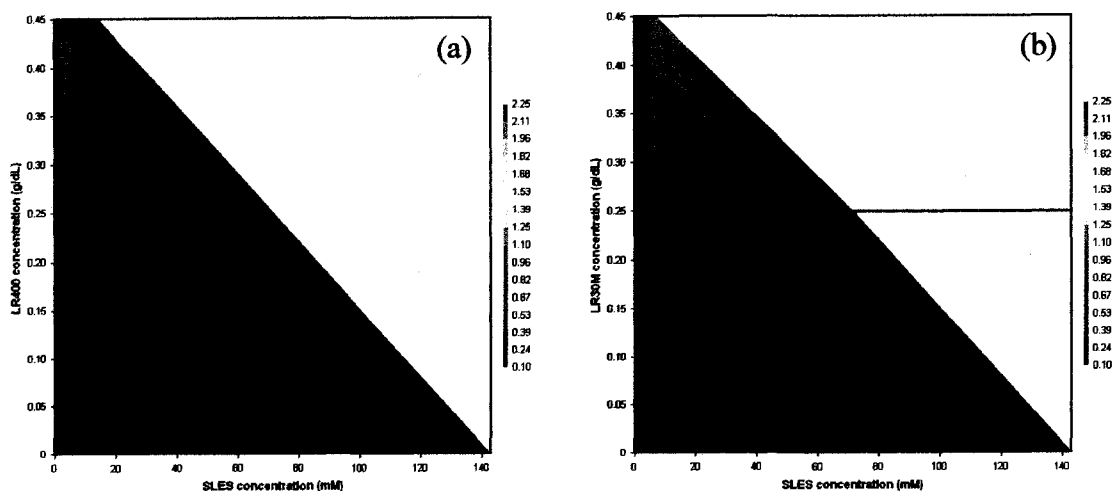


Figure 4B-12. Contour phase diagrams of (a) LR400 and (b) LR30M with SLES. Molecular weight increases from left to right.

Comparing the contour phase diagrams of these two polymers, it is again evident that molecular weight is an important factor in the amount of coacervate formed. Nearly all two-phase regions were observed above c^* for the LR30M-SLES system. Although the viscosity scaling in this regime is characteristic of a non-ionic polymer there was clearly enough charge present on the polymer to cause coacervation.

From these high-throughput molecular weight studies we can conclude that, in general, an increase in molecular weight causes an increase in coacervate amount and compositional range of coacervate formation. We can also conclude that polymer entanglement influences coacervate formation, with an increase in coacervate amount observed above c^* of the polymer.

Detailed Investigation of Specific Systems

The contour phase diagrams for the JR400-SLES and the JR30M-SLES systems were used to select compositions for more detailed study. The compositions chosen were at a constant polymer concentration of 0.35 g/dL and a surfactant concentration range of 0.10 – 43 mM. This compositional region was chosen because it exemplifies the general principles of coacervate formation and presents a region above c^* for JR30M and below c^* for JR400 which would allow us to probe the molecular mechanisms involved in coacervate formation for both a dilute and semi-dilute polymer system.

Surface Tensiometry

Surface tension measurements were performed over the selected SLES concentration range to evaluate the onset of interaction between the polymer and surfactant, a parameter that was not determined using high-throughput screening. The CMC of the surfactant was also determined for reference. The plot of surface tension versus surfactant concentration for the JR400-SLES system is shown in Figure 4B-13.

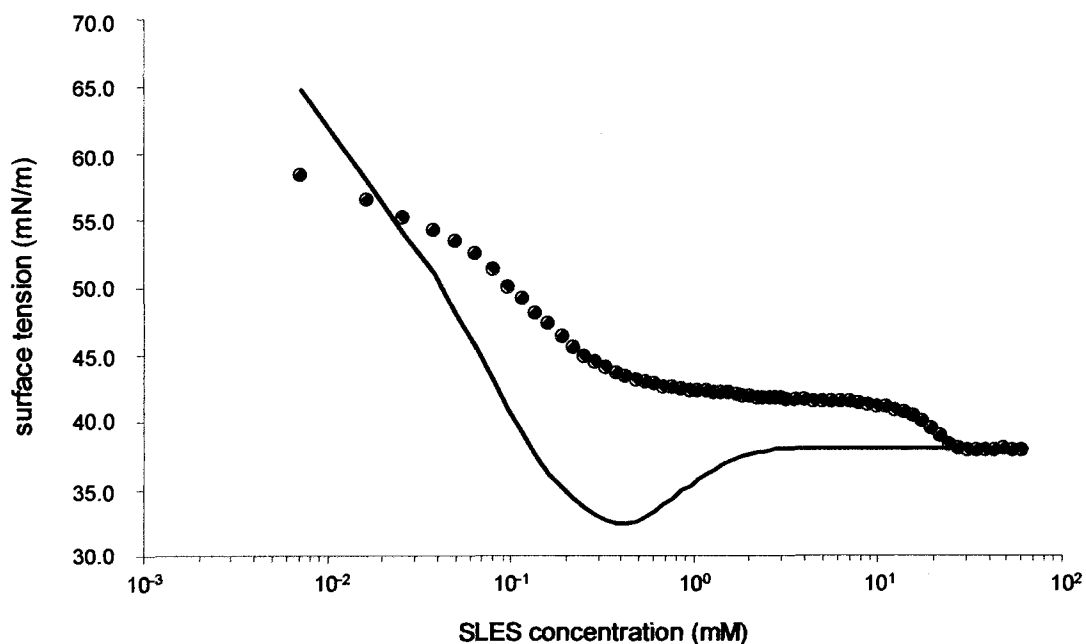


Figure 4B-13. Surface tension versus surfactant concentration data for 0.35 g/dL JR400 with SLES. — SLES; ♦ JR400-SLES mixture, Run 1; ● JR400-SLES mixture, Run 2.

The CMC of SLES in the absence of polymer was determined to be 3.0 mM. Despite the pre-CMC dip in the curve, due to impurities, the experimentally determined CMC is in good agreement with previously reported values.^{105, 106} Multiple runs were performed on the JR400-SLES mixture series, exhibiting excellent reproducibility in the data.

At very low surfactant concentrations the surface tension was lower in the mixture than in the pure SLES system, which is consistent with the formation of a highly surface-active complex between the polymer and surfactant monomers.⁷ Thus, the onset of polymer-surfactant interaction, or the critical aggregation concentration (CAC), occurred at very low surfactant concentrations, below 7.1×10^{-3} mM SLES. At a surfactant concentration of 2.1×10^{-2} mM the curves intersect and the surface tension of the mixture remained higher than that of the pure surfactant until a surfactant concentration of 31 mM. This higher surface tension compared to pure surfactant is indicative of

polymer-surfactant interaction where the surfactant interacts preferentially with the polymer rather than the surface. Electrostatic interaction between surfactant head groups and cationic charges along the polymer are enthalpically and entropically favorable^{7, 18} and from the increase in surface tension we can conclude that the free energy of interaction of SLES with JR400 is lower than the free energy of adsorption of surfactant monomers at the air/water interface.

The large plateau region between 0.50 – 24 mM SLES (approximately 1.5 decades) is indicative of strong interactions between the polymer and surfactant, likely due to the attraction of the oppositely-charged species¹³⁰ and this corresponds to complex coacervate formation observed in the contour phase diagram (Figure 4B-5a). The plateau region extends from an anionic:cationic charge ratio of 0.1:1 to 3:1. Therefore the complex coacervate forms over a range of stoichiometries encompassing the 1:1 charge ratio.

The CMC in the presence of polymer was shifted to a higher surfactant concentration of 31 mM. At this point the two curves converge, indicating the presence of free micelles in the system. This corresponds with the resolubilization observed in the contour phase diagram (Figure 4B-5a). The anion:cation stoichiometric ratio at this CMC is 7:1, or seven surfactant molecules per cationic group. Yamato and Lochhead observed a similar size for hemi-micelles in the JR400-SDS system.⁷³

Surface tension measurements were also performed for the JR30M-SLES system, which was above c^* at 0.35 g/dL JR30M (Figure 4B-14).

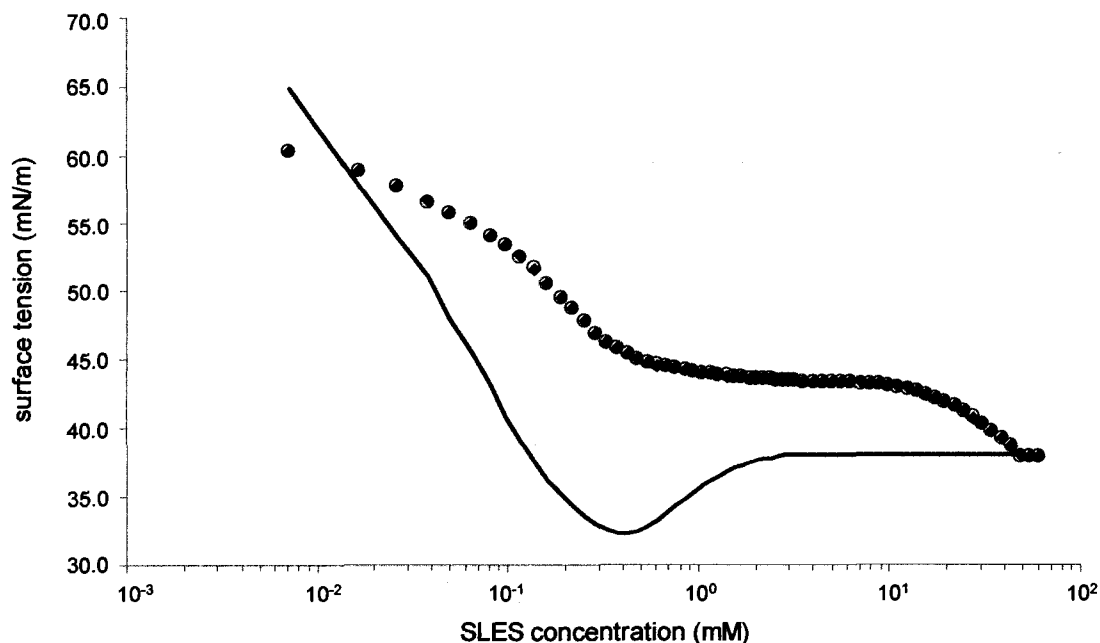


Figure 4B-14. Surface tension versus surfactant concentration data for 0.35 g/dL JR30M with SLES. — SLES; ◆ JR30M-SLES mixture, Run 1; ● JR30M-SLES mixture, Run 2.

As in the JR400-SLES system, the surface tension for the JR30M-SLES system was lower than that of pure SLES at very low surfactant concentrations, indicating the formation of a highly surface-active complex between the polymer and surfactant monomers with a CAC below 7.1×10^{-3} mM SLES.⁷ The SLES and JR30M-SLES mixture curves intersect at 1.4×10^{-2} mM SLES and the surface tension of the mixture remained higher than that of the pure surfactant until a surfactant concentration of 50 mM. Initial interactions occurred at a lower surfactant concentration and CMC was reached at a much higher surfactant concentration for the JR30M-SLES system compared to the JR400-SLES system. The larger value of CMC in the JR30M-SLES system is attributed to the entangled polymer network and is in agreement with the observation of a two-phase system up to ~ 48 mM SLES in the contour phase diagram (Figure 4B-5b).

The plateau region was approximately the same length as in the JR400-SLES system indicating that the strength of interactions is similar with both polymers.⁷⁸ The anion:cation stoichiometric ratio was 11:1 at the CMC in the presence of polymer, or eleven surfactant molecules per cationic group, which is greater than that for JR400-SLES.

Interactions between macromolecules and amphiphilic molecules (surfactants) occur only if the free energy gained by their association exceeds the free energy gained by other processes available to the surfactant.¹³¹ One such process having a favorable gain in free energy is micelle formation, since the hydrophobic portions of the surfactant molecule are driven towards association. We observed that coacervate formation occurred at concentrations well above the pure surfactant CMC indicating that polymer-surfactant interaction was more favorable than micelle formation in both the JR400-SLES and JR30M-SLES systems. Micellization is governed by both electrostatic repulsive forces (increase in free energy of association) and hydrophobic associations (decrease in free energy of association). The interaction of oppositely-charged polymer and surfactant is governed by electrostatic attractive forces and hydrophobic associations, both of which lower the free energy of association. Therefore, it is reasonable that the formation of coacervate was more favorable than micellization in these systems. At the CMC₂, the CMC in the presence of polymer, the surfactant and polymer-surfactant surface tension curves converge and above this concentration the chemical potential of polymer-surfactant complexation and the chemical potential of micelle formation are equal so that polymer-surfactant complexes and free micelles coexist.

Dynamic Light Scattering

Dynamic light scattering (DLS) measurements were performed to investigate the formation of polymer-surfactant complexes over the selected concentration range. Polymer in the absence of surfactant and surfactant in the absence of polymer were also investigated. It is important to note that these systems were studied in salt-free aqueous solutions. Because polyelectrolyte solutions consist of polyions, counterions, co-ions and solvent, scattering studies are more complex than with their neutral analogues.¹³² The long-range electrostatic interactions between polyions in solution provide a much faster diffusion rate than their neutral analogues¹³² and because the radius of hydration (R_H) is determined using the Stokes-Einstein equation

$$D = \frac{kT}{6\pi\eta R_H} \quad \text{Equation 4B-5.}$$

where D is the diffusion coefficient and η is the viscosity of the solution, a faster diffusion can lead to error in determination of polyelectrolyte particle size. Thus, the apparent R_H presented in these studies is not indicative of the true polymer R_H . However, for comparison of particle size in pure polymer solution with particle size in polymer-surfactant solutions, the polymer apparent hydrodynamic diameter (D_H) was employed, similar to studies by Zhou et al.⁹⁵

The apparent D_H of the surfactant over a wide range of concentrations was also determined for comparison with polymer-surfactant solutions. A decrease in D_H was observed with increasing surfactant concentration, which was attributed to long chain alcohol impurities in the surfactant (discussed previously), and those impurities being solubilized at higher surfactant concentrations. It is also probable that as concentration was increased the electrostatic repulsions between surfactant head groups became

stronger causing monomers and micelles to diffuse more rapidly in solution. As discussed with the polyelectrolytes in salt-free solution, this caused a reduction in apparent R_H . For comparison of particle size in pure surfactant solution with particle size in polymer-surfactant solutions, the apparent D_H values were used.

DLS studies of polymer-surfactant solutions were performed at a constant polymer concentration (0.35 g/dL) and surfactant concentrations above and below the CMC. The DLS results for the JR400-SLES system are shown in Figure 4B-15.

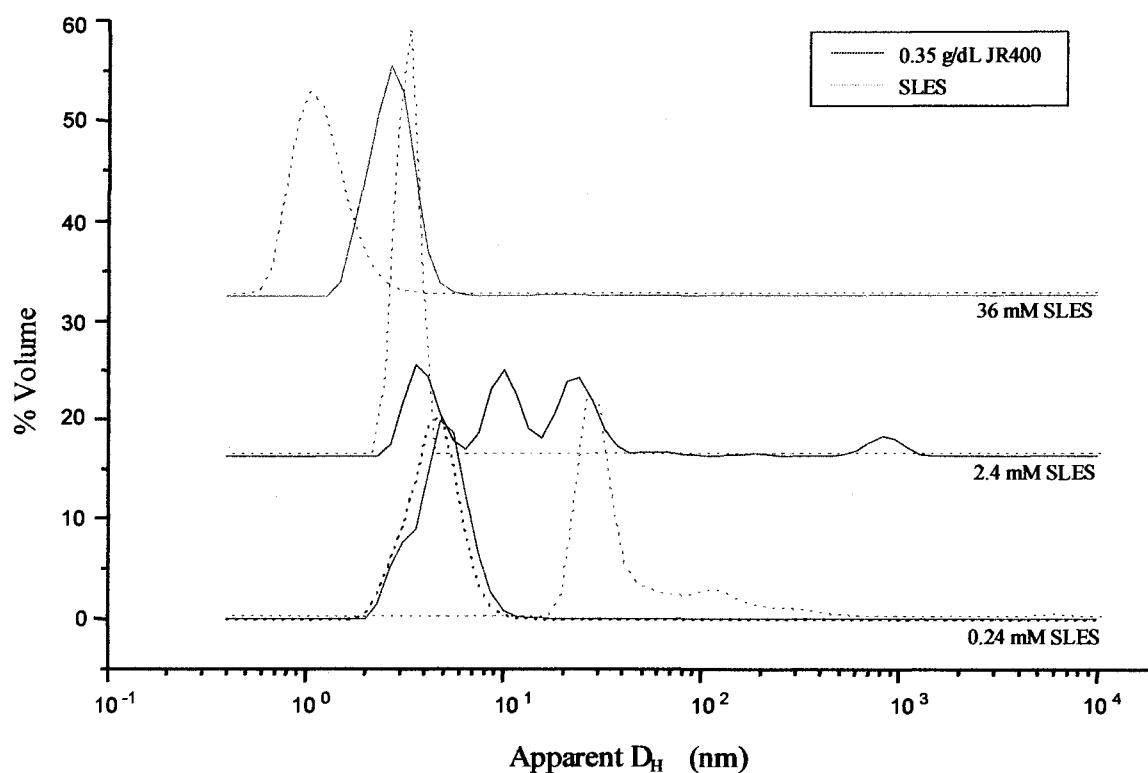


Figure 4B-15. Dynamic light scattering data for 0.35 g/dL JR400 – SLES mixtures.

The 0.35 g/dL JR400 - 0.24 mM SLES system showed a very similar distribution to the pure polymer, with a hydrodynamic diameter of 4.9 nm. A small shoulder was observed

on the left side of this peak indicating that a possible smaller second particle size was present. From the surface tension studies, this system is above the CAC so that surfactant molecules are electrostatically bound along the polymer chain. The similarity in D_H between the pure polymer and the JR400-SLES complexes indicates that minimal hydrophobic association is occurring between polymer-bound surfactant molecules. This is reasonable because association between bound hydrophobes would result in a conformational entropic penalty for the polymer molecule.¹³³ An absence of complexes at high D_H indicates that intermolecular interactions did not occur in this system.

The apparent D_H profile was dramatically different for the 0.35 g/dL JR400 - 2.4 mM SLES system compared to the pure polymer and surfactant solutions. The sample used for this study contained two phases, and a random sample was used for the DLS measurement (i.e., DLS was not performed solely on the supernatant). Three peaks of nearly equal volume distribution were present below 100 nm, with diameters of 3.6 nm, 10 nm, and 24 nm. The diameter of the smaller peak at the far right is 830 nm. The four distinct peaks are convincing evidence of the coexistence of micelles (3.6 nm), soluble complexes (10 and 24 nm) and coacervate (830 nm). The micelle peak at 3.6 nm (shoulder in previous mixture) was visible in this system because the polymer peak was not present and baseline resolution was attained. At this SLES concentration, slightly below CMC, the soluble complex peaks with D_H larger than the polymer in solution may be attributed to intermolecular hydrophobic interactions of bound surfactant molecules along neighboring polymer chains, as was shown by Zhou et. al.⁹⁵ The peak corresponding to 830 nm is in agreement with the visual observation of a two-phase system.

For the 0.35 g/dL JR400 – 36 mM SLES system a single peak was observed, with a particle size of 2.7 nm. From the contour phase diagram and from visual observation a one-phase system exists at this composition. According to the general principles of coacervation, this system is in a region of resolubilization with an anion:cation stoichiometric ratio of 8:1. This system was above the CMC in the presence of polymer (Figure 4B-13) so it is likely that excess surfactant molecules have associated with bound surfactant molecules through hydrophobic associations, limiting the contact of the hydrophobic tail groups with water and decreasing the free energy of the system. These excess surfactant molecules may now form hemi-micelles along the polymer chains with head groups oriented into solution⁷³, which causes redissolution of the phase separated complexes, producing small polymer-surfactant complexes. Zhou and coworkers observed similar interactions and dissociations with PQ-10-SDS systems.⁹⁵

The DLS results for the JR30M-SLES system are shown in Figure 4B-16. The polymer was above c^* at the concentration studied.

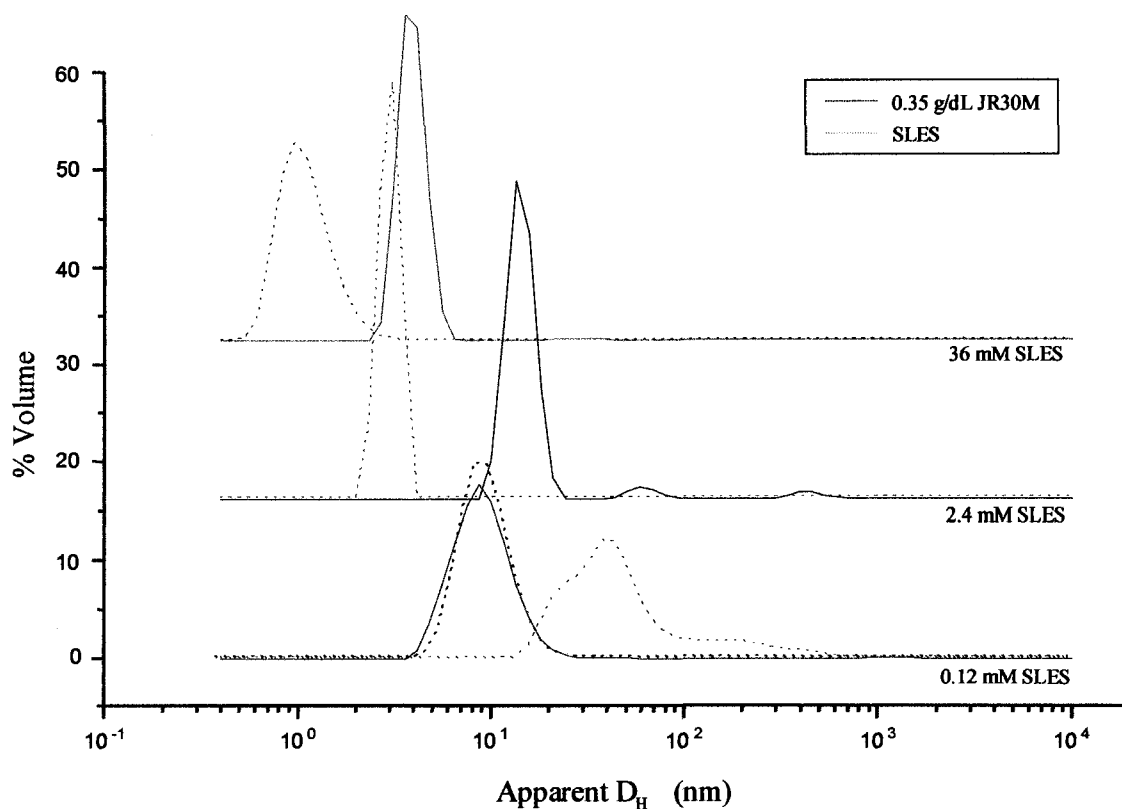


Figure 4B-16. Dynamic light scattering data for 0.35 g/dL JR30M with SLES.

For JR30M, the D_H of the pure polymer solution at 0.35 g/dL was 8.7 nm. As previously discussed, the polymers were studied in salt-free aqueous solution. The difference observed in apparent D_H between JR400 and JR30M can be deconvoluted from their time autocorrelation functions and is discussed in more detail in Appendix I.

A single peak was observed for the 0.35 g/dL JR30M - 0.12 mM SLES system, with a very similar D_H to the pure polymer solution (8.7 nm). This system is above the CAC (Figure 4B-14) so surfactant molecules are electrostatically associated with the polymer chain. From the c^* measurements, we know that the polymer exists in an entangled network in this system. The absence of change in D_H with the addition of

surfactant indicates that this small concentration of surfactant does not significantly affect inter- or intramolecular associations within the entangled polymer network.

The apparent D_H profile was different for the 0.35 g/dL JR30M - 2.4 mM SLES system compared to the pure polymer and surfactant solutions. The sample used for this study contained two phases, and a random sample was used for the DLS measurement (i.e., DLS was not performed solely on the supernatant). Three peaks were observed, one with a much greater volume distribution. The D_H of this peak was 14 nm. The hydrodynamic diameters of the two peaks with low volume distribution were 68 nm and 460 nm. The presence of three distinct peaks, all with a diameter greater than that of the polymer in solution indicates that intermolecular interactions occurred at this surfactant concentration and it is likely that polymer-surfactant complexes aggregated to produce the high D_H of 460 nm. No micelle peak was observed in this system indicating that polymer-surfactant interaction was highly favored in the entangled system. The large volume distribution of particles with D_H of 14 nm may be due to swelling of the entangled network by the addition of surfactant molecules bound to the polymer chains. At this SLES concentration (2.4 mM), the particle sizes for the JR30M-SLES system are overall larger than in the JR400-SLES system, which can be attributed to the existing network structure in the former.

A single peak at 3.6 nm was observed for the 0.35 g/dL JR30M - 36 mM SLES system. Contrary to the JR400-SLES system at this composition, a two-phase system was observed visually and from the contour phase diagram for the JR30M-SLES system. The separated phase of the 0.35 g/dL JR30M - 36 mM SLES system was more compact than the 0.35 g/dL - 2.4 mM SLES separated phase so DLS measurements were

performed solely on the supernatant. The decreased particle size in this system compared to pure polymer indicates that complexes were present in solution despite the presence of a separated phase.

Viscometry

Zero-shear viscosity measurements were also performed on polymer-surfactant solutions over the selected concentration range. Polymer concentration remained constant (0.35 g/dL) and surfactant concentrations above and below the CMC were studied. The results for JR400-SLES mixtures are shown in Figure 4B-17.

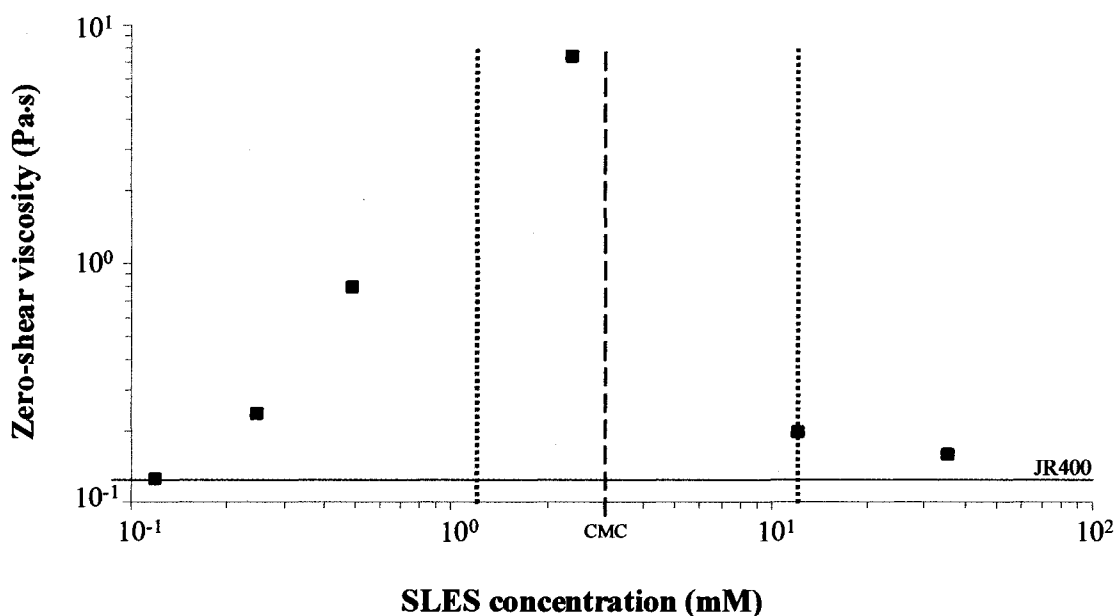


Figure 4B-17. Zero-shear viscosities of 0.35 g/dL JR400-SLES mixtures.
 Precipitation boundary; --- CMC in the absence of polymer.

An increase in zero-shear viscosity with increasing SLES concentration was observed in single phase solutions up to the precipitation boundary at 1.2 mM SLES. This is in agreement with complex formation observed in the DLS studies for the 0.35 g/dL JR400

– 0.24 mM SLES system. A peak in viscosity occurred at 2.4 mM. As was discussed with the DLS studies, the viscosity measurement of the 0.35 g/dL JR400 – 2.4 mM SLES mixture was performed on the two phase dispersed system, not solely on the supernatant. The peak viscosity at this composition is in agreement with the presence of multiple large particle sizes observed in the DLS studies. It is also in agreement with the viscosity increase observed by Leung and Goddard in JR400-SDS systems, which they attributed to association of bound surfactant hydrophobic tail groups along neighboring polymer chains.¹³ The decrease in viscosity at higher surfactant concentrations is also in agreement with the decrease in particle size observed with DLS and can be attributed to resolubilization of coacervate complexes.

The zero-shear viscosity results for the JR30M-SLES mixtures are shown in Figure 4B-18.

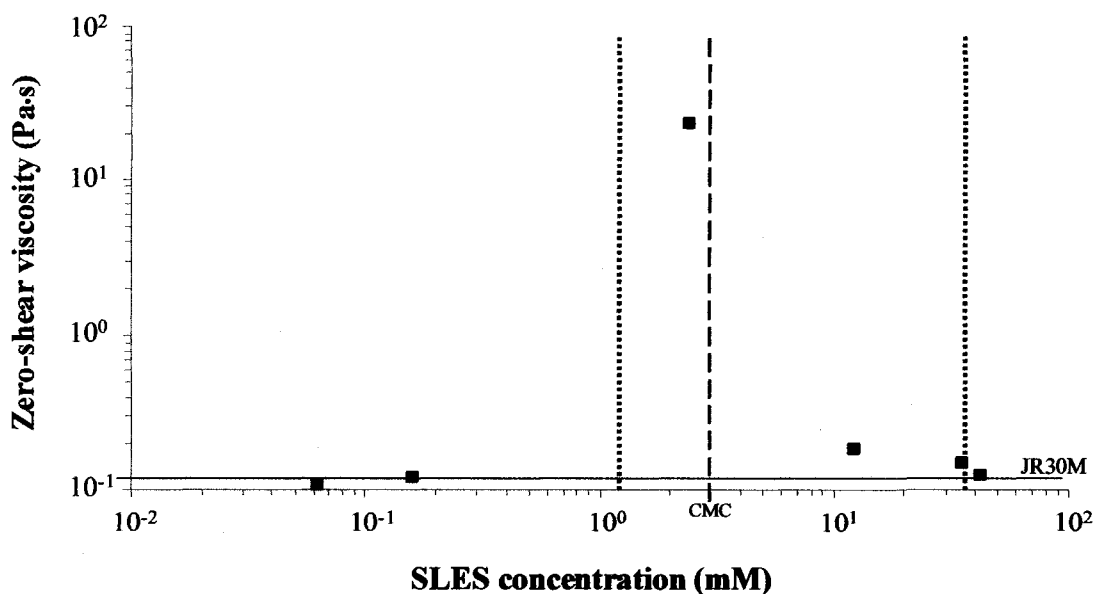


Figure 4B-18. Zero-shear viscosities of 0.35 g/dL JR30M-SLES mixtures.
 Precipitation boundary; --- CMC in the absence of polymer.

Below the precipitation boundary, the zero-shear viscosity increased only slightly with increasing surfactant concentration and was similar to the polymer solution viscosity at 0.35 g/dL. This is in agreement with the absence in D_H change for the 0.35 g/dL JR30M – 0.12 mM SLES system observed with DLS. The viscosity increased dramatically at 2.4 mM SLES, where as was discussed with the DLS studies, the viscosity of the JR30M-SLES mixture was performed on the two phase dispersed system, not solely on the supernatant. The high viscosity of this mixture is in agreement with the presence of multiple large particle sizes determined via DLS. Within the precipitation boundary, as the surfactant concentration increased the viscosity decreased, which can be attributed to solubilization of some of the complexes. The low viscosities above 12 mM SLES are in agreement with the decrease in D_H observed with DLS for the 0.35 g/dL JR30M – 36 mM SLES, supporting the presence of small complexes in solution for two-phase systems and partial resolubilization of coacervate complexes in the single-phase systems.

Data Summary

In order to provide an overall picture of coacervate formation in these systems the data from high-throughput screening, surface tension, DLS, and viscometry measurements were compiled for the JR400-SLES system (Figure 4B-19). Figure 4B-19a shows the amount of coacervate formed at 0.35 g/dL polymer as a function of surfactant concentration using the same color-coding as the contour phase diagram. Figure 4B-19b is the zero shear viscosity as a function of surfactant concentration for 0.35 g/dL JR400 –SLES mixtures. Figure 4B-19c is a representation of apparent D_H as a function of surfactant concentration. Figure 4B-19d is the surface tension data represented in its entirety.

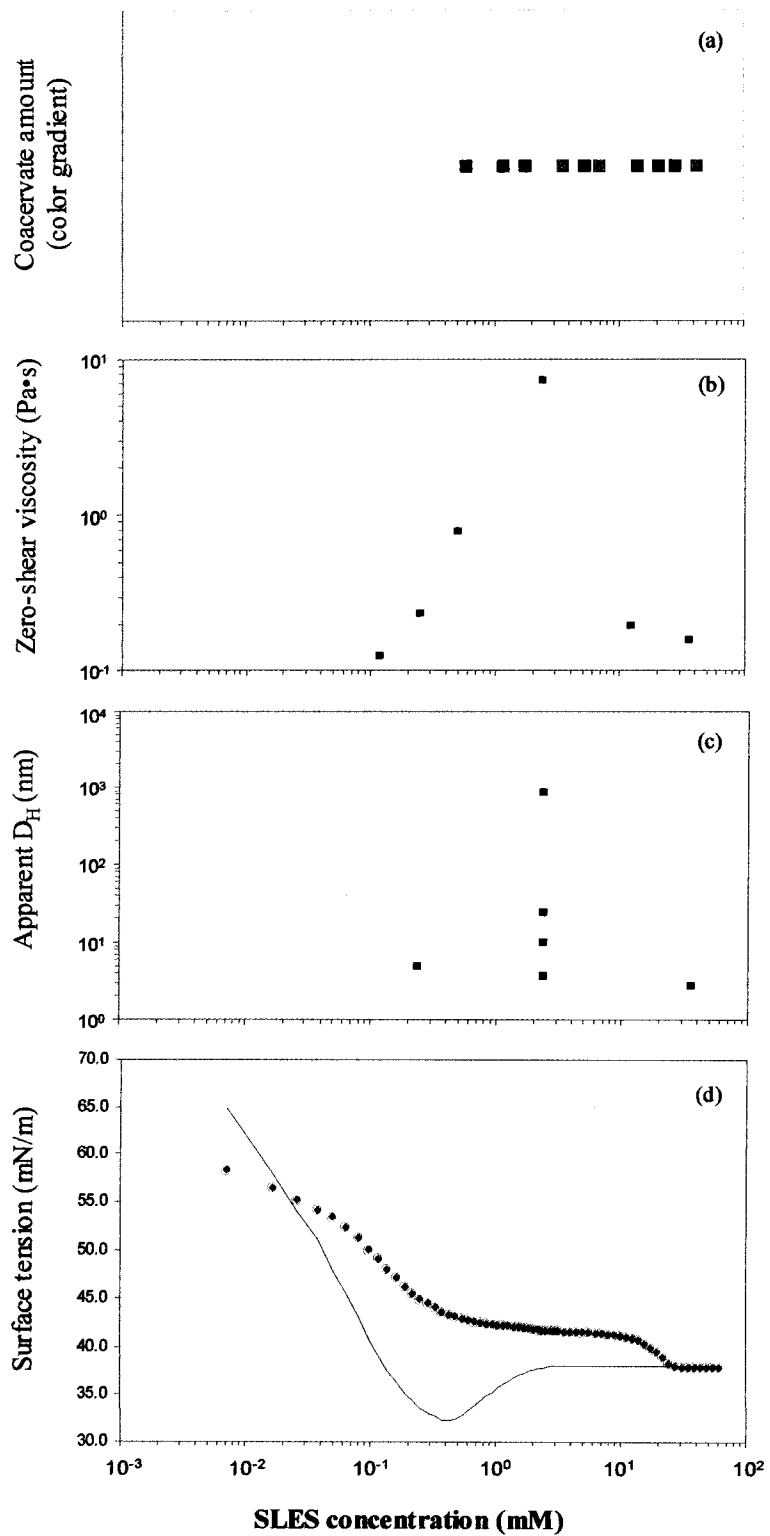


Figure 4B-19. Data compilation for the 0.35 g/dL JR400 - SLES system.

The phase separation range of the JR400-SLES system at 0.35 g/dL polymer was observed visually from 1.2 mM to 12 mM SLES, which corresponds to the region of phase separation in the contour phase diagram (Figure 4B-19a). As discussed previously, viscosity increased with the increasing SLES concentration and a maximum was reached in the two-phase region. The maximum viscosity at 0.35 g/dL - 2.4 mM SLES is in agreement with the coexistence of soluble complexes and aggregates as shown by DLS, and corresponds to the plateau region of the surface tension plot, which was previously designated as a region of complex coacervate formation. The decrease in viscosity at higher surfactant concentrations is in agreement with the decrease in particle size observed with DLS, the one-phase regions (blue) observed with high-throughput screening, and the presence of micelles observed in the surface tension data. Zhou *et. al.* observed a similar trend and attributed it to a polymer chain that has been saturated with SDS micelles and the break up of large complex particles into small complex particles as a result of the repulsion between SDS micelles.⁹⁵

The data from high-throughput screening, surface tension, DLS, and viscometry measurements were compiled for the JR30M-SLES system as well (Figure 4B-20). All plots are the same as those described for the JR400-SLES system (Figure 4B-19).

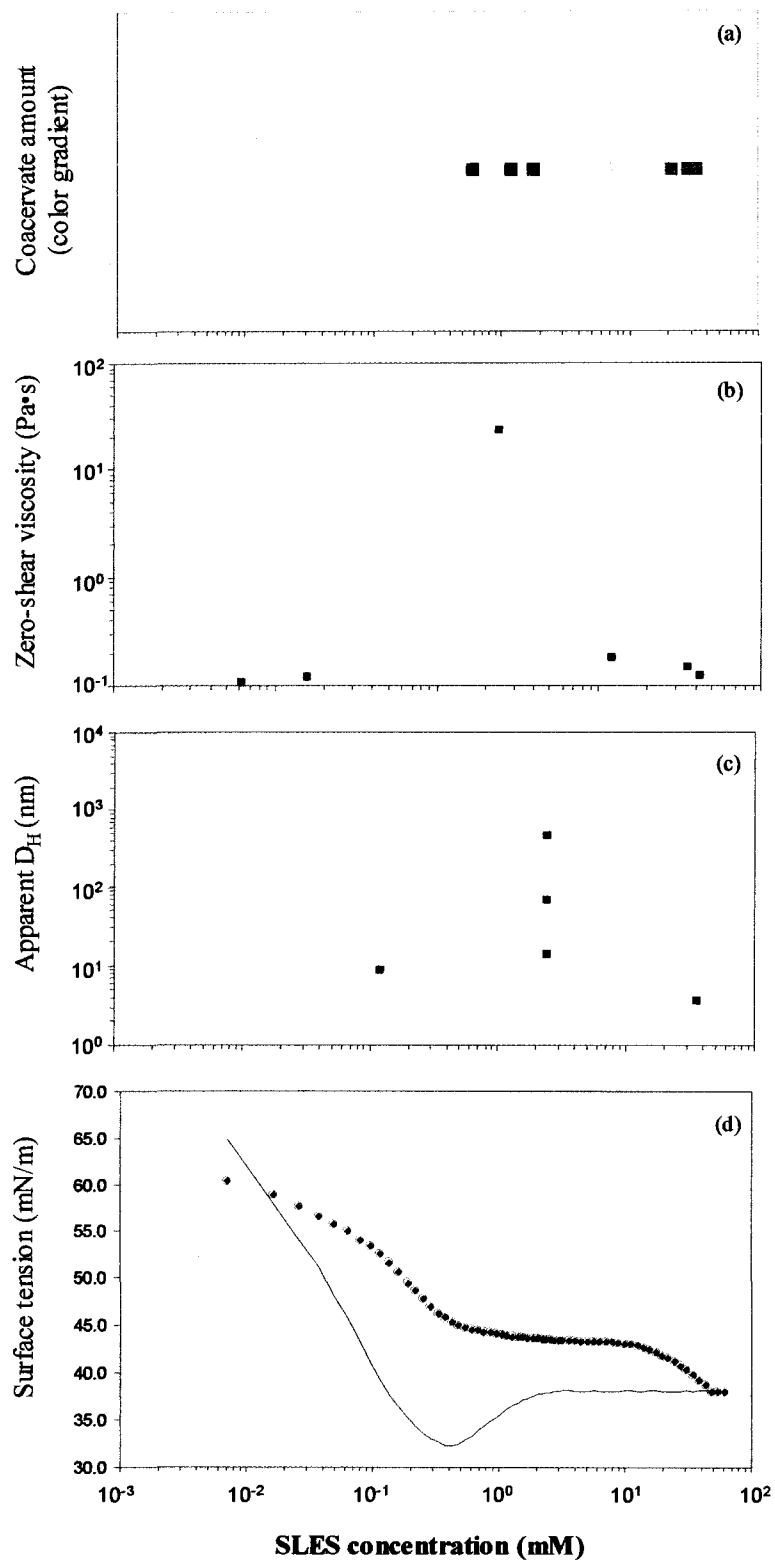


Figure 4B-20. Data compilation for the 0.35 g/dL JR30M - SLES system.

The data and our interpretation of the data for the JR30M-SLES system are similar to that already rendered for the JR400-SLES system, with the exception of an extension of the phase separation region to higher surfactant concentrations, which is also manifested in the plateau region of the surface tension versus surfactant concentration curve. It is notable that the charge substitution is the same for both polymers, but that the molecular weight of JR30M is approximately three times greater than the molecular weight of JR400. The systems studied with JR400 were below c^* whereas the JR30M systems were above c^* . Therefore, the differences we observed in complexation and coacervate formation must be due to the different molecular weights and/or the fact that one system was in the dilute regime and the other was in the semi-dilute regime.

CHAPTER IV-C

CATIONIC POLYSACCHARIDE – ANIONIC SURFACTANT INTERACTIONS AS
A FUNCTION OF POLYMER AND SURFACTANT PROPERTIES

Polymer Structural Effects

In Chapter IV-B, the effect of polymer molecular weight on coacervate formation was investigated for a series of polyquaternium-10 polymers with SLES and, at constant charge substitution (CS), a dependence of coacervate formation and coacervate amount on polymer molecular weight was observed. Our broader goal is to gain a better understanding of the polymer and surfactant properties that underpin the phase separation behavior of oppositely charged polymer-surfactant complexes. To achieve this goal we expanded our studies to encompass a range of cationic polysaccharides that included cellulosic polymers, hydrophobically-modified cationic cellulose, and cationic galactomannans. These classes of polysaccharides were investigated in order to probe the effect of a range of polymer charge substitutions and molecular weights and the effect of polymer backbone structure on coacervate phase behavior.

Degree of Charge Substitution

In previous research on complex coacervation, polymer CS has usually been considered to be of primary importance.⁷ In the present study this was investigated by comparing three polymers (LK, LR400, and JR125) with approximately the same molecular weight (350 000 – 400 000 g/mol, Table 4B-I) but different charge substitutions ($CS_{LK} = 0.13$, $CS_{LR400} = 0.25$, $CS_{JR125} = 0.48$). The contour phase diagrams for these polymers with SLES are shown in Figure 4C-1. All polymers were below c^* for all compositions investigated.

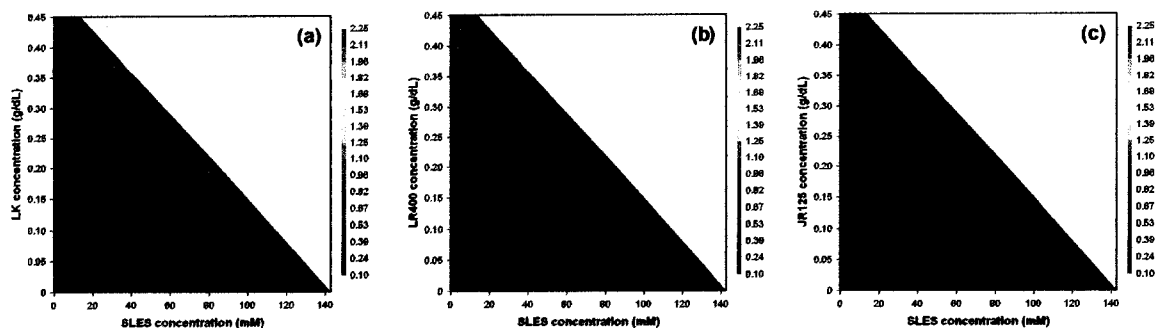


Figure 4C-1. Contour phase diagrams of (a) LK, (b) LR400, and (c) JR125 with SLES. Charge substitution increases from left to right.

Polymer LK has a very low degree of CS (0.13) and shows almost no coacervate formation. This can be attributed to the low amount of electrostatic interaction resulting in less hydrophobic tail group associations. Two-phase regions occurred at similar compositions for the LR400-SLES and JR125-SLES systems, near the 1:1 stoichiometric ratio. The amount and compositional range of coacervate formation increased with increasing CS of the polymer. The same trend was observed for the high molecular weight polymers LR30M and JR30M (1 300 000 – 1 500 000 g/mol) with SLES, shown in Figure 4C-2. The degree of CS is 0.25 for LR30M and 0.48 for JR30M. Both polymers were studied above and below their c^* ($c^*_{\text{LR30M}} = 0.25$ g/dL; $c^*_{\text{JR30M}} = 0.30$ g/dL).

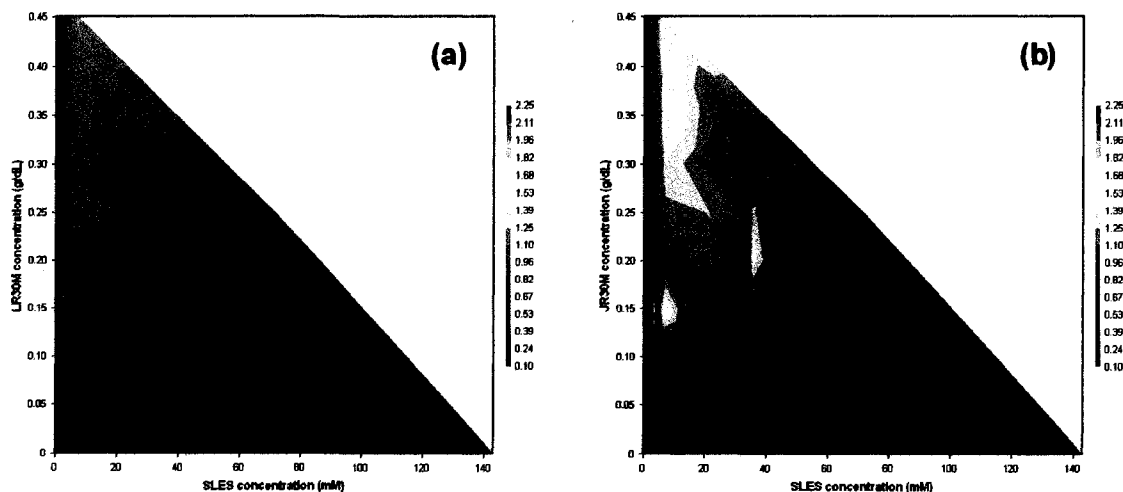


Figure 4C-2. Contour phase diagrams of (a) LR30M and (b) JR30M with SLES. Charge substitution increases from left to right.

Both the LR30M-SLES and JR30M-SLES systems showed maximum coacervate formation above c^* , as was discussed in Chapter IV-B. As in the systems with low molecular weight polymer, the amount and compositional range of coacervate formation was less for the polymer with lower CS.

From these studies we confirm that polymer CS is an important factor in coacervate formation. For low and high molecular weight polymers, an increased amount of coacervate, as well as an increased compositional range of coacervate formation, occurred in systems with higher charge substituted polymers. In Chapter IV-B, we determined that polymer molecular weight and c^* were also important factors in coacervate formation. The relationship among the polymer structural properties of molecular weight, CS, and c^* and phase behavior in PQ-10-SLES systems is summarized in Figure 4C-3.

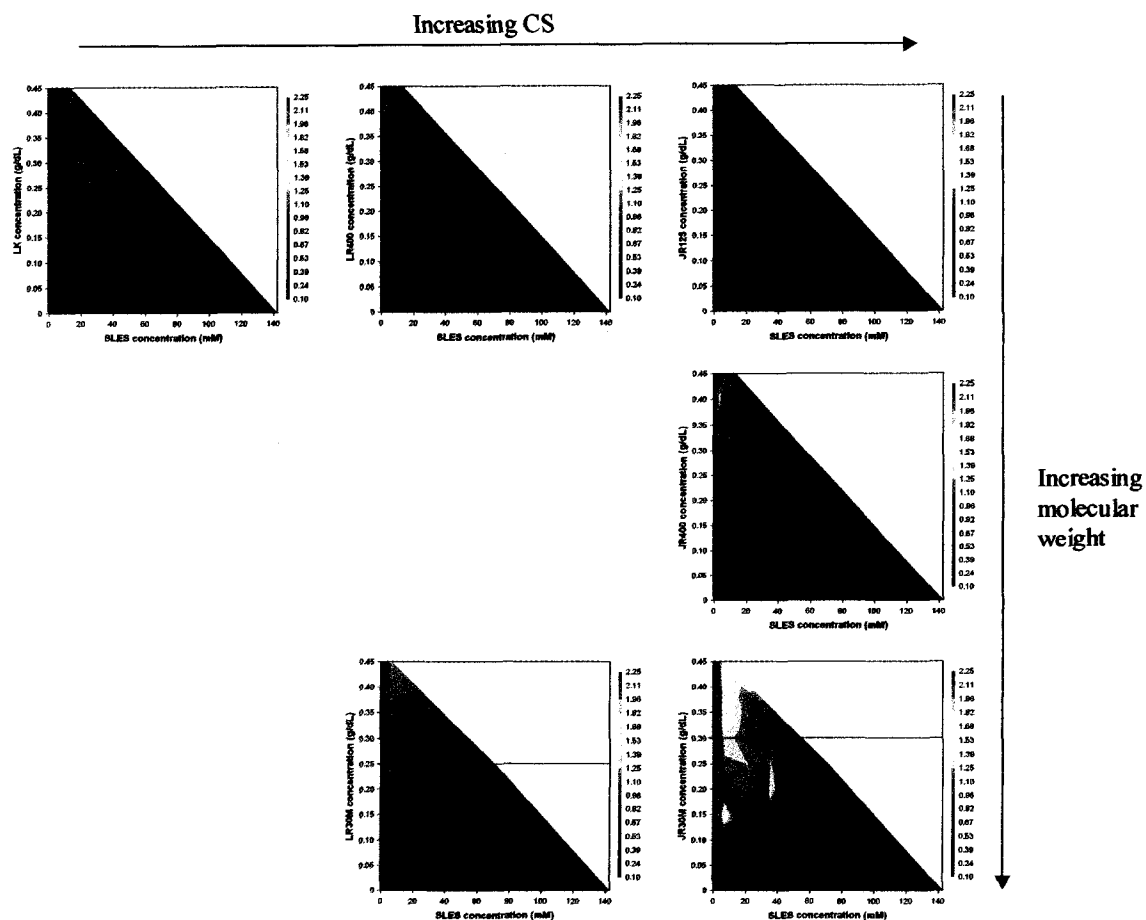


Figure 4C-3. Relationship between polymer structural properties and coacervate formation for the PQ-10 series with SLES.

Polymer Backbone Structure

A second class of cationic polysaccharides, cationic galactomannans, was investigated to determine whether the coacervation trends discussed above could be extended to polysaccharides with a different backbone structure. Cationic galactomannans have rigid backbones, similar to cationic HEC, but with a more regular structure in regards to pendant group positioning (Figure 3-3).¹³⁴ As with polyquaternium-10, a series of cationic galactomannans (cationic guar) including a range of molecular weights and degrees of CS was studied (Table 4C-I).

Table 4C-I. Guar hydroxypropyltrimonium chloride series properties.¹⁰⁰

Polymer	M_w (10^3 g/mol)	CS
C-1000	1 000	0.14
Excel	1 500	0.14
C-14S	2 000	0.14
C-17	2 000	0.17

The relationship between the cationic guar structural properties of molecular weight and CS and phase behavior in systems with SLES is summarized in Figure 4C-4.

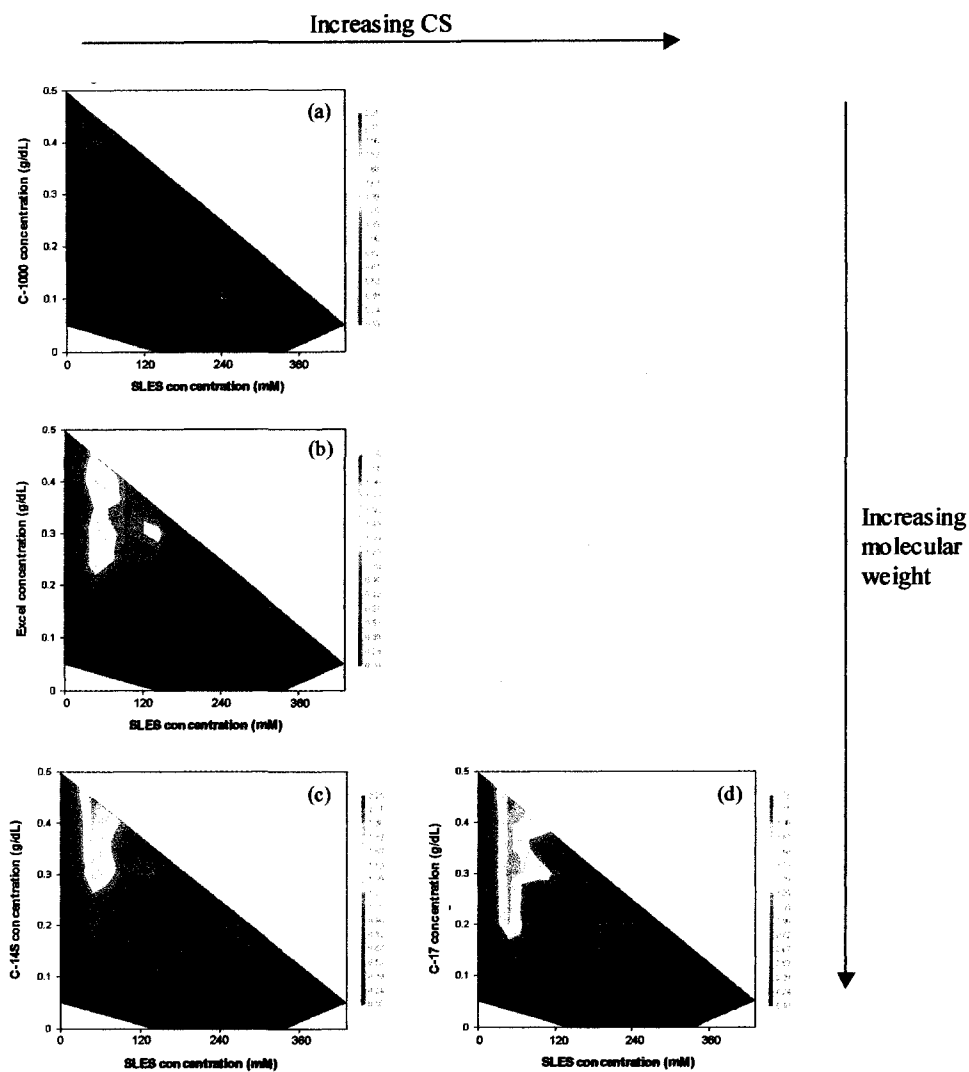


Figure 4C-4. Relationship between polymer structural properties and coacervate formation for the cationic guar series with SLES: (a) C-1000, (b) Excel, (c) C-14S, and (d) C-17.

A broader range of surfactant concentrations was investigated with the cationic guar-SLES systems (up to 480 mM SLES) than with the PQ-10-SLES systems (up to 140 mM SLES). Considering only the portion of the cationic guar-SLES phase diagrams below 140 mM SLES, comparable trends as a function of molecular weight and CS were observed for both polymer types. At low polymer molecular weight (C-1000) coacervate

amount was low and only observed at very high polymer concentrations. At higher molecular weights, the compositional range of coacervate formation became broader, as was observed in the PQ-10 series. At the highest molecular weight (C14-S) coacervate amount was greatest and coacervate formation occurred over the broadest compositional range. Although CS for the cationic guar varied only from 0.14 to 0.17 (C-14S and C-17, respectively), which was a narrower CS range than that studied with the PQ-10 series, the increase in CS provided an increase in the amount of coacervate formed. This was comparable to the CS effect observed with LR30M-SLES and JR30M-SLES (Figure 4C-2).

For the cationic guar series, all systems showed some two-phase region(s) at high surfactant concentration (above 140 mM SLES), with the amount and compositional range of coacervate increasing at higher in molecular weights. Conventional thinking dictates that, at high surfactant concentrations, coacervate that had been formed would be resolubilized via comicellization.^{7, 16, 72} However, Panmai and coworkers proposed a model for hydrophobically-modified polymer-surfactant interactions where polymer cationic groups acted as crosslinks between multiple anionic surfactant micelles creating a network structure.⁵⁹ It is compelling to adopt Panmai's model to explain the large amount of coacervate that we observed at these high surfactant concentrations.

Hydrophobic Modification

The presence of hydrophobic groups along the polymer backbone has been shown to alter the ion-exchange and hydrophobic interaction cooperativity of the polymer-surfactant interaction mechanism.⁷ Smith and McCormick demonstrated that both electrostatic and hydrophobic interactions occurred with hydrophobic terpolymers and

CTAB²⁹, however association between hydrophobic tail groups and hydrophobic groups along the polymer chain imparted a specificity to these interactions.⁷ The potential alteration of the mechanism of coacervate formation with the addition of hydrophobic moieties was investigated for a series of hydrophobically-modified cationic HEC polymers, polyquaternium-67 (PQ-67), with SLES using high-throughput screening. The PQ-67 series consists of polymers of constant molecular weight range (200 000 – 800 000 g/mol) and constant CS (0.25) with different degrees of hydrophobic substitution. Contour phase diagrams for this series with SLES are shown in Figure 4C-5.

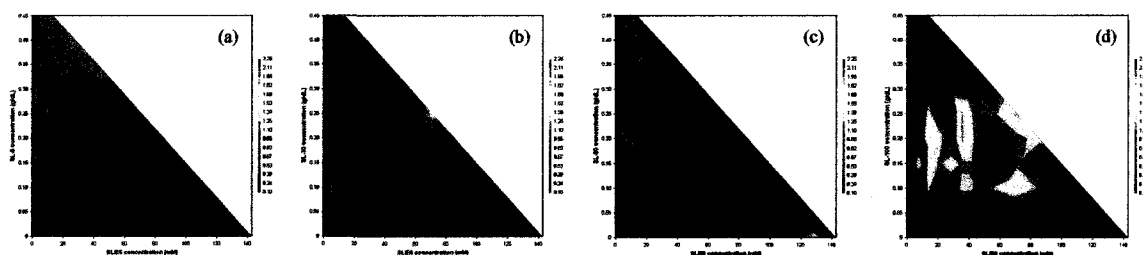


Figure 4C-5. Contour phase diagrams for PQ-67 series with SLES: (a) SL-5, (b) SL-30, (c) SL-60, and (d) SL-100. The degree of hydrophobic substitution increases from left to right.

In general, the amount of coacervate and the compositional range of coacervation increased with higher degrees of hydrophobic substitution. A shift in the compositional range of coacervate formation was observed between the system with the lowest degree of hydrophobic substitution (SL-5-SLES, Figure 4C-5a) and the systems with polymers with higher degrees of hydrophobic substitution. The low degree of hydrophobic substitution for SL-5 ($HS = 5 \times 10^{-4}$) provided a polymer very similar to LR400 or LR30M and coacervate formation at similar compositions and in similar amounts was observed. As the amount of hydrophobic substitution on the polymer chain increased, the

region of coacervate formation was shifted to lower polymer concentration. This shift in compositional range can be attributed to the variation of the cooperative mechanism of coacervate formation with hydrophobically-modified polyelectrolytes.

An increased amount of coacervate and increased range of coacervate formation was also observed at higher degrees of hydrophobic substitution. Panmai et. al. demonstrated that in the presence of hydrophobically-modified polymer surfactant micelles incorporate hydrophobic moieties of multiple polymer chains into their core, forming cross-links and a subsequent network structure that can lead to phase separation.^{7, 59} Using viscosity measurements, they determined that the number of potential crosslinking sites increased with an increased degree of hydrophobic substitution.⁵⁹ Our observation of the highest amount of coacervate in the most hydrophobically-substituted SL-100-SLES system ($HS = 1 \times 10^{-2}$) compared to the SL-30-SLES and SL-60-SLES ($HS = 5 \times 10^{-3}$) systems is consistent with the formation of micellar junction zones between polymer chains as hypothesized by Panmai et. al.⁵⁹

Surfactant Structural Effects

Micelle Charge Density

The surface charge of colloidal particles, such as surfactant micelles, is known to influence their adsorption characteristics.²¹ For oppositely-charged polymers and surfactants, this property is of particular importance due to the ion-exchange interaction mechanism that contributes to polymer-surfactant interaction. Dubin and coworkers have extensively investigated the effect of micelle surface charge density on oppositely-charged polymer-surfactant interactions.^{7, 14, 15, 79, 80} They have observed that above a

critical micelle surface charge density complex formation occurs, with increasing coacervate formation as micelle surface charge density increases.⁸⁰ This behavior was attributed to polymer-surfactant association via a different mechanism than that proposed by Goddard¹⁵ and this is discussed in more detail in Chapter IV-E.

The examination of micelle charge density and its effects on coacervate formation was investigated by studying surfactants with various degrees of surfactant ethoxylation (EO). This effect was investigated using JR30M and LR30M with ammonium lauryl ether sulfates (ALES) with different EO lengths (3 EO, 12 EO, and 30 EO). The results are shown in Figure 4C-6.

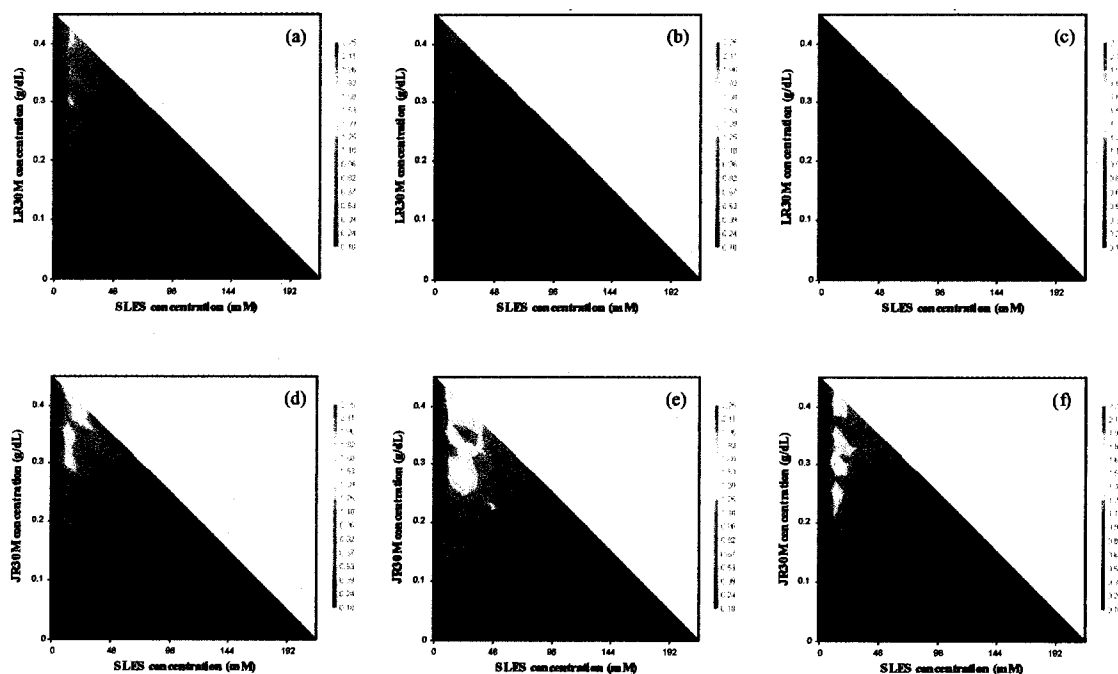


Figure 4C-6. Contour phase diagrams of JR30M (a-c) and LR30M (d-f) with ammonium lauryl ether sulfates with increasing EO lengths from left to right.

For both polymers, increasing the EO length of the surfactant caused a decrease in the compositional range and amount of coacervate formation. The inclusion of a

poly(ethylene oxide) spacer would be expected to increase the size of the palisade layer of the micelle, and in turn decrease the net charge density of the micelle. The decrease in coacervate with a decrease in micelle charge density is in agreement with Dubin's hypothesis.

The examination of micelle charge density and its effects on coacervate formation was also performed using the mixed nonionic/anionic surfactant system, PEG-12 with ALES. In this case the incorporation of a nonionic surfactant can be expected to decrease the surface charge density of the resulting mixed micelle.¹³⁵ The contour phase diagrams for JR30M-SLES and JR30M with the mixed micelle system are shown in Figure 4C-7.

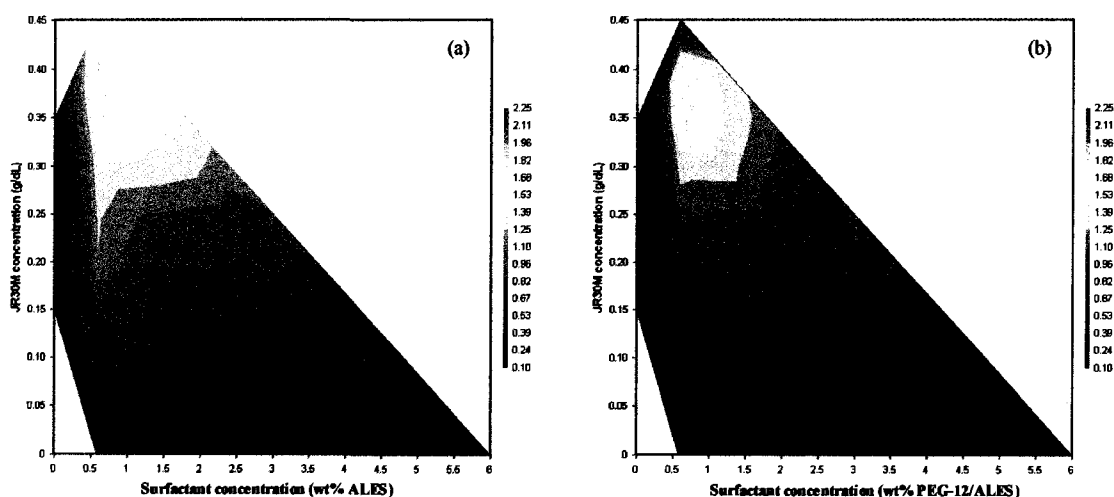


Figure 4C-7. Contour phase diagrams of JR30M with (a) ALES and (b) PEG-12/ALES premixed in a 2:1 ratio.

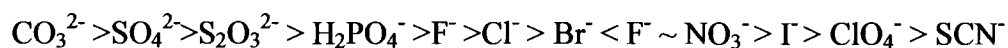
For all compositions, ALES and PEG-12 were premixed at a constant ratio of 2:1 PEG-12:ALES before addition to the polymer, and polymer was added to a 0.17 M NaCl solution in the initial step of sample preparation.

Coacervate formation was observed over a similar compositional range for the anionic surfactant system (Figure 4C-7a) and the nonionic/anionic surfactant system (Figure 4C-7b). The amount of coacervate formed was less in the mixed micelle system, which is in agreement with studies by Dubin where a decrease in micelle charge density results in decreased coacervate formation between polymer and surfactant micelles.²⁰ From the similarity in the phase diagrams, it could be inferred that in the mixed micelle system there could be specific and cooperative binding of the anionic surfactant to the cationic polymer that may cause demixing of the anionic from nonionic surfactant components of the mixed micelles. This is an interesting result that merits further study.

CHAPTER IV-D

CATIONIC HYDROXYETHYLCELLULOSE – ANIONIC SURFACTANT INTERACTIONS IN THE PRESENCE OF SODIUM CHLORIDE

The theories of coacervate formation discussed in Chapters I and IV-B include a dependence on electrostatic interactions between the polymer and surfactant and hydrophobic associations between surfactant tail groups, thus interference with these interactions would be expected to affect coacervate formation.^{7, 20} It is generally accepted that the addition of salt causes screening of either inter- or intramolecular electrostatic interactions.^{7, 16, 18-20} Dubin and coworkers attributed a decrease in coacervate amount due to salt ion screening of intermolecular electrostatic interactions between the polymer and surfactant micelles.²⁰ Conversely, Picullel and Guillemet attributed an increase in coacervate amount to screening of the electrostatic repulsions between anionic surfactant head groups causing an increase in micelle size.^{20, 82} Salts also have an effect on hydrophobic interactions which has been shown for amphipathic systems (PNIPAM) by Bergbreiter and coworkers.¹³⁶ Using a high-throughput gradient method, they investigated the effects of multiple ions from the Hofmeister series,



where the position of the ion in the series is related to its ability to precipitate soluble proteins from aqueous solution.¹³⁷ Ions to the left in the Hofmeister series are usually called kosmotropes (water-structure making). Bergbreiter and coworkers determined that kosmotropes caused the emergence of two distinct steps in the LCST of PNIPAM. They explained the effects of the kosmotropes on the basis of three distinct interactions: (i) polarization by anions of the water molecules that are positioned to hydrogen-bond with

the polymer amide groups, (ii) interference of anions with the hydrophobic hydration and a subsequent reduction in the interfacial tension of the cavity surrounding the polymer backbone and the isopropyl group, and (iii) direct binding of anions to the polyamide.¹³⁶ Analogous effects could occur with the amphipathic surfactant molecules in polymer-surfactant systems, thus interfering with polymer-surfactant interaction.

In addition to the possible effects observed by Bergbreiter and coworkers, salt can interact with each of the components of an oppositely-charged polymer-surfactant system in various ways. An increase in ionic strength could cause conformational collapse of the polyelectrolyte, an increase in size of the surfactant micelles, and/or shielding of the polymer-surfactant ion-ion interaction. At the present time we cannot predict the relative contributions of each of these phenomena to the eventual outcome.

Naderi and coworkers investigated the effect of addition order on polymer-surfactant interactions and coacervate formation in the presence of salt and determined that the order of addition was important, due to interactions at the interface of the polymer and surfactant layers before homogeneous distribution within the sample was achieved.¹⁶ We have expanded upon this idea and using high-throughput screening we have studied the effect of all possible addition orders for the three-component system (polyelectrolyte, surfactant, salt) for a series of PQ-10 polymers with differing molecular weight and charge substitution. The effect of salt concentration on interactions between oppositely-charged polymer and surfactant, relative to polymer CS, was also investigated in this research over a range of surfactant concentrations encompassing the CMC and substantially greater than the CMC.

Effect of Addition Order

The effect of NaCl on PQ-10-SLES interactions was investigated by premixing NaCl with SLES (30:1 SLES:NaCl) before sample preparation. The interactions of LR400, JR125, and JR400 with the SLES-NaCl mixture were investigated. The contour phase diagrams in the absence and presence of salt are shown in Figure 4D-1.

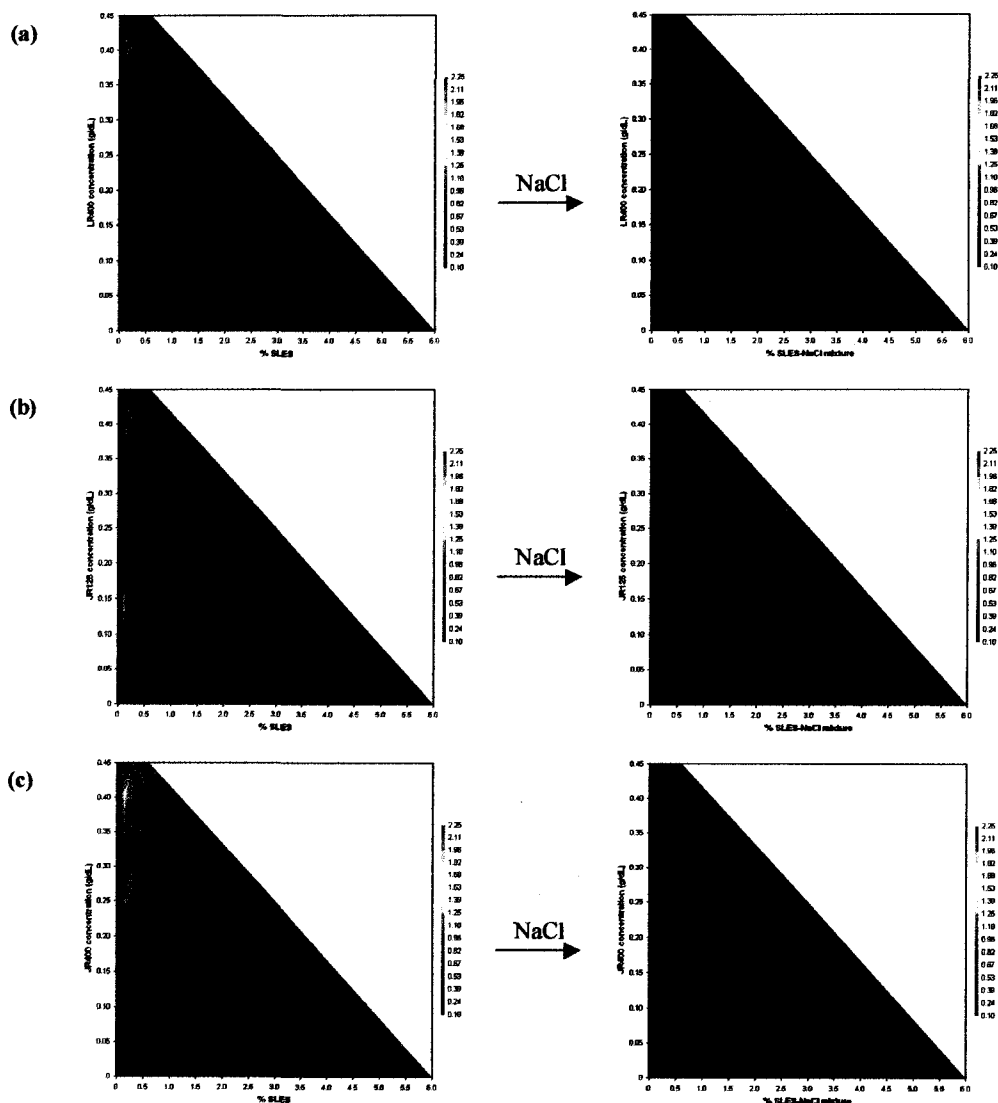


Figure 4D-1. Contour phase diagrams for (a) LR400, (b) JR125, and (c) JR400 with SLES in the absence (left) and presence (right) of NaCl. The SLES-NaCl mixture contains a constant 30:1 ratio of SLES:NaCl.

In all PQ-10-SLES systems, in the absence of NaCl, coacervate formation was observed at low surfactant concentrations. The amount of coacervate formed was dependent on the polymer CS (LR400, JR125) or molecular weight (JR125, JR400), as discussed in Chapter IV-C. In the premixed SLES/NaCl systems, coacervate formation was absent at low surfactant concentrations independent of CS or molecular weight. Coacervate formation was observed at intermediate surfactant concentrations in the presence of salt (1-3 % SLES/NaCl), but was again absent at higher surfactant concentrations. A similar trend was observed by Wang and coworkers with NaCMC and DTAB¹⁹ and they attribute this behavior to screening of polymer-surfactant interactions at low surfactant concentrations and as surfactant concentration increased the micelles became large enough that interactions between the polymer and micelles occurred, resulting in complex formation.¹⁹ Solubilization was observed at high surfactant concentrations.

It is commonly acknowledged that order of addition of components can affect the observed physical state of these polyelectrolyte-surfactant-salt systems.¹⁶ Therefore, it was of interest to investigate the effect of addition order on coacervate formation in the PQ-10-SLES-NaCl systems. This allows us to understand the overall effect of addition order on coacervate formation and will provide insight into the relative importance of the effect of electrolyte on each of the components.

All possible addition orders were examined for three polymers (LR30M, JR30M, and JR400) with SLES and NaCl using the Salt Gradient method (Chapter III).

Abbreviations are used to identify the addition orders, where P represents polymer, S represents surfactant, and E represents electrolyte (salt). The order of the letters is indicative of the order of addition of the components, for example PSE means the

addition order was polymer first, surfactant second, and electrolyte last. For reference, the polymer-SLES contour phase diagrams with no salt added are shown in Figure 4D-2.

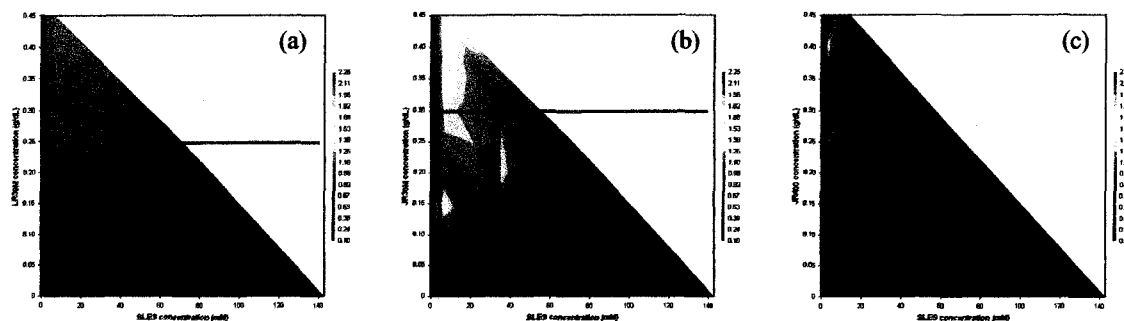


Figure 4D-2. Contour phase diagrams of (a) LR30M, (b) JR30M, and (c) JR400 with SLES in the absence of salt. c^* is represented by the red line.

As discussed in Chapter IV-B, coacervate formation was observed at low surfactant concentrations and as the amount of surfactant increased solubilization occurred for all polymer-SLES systems. This phase separation was attributed to ionic attachment of hydrophobes to the hydrophilic polymer chain and formation of a mesh even below the measured c^* . In JR30M-SLES and LR30M-SLES systems, the highest amount of coacervate was observed above the polymer c^* . In these compositions a polymer entangled network structure is present and with an entangled network, the bound surfactant tail groups are likely to form hydrophobic associations that enhance the mesh structure. Coacervate formation was observed over the broadest compositional range for the high CS, high molecular weight JR30M-SLES system. The ‘no salt’ diagrams (Figure 4D-2) were used as a baseline for understanding the effects of addition order in the presence of salt. The contour phase diagrams for all addition orders with the polymer-SLES-NaCl systems are shown in Figure 4D-3.

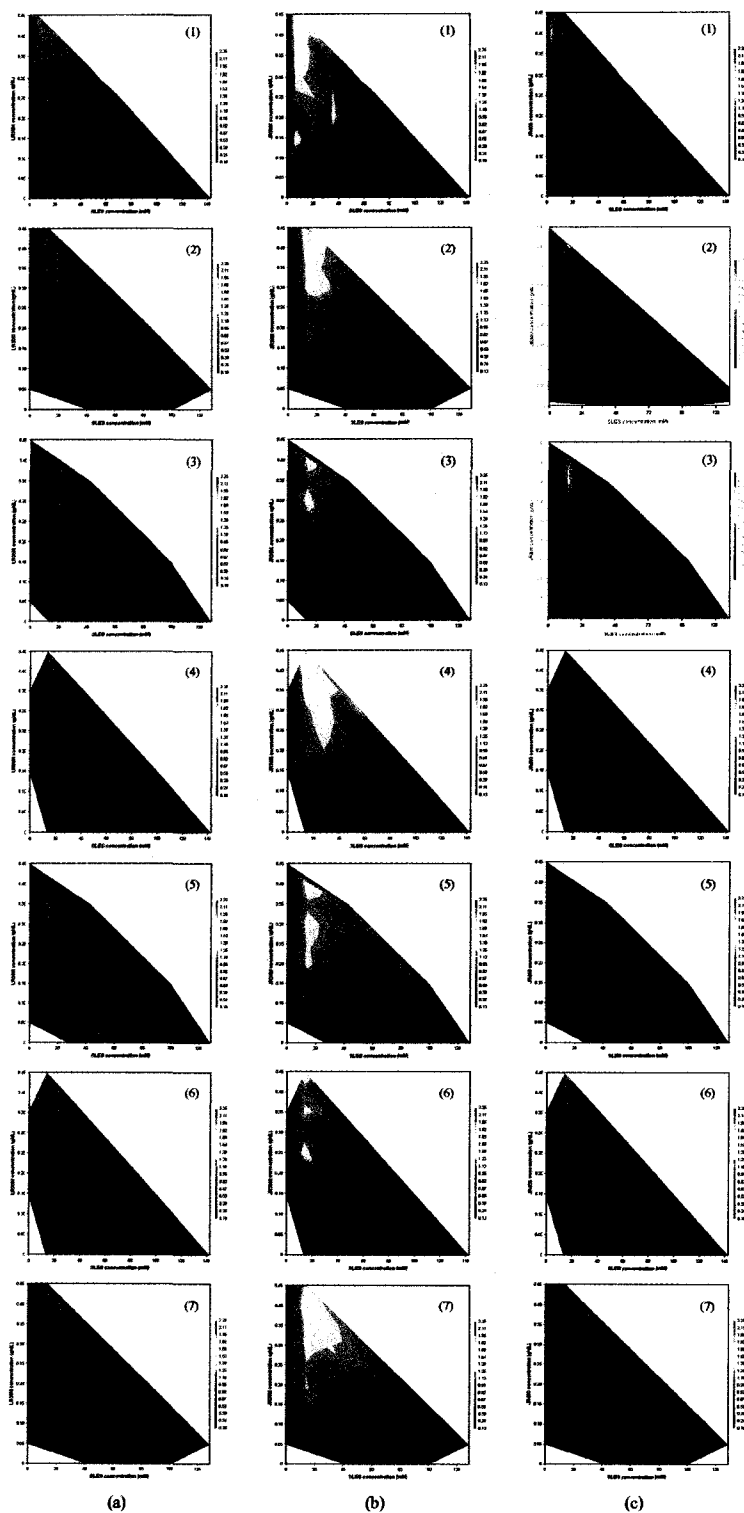


Figure 4D-3. PQ-10-SLES-NaCl contour phase diagrams: (a) LR30M, (b) JR30M, and (c) JR400 with (1) no salt and addition (2) salt, polymer, surfactant; (3) polymer, salt, surfactant; (4) salt, surfactant, polymer; (5) surfactant, salt, polymer; (6) polymer, surfactant, salt; (7) surfactant, polymer, salt.

We observed that the addition of even a small amount of NaCl changes the phase diagram for all systems and this observed change depends on the addition order. It is obvious from these diagrams that the addition of NaCl curtails coacervate formation in dilute solution (< 10 mM) for all systems. This is consistent with dilute solution studies of Dubin and coworkers, who attribute this to screening of intermolecular electrostatic interactions between the polymer and surfactant molecules.²⁰

With addition orders where polymer and salt were added first or second (salt, polymer, surfactant (Figure 4D-3-2) and polymer, salt, surfactant (Figure 4D-3-3)) coacervate formation was dependent on addition order and polymer properties. With the EPS addition order the amount and compositional range of coacervate formation was similar to the no salt system for all polymers. Using the PES addition order coacervate amount decreased for JR30M, but the amount and compositional range of coacervate formation increased slightly for LR30M and significantly for JR400.

With addition orders where surfactant and salt were added first or second (salt, surfactant, polymer (Figure 4D-3-4) and surfactant, salt, polymer (Figure 4D-3-5)) coacervate formation was again dependent on addition order and polymer properties. Using the ESP addition order, a higher coacervate amount and compositional range of coacervate formation were observed with high CS polymers (JR30M, JR400). With the SEP addition order an increased compositional range of coacervate formation was observed for the high molecular weight polymers (LR30M, JR30M) and a decreased coacervate amount was observed for all systems compared to the no salt systems and the ESP addition order. The increased compositional ranges of coacervate formation are

reasonable based on an expected increase in micelle size with the addition of salt to an ionic surfactant.^{7, 18, 19, 60}

With addition orders where surfactant and polymer were added first or second (polymer, surfactant, salt (Figure 4D-3-6) and surfactant, polymer, salt (Figure 4D-3-7)) we observed a decrease in coacervate amount and compositional range of formation with the high molecular weight polymers (LR30M, JR30M) using the PSE addition order and an increase in range and amount with the SPE addition order. Conversely, with low molecular weight JR400 coacervate amount and compositional range of formation increased with the PSE addition order and decreased with the SPE addition order.

Effect of Salt Concentration

The Salt Gradient method was used to emphasize the effect of order of addition in systems including salt. To better understand the effect of ionic strength it was important to construct phase diagrams at constant salt concentration. The Constant Salt method (Chapter III) was used for preparation of these phase diagrams and the addition order was PES. Interactions of LR30M and JR30M with SLES in the presence of NaCl were studied and three contour phase diagrams were generated for each polymer-SLES system: no salt, 43 mM NaCl, and 130 mM NaCl. The LR30M-SLES-NaCl and JR30M-SLES-NaCl contour phase diagrams are shown in Figure 4D-4.

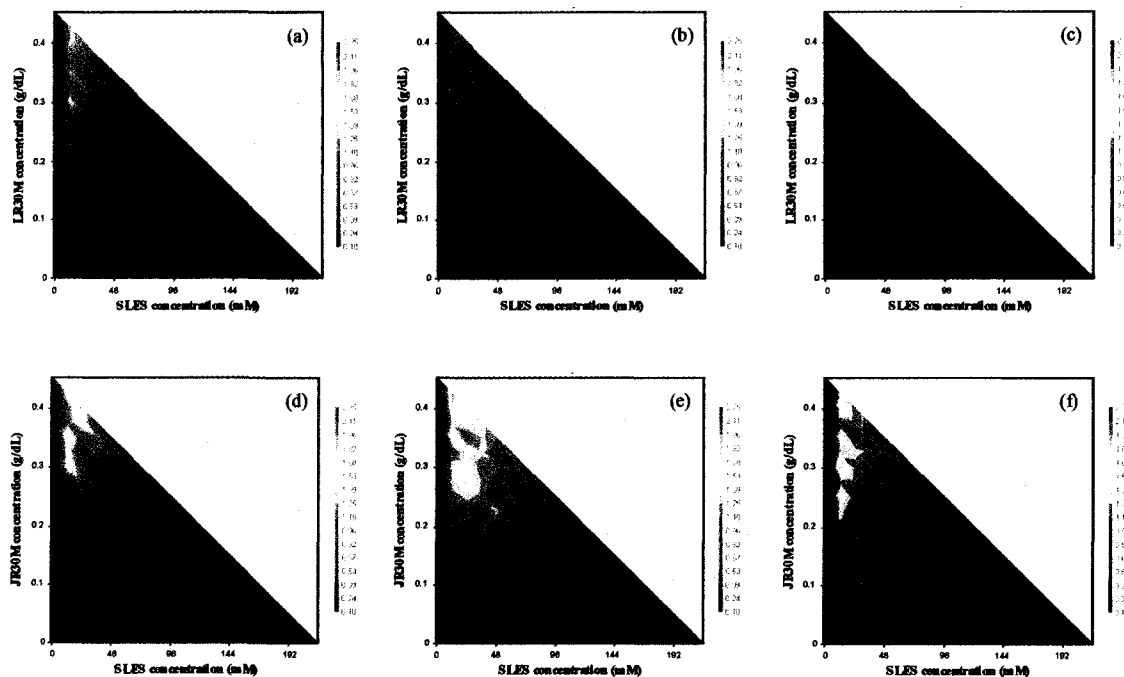


Figure 4D-4. Contour phase diagrams of LR30M - SLES (a-c) and JR30M – SLES (d-f) with 0 mM, 43 mM, and 130 mM NaCl. NaCl concentration increases from left to right.

In the LR30M-SLES ‘no salt’ phase diagram (Figure 4D-4a) coacervate formation similar to that discussed in Chapter IV-C was observed. With the addition of 43 mM NaCl (Figure 4D-4b), the amount of coacervate formed was less than in the ‘no salt’ system. This is likely due to screening of ion-ion interactions between the polymer and surfactant by the salt molecules, inhibiting coacervate formation. However, the compositional range of coacervate formation increased to include lower polymer concentrations. At 130 mM NaCl (Figure 4D-4c), very little coacervate formation was observed. This is probably due to near complete screening of polymer-surfactant interactions at this high salt concentration. Similarly, Wang and coworkers observed complete screening of electrostatic interactions with poly(dimethyldiallylammonium chloride)-SDS/Triton X-100 systems at high surfactant concentrations.²⁰

In the JR30M-SLES 'no salt' phase diagram (Figure 4D-4d) coacervate formation similar to that discussed in Chapter IV-C was observed. With the addition of 43 mM NaCl (Figure 4D-4e) the amount of coacervate and the compositional range of coacervate formation increased. The compositional range of coacervate formation increased further in the 130 mM NaCl system relative to the 43 mM NaCl system, however where coacervate occurred in both diagrams, there was a lesser amount at the higher salt concentration. This could be due to enhanced screening of electrostatic interactions at the high salt concentration causing a reduction in the amount of coacervate formed. The increased compositional range of coacervate formation could be due to either "salting out" of the polymer-surfactant complex or the formation of larger surfactant micelles.

Polymer charge substitution can be expected to influence the degree of surfactant binding in the presence of added salt because salt interferes with electrostatic attractions.¹⁹ This parameter was explored using LR30M and JR30M, both with approximately the same molecular weight, but the charge substitution of JR30M is twice that of LR30M (0.48 and 0.25, respectively). In general, coacervate amount was greater for the JR30M-SLES-NaCl systems, which can be attributed to increased surfactant binding with increased charge substitution, as discussed in Chapter IV-C. With 43 mM NaCl the amount of coacervate formed increased compared to the 'no salt' system for JR30M-SLES, but decreased for LR30M-SLES. It is probable that screening of electrostatic interactions by salt molecules was more efficient in the lower charge substituted LR30M-SLES system, thus less coacervate was able to form. With 130 mM NaCl, coacervate formation was completely screened in the LR30M-SLES system, and despite the compositional range of coacervate formation increasing for the JR30M-SLES

system, the amount of coacervate formed was less with 130 mM NaCl than with 43 mM NaCl at specific compositions. We conclude that the interactions between low charge substituted PQ-10 and oppositely-charged surfactant are readily shielded by salt, whereas the interactions between high charge substituted PQ-10 and oppositely-charged surfactant persist and extend over a broader compositional range in the presence of NaCl up to 130 mM.

It is important to note that for the LR30M-SLES-NaCl system, similar trends in coacervate formation were observed with the Salt Gradient method (10-40 mM NaCl) and the Constant Salt method. In both methods, an increase in compositional range of coacervate but decrease in coacervate amount was observed. On the contrary, for the JR30M-SLES-NaCl system, opposing trends were observed between the two salt addition methods. At a comparable salt concentration, the compositional range and amount of coacervate increased with the Constant Salt method but compositional range was approximately constant and coacervate amount decreased with the Salt Gradient method. From these results, it appears that optimum conditions are required for coacervate to form. As discussed previously, salt may affect polymer-surfactant interactions through a variety of pathways, including screening of ion-ion interactions, induction of polymer collapse, or increasing the size of the surfactant micelle. In a single polymer-surfactant system, competition between these effects could lead to a multitude of end results. Certainly, these effects and the end results are also dependent on the polymer and surfactant properties, the component concentrations, and the addition order of multiple components. With this vast array of possible interactions and influencing factors, the

research presented here provides a valuable basis for future studies in the area of polymer-surfactant interaction in the presence of salt.

CHAPTER IV-E

INVESTIGATION OF CATIONIC POLY(VINYLPYRIDINIUM HYDROCHLORIDE)
– ANIONIC SURFACTANT INTERACTIONS

In the previous chapters, the interactions of cationic polysaccharides with oppositely-charged surfactants were found to be dependent on a number of polymer properties, including molecular weight and charge substitution. All interactions between these polymers and surfactant occurred via the cooperative mechanism of coacervate formation described by Goddard.^{7,8} However, as discussed in Chapter I, two potential mechanisms of coacervate formation have been described for oppositely-charged polymer-surfactant complexes, the Goddard mechanism and the Dubin mechanism.²⁰ In the Goddard mechanism, site-specific interactions occur, driven through ion-ion interaction and hydrophobic association. In the Dubin mechanism, interactions occur between two macroions, such as the polymer interacting with surfactant micelles. The Goddard mechanism has been postulated for a variety of polymer systems, while the Dubin mechanism has been primarily discussed for PDADMAC.

It was of interest in this research to investigate systems that differed fundamentally from polysaccharides in order to attempt to understand the verisimilitude of each of the Goddard and the Dubin theories. Cationic poly(vinylpyridines) were chosen because, in contrast to the cellulose derivatives, they have a hydrophobic and flexible backbone and two isomers are readily available so that the influence of the position of the cationic charge relative to the polymer backbone could be investigated. The polymers used in this research were prepared via RAFT so the PDI values were low,

which was important because polymer molecular weight has been shown to influence polymer-surfactant interactions.^{15, 62-64}

Polymer Solution Conformation

The solution properties of poly(4-vinylpyridinium hydrochloride) (P4VP) and poly(2-vinylpyridinium hydrochloride) (P2VP) were investigated to gain understanding of the effects of charge isomerization on solution properties that could impact the interaction of these polymers with anionic surfactant.

Static Light Scattering

Static light scattering (SLS) was performed using the cationically-charged polymers in salt-free aqueous solution to directly mimic the systems investigated via high-throughput screening and other techniques. Low molecular weight P4VP (9 000 g/mol) was investigated at five concentrations (Figure 4E-1).

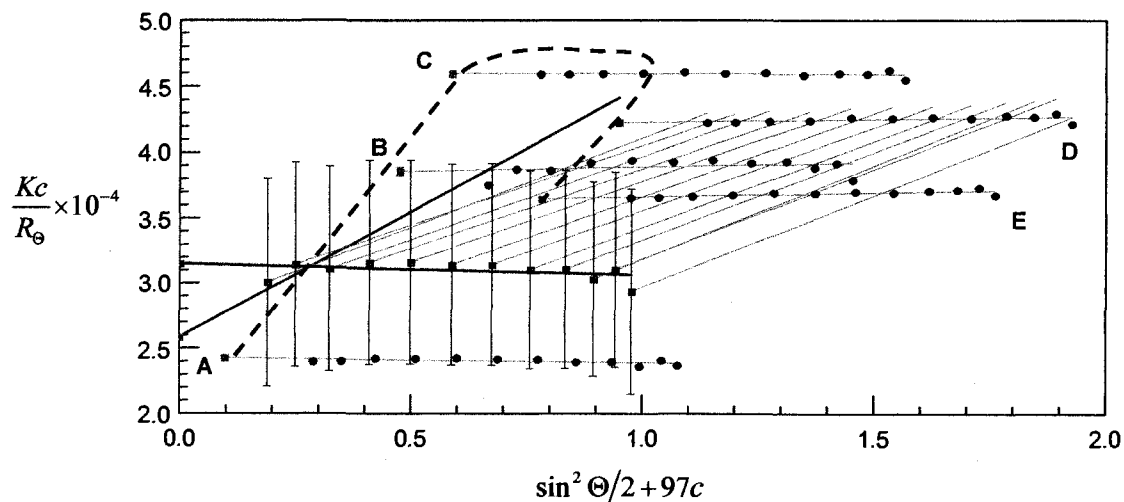


Figure 4E-1. Zimm plot of low molecular weight P4VP in filtered HPLC grade water. A-E indicate concentrations of P4VP investigated (1.0, 4.9, 6.0, 8.0, 9.7 mg/mL). Blue dashed line follows curvature of the plot.

Positive curvature of Zimm plots is common in protein and polyelectrolyte solutions, where the curvature is indicative of association between solute molecules and aggregation of macromolecules at high concentrations.¹³⁸ Aggregation at high concentrations may be due to blocky charge distribution, too few charges, and/or temporal complexes between polymers where counterions are associated with more than one polyelectrolyte. In our system, the formation of aggregates due to a small amount of charge was unlikely because the percent ionization for P4VP was 86 % (Chapter III). In order to determine the second virial coefficient (B), the high concentrations that were responsible for curvature were eliminated (Figure 4E-2).

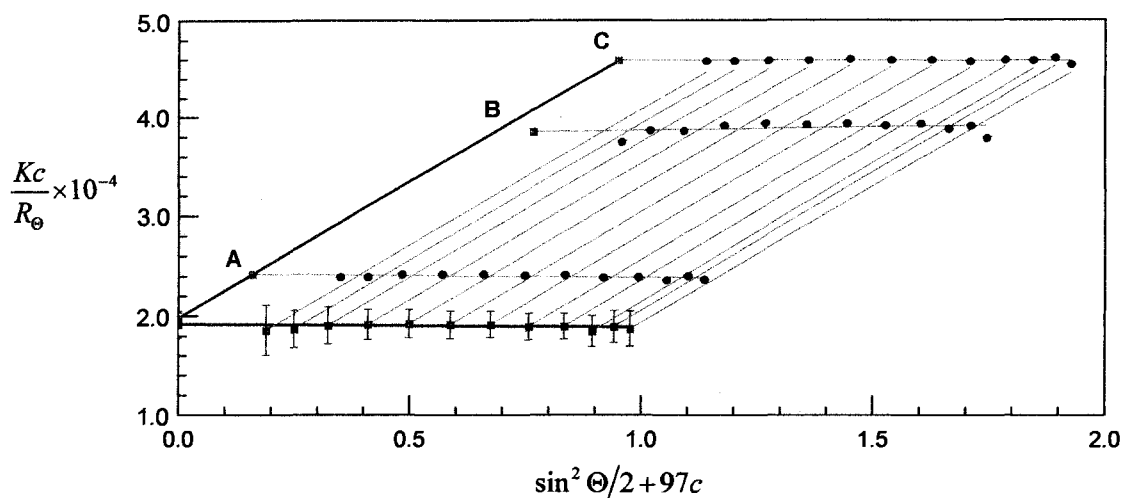


Figure 4E-2. Zimm plot of low molecular weight P4VP in filtered HPLC grade water at low concentrations (A-C = 1.0, 4.9, 6.0 mg/mL).

For P4VP, B was 2.2×10^{-2} (Equation 3-8). The positive number indicates that water is a good solvent for this cationic polymer.

Low molecular weight P2VP (6 000 g/mol) was investigated at four concentrations (Figure 4E-3).

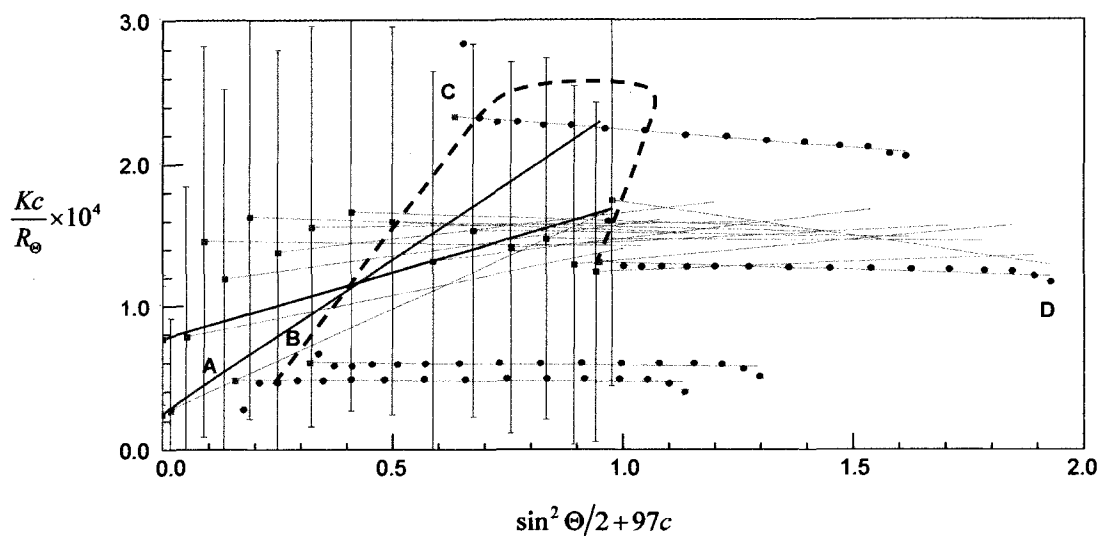


Figure 4E-3. Zimm plot of low molecular weight P2VP in filtered HPLC grade water. A-D indicate concentrations of P2VP investigated (1.0, 2.0, 4.0, 6.0 mg/mL). Blue dashed line follows curvature of the plot.

Similar to the P4VP Zimm plot with high concentrations, curvature was observed with P2VP, again indicative of macromolecular associations at high concentrations.¹³⁸ The highest concentration was eliminated from this data set to determine B (Figure 4E-4).

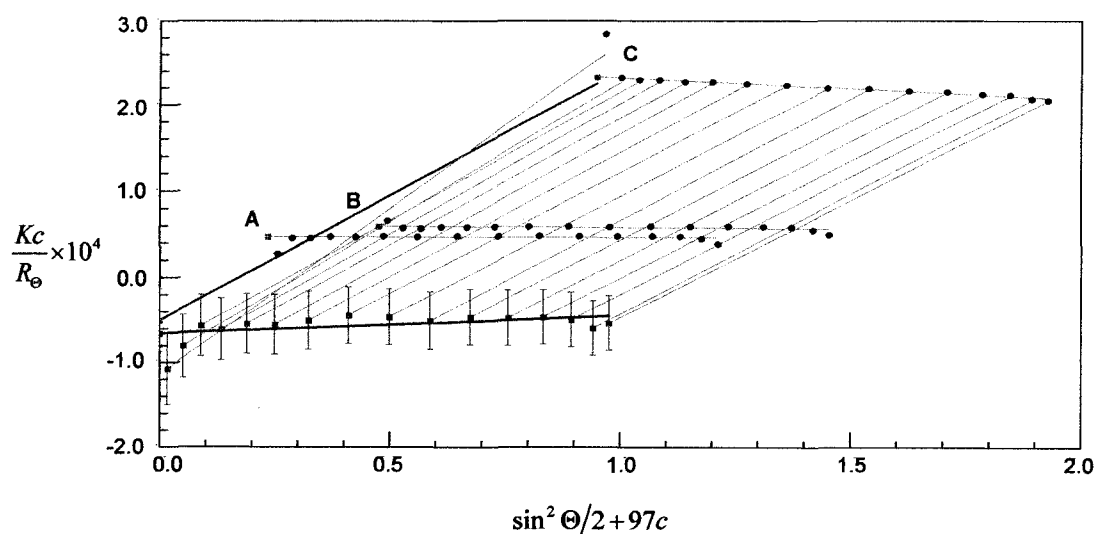


Figure 4E-4. Zimm plot of low molecular weight P2VP in filtered HPLC grade water at low concentrations (A-C = 1.0, 2.0, 4.0 mg/mL).

For P2VP, B was -1.4×10^{-1} . Negative B values have been attributed to both association of solute molecules and charge fluctuations in macro-ion solutions. The latter has been reserved for macroions with differing charges, but an average net charge of zero, such as proteins and weak electrolytes.¹³⁸ P2VP does not have a net charge of zero, thus the negative B value was attributed to poor polymer-solvent interactions.

Surface Tensiometry

Surface tension measurements were also performed on P4VP and P2VP in salt-free aqueous solution, with initial solution concentrations of 0.15 g/dL. The results are presented in Figure 4E-5 with the sodium dodecylbenzene sulfonate (SDBS) surface tension curve as a point of reference (Chapter III).

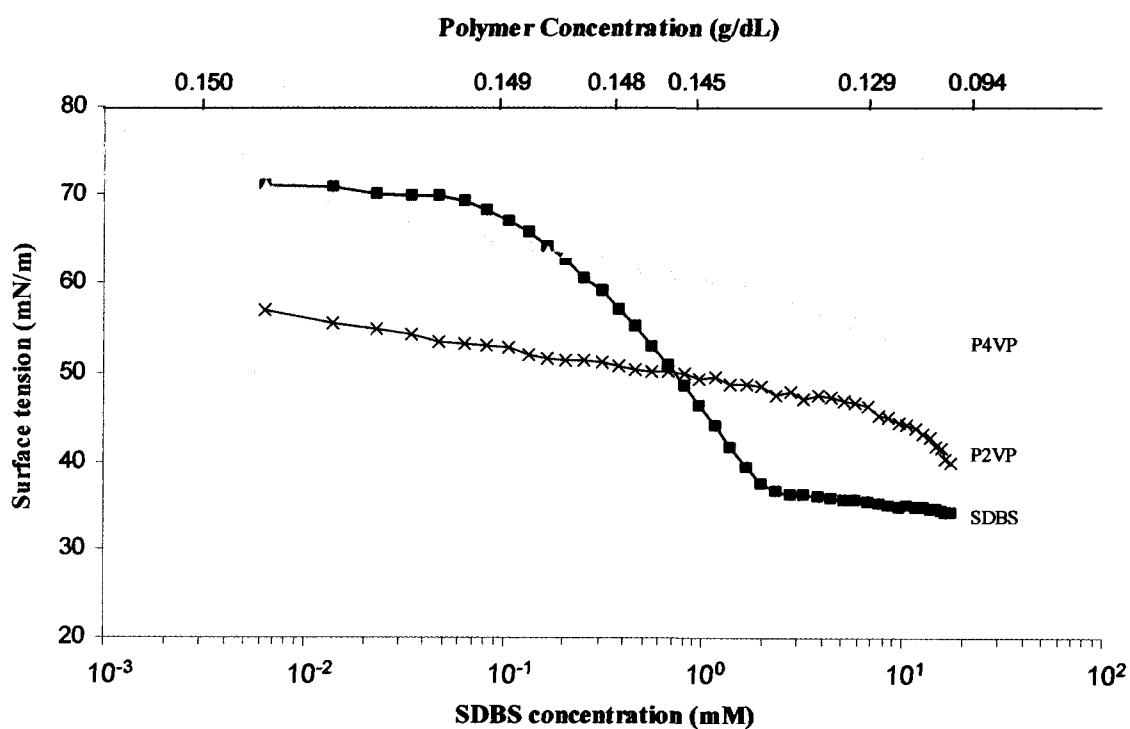


Figure 4E-5. Surface tension as a function of concentration.

It is clear from Figure 4E-5 that while both P4VP and P2VP adsorb at the air/water interface, P2VP was more surface active than P4VP. The increased surface activity of P2VP compared to P4VP is in agreement with the B values determined with SLS, where P2VP has poorer interaction with water. It is possible that the cationic groups of P4VP are oriented in such a way that they are more accessible to water, masking the hydrophobicity of the polymer backbone.

Dynamic Light Scattering

Dynamic light scattering (DLS) is commonly used to determine the hydrodynamic size of polymers in solution, however, as discussed in Chapter IV-B, error is inherent in determination of the hydrodynamic size of polyelectrolytes in salt-free solution due to electrostatic effects on polymer diffusion.¹³² Sedláč has demonstrated that the fast diffusion mode (D_f) is sensitive to charge interaction parameters.¹³² DLS studies were performed for both P4VP and P2VP in salt-free aqueous solution at a constant concentration of 0.15 g/dL and the plot of relaxation time (τ) for both polymers is shown in Figure 4E-6.

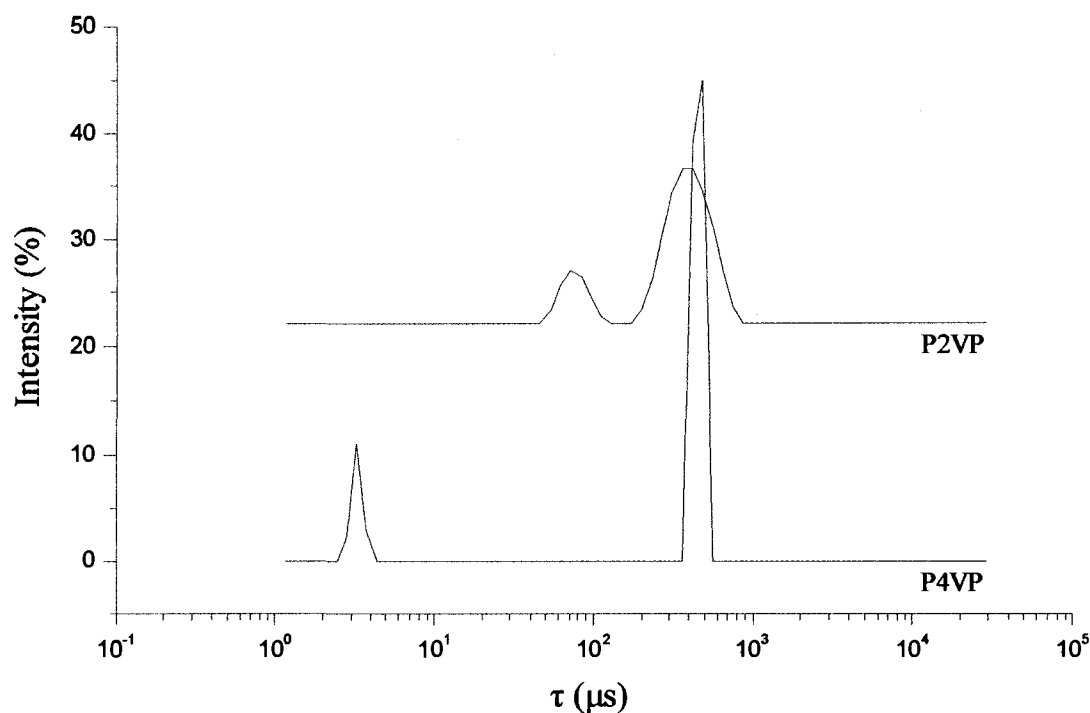


Figure 4E-6. Relaxation time (τ) of 0.15 g/dL P4VP and P2VP.

In both polymer solutions we observed a bimodal distribution of relaxation times, which has been observed previously by Schmidt and coworkers for quaternized P2VP.¹³⁹ The slow mode diffusion rate, D_s , was approximately the same for both P4VP and P2VP ($4.8 \times 10^2 \mu\text{s}$), which is reasonable given the similarity in polymer structure and molecular weight and the low response of D_s to changes in polymer-solvent compatibility.¹³² The fast diffusion process of P4VP (3.3 μs) was much faster than that of P2VP (71 μs). This large difference is in agreement with the sensitivity of D_f to charge interactions.¹³² It is generally known that the diffusion of polyelectrolytes in salt-free solution is faster than that of analogous neutral polymers due to the intermolecular electrostatic repulsions.¹³² The faster diffusion of P4VP in the fast mode is indicative of

greater intermolecular electrostatic repulsions in this polymer solution compared to the P2VP solution.

Solution Viscometry

Polymer critical overlap concentration (c^*) was shown to have an impact on coacervate formation in the polysaccharide systems (Chapter IV-B) so c^* values were determined for all poly(vinylpyridinium hydrochloride) polymers studied in this research.

Apparent viscosities were measured and reduced viscosity, $\frac{\eta_{sp}}{c}$, was calculated as

described in Chapter III. The reduced viscosities were plotted versus the polymer concentration (c) (Figure 4E-7).

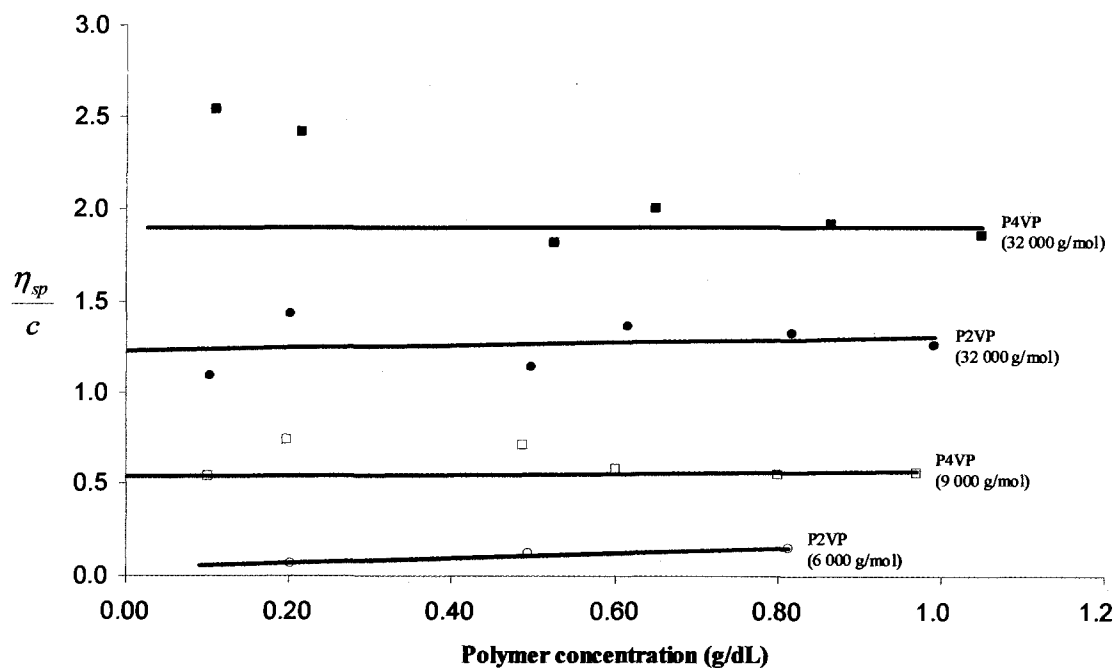


Figure 4E-7. Reduced viscosities of high and low molecular weight P4VP and P2VP in DI water at 25 °C.

Despite the absence of salt in these systems, the deviation of the reduced viscosity curve from linearity ordinarily observed with polyelectrolytes occurred only in the high

molecular weight P4VP system; only points in the linear region were considered in determining intrinsic viscosity, $[\eta]$, for this system.¹⁴⁰ The reduced viscosities were found to be practically linear over the appropriate concentration ranges and $[\eta]$ was obtained by extrapolation of the reduced viscosities to infinite dilution, while neglecting data points that were clearly high due to polyelectrolyte expansion.¹⁴⁰ The linearity of the curves also allows for calculation of the Huggins constant (k') using the Huggins equation

$$\frac{\eta_{sp}}{c} = [\eta] + k'[\eta]^2 c \quad \text{Equation 4E-1.}$$

The Huggins constant is a parameter describing solute-solvent interaction and has been shown to decrease as polymer molecules become more extended in solution.¹⁴⁰⁻¹⁴³ The experimentally determined intrinsic viscosities were employed in calculating c^* from the Berry number, $[\eta]c^*$, with the assumption of non-interacting Gaussian coils so that $[\eta]c^* = 1$. The P4VP and P2VP values for $[\eta]$, k' , and c^* are shown in Table 4E-I.

Table 4E-I. P4VP and P2VP values for $[\eta]$, k' , and c^* .

Polymer	\overline{M}_n (g/mol)	$[\eta]$	k'	c^* (g/dL)
P4VP	9 000	0.54	0.080	1.9
P4VP	32 000	1.9	0.034	0.53
P2VP	6 000	0.045	67	22
P2VP	32 000	1.2	0.047	0.83

The solution viscometry studies correspond with the observations from the light scattering and surface tensiometry studies. Polymers in a good solvent are expected to

have higher viscosities than polymers in a poor solvent, and this was observed for both the high and low molecular weight P4VP compared to the corresponding P2VP. In a good solvent, the polymer will be hydrated and swollen providing a higher viscosity. Polymer in a poor solvent will exist in a collapsed conformation, which causes the viscosity to be lower. This is also in agreement with the observation of the polyelectrolyte effect only in the high molecular weight P4VP system. Huggins constant values greater than 1 generally imply aggregation.¹⁴⁴ The low Huggins constants for high and low molecular weight P4VP indicate little hydrodynamic interaction, and thus little or no aggregation of polymer molecules in solution. The apparent viscosities measured for the low molecular weight P2VP were similar to that of the solvent and therefore the calculated $[\eta]$ may be artificially low. This resulted in the very high Huggins constant and c^* for low molecular weight P2VP. Despite this instrumental limitation, it is clear that low molecular weight P2VP was below c^* at these concentrations. The concentration of the P4VP and P2VP premixes used in our research was 0.25 g/dL so all compositions investigated for both polymers were below c^* .

From the polymer solution studies, we know that water is a good solvent for P4VP. In dilute aqueous solution, it is likely that this polymer adopts an extended conformation where the cationic charges are presented to the solvent and the hydrophobic backbone is shielded from the water. The P2VP system contrasts with that of P4VP. Water is a poor solvent for P2VP, although it is soluble in aqueous solution due to the presence of the cationic charges. The surface tension of water was considerably reduced in the presence of P2VP, indicating hydrophobicity of the polymer. The positioning of the cationic charge near the polymer backbone possibly requires adoption of a polymer

conformation where both the cationic charges and the hydrophobic polymer backbone are in contact with water, possibly in a collapsed or coiled conformation as evidenced by the viscometry studies.

Polymer – Surfactant Complex Formation

Coacervate Physical Description

It was observed visually that the coacervate formed in poly(vinylpyridinium hydrochloride)-surfactant systems had different physical characteristics than that of the polysaccharide-surfactant systems discussed in Chapters IV-B-D. The separated phase consisted of a fine particulate colloidal dispersion. Photographic images of representative samples are shown in Figure 4E-8.

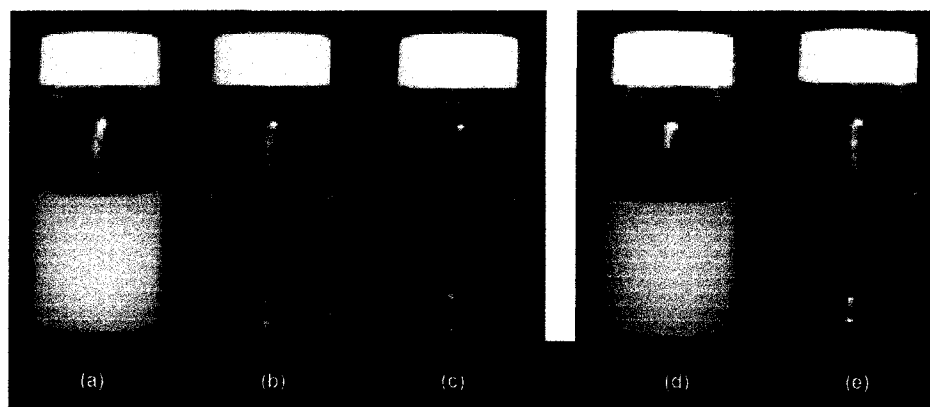


Figure 4E-8. Photographic images of coacervate formed in cationic poly(vinylpyridinium hydrochloride)-anionic surfactant mixed systems at different compositions: (a) P4VP-SDBS, high coacervate; (b) P4VP-SDBS, low coacervate; (c) P4VP-SDBS, no coacervate; (d) P2VP-SDBS, high coacervate; (e) P2VP-SDBS, no coacervate.

The first three samples (Figure 4E-8a-c) were formed using the P4VP-SDBS system and the last two samples (Figure 4E-8d-e) were formed using the P2VP-SDBS system. The

coacervate formed in these systems was representative of that formed for all poly(vinylpyridinium hydrochloride)-surfactant systems. The yellow tint observed with P2VP, due to the chain transfer agent, did not affect the transmittance measurements. It was apparent from visual observation that the macroscopic coacervate properties were similar across these systems. Due to the difference in coacervate appearance, and subsequently a difference in the color gradient scale and the maximum absorbance measurements, contour phase diagrams of poly(vinylpyridinium hydrochloride) and polysaccharide systems were not directly comparable.

Poly(vinylpyridines) are intrinsically hydrophobic and insoluble in water, but become cationically charged and water-soluble at acidic pH. In our experiments we chose to use an initial solution of the poly(vinylpyridine) at approximately 86 % ionization (Chapter III). The anionic surfactants studied in this research have neutral or slightly basic pH values and were added directly to the poly(vinylpyridinium hydrochloride) solution. It would have been possible to work at constant pH by performing back titration of the final mixture with a suitable acid. However, back titration would inevitably change the ionic strength of the system, which has previously been shown to change the characteristics of the coacervate system.^{19,20} This would have introduced an uncontrollable variable and back titration was therefore not performed.

Because an increase in pH upon combination with surfactant could potentially affect the percent ionization of the polymer, causing insolubility, the effect of pH increase on poly(vinylpyridinium hydrochloride) water solubility was investigated to ensure that phase separation observed upon surfactant addition was due to coacervate formation. The pH of five representative samples was determined using an Accumet

Scientific AR-15 pH meter after all components were added and the samples were mixed (Table 4E-II). The pH of the initial P2VP solution was 2.74 and the pH of the surfactant used was 7.04.

Table 4E-II. pH readings of representative polymer-surfactant mixtures.

Sample	P2VP concentration (g/dL)	SDBS concentration (mM)	pH reading	Phase separation
1	0.1	0.0	2.8	clear
2	0.2	0.0	2.6	clear
3	0.09	160	5.1	hazy
4	0.04	220	5.6	clear
5	0.01	240	6.6	clear

A sample of 0.04 g/dL P2VP was titrated with 1.0 *N* NaOH and phase separation due to water insolubility was observed at pH 4.6. The addition of surfactant increased the pH of samples 1-3 above 4.6, but phase separation was observed only in sample 3. The lack of phase separation for P2VP- SDBS systems at pH > 5.1 (samples 4-5) indicated that surfactant was bound to the polymer and resolubilization occurred at these surfactant concentrations. These are the characteristics normally associated with polymer-surfactant complex coacervates.

Titration of 0.04 g/dL P4VP with 1.0 *N* NaOH produced a yellow, dispersed, separated phase at pH 4.2. A 0.04 g/dL P4VP- 220 mM SDBS mixture was investigated and the pH was 6.1. A white, hazy and dispersed separated phase was observed in this sample. The difference in appearance of the separated phase again indicated that phase separation was not due to inherent water insolubility of the polymer as a function of pH increase.

P4VP-SDBS Interactions

Surface tension measurements were utilized to determine the critical aggregation concentration (CAC) and the critical micelle concentration in the presence of polymer (CMC2) of the P4VP-SDBS system. The P4VP concentration was held constant at 0.15 g/dL and the surface tension was recorded as a function of increasing surfactant concentration. The results are shown in Figure 4E-9. The surface tension curves of pure SDBS and P4VP are included for reference.

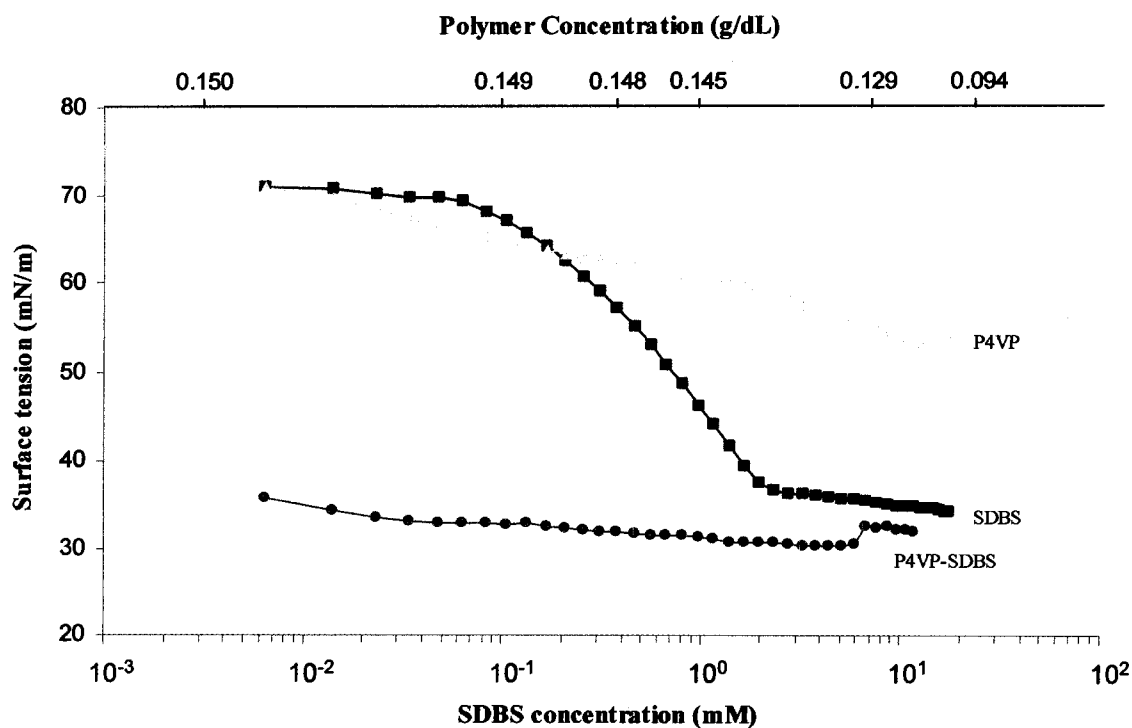


Figure 4E-9. Surface tension as a function of concentration.

As shown in Figure 4E-5, the surface tensions of P4VP at 0.15 g/dL and SDBS at 6.4×10^{-3} mM individually were each close to that of water (72 mN/m). However, when P4VP and SDBS were combined at this composition, the measured surface tension was 35 mN/m. This indicated strong polymer-surfactant interaction to form surface-active

species upon combination of the polymer and surfactant at very low surfactant concentrations. In this system, the interactions were so strong that neither a CAC nor a CMC2 were detected in the range studied. It is likely that the CAC occurred at a concentration less than 6.4×10^{-3} mM and therefore all systems investigated using high-throughput screening were at concentrations well above the CAC.

The interaction of P4VP and SDBS at three different polymer concentrations was also investigated using surface tensiometry. The polymer concentrations were held constant (0.15, 0.10, and 0.050 g/dL) while the surfactant concentration was increased (Figure 4E-10).

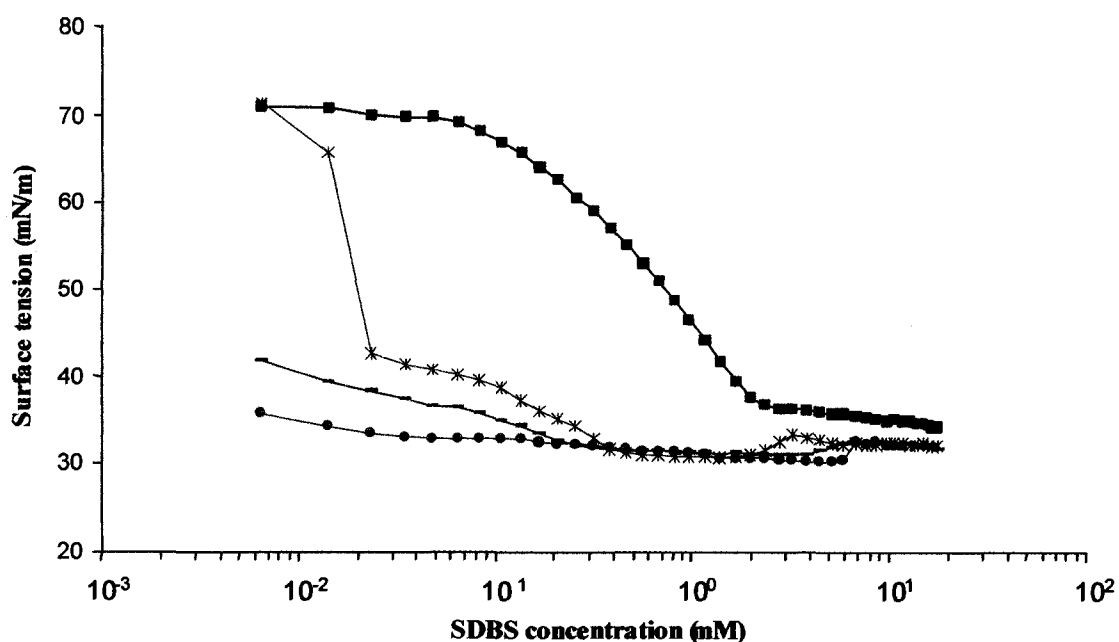


Figure 4E-10. Surface tension as a function of surfactant concentration. ■ SDBS, ● 0.15 g/dL P4VP-SDBS, - 0.10 g/dL P4VP-SDBS, * 0.050 g/dL P4VP-SDBS.

The 0.15 g/dL and 0.10 g/dL P4VP-SDBS curves both showed the presence of a highly surface active species, with the higher P4VP concentration being the more surface active. At 0.21 mM these two curves converged on one another. The 0.050 g/dL P4VP-SDBS

system had a different profile than the others. Below 6.4×10^{-3} mM the surface tension was 72 mN/m, the same as the pure polymer, pure surfactant, and water. Beginning at 6.4×10^{-3} mM a decrease in surface tension was observed, ending in a plateau at 2.9×10^{-2} mM, corresponding to the CAC of this system. A second plateau occurred at 45 mM corresponding to the CMC2. In surface tensiometry of polymer-surfactant complexes, the initial lowering of surface tension is attributed to adsorption of polymer-surfactant complexes at the air-water interface, where the hydrophobicity of the complexes formed is the primary driving force.⁷ The water-solubility of P4VP is conferred by the cationic charges imparted along the hydrophobic backbone. Thus electrostatic interaction of these charges with SDBS formed complexes consisting of a hydrophobic polymer backbone with bound surfactant groups. The very low surface tensions observed in Figure 4E-10 show that these hydrophobic complexes were driven strongly to the air-water interface. As discussed previously, P4VP was below c^* at all concentrations investigated so that the only difference in solution properties for 0.15 g/dL, 0.1 g/dL and 0.05 g/dL P4VP was the number of polymer molecules in solution. At 0.15 g/dL P4VP the surface was saturated at a concentration less than 6.4×10^{-3} mM indicating significant complexation. At 0.05 g/dL P4VP, the onset of surface activity occurred between 6.4×10^{-3} mM SDBS and 1.4×10^{-2} mM SDBS, which is more than one order of magnitude lower than SDBS alone. For this polymer concentration both a CAC and CMC2 were distinguishable, the CAC at 2.3×10^{-2} mM SDBS and the CMC2 at about 0.4 mM SDBS. These values are lower than the CMC of SDBS alone, 2.4 mM, and this lends credence to the idea that P4VP-SDBS surface-active complexes

are formed and that these are more surface active than either the polymer or the surfactant.

Dynamic light scattering was used to investigate complex formation between P4VP and SDBS. As discussed previously, the apparent hydrodynamic diameter (D_H) determined in DLS studies of polyelectrolyte in salt-free solutions is not indicative of the true polymer D_H . However, for comparison of particle size in pure polymer solution with particle size in polymer-surfactant solutions, the polymer D_H was employed, similar to studies by Zhou et al.⁹⁵ DLS studies of P4VP-SDBS solutions were performed at constant polymer concentration (0.15 g/dL) and surfactant concentrations above and below the CMC (between 0.029 - 43 mM) and the results are shown in Figure 4E-11.

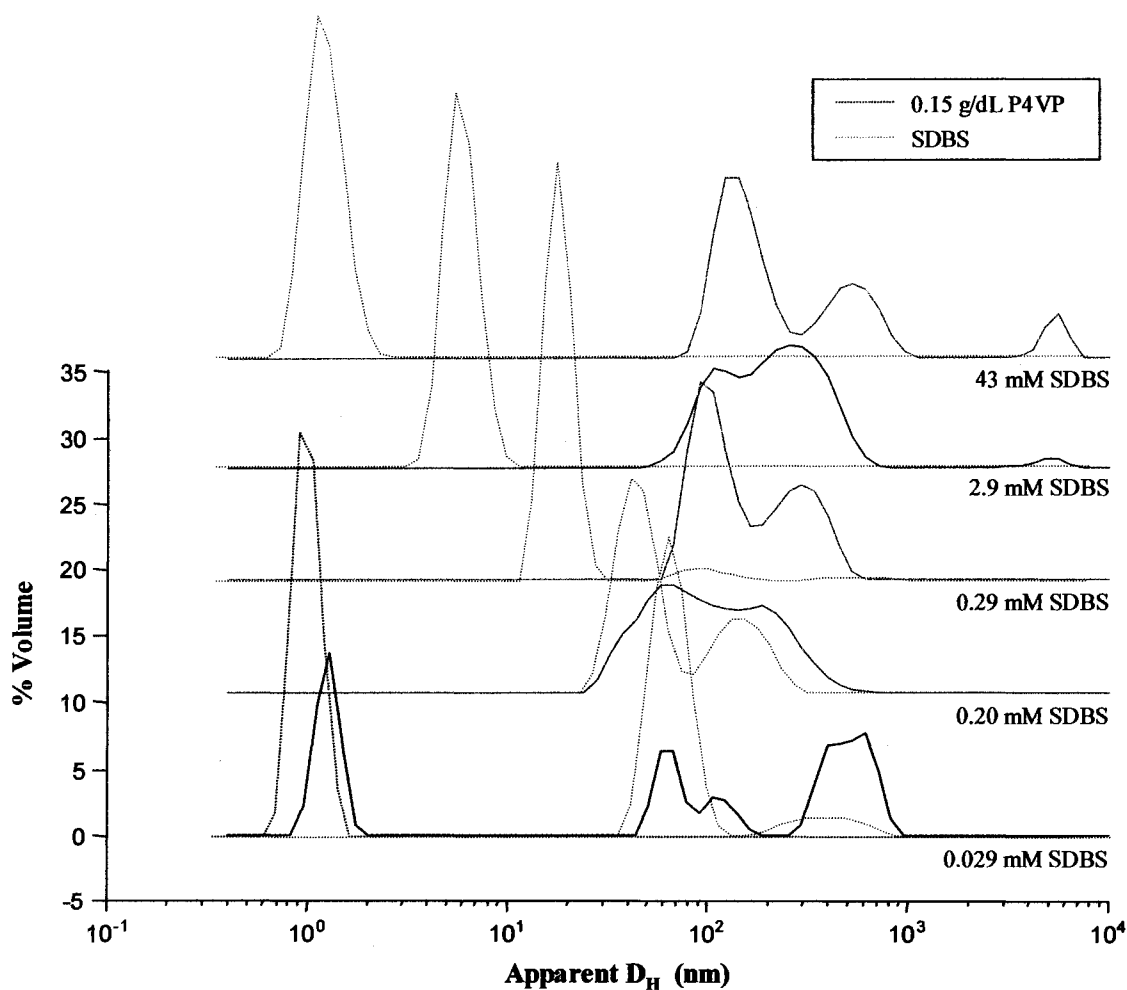


Figure 4B-11. Dynamic light scattering data for 0.15 g/dL P4VP – SDBS mixtures.

As discussed previously (Figure 4E-6), P4VP in salt-free solution exhibited a fast diffusion process due to intermolecular electrostatic repulsions that results in an artificially low value of D_H . Thus the peak at 1.1 nm for P4VP corresponds to the character of the polyelectrolyte solution and not the actual size of polymer in solution. This peak was observed in the P4VP-SDBS mixture with the lowest SDBS concentration (0.029 mM SDBS), but for all P4VP-SDBS compositions with SDBS greater than 0.029 mM SDBS, the peak at 1.1 nm corresponding to uncomplexed P4VP was not present.

This indicates that uncomplexed P4VP was present with 0.029 mM SDBS, and that all polymer was complexed at SDBS concentrations above 0.029 mM SDBS. This agrees with the strong interactions between P4VP and SDBS observed in surface tensiometry studies.

The D_H was also determined for SDBS in salt-free solution for all concentrations studied with DLS. A decrease in D_H was observed with increasing SDBS concentration, with large values below CMC. This is likely an artifact due to impurity in the surfactant, as discussed for SLES (Chapter IV-B). For the P4VP-SDBS system at 0.029 mM SDBS, a peak at 400 nm was observed that corresponded with a peak observed in SDBS solution at this concentration, and is likely due to surfactant impurity. A similar peak was observed at 0.20 mM SDBS, but at higher SDBS concentrations this peak was absent.

A bimodal peak corresponding to polymer-surfactant complexes was observed for all P4VP-SDBS compositions studied. At 0.029 mM SDBS, a total of four peaks were observed for the P4VP-SDBS mixture, corresponding to the character of pure polymer (1.1 nm) and pure surfactant (400 nm), and polymer-surfactant complexes (60 nm and 120 nm). This is indicative of coexistence of polymer, surfactant and complexes at this low surfactant concentration. Complex formation between the polymer and surfactant at this low SDBS concentration is in agreement with the strong interactions observed with surface tensiometry. At 0.20 mM SDBS and 0.29 mM SDBS, only the bimodal peaks corresponding to P4VP-SDBS complexes were observed, and the peak size increased with increasing SDBS concentration. Above the CMC ($CMC_{SDBS} = 2.4$ mM), the bimodal peak and an additional peak with high D_H (5560 nm) were observed. These samples were visually hazy so the larger particle sizes were likely due to aggregate

formation. The volume percent of the peak at 5560 nm increased with 43 mM SDBS, indicating increased aggregation with additional surfactant. The continuity of the bimodal peaks throughout all compositions studied is in agreement with the cooperative binding mechanism described by Goddard^{7,8} and with the lack of resolubilization observed with high-throughput screening (*vide infra*).

The formation of complexes and subsequent aggregation at high surfactant concentrations was also observed in solution viscometry studies (Figure 4E-12). The concentration of P4VP was held constant at 0.15 g/dL P4VP and the SDBS concentration differed as described for the DLS studies.

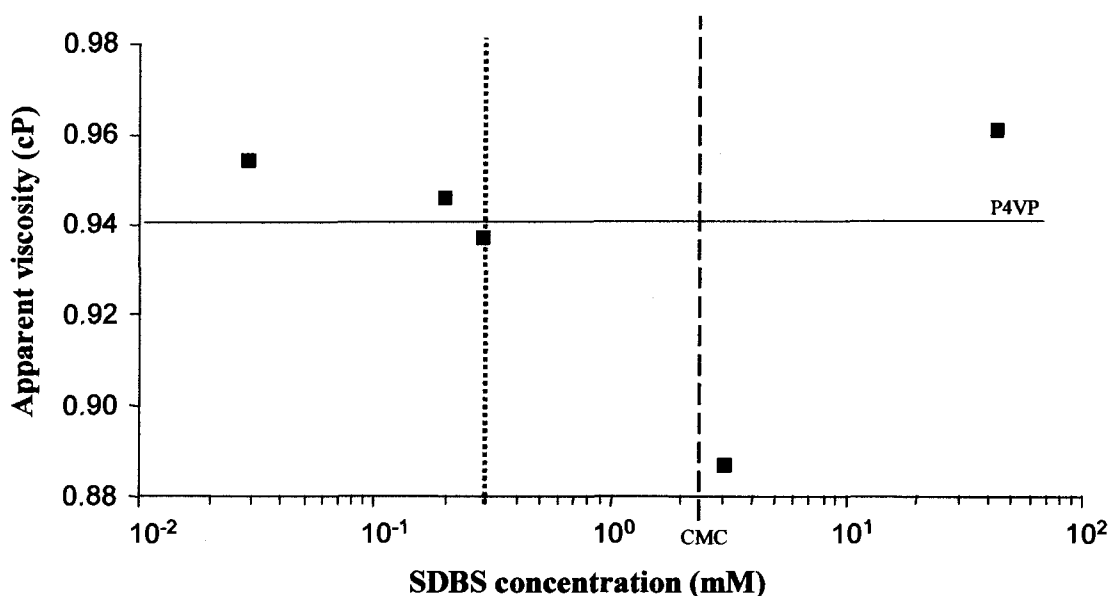


Figure 4E-12. Apparent viscosities of 0.15 g/dL P4VP – SDBS mixtures.
 Precipitation boundary; --- CMC in the absence of polymer.

A slight increase in viscosity occurred with the addition of 0.029 mM SDBS, which may be due to the coexistence of polymer, surfactant, and polymer-surfactant complexes

observed with DLS. As SDBS concentration increased, a decrease in viscosity was observed up to 2.9 mM, where a minimum occurred. Aggregate formation was observed at 43 mM SDBS in DLS studies, which is in agreement with the large increase in viscosity for this composition. From these studies we can conclude that interactions between P4VP and SDBS are strong and that complex formation occurs at very low surfactant concentration and continues for surfactant concentrations above CMC.

P2VP-SDBS Interactions

As with the P4VP-SDBS system, surface tension measurements were utilized to determine the CAC and the CMC2 for the P2VP-SDBS system, with the P2VP concentration held constant at 0.15 g/dL. The results are shown in Figure 4E-13. The surface tension curves of pure SDBS and P2VP are included for reference.

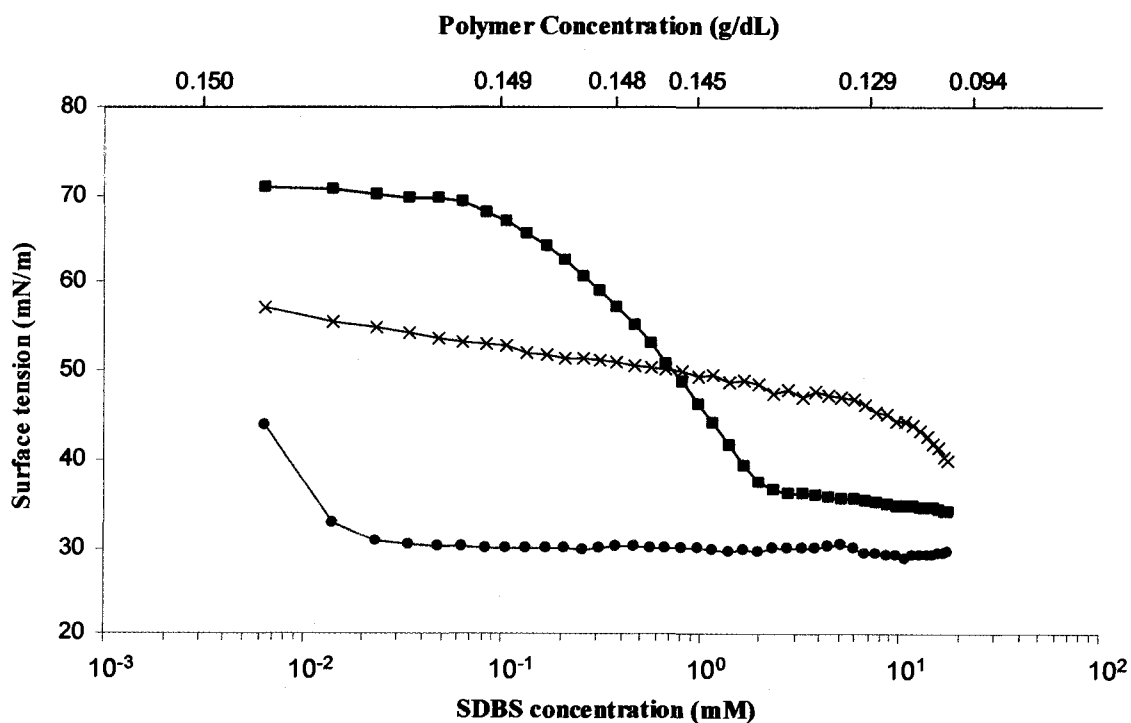


Figure 4E-13. Surface tension as a function of concentration.

As discussed in Figure 4E-5, the surface tension of pure P2VP at 0.15 g/dL was 57 mN/m, indicating surface activity of the polymer at this concentration. We also observed that P2VP is a more surface-active, and therefore a more hydrophobic polymer than P4VP. However, at 0.15 g/dL polymer, the addition of 6.4×10^{-3} mM SDBS to P2VP yields a moiety that is less hydrophobic than that which is formed under the same conditions with P4VP and SDBS. This could indicate that the surfactant interacts less intensely with P2VP than it does with P4VP or that the organization of bound surfactant molecules along the polymer backbone is different for P2VP and P4VP. However, the lowest surface tension reached is approximately the same for both P2VP-SDBS and P4VP-SDBS, indicating that the complexes, once formed, are about equal in surface activity.

The surface tension decrease beginning at 6.4×10^{-3} mM and ending in a plateau at 2.4×10^{-2} mM indicates the progressive formation of a surface-active complex. As in the P4VP-SDBS system, the CAC occurred at an SDBS concentration less than 6.4×10^{-3} mM, and all compositions studied with high-throughput screening were well above CAC. A CMC2 could not be detected in the P2VP-SDBS.

The interactions of P2VP with SDBS were also investigated using DLS, where the P2VP concentration was held constant at 0.15 g/dL and surfactant concentrations between 0.029 - 43 mM were studied (Figure 4E-14).

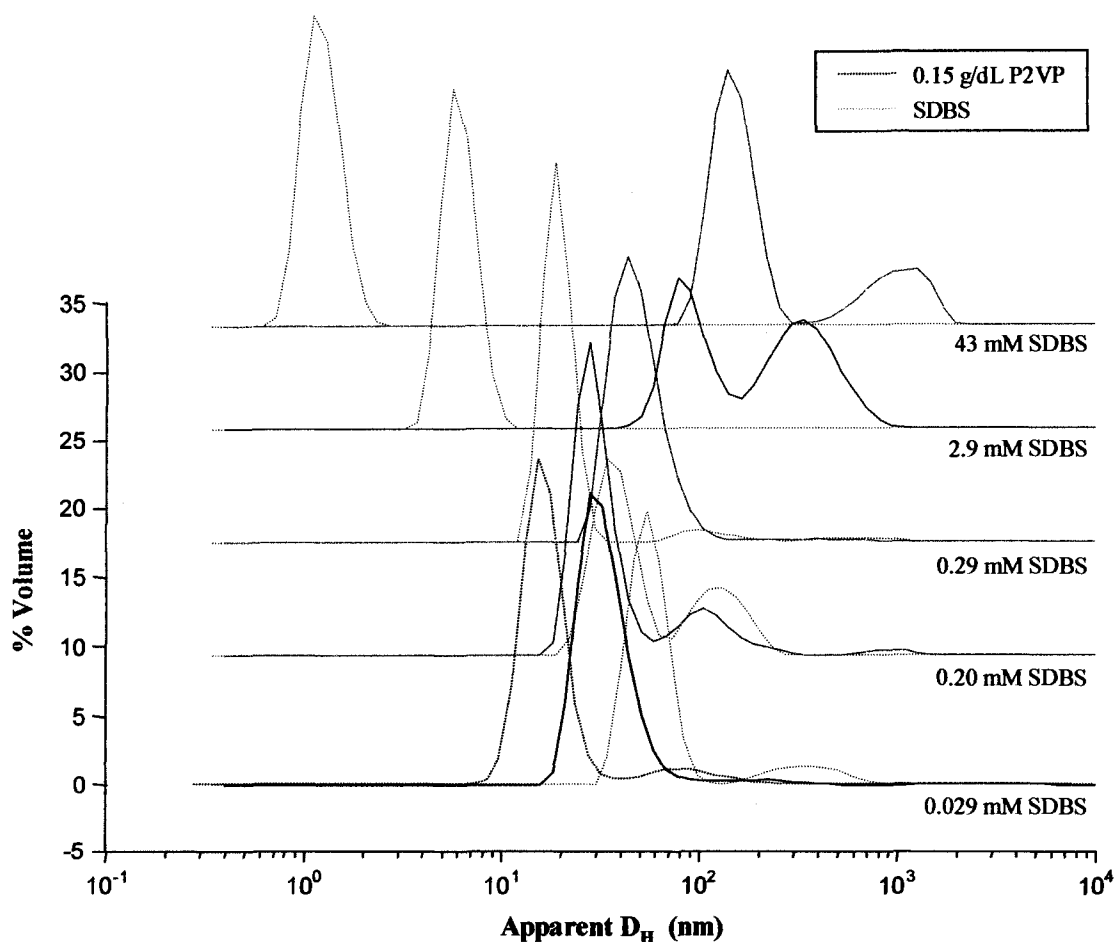


Figure 4E-14. Dynamic light scattering data for 0.15 g/dL P2VP – SDBS mixtures.

As with P4VP, P2VP in salt-free aqueous solution displayed a fast diffusion process, which resulted in a D_H that is artificially low (21 nm). Also, the SDBS D_H values decreased with increasing concentration, with large D_H at concentrations below CMC likely due to impurities. Contrary to the P4VP-SDBS systems, the presence of unimodal or bimodal peaks was dependent on surfactant concentration. A single unimodal peak was observed for all P2VP-SDBS composition below the SDBS CMC (2.4 mM); the small shoulder with 0.20 mM SDBS was similar to a peak observed in the SDBS solution and was attributed to surfactant impurity. The presence of only a single peak for these

compositions indicates that coexistence of polymer, surfactant and polymer-surfactant complexes did not occur for P2VP-SDBS. The interaction of P2VP and SDBS at low SDBS concentrations is in agreement with the surface tensiometry results (Figure 4E-13). The size of the unimodal peak corresponding to P2VP-SDBS complexes was similar for the 0.029 mM SDBS and 0.20 mM SDBS systems (30 nm). At 0.29 mM SDBS, the peak size was 44 nm; the complex size increased with increasing surfactant concentration. Up to 2.9 mM SDBS, the complexes formed with P2VP-SDBS were generally smaller than those with P4VP-SDBS, which may be due to less bound surfactant molecules or a different structuring of the surfactant molecules around the polymer chain.

Above CMC, bimodal peaks or two distinct peaks corresponding to P2VP-SDBS complex formation were observed. At 2.9 mM SDBS, the D_H values were larger than observed at lower SDBS concentrations (100 nm and 300 nm). Two distinct peaks were also observed at 43 mM SDBS and the D_H was again higher (150 nm and 1000 nm). These were two-phase systems and it is probable that the particles at large D_H were due to aggregation of complexes.

Solution viscometry was performed on the P2VP-SDBS compositions explored with DLS (Figure 4E-15).

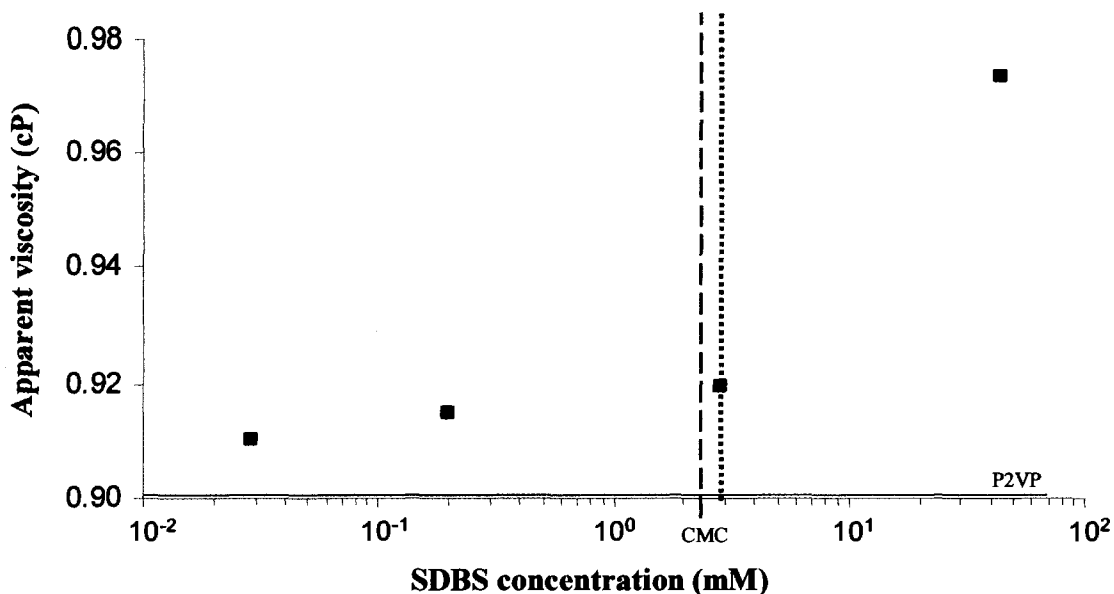


Figure 4E-15. Apparent viscosities of 0.15 g/dL P2VP – SDBS mixtures.
 Precipitation boundary; --- CMC in the absence of polymer.

An initial increase in viscosity was observed with the addition of 0.029 mM SDBS, and a gradual increase in viscosity was observed up to 2.9 mM, which was the onset of macroscopic phase separation. Contrary to the P4VP-SDBS system, a viscosity decrease and minimum were not observed in the P2VP-SDBS system. At 43 mM SDBS, a sharp increase in viscosity was observed, which is in agreement with the large D_H observed in the DLS studies possibly due to aggregation of P2VP-SDBS complexes. From these studies we can conclude that interaction between P2VP and SDBS is strong and that the mechanism of complex formation and the resulting polymer-surfactant complexes are different than those formed with P4VP-SDBS.

Polymer – Surfactant Contour Phase Diagrams

P4VP – Surfactant Coacervation

The interaction of low molecular weight P4VP (9 000 g/mol) with SDBS was investigated using high-throughput screening over a wide range of surfactant concentrations. The stability of the formed coacervate was studied, where the samples prepared for the initial phase diagram were analyzed after 24 hours (Figure 4E-16).

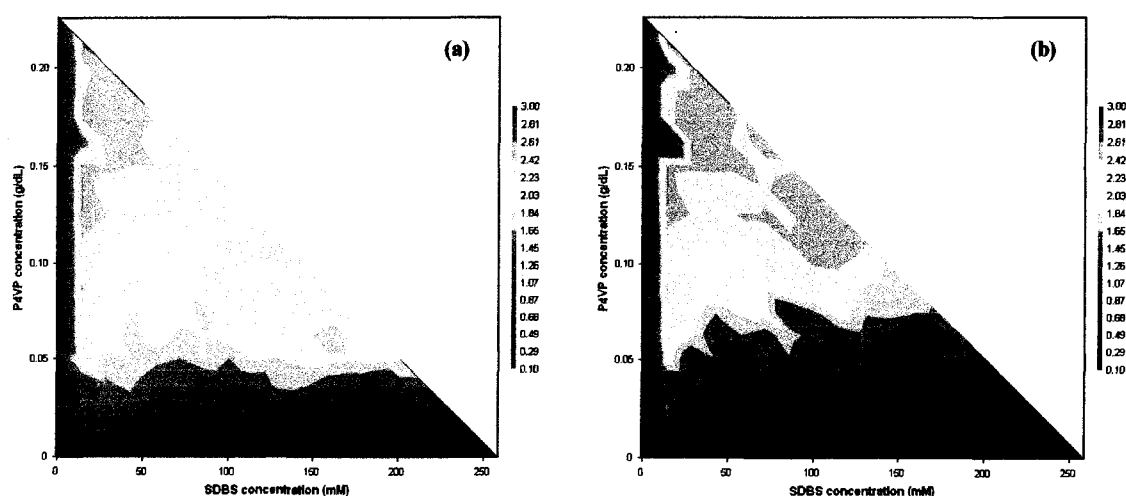


Figure 4E-16. Contour phase diagrams for P4VP-SDBS (a) initial analysis and (b) analysis after 24 hours.

All P4VP-SDBS compositions were essentially unchanged after 24 hours, indicating that very stable complexes had been formed in the P4VP-SDBS system. The 24 hour data were taken as equilibrium condition for these samples and this diagram is represented in Figure 4E-17.

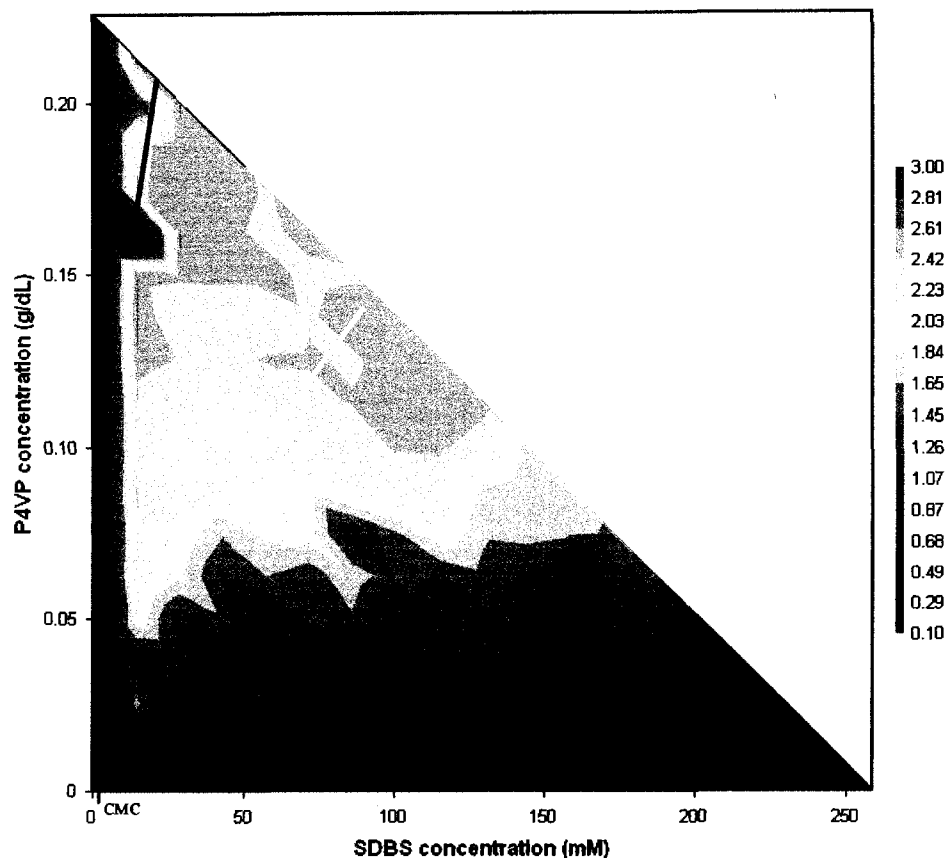


Figure 4E-17. Contour phase diagram of P4VP-SDBS. The 1:1 stoichiometric ratio is designated by the solid black line. Above the dashed white line coacervate amount was dependent on polymer and surfactant concentration.

It is important to note that for the P4VP-SDBS system shown in Figure 4E-17 the lowest concentration of SDBS investigated was 14 mM SDBS. As discussed in Chapter IV-A, the gradient in color seen between 0 – 14 mM SDBS was an artifact of the mesh technique employed by the plotting software. Therefore, the color gradient presented in this range was artificial and was not considered in data analysis.

According to the cooperative coacervation mechanism described for the dilute regime, maximum precipitation should occur near a 1:1 charge ratio of anionic:cationic charges, designated by the solid black line in Figure 4E-17.⁷ For the P4VP-SDBS

system, maximum coacervate formation was observed near the 1:1 charge ratio, with coacervate formation on either side of this line as well, which is in agreement with Goddard's observations of coacervate formation.⁶ Generally, the absence of coacervate at high surfactant concentrations is described in terms of 'resolubilization' of coacervate that was formed at lower surfactant concentrations (Chapter I, Figure 1-5).⁷ In our sample preparation method, surfactant concentrations are added discretely so it is more appropriate to discuss an absence of coacervate at higher surfactant concentrations as 'solubilization'. In the P4VP-SDBS system, complete resolubilization, or solubilization, of the coacervate was not observed in the surfactant concentration range studied, however at some constant polymer concentrations a decrease in the amount of coacervate formed was observed as surfactant concentration increased, indicating some solubilization. The low degree of solubilization is in agreement with studies by Chen et. al. where resolubilization was absent in high polymer charge density systems.²

In general, high coacervate amounts were produced at nearly all compositions studied in the P4VP-SDBS system, with the highest coacervate amounts near the 1:1 stoichiometric ratio. Two trends in coacervate formation were observed, dependent on the polymer and surfactant concentrations. At polymer concentrations above the dashed white line in Figure 4E-17, phase separation was dependent on both polymer and surfactant concentration. Below this line there was a region below 0.05 g/dL P4VP where coacervate amount was independent of surfactant concentration but had a strong dependence on polymer concentration. A transition region also occurred below this line, where both trends were observed between 0.05 - 0.125 g/dL P4VP.

The interactions of P4VP and SDBS were also investigated at a higher polymer molecular weight (32 000 g/mol) (Figure 4E-18). The low molecular weight P4VP-SDBS (9 000 g/mol) phase diagram is included for reference.

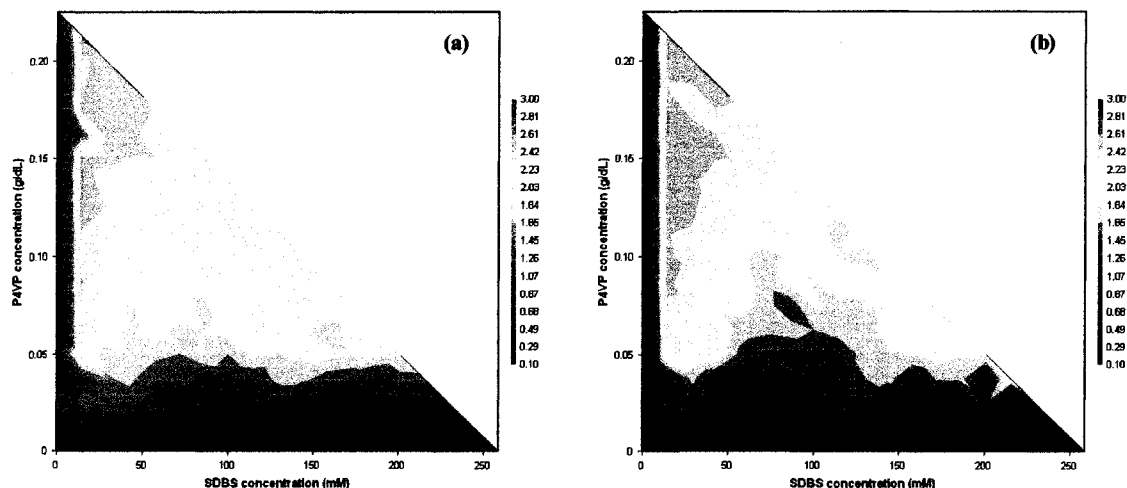


Figure 4E-18. Contour phase diagrams of P4VP-SDBS with P4VP molecular weights of (a) 9 000 g/mol and (b) 32 000 g/mol.

Based on the work of Li and coworkers with PDMDAAC and SDS/TX100 systems¹⁵, a decrease in coacervate amount could be expected for the high molecular weight P4VP-SDBS system (Figure 4E-18b), however we observed little difference between the amounts and compositions of coacervate formation with different polymer molecular weights. The second virial coefficient for high molecular weight P4VP was investigated using SLS and the resulting Zimm plot is shown in Figure 4E-19.

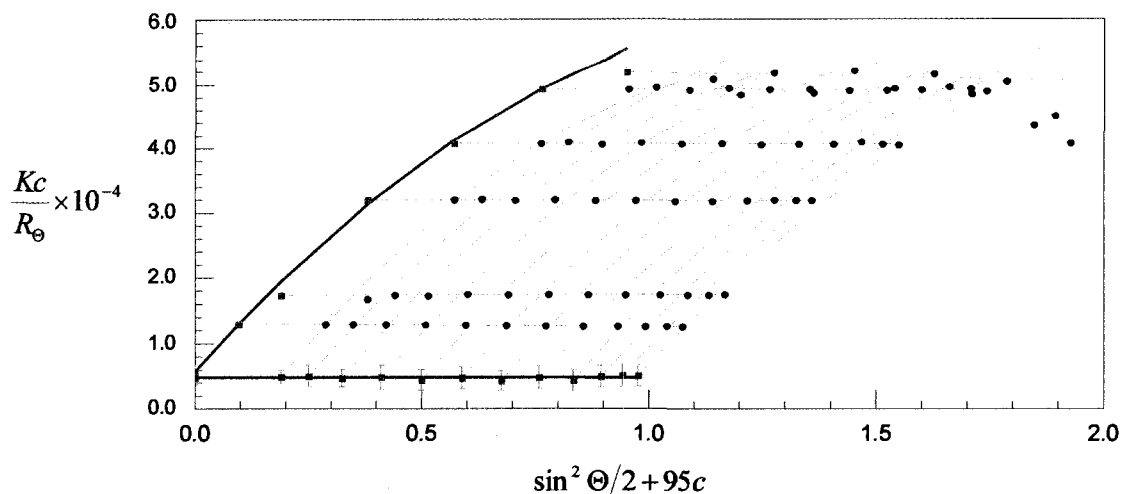


Figure 4E-19. Zimm plot of high molecular weight P4VP in filtered HPLC grade water at all concentrations studied (1.0, 2.0, 4.0, 6.0, 8.0, 10.0 mg/mL).

The curvature of the plot was not as extreme as observed for the low molecular weight polymer (Figure 4E-1) so all six P4VP concentrations investigated were used in calculation of B . For high molecular weight P4VP, B was 3.7×10^{-2} , which was similar to the second virial coefficient of low molecular weight P4VP and indicates that water was a good solvent for this polymer. The similarity in the contour phase diagrams with a difference in molecular weight but a similarity in polymer-solvent interaction demonstrates a probable relationship between polymer conformation and coacervate formation for the P4VP-SDBS systems.

Coacervation of low molecular weight P4VP with sodium capryl sulfonate (SCS) was also investigated using high-throughput screening. SCS has the same sulfonate head group as SDBS, but a C_8 linear tail group, which contains no aromatic moieties and is less bulky and less hydrophobic than the SDBS tail group (Chapter III). It is important to note that, in this study, poly(vinylpyridinium hydrochloride)-surfactant studies were performed over the same surfactant wt % concentration range, however the molar

concentrations range varies due to surfactant molecular weight differences. The initial and equilibrium contour phase diagrams of P4VP-SCS are shown in Figure 4E-20.

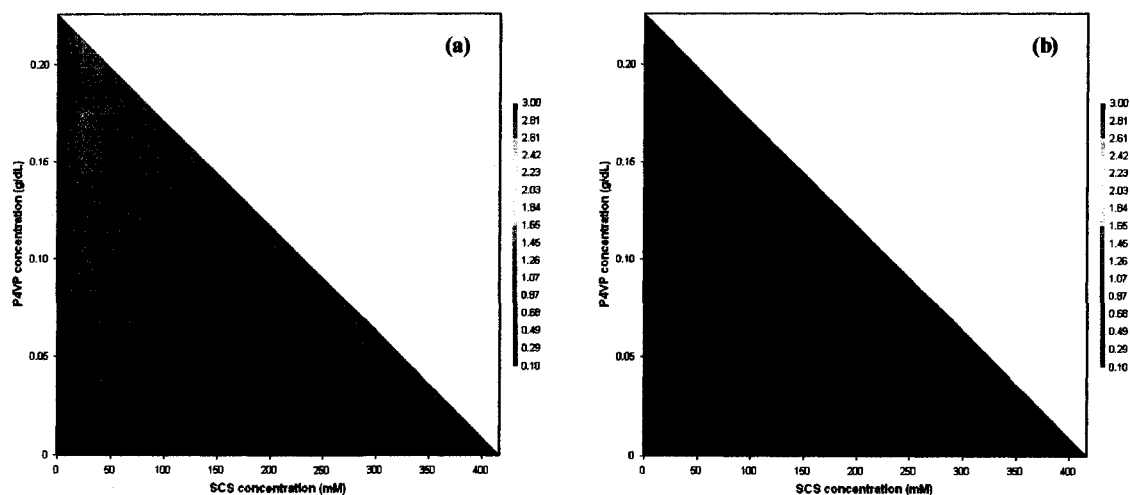


Figure 4E-20. Contour phase diagrams of P4VP-SCS (a) initial analysis and (b) analysis after 24 hours.

After 24 hours, coacervate formed was completely or nearly completely resolubilized indicating that complexes formed between P4VP and SCS were not stable. The formation of transient complexes during initial sample analysis (Figure 4E-20a) demonstrates that interactions occur between P4VP and SCS and it is probable that thermodynamically stable complexes would form in more concentrated systems or at a polymer-surfactant ratio not explored in this research.

The interaction of P4VP with sodium xylene sulfonate (SXS) produced a similar outcome. SXS has a sulfonate head group and an aromatic tail group with very low hydrophobicity, so much so that micelles do not form in solution. The contour phase diagrams for P4VP-SXS at initial and 24 hour time points are shown in Figure 4E-21.

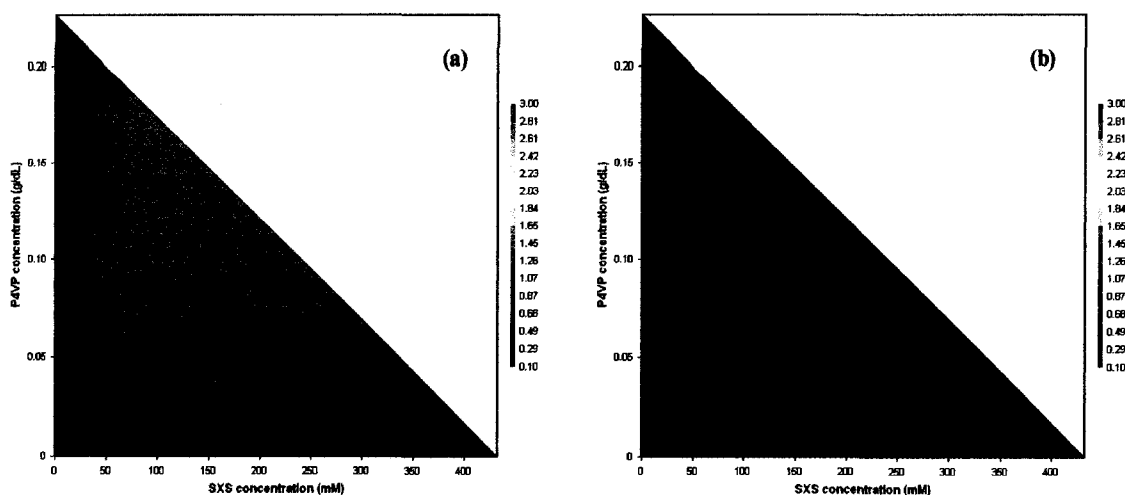


Figure 4E-21. Contour phase diagrams of P4VP-SXS (a) initial analysis and (b) analysis after 24 hours.

In the P4VP-SXS system, coacervate was initially observed over a wide range of compositions and in amounts greater than P4VP-SCS but less than P4VP-SDBS. However, at equilibrium complete dissolution was observed indicating instability of complexes that were initially formed. The absence of coacervate at equilibrium with P4VP-SCS and P4VP-SXS compared to the presence and stability of coacervate formed with P4VP-SDBS indicates that surfactant tail group architecture is critical for formation of thermodynamically stable complexes with P4VP. The surfactant molecules with only an aromatic moiety or only a hydrophobic moiety are inefficient at producing stable coacervate. However, a surfactant architecture that combines both an aromatic and a hydrophobic moiety of sufficient size produces stable coacervate.

P2VP – Surfactant Coacervation

The interaction of low molecular weight P2VP (6 000 g/mol) with SDBS was also investigated using high-throughput screening over the same wide range of surfactant concentrations studied with P4VP-SDBS. The stability of the formed coacervate was

studied, where the samples prepared for the initial phase diagram were analyzed after 24 hours (Figure 4E-22).

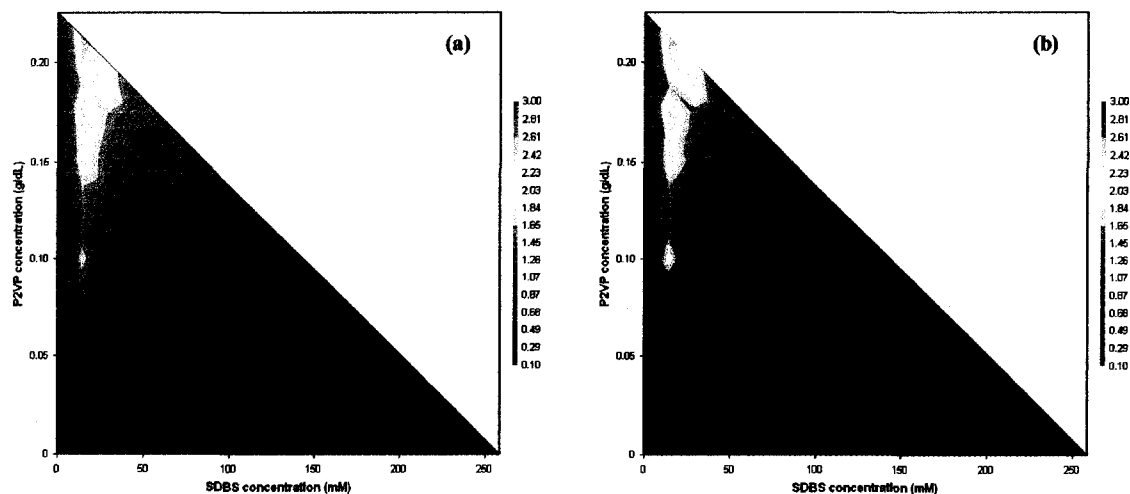


Figure 4E-22. Contour phase diagrams for P2VP-SDBS (a) initial analysis and (b) analysis after 24 hours.

As with the P4VP-SDBS systems, the coacervate formed in the P2VP-SDBS system was stable after 24 hours and this 24 hour contour phase diagram was taken as the equilibrium phase diagram (Figure 4E-23).

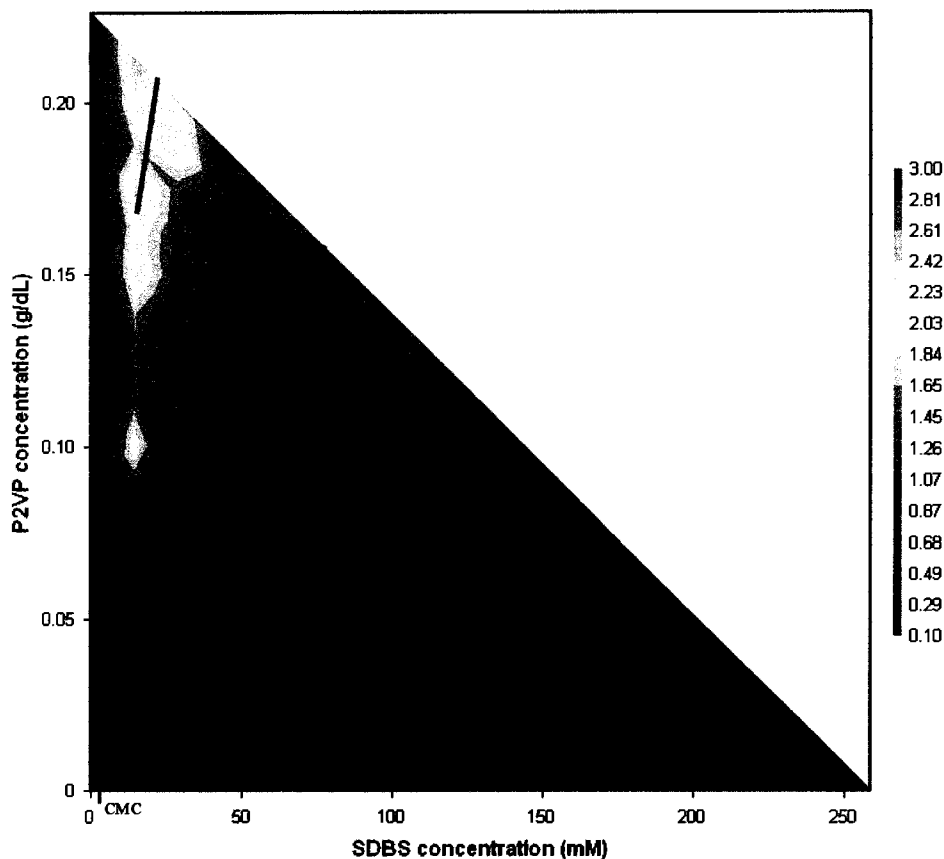


Figure 4E-23. Contour phase diagram of P2VP-SDBS. The 1:1 stoichiometric ratio is designated by the solid black line. Resolubilization is designated by the dotted black line.

As previously discussed, the coacervate amounts indicated below 14 mM SDBS were an artifact of the mesh technique of the software program and were not considered in our analysis of the data. Similar to the P4VP-SDBS system (Figure 4E-17), maximum coacervate formation occurred near the 1:1 charge ratio for the P2VP-SDBS system (solid black line, Figure 4E-23). Thus, phase separation in this region was in agreement with the observations of Goddard for the dilute surfactant regime.⁷

Coacervate formation in the P2VP-SDBS system only occurred in the previously-designated “polymer and surfactant dependent” region. Coacervate amount was highest above 0.2 g/dL P2VP; however the regions of coacervate were localized and non-

continuous. The lower coacervate amounts and smaller compositional range of coacervate formation with P2VP-SDBS compared to P4VP-SDBS may be due to the difference in polymer solution conformation and is likely attributable to steric hindrance of cationic charges due to their position near the polymer backbone. With increasing surfactant concentration, some degree of solubilization was observed at all P2VP concentrations, with complete solubilization below 0.1 g/dL P2VP. Complete, or near complete solubilization occurred at a constant surfactant : polymer concentration ratio, designated by the dotted black line in Figure 4E-23. The number of surfactant molecules required for solubilization was calculated based on this concentration ratio. Using the coordinate (40, 0.1) from the solubilization line the anionic:cationic molar ratio was calculated. Since not all ionizable groups on the polymer chain were ionized, the equivalent mass of polymer per unit cationic charge was determined. In order to calculate this value, the P2VP degree of polymerization (\bar{X}_n) was determined using Equation 4E-2

$$M_n = M_o(\bar{X}_n) + M_{eg} \quad \text{Equation 4E-2.}$$

where M_n is the number average molecular weight (6 000 g/mol), M_o is the molecular weight of the repeat unit (105 g/mol), and M_{eg} is the molecular weight of the end groups (364 g/mol). The number of repeat units was calculated to be 54, and at 85 % ionization there were 46 cationically charged repeat units. The fraction of charged units was 46 / 54, or 7 / 8, meaning that seven of every eight units were charged. Distributing the molecular weight of the one uncharged repeat unit among the seven charged units gives an equivalent mass per unit cationic charge of 120 g/mol. At the point (40, 0.1) there are 1.2×10^{-5} moles anionically charged units and 2.4×10^{-6} moles cationically charged units,

giving a molar ratio of anionic:cationic charges of 5:1, or five surfactant molecules per cationic charge were required for solubilization.

The effect of polymer molecular weight on coacervate formation was also investigated for the P2VP-SDBS system. The interactions of low molecular weight P2VP (6 000 g/mol) with SDBS were compared to the interactions of high molecular weight P2VP (32 000 g/mol) with SDBS (Figure 4E-24).

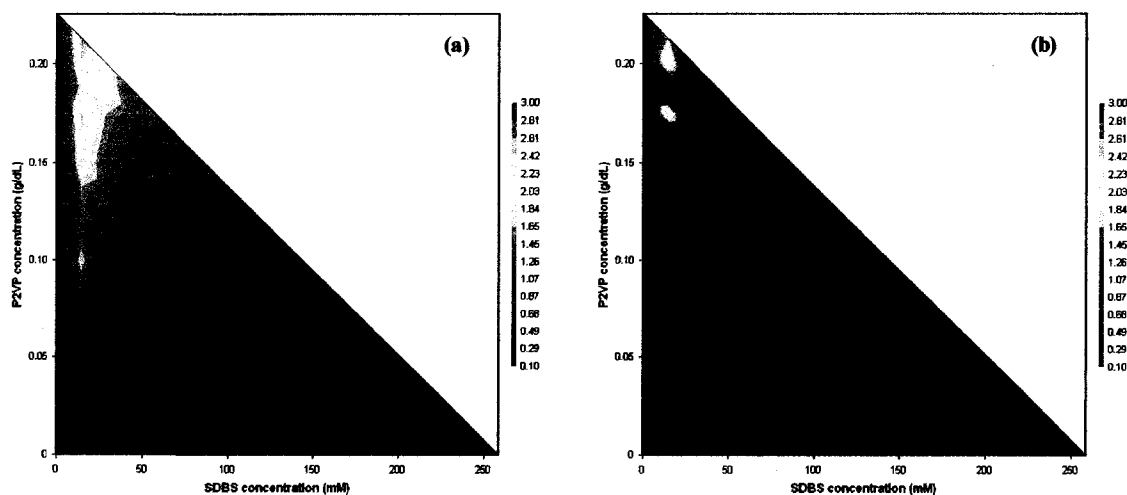


Figure 4E-24. Contour phase diagrams of P2VP-SDBS with P2VP molecular weights of (a) 6 000 g/mol and (b) 32 000 g/mol.

A large decrease in coacervate formation was observed with the increase in polymer molecular weight, which is contrary to the consistent coacervate formation observed in the P4VP molecular weight studies, but is in agreement with the observations by Li and coworkers of decreased coacervation with increasing molecular weight of PDMDAAC.¹⁵ The influence of molecular weight on the P2VP conformation was investigated using SLS and the Zimm plot is shown in Figure 4E-25.

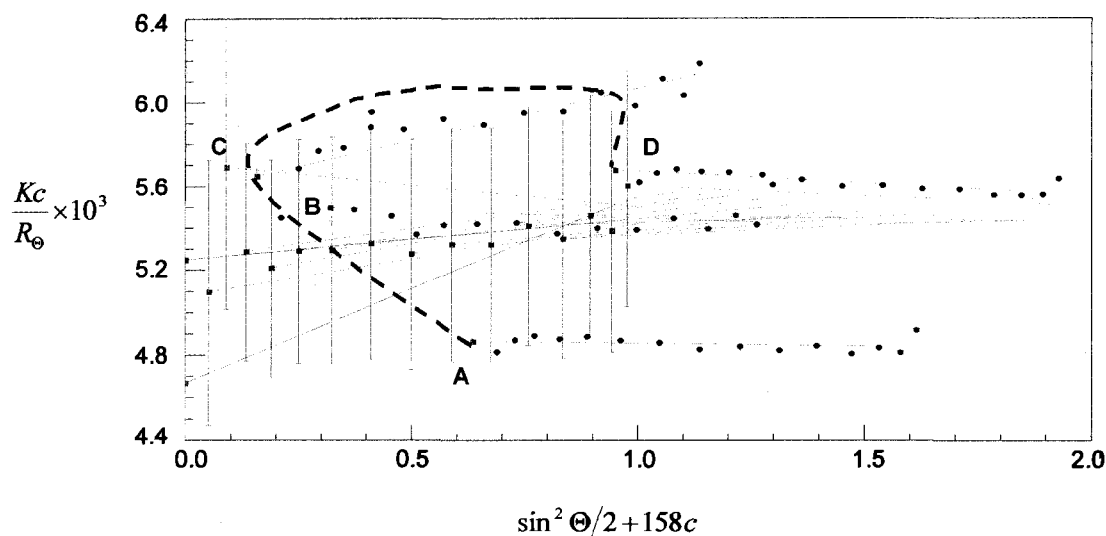


Figure 4E-25. Zimm plot of high molecular weight P2VP in filtered HPLC grade water. A-D indicate concentrations of P2VP investigated (1.0, 2.0, 4.0, 6.0 mg/mL). Blue dashed line follows curvature of plot.

As with the low molecular weight P2VP (Figure 4E-3), curvature of the Zimm plot was observed when all concentrations were included. The highest concentration was removed for determination of B (Figure 4E-26).

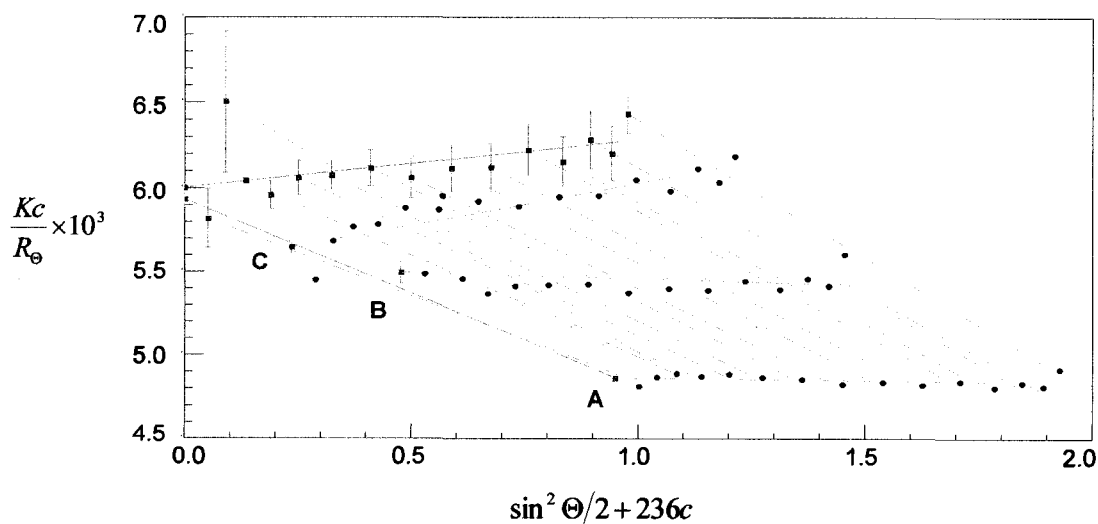


Figure 4E-26. Zimm plot of low molecular weight P2VP in filtered HPLC grade water at low concentrations (A-C = 1.0, 2.0, 4.0 mg/mL).

For high molecular weight P2VP, B was 3.8×10^{-3} , which is greater than the negative B value obtained for low molecular weight P2VP, but the low number is indicative of poor polymer-solvent interactions. In addition, a negative curvature of the Zimm plot was observed, which can be attributed to collapse of the polyions at high concentrations. The collapse of the high molecular weight P2VP chains is in agreement with the lower coacervate amount produced in the high-throughput screening studies. Increased coiling of the polymer could result in the cationic charges being more sterically-hindered than in the low molecular weight system. Such steric hindrance could restrict direct ion-ion interaction with surfactant molecules, or micelles, and this would be consistent with the observed inverse dependence of coacervate formation on P2VP molecular weight. This P2VP molecular weight study supports the conclusion that polymer conformation has an effect on coacervate formation in P2VP-SDBS systems.

Coacervation of low molecular weight P2VP with SCS was also investigated using high-throughput screening and the initial and equilibrium contour phase diagrams of P4VP-SCS are shown in Figure 4E-27.

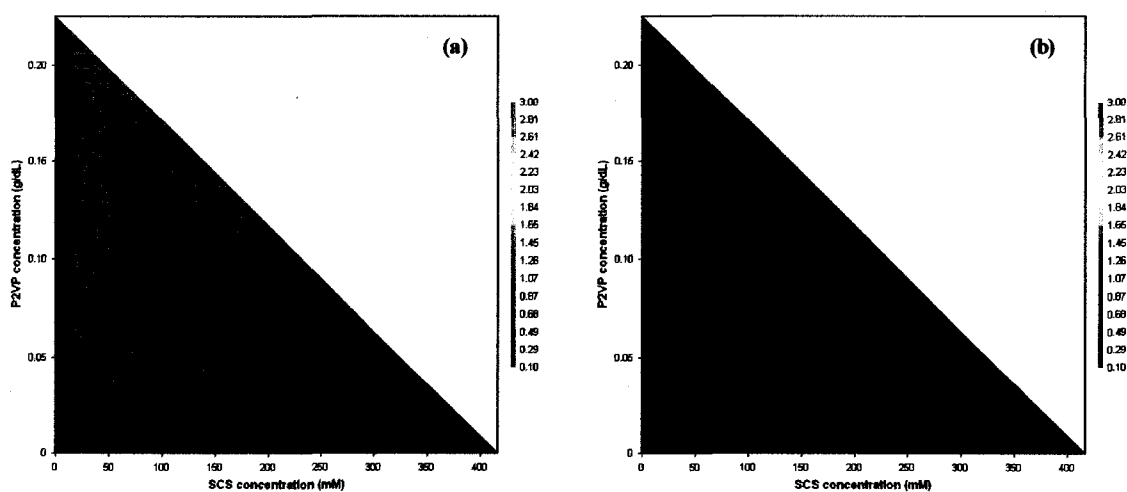


Figure 4E-27. Contour phase diagrams of P4VP-SCS (a) initial analysis and (b) analysis after 24 hours.

As with P4VP-SCS, coacervate was formed initially with P2VP-SCS and the coacervate formed was completely resolubilized after 24 hours, indicating that the complexes formed between P2VP and SCS were thermodynamically unstable.

Contour phase diagrams for P2VP-SXS formed initially and after 24 hours are shown in Figure 4E-28.

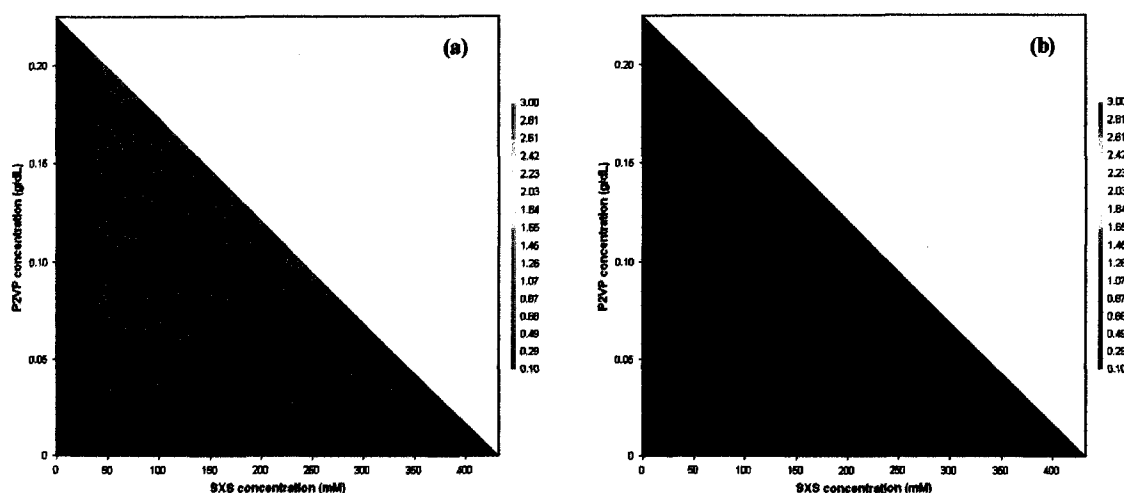


Figure 4E-28. Contour phase diagrams of P2VP-SXS (a) initial analysis and (b) analysis after 24 hours.

In the P2VP-SXS system, coacervate was initially observed over a wider range of compositions than the P2VP-SDBS and P2VP-SCS systems. In fact, the compositional range and coacervate amounts were comparable to that of P4VP-SXS (Figure 4E-21a). Similar to P4VP-SXS and P2VP-SCS, complete dissolution was observed after 24 hours in the P2VP-SXS system. This instability of formed coacervate with SCS and SXS is again indicative of the need for both aromatic and hydrophobic surfactant tail group moieties for coacervate formation with poly(vinylpyridinium hydrochloride) polymers.

Effects of Polymer and Surfactant Structure on Coacervate Formation

Using surface tensiometry, dynamic light scattering, viscometry, and high-throughput screening we observed that coacervate formation with SDBS differed greatly between P4VP and P2VP. Coacervate formed readily with both P4VP-SDBS and P2VP-SDBS, but the amount of coacervate was much greater for P4VP than for P2VP and solubilization was not observed in the former, but was prominent in the latter.

Interactions between polymer and surfactant occurred at very low concentrations for both systems, but the coacervate complexes that were formed differed in hydrodynamic size and the effect of surfactant concentration on complex size was more substantial for the P2VP-SDBS system. Based on the polymer solution studies and the polymer-surfactant interaction studies it is evident that polymer solution conformation in regards to the position of the cationic charge has a direct bearing on the interaction of the polymer with oppositely-charged surfactant.

The conformation of P4VP, with cationic groups in the 4-position rather than the more sterically-hindered 2-position may favor ion-ion association with the large SDBS anions and hydrophobic association of the hydrocarbon tail groups of SDBS when bound electrostatically to the polymer chain. Chen and coworkers² investigated polymer-surfactant interactions of a high charge density ionene bromide polymer (3,3-ionene bromide) with SDS and observed the formation of irreversible, stable complexes that remained insoluble even at high surfactant concentrations. The authors attributed this insolubility to strong side-by-side hydrophobic associations between bound surfactant tail groups, forming a lamellar-like packing.² It is reasonable to expect that a similar complex structure was formed with the P4VP-SDBS system, where the lack of

solubilization was due to the free energy of micelle formation along the polymer chain being less favored than the existing highly-ordered tail group structure such that no driving force existed for resolubilization at increased surfactant concentrations.¹⁴⁵ In the P4VP-SCS system, contrary to the P4VP-SDBS system, resolubilization was observed at all compositions after 24 hours. Site-specific interactions were likely in this system as well, but it could be argued that the smaller hydrophobic tail groups provided hydrophobic interaction insufficient to prevent resolubilization to a micellar state with lower free energy.

Contrary to P4VP, the second virial coefficient of the P2VP polymer indicates a polymer close to theta conditions. From the chemical structure and the polymer solution measurements, the cationic groups are sterically-hindered by the polymer backbone. Steric hindrance would limit the number of bulky surfactant molecules that could bind to each cationic charge due to space restrictions. Interactions between P2VP and SDBS were observed below and above the CMC, however the mechanism of coacervate formation does not neatly fit into either the site-specific (Goddard) or macroion-macroion (Dubin) interaction models. Rather, it shows characteristics of each of these models depending upon the conditions of the system. The charge density of P2VP was similar to that of P4VP so the solubilization of P2VP-SDBS complexes indicates that structuring of bound surfactant tail groups was not favored in the P2VP-SDBS system. This is in agreement with a coiled solution conformation and sterically-hindered cationic charges. It is possible that at surfactant concentrations near and above CMC this solution conformation promoted macroion-macroion interactions as described by Dubin.²⁰ The interaction of P2VP with SCS produced unstable coacervate that was completely

resolubilized after 24 hours, which did not clarify the mechanism of P2VP-surfactant interaction. The initial contour phase diagram for P2VP-SXS was nearly identical to that of P4VP-SXS, which may indicate site-specific interactions in this system.

As indicated in the above discussions, the surfactant tail group structure affected coacervate formation and coacervate stability. Initially, coacervate formation was observed for P4VP and P2VP with all surfactants studied, however only coacervate formed between P4VP-SDBS and P2VP-SDBS was stable over 24 hours. The instability of the coacervate formed initially with SCS and SXS compared with the stability of the coacervate initially formed with SDBS indicates that neither an aromatic group nor a short hydrophobic alkyl chain is sufficient to provide thermodynamically stable coacervate complexes. In fact, a hydrophobic chain with sufficient length and/or an aromatic group is necessary to form thermodynamically stable coacervate.

Combining the understandings gained from the detailed investigations of poly(vinylpyridinium hydrochloride) interactions with SDBS with the macroscopic and wide compositional range investigations of the polymers with surfactants of different tail group architecture, we can conclude that the mechanism of polymer-surfactant interaction and coacervate formation differs depending on the position of the cationic group along the polymer backbone, and in some cases the surfactant tail group architecture.

Salt Addition Studies

Using multiple methods we determined that P4VP-SDBS interactions occur through site-specific interactions, probably forming highly-ordered complex structures and that the formation of these structures is a function of the polymer solution

concentration, the position of the cationic group in the macromolecule, and the packing ability of the surfactant hydrophobic tail group. It was of interest to understand how the addition of the common ion salt, sodium chloride, would influence these interactions due to its propensity to alter the solution properties of polyelectrolytes and surfactant molecules.¹⁴⁶ For example, salt in sufficient concentration can cause dissociation of oppositely charged ion-ion complexes, but salt also causes surfactant micelles to grow in size.

The effect of salt on P4VP was studied using DLS (Figure 4E-29). The P4VP concentration was 0.15 g/dL and the NaCl concentration was 8.6 mM.

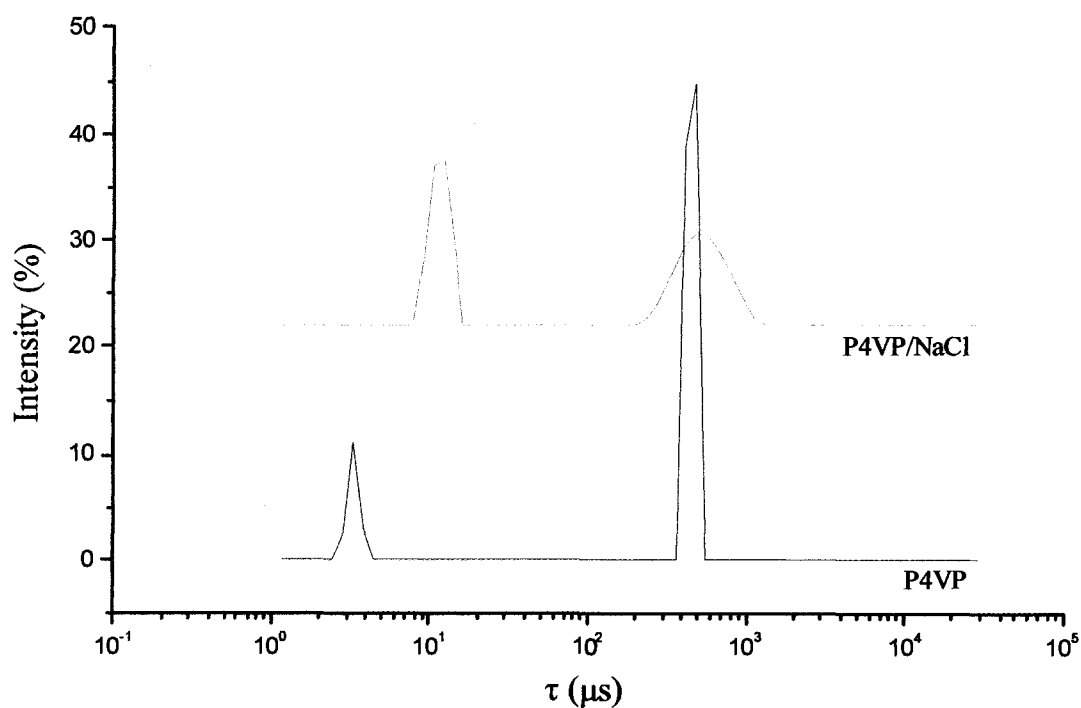


Figure 4E-29. Relaxation time (τ) of 0.15 g/dL P4VP and 0.15 g/dL P4VP with 8.6 mM NaCl.

As discussed in the P4VP solution studies (Figure 4E-6), P4VP in salt-free solution exhibits a bimodal diffusion due to the polymer charge. A bimodal distribution was also observed for the P4VP/NaCl solution. The fast diffusion mode for P4VP in salt solution was observed at a higher relaxation time (12 μ s) indicating a decreased rate of diffusion. The slower D_f of polymer in the salt solution suggests screening of intermolecular electrostatic repulsions; however bimodality indicates that the concentration of NaCl was not high enough to screen all electrostatic repulsions. Diffusion in the slow mode was identical for P4VP in aqueous and salt solutions, which is reasonable given the lack of sensitivity of the slow mode to charge interaction parameters.¹³²

The effect of NaCl on SDBS particle sizes in solution was also investigated using DLS. Previous DLS studies with P4VP and SDBS focused on low surfactant concentrations. When exploring the impact of salt on coacervate formation, higher surfactant concentrations were explored because significant differences were observed in high-throughput experiments over a wide range of surfactant concentrations. The D_H values were similar ($D_H = 1.3 - 2.0$ nm) for all concentrations studied above CMC (29 - 200 mM SDBS). The consistent diameters at these concentrations indicated that micelle growth at high surfactant concentrations was not predominant in this system. For comparison, D_H was 1.1 nm in this concentration range for salt-free SDBS solutions. Micelle theory describes micelle growth with the addition of salt due to shielding of head group repulsions.^{20, 82} The absence of micelle growth in our systems can be attributed to the low concentration of NaCl used in these studies.

Investigation of the effects of salt on coacervate formation was studied using high-throughput screening. Two addition orders were investigated for the P4VP-SDBS-

NaCl system: Polymer, Salt, Surfactant (PES) and Surfactant, Salt, Polymer (SEP).

Complementary DLS studies were attempted; however settling of the coacervate in a short time was observed so high-throughput screening proved to be a more beneficial tool for investigating these systems. For reference, the P4VP-SDBS contour phase diagram with no salt added is shown in Figure 4E-30.

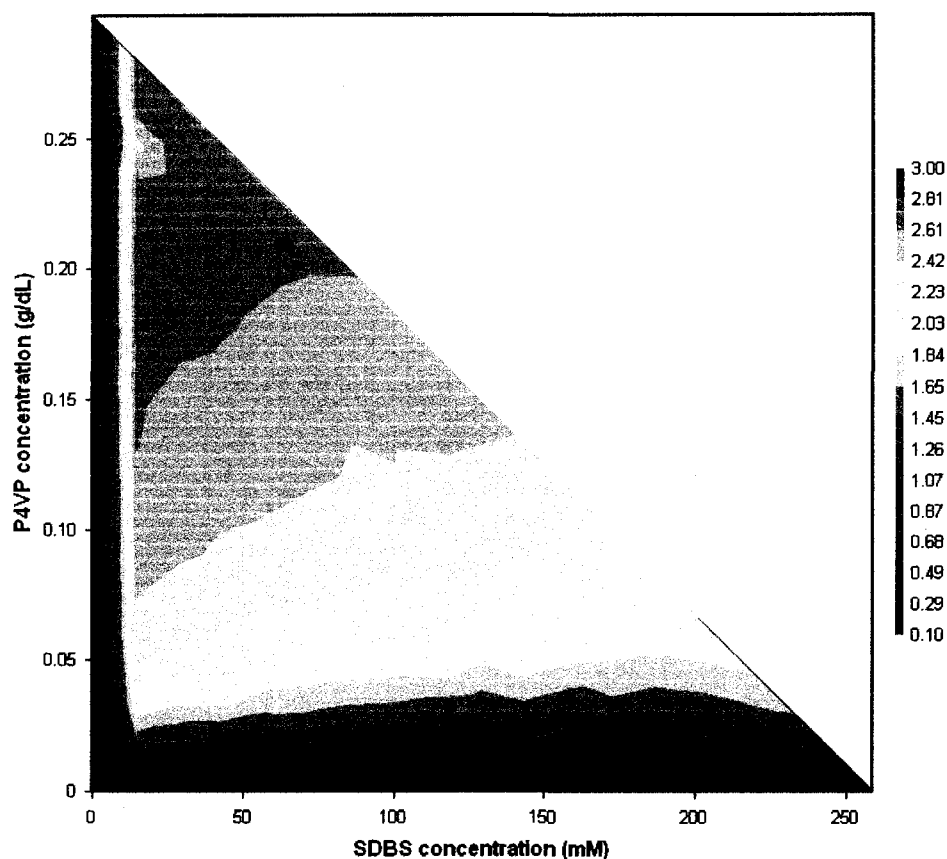


Figure 4E-30. Contour phase diagram of P4VP-SDBS in salt-free aqueous solution.

As discussed earlier, coacervate formation in the P4VP-SDBS system was due to site-specific interactions and possible high-ordered packing of surfactant tail groups forming a complex with an ordered structure. Solubilization was not observed for this system and at low polymer concentrations these ordered structures were unaffected by the high

surfactant concentrations, which was attributed to the associations in the tightly packed system of bound tail groups being more favorable than comicellization. The “no salt” diagram was used as a baseline for understanding the effects of addition order in the presence of salt.

Coacervate formation with the addition of NaCl was affected differently based on the addition order used. The contour phase diagrams for both addition orders are shown in Figure 4E-31.

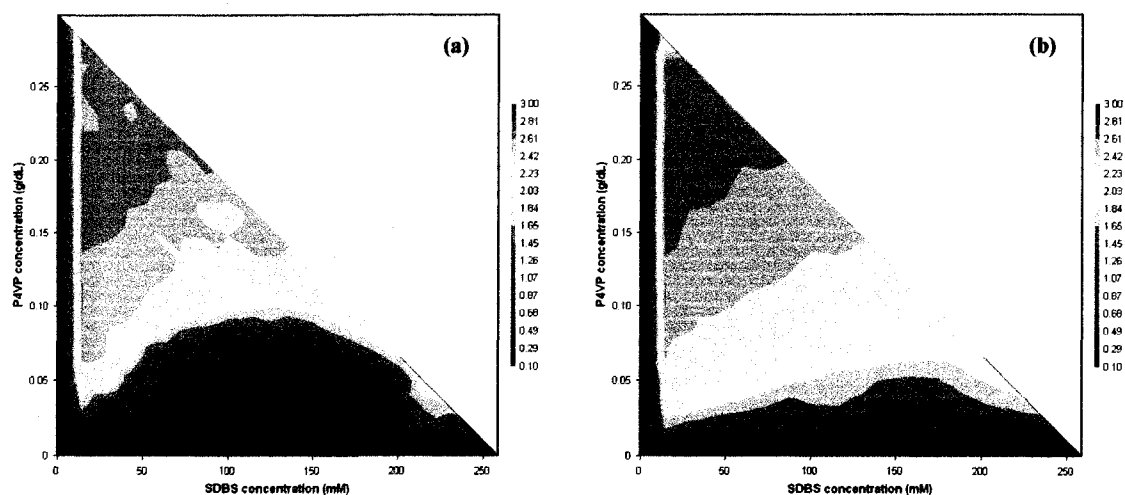


Figure 4E-31. Contour phase diagrams of P4VP-SDBS in 8.6 mM NaCl solution, combined using the addition orders of (a) polymer, salt, surfactant and (b) surfactant, salt, polymer.

The phase diagrams shown in Figure 4E-31 were prepared using the Constant Salt method (Chapter III), so there was a constant salt concentration of 8.6 mM for all points on the diagram.

In the PES system (Figure 4E-31a), we observed that the addition of salt affected the amount of coacervate formed at some, but not all compositions investigated. At P4VP concentrations greater than 0.15 g/dL, coacervate formation was similar to the “no

salt” system. With this addition order, salt and polymer interacted before the addition of surfactant and from the DLS studies we know that addition of NaCl to P4VP caused screening of some intermolecular electrostatic repulsions. Shielding of electrostatic interactions between P4VP and SDBS would therefore be expected with the addition of salt; however the lack of effect of salt at low surfactant concentrations indicated that this was not a predominant effect, and it is probable that the complexes formed at high P4VP concentration in the presence of NaCl were similar to those formed in the salt-free solutions.

Below 0.1 g/dL P4VP, coacervate formation was significantly decreased for almost all compositions compared to the “no salt” system. Since salt concentration was constant at all compositions, screening is inferred to be more effective at these low polymer concentrations. It is well known that salt causes polyelectrolyte conformational collapse. It is reasonable to expect that in this collapsed conformation the availability of the ionic nitrogens would be lessened. This would result in a lesser degree of polymer-surfactant interaction and highly ordered packing of bound surfactant tail groups would be absent. The absence of coacervate at intermediate surfactant concentrations can be attributed to solubilization of complexes by free surfactant due to a lack of highly ordered bound surfactant tail group packing. At low surfactant concentrations, the free surfactant concentration is not sufficient to cause solubilization of complexes. The presence of coacervate at high surfactant concentration would theoretically be attributed to micelle growth, however the DLS results do not show larger particle sizes and therefore coacervation in this region is not completely understood.

In the SEP system (Figure 4E-31b), coacervate formation was very similar to the “no salt” system at all compositions investigated. With this addition order, surfactant and salt interacted before the addition of P4VP. The DLS studies showed little effect of salt on micelle size and a constant micelle size between 120 – 200 mM SDBS with salt, despite the increased surfactant concentration. From all of the foregoing results, we can confidently predict that, with this order of addition, the polymer molecules would be in an expanded conformation when introduced to the surfactant molecules. This would explain why there is no difference between the SEP and the “no salt” phase diagrams.

Concluding Remarks

As a result of the combination of high-throughput screening experimentation with more detailed techniques we have determined that coacervate formation could occur by either the Goddard mechanism or the Dubin mechanism, dependent on the polymer solution conformation, which was ultimately dependent on the position of the cationic charge along the polymer backbone. We have shown that P4VP interacts with anionic surfactant by a site-specific Goddard mechanism. Alternatively, P2VP appears to interact with anionic surfactant via a mixed mechanism comprising elements from both site-specific (Goddard) and macroion-macroion (Dubin) interactions. We also determined that polymer-surfactant interaction and coacervate formation was dependent on surfactant tail group architecture. The existing theoretical models present two distinct viewpoints based on only a few polymers and surfactants. We have shown that in fact the mode of interaction depends critically on the detailed polymer and surfactant molecular structures.

CHAPTER V

CONCLUSIONS

Two classes of polymers, polysaccharides and poly(vinylpyridines), were chosen to enhance our understanding of the effects of various polymer, surfactant and solution properties on interactions between polymer and surfactant, and subsequent coacervate formation. A cationic polysaccharide series, polyquaternium-10 (PQ-10), was chosen because a range of molecular weights and degrees of charge substitution is available, and these polymers are traditionally used to study polymer-surfactant interactions. The molecular weight and PDI of each PQ-10 polymer was characterized using SEC-MALLS and the c^* in salt-free solution was measured using solution viscometry. The effect of molecular weight on interactions between PQ-10 and the anionic surfactant sodium lauryl ether sulfate (SLES) was studied for the JR400 and JR30M polymers using surface tensiometry, dynamic light scattering and viscometry. Both polymer-surfactant systems exhibited interaction at very low surfactant concentrations. Formation of polymer-surfactant complexes was observed at surfactant concentrations below and above the surfactant CMC. Below CMC, minimal hydrophobic association occurred between polymer bound surfactant molecules. At higher surfactant concentrations, near the 1:1 stoichiometric ratio, hydrophobic associations between polymer bound surfactant molecules did occur and complexes larger than the pure polymer were produced. This is consistent with the theories of cooperative interaction between oppositely-charged polymer and surfactant.

The effects of polymer molecular weight and charge substitution (CS) on coacervate formation were systematically studied using this PQ-10 series and a novel

high-throughput screening method developed in this research. This method allowed rapid and reproducible preparation and analysis of multi-component polymer-surfactant systems and representation using contour phase diagrams showing the compositions exhibiting coacervate formation and the amount of coacervate formed at each composition. Maximum coacervate formation was observed near the 1:1 stoichiometric ratio for all PQ-10-SLES systems, and coacervate formation was consistent with the traditional JR400-SDS system. The effect of CS on coacervate formation was studied by holding the polymer molecular weight approximately constant across multiple polymer systems. A minimal amount of coacervate was produced at very low CS and the amount of coacervate and the compositional range of coacervate formation increased with higher CS. This same trend was observed with both low and high molecular weight polymers. The effect of polymer molecular weight at constant CS was also studied. At constant CS the amount of coacervate increased, as did the compositional range of coacervate formation, with increasing polymer molecular weight. This same trend was observed with both low and high charge substituted polymers. Also with both low and high CS, the amount and compositional range of coacervate formation showed a dependence on the polymer critical overlap concentration (c^*). Coacervate formation was observed below c^* in all systems studied, and for the polymers that were also studied above c^* , the coacervate amount and compositional range increased near and above c^* . This effect of polymer molecular weight, and c^* , on coacervate formation and coacervate amount was attributed to hydrophobic associations of surfactant molecules along the polymer chain decreasing the effective mesh size of the polymer chain, lowering the configurational and conformational entropy of the polymer chains, and thus increasing the free energy of

mixing so that phase separation was favorable. Overall, the highest amount and compositional range of coacervate formation was observed for the polymer with the highest molecular weight and CS in this PQ-10 series.

The effects of polymer backbone structure and micelle charge density on coacervate formation were studied using different series of cationic polysaccharides, interacting with anionic surfactants and analyzed using high-throughput screening. Cationic guar has molecular weights similar to the PQ-10 series, but a different backbone structure, with similar rigidity but more regularity in pendant group positioning. Despite the difference in backbone structure, the trends in coacervate formation with SLES, as a function of polymer molecular weight and CS, were similar to that of PQ-10. The highest amount of coacervate and broadest compositional range of coacervate formation was observed for the cationic guar with the highest molecular weight and CS. The effect of hydrophobic substitution along the polymer backbone, including the degree of hydrophobic substitution, was studied using a series of polymers similar to PQ-10 polymers. At low degree of hydrophobic substitution, the amount and compositional range of coacervate formation was similar to that of the unsubstituted polymer. With higher degrees of hydrophobic substitution the compositional range of coacervate formation shifted to lower polymer concentrations and as the degree of hydrophobic substitution increased this shifted compositional range of coacervate formation was maintained and the amount of coacervate formed increased. This shift in compositional range was attributed to the variation of the cooperative mechanism of coacervate formation with hydrophobically-modified polyelectrolytes and the increased coacervate amount with increasing degree of hydrophobic substitution was attributed to

the formation of micellar junction zones between polymer chains. High-throughput screening was also used to study the effect of micelle charge density on PQ-10-surfactant interactions. In systems with surfactants of differing EO lengths a decrease in coacervate formation with a decrease in micelle charge density was observed. A similar trend was observed with mixed nonionic/anionic surfactant systems, where coacervate amount decreased with a decrease in micelle charge density, although the compositional range of coacervate formation was relatively unaffected by micelle charge density.

Poly(vinylpyridines), cationically-modified via pH adjustment, were chosen because they have flexible, hydrophobic backbones and offer isomers with different positioning of the cationic charge relative to the backbone. This allowed investigation of the site-specificity of polymer-surfactant interaction as well as the investigation of the effects of polymer solution properties and charge isomerism on polymer-surfactant interaction and coacervate formation. The molecular weight and PDI of the uncharged polymers was determined using SEC-MALLS and it was determined from solution viscometry that the polymers were below c^* at all concentrations studied. The solution properties of P4VP and P2VP in salt-free solution were studied. Using static light scattering and solution viscometry, it was determined that water was a good solvent for P4VP but a poor solvent for P2VP. Surface tensiometry indicated that P2VP was more surface active than P4VP. The fast diffusion process observed with dynamic light scattering was faster with P4VP than P2VP, due to enhanced intermolecular electrostatic repulsions in the former. Based on these results, we deduced that the cationic groups of P4VP were oriented into solution, shielding the hydrophobic backbone from the solvent,

whereas the cationic groups of P2VP were exposed to water, providing solubility, but the polymer likely adopted a collapsed solution conformation.

The effect of charge isomerism on the interactions, and subsequent coacervate formation, between polymer and surfactant was studied using surface tensiometry, dynamic light scattering, viscometry, and high-throughput screening. In all techniques, coacervate formation between polymer and the anionic surfactant sodium dodecylbenzene sulfonate (SDBS) differed greatly between P4VP and P2VP. Coacervate formed readily with both P4VP-SDBS and P2VP-SDBS, but the amount of coacervate was much greater for P4VP than for P2VP and solubilization was not observed in the former, but was prominent in the latter. Interactions between polymer and surfactant occurred at very low concentrations for both systems, but the coacervate complexes that were formed differed in hydrodynamic size and the effect of surfactant concentration on complex size was more substantial for the P2VP-SDBS system. Based on the polymer solution studies and the polymer-surfactant interaction studies it is evident that polymer solution conformation in regards to the position of the cationic charge has a direct bearing on the interaction of the polymer with oppositely-charged surfactant and it is deduced that this affects the mechanism of polymer-surfactant interaction.

The conformation of P4VP, with cationic groups in the 4-position rather than the more sterically-hindered 2-position may favor cooperative binding via ion-ion association with the large SDBS anions and hydrophobic association of the hydrocarbon tail groups of SDBS when bound electrostatically to the polymer chain. Contrary to P4VP, the second virial coefficient of the P2VP polymer indicates a polymer close to theta conditions. From the chemical structure and the polymer solution measurements, the

cationic groups are sterically-hindered by the polymer backbone. Steric hindrance would limit the number of bulky surfactant molecules that could bind to each cationic charge due to space restrictions. Interactions between P2VP and SDBS were observed below and above the CMC, however the mechanism of coacervate formation does not neatly fit into either the site-specific (Goddard) or macroion-macroion (Dubin) interaction models. Rather, it shows characteristics of each of these models depending upon the conditions of the system.

The effect of surfactant tail group structure on coacervate formation was also studied using high-throughput screening. Initially, coacervate formation was observed for P4VP and P2VP with all surfactants studied, however only coacervate formed between P4VP-SDBS and P2VP-SDBS was stable over 24 hours. The instability of the coacervate formed initially with sodium capryl sulfonate and sodium xylene sulfonate compared with the stability of the coacervate initially formed with SDBS indicates that neither an aromatic group nor a short hydrophobic alkyl chain is sufficient to provide thermodynamically stable coacervate complexes. Combining the understandings gained from the investigations of P2VP and P4VP interactions with SDBS with the macroscopic investigation of coacervate formation with these polymers and surfactants of different tail group architecture, we can conclude that the mechanism of polymer-surfactant interaction and coacervate formation differs depending on the position of the cationic group along the polymer backbone and the surfactant tail group architecture.

The effects of solution properties on polymer-surfactant interaction and coacervate formation were studied with both classes of polymer. The effects of surfactant concentration on interactions between polymer and surfactant were studied

using surface tensiometry, dynamic light scattering and viscometry and the interactions were observed to be affected by concentration in manners similar to conventional coacervate mechanisms of interaction as described by Goddard (PQ-10, P4VP, P2VP) and Dubin (P2VP). The effect of salt concentration and addition order was systematically studied using high-throughput screening with both classes of polymers. Using a constant salt high-throughput method, the effect of salt concentration was investigated using high molecular weight PQ-10 polymers, one with low and one with high CS. In the low CS polymer-salt-surfactant system, the amount of coacervate decreased with increasing salt concentration. Initially, with the addition of salt the compositional range of coacervate formation increased but at a much higher salt concentration the compositional range was less than that of the polymer-surfactant system in the absence of salt. In the high CS polymer-salt-surfactant system, the compositional range of coacervate formation increased with increasing salt concentration. However, at high salt concentration the amount of coacervate formed decreased. The increased compositional range of coacervate formation in both systems was attributed to “salting out” of the polymer-surfactant complex and the decreased coacervate amounts were due to screening of the electrostatic charges by the salt molecules, which was more efficient in the system with the low charge substituted polymer.

The effect of addition order in the presence of salt was studied using a high-throughput gradient method with PQ-10 polymers and SLES. Overall, The addition of even a small amount of NaCl changed the phase diagram for all systems, with the degree of change dependent on the addition order. For all polymer molecular weights and CS, the addition of NaCl curtailed coacervate formation in dilute solution. A decrease in

coacervate amount with the addition of salt was observed with addition orders where salt and polymer interacted before sample mixing. The addition of surfactant and salt before polymer addition caused an increase in coacervate amount and compositional range for all systems. The effect of addition order in the presence of salt was studied using the high-throughput constant salt method with P4VP and SDBS. Dynamic light scattering studies of the polymer in salt solution and surfactant in salt solution indicated that at the NaCl concentration studied, some screening of electrostatic interactions occurred however the interactions were not fully screened. These studies also indicated that the NaCl concentration was not sufficient to cause a measurable increase in micelle size. Coacervate formation with the addition order of surfactant, salt, polymer was nearly identical to that of the salt-free system. However, an absence of coacervate was observed at intermediate surfactant concentrations for the polymer, salt, surfactant system and this was attributed to inability of polymer bound surfactant tail groups to associate due to polymer-salt interaction leading to complex solubilization.

CHAPTER VI

RECOMMENDATIONS FOR FUTURE RESEARCH

The cationic polymer-anionic surfactant systems studied in this research have proven to be effective model systems for investigating the interaction of polymer and surfactant and the subsequent formation of coacervate. The effects of various polymer properties have been studied and the effects of these properties in salt-free solutions are now well understood. These model systems were also studied in the presence of salt, and specifically the order of addition of components was investigated. These results have provided the base knowledge that addition order does affect coacervate formation, and likely affects the mechanism of interaction of polymer and surfactant. However, the studies of salt and addition order discussed in this work only represent preliminary endeavors that are a component of a larger research program dedicated to understanding the effect of salt, and specifically of addition order on coacervate formation. It would be advantageous to understand the time-scale of component distribution in solution compared to the time-scale of complex formation. The high-throughput screening method could be advantageous for these studies, with some modification such that mixing time of individual components is controlled to ensure molecular scale intermixing before introduction of additional components. Dynamic light scattering, combinatorial or traditional, is a necessary supplemental technique to observe the occurrence of polymer collapse and/or micelle growth with the addition of salt to either component. This instrumental method could provide information on the size of the polymer-surfactant complexes formed as a function of addition order to provide insight into the mechanism

of interaction. These time study investigations could also be beneficial in gaining a better understanding of whether coacervate formation is kinetically or thermodynamically controlled, or both.

Another area of research that merits further investigation as a larger research program is the characterization of the rheological and structural properties of the coacervate formed in the different polymer-surfactant systems. The coacervate was described based on visual observation for both the PQ-10-SLES and P4VP-SDBS/P2VP-SDBS systems, and the coacervates were visually very different with these different polymers. Rheological measurements of the coacervate complexes may further enhance the understanding in regards to a reduction in mesh size proposed with the PQ-10-SLES systems and the effect of polymer c^* on coacervate amount. Previous researchers have demonstrated the usefulness of X-ray scattering and neutron scattering techniques in determining the presence or absence of an ordered network structure in coacervate complexes. This understanding would enhance the preliminary conclusions drawn from the current P4VP-SDBS studies of formation of a highly-ordered packing of bound SDBS tail groups along the polymer chain, which would enhance the understanding of the mechanism of polymer-surfactant interaction.

APPENDIX

As discussed in Chapter IV-B, dynamic light scattering (DLS) measurements were performed on polyquaternium-10 polymers in salt-free aqueous solutions and due to the long-range electrostatic interactions between polyions in solution the diffusion rate is generally much faster than their neutral analogues.¹³² This increased rate of diffusion can lead to error in determination of polyelectrolyte particle size, however, for comparison of particle size in pure polymer solution with particle size in polymer-surfactant solutions, the polymer apparent hydrodynamic diameter (D_H) was employed. JR400 (MW = 500×10^3 g/mol) and JR30M (MW = $2\,000 \times 10^3$ g/mol) were studied using this method and the time autocorrelations for both polymers were deconvoluted to understand their observed differences in D_H (Figure AI-1).

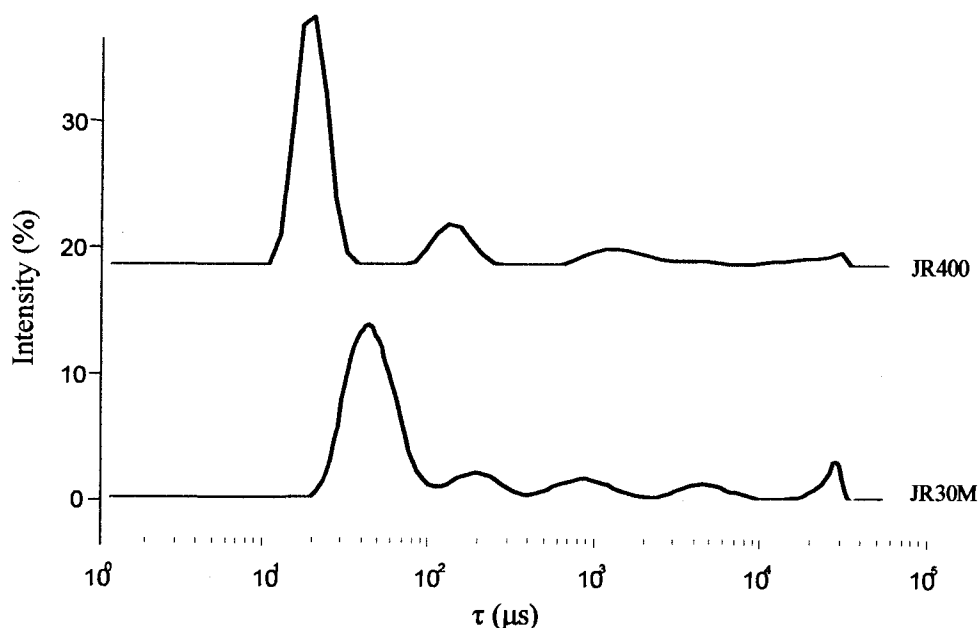


Figure AI-1. Relaxation time (τ) of 0.35 g/dL JR400 and 0.35 g/dL JR30M in aqueous solution.

In both polymers solutions a multimodal distribution of relaxation times was observed, including a fast diffusion process (D_f) and a slow diffusion process (D_s), as well as intermediate diffusion processes (D_i). The slow mode diffusion rate was approximately the same for both JR400 and JR30M ($3.0 \times 10^4 \mu\text{s}$). Generally, D_s is dependent on molecular weight¹⁴⁷ so the similarity observed in these systems is surprising. The difference in D_f between these polymers was also surprising because D_f is generally independent of molecular weight.¹⁴⁷ Diffusion in the fast mode has been attributed to coupled diffusion of a portion of the polyion chain and counterions¹⁴⁷ so a possible explanation of the difference observed with molecular weight may be a difference in association due to non-homogeneous distribution of cationic charges along the polymer backbone, as discussed in Chapter III. The appearance of D_i is consistent with the broad PDI values for these polymers as determined by SEC-MALLS (Chapter III). Polyelectrolyte interaction modes have been observed at diffusion rates slower than D_f and have been attributed to a mixture of two or more polyelectrolytes with different molecular weight.¹³²

REFERENCES

1. Ananthapadmanabhan, K. P., Lueng, P. S., Goddard, E. D. *Colloids and Surfaces* **1985**, 13, 63-72.
2. Chen, L., Yu, S., Kagami, Y., Gong, J., Osada, Y. *Macromolecules* **1998**, 31, 787-794.
3. Chronakis, I. S., Alexandridis, P. *Macromolecules* **2001**, 34, 5005-5018.
4. Dubin, P., Bock J., Davies, R. M., Schulz, D. N., Thies, C., *Macromolecular Complexes in Chemistry and Biology*. Springer-Verlag: Berlin, 1994.
5. Goddard, E. D., Phillips, T. S., Hannan, R. B. *Journal of Society of Cosmetic Chemists* **1975**, 26, 461-475.
6. Goddard, E. D., Hannan, R. B. *Journal of the American Oil Chemists Society* **1977**, 54, 561-566.
7. Goddard, E. D., Ananthapadmanabhan, K. P., eds., *Interactions of Surfactants with Polymers and Proteins*. CRC Press: Boca Raton, FL, 1993; p Chapters 2-4.
8. Holmberg, K., Jonsson, B., Kronberg, B., Lindman, B., *Surfactants and Polymers in Aqueous Solution*. 2nd ed.; John Wiley & Sons Ltd.: West Sussex, England, 2003.
9. Jonsson, M., Linse, P. *Journal of Chemical Physics* **2001**, 115, (23), 10975-10985.
10. Kogej, K., Skerjanc, J. *Langmuir* **1999**, 15, 4251-4258.
11. Kogej, K., Evmenenko, G., Theunissen, E., Berghmans, H., Reynaers, H. *Langmuir* **2001**, 17, 3175-3184.
12. Kogej, K., Theunissen, E., Reynaers, H. *Langmuir* **2002**, 18, 8799-8805.
13. Leung, P. S., Goddard, E. D., Han, C., Glinka, C. J. *Colloids and Surfaces* **1985**, 13, 47-62.

14. Li, Y., Xia, J., Dubin, P. L. *Macromolecules* **1994**, *27*, 7049-7055.
15. Li, Y., Dubin, P. L., Dautzenberg, H., Luck, U., Hartmann, J., Tuzar, Z. *Macromolecules* **1995**, *28*, 6795-6798.
16. Naderi, A., Claesson, P. M., Bergstrom, M., Dedinaite, A. *Colloids and Surfaces A* **2005**, *253*, 83-93.
17. Svensson, A., Sjostrom, J., Scheel, T., Picullel, L. *Colloids and Surfaces, A* **2003**, *228*, 91-106.
18. Wang, C., Tam, K. C. *Langmuir* **2002**, *18*, 6484-6490.
19. Wang, X. L., Y.; Li, J.; Wang, J.; Wang, Y.; Guo, Z.; Yan, H. *Journal of Physical Chemistry B* **2005**, *109*, 10807-10812.
20. Wang, Y., Kimura, K.; Huang, Q., Dubin, P. L., Jaeger, W. *Macromolecules* **1999**, *32*, 7128-7134.
21. Yamaguchi, Y., Inaba, Y., Uchiyama, H., Kunieda, H. *Colloid and Polymer Science* **1999**, *277*, 1117-1124.
22. Zheng, X.-L., Cao, W-X. *Polymer International* **1998**, *46*, 285-288.
23. Zheng, X.-L., Cao, W-X. *Polymer International* **2001**, *50*, 484-486.
24. Anghel, D. F., Toca-Herrera, J. L., Winnik, F. M., Rettig, W., Klitzing, R. v. . *Langmuir* **2002**, *18*, 5600-5606.
25. Bergstrom, M., Mikael Kjellin, U. R., Claesson, P. M., Pedersen, J. S., Nielsen, M. M. *Journal of Physical Chemistry B* **2002**, *106*, 11412-11419.
26. Chang, Y., Lochhead, R. Y., McCormick, C. L. *Macromolecules* **1994**, *27*, 2145-2150.
27. Meszaros, R., Thompson, L., Bos, M., Varga, I., Gilanyi, T. *Langmuir* **2003**, *19*, 609-615.

28. Nisha, C. K., Basak, P., Manorama, S. V. *Langmuir* **2003**, 19, 2947-2955.
29. Smith, G. L., McCormick, C. L. *Langmuir* **2001**, 17, 1719-1725.
30. Zhou, S., Burger, C., Chu, B. *Journal of Physical Chemistry B* **2004**, 108, 10819-10824.
31. Armstrong, R. W., Strauss, U. P., *Encyclopedia of Polymer Science and Technology: Polyelectrolytes*. John Wiley & Sons: New York, NY, 1969; Vol. 10, p 781-861.
32. Donnan, F. G. *Chem. Revs. I* **1924**, 80, (73-90).
33. Everett, D. H. I. M. *Pure Appl. Chem.* **1972**, 31, (4), 619.
34. Oman, S. F. *Acta Chim. Slov.* **2000**, 47, 519-534.
35. Chapman, D. L. *Phil. Mag.* **1913**, 6, 475.
36. Gouy, G. *J. Phys.* **1910**, 4, 457.
37. Guoy, G. *Comt. Rend.* **1909**, 149, 654.
38. Stern, O. Z. *Electrochem.* **1924**, 30, 508.
39. Stigter, D. *J. Coll. Int. Sci.* **1967**, 23, 379.
40. de Gennes, P. G., *Scaling Concepts in Polymer Physics*. Cornell University Press: Ithaca, NY, 1979; p Chapter 2.
41. Kratky, O., Porod, G. *Recl. Trav. Chim. Pays. Bas.* **1949**, 68, 1106.
42. Carpenter, D. K., *Encyclopedia of Polymer Science and Technology: Colloids*. John Wiley & Sons: New York, NY, 1966; Vol. 4, p 16-73.

43. Hodgson, D. F., Amis, E. J. *Journal of Chemical Physics* **1991**, 95, 7653-7663.
44. Kuang, M., Duan, H., Wang, J., Jiang, M. *Journal of Physical Chemistry B* **2004**, 108, 16023-16029.
45. de Gennes, P. G., Pincus, P., Velasco, R. M., Brochard, F. *Journal of Physics Paris* **1976**, 37, 1461-1473.
46. Fuoss, R. M., Katchalsky, A., Lifson, S. *Proceedings of the National Academy of Sciences* **1951**, 37, 579-589.
47. Gao, J. Y., Dubin, P. L., Sato, T., Morishima, Y. *Journal of Chromatography A* **1997**, 766, 232-236.
48. Manning, G. S. *Quarterly Reviews of Biophysics* **1978**, 2, (179-246).
49. Osawa, F., *Polyelectrolytes*. Marcel Dekker: New York, NY, 1971.
50. Ritacco, H., Kurlat, D., Langevin, D. *Journal of Physical Chemistry B* **2003**, 107, 9146-9158.
51. Flory, P. J., *Principles of Polymer Chemistry*. Cornell University Press: Ithaca, NY, 1953.
52. Wang, L., Bloomfield, V.A. *Macromolecules* **1990**, 23, 804-809.
53. Ezzell, S. A., McCormick, C. L. *Macromolecules* **1992**, 25, 1881-1886.
54. Ezzell, S. A., Hoyle, C. E., Creed, D., and McCormick, C. L. *Macromolecules* **1992**, 25, 1887-1895.
55. Rosen, M. J., *Surfactants and Interfacial Phenomena*. Third Edition ed.; John Wiley & Sons: Hoboken, NJ, 2004.
56. Franks, F., *Water, a comprehensive treatise*. Plenum Press: New York, NY, 1972; Vol. 1.

57. Israelichvili, J. N., Mitchell, D. J., Ninham, B. W. *Journal of the Chemical Society Faraday Transactions* **1976**, 72, 1525.
58. Mitchell, D. J., Ninham, B. W. *Journal of the Chemical Society Faraday Transactions* **1981**, 77, 601-629.
59. Panmai, S., Prud'homme, R. K., Peiffer, D. G. *Colloids and Surfaces A* **1999**, 147, 3-15.
60. Flood, C., Dreiss, C. A., Croce, V., Cosgrove, T. *Langmuir* **2005**, 21, 7546-7652.
61. Burgess, D. J. *Journal of Colloid and Interface Science* **1990**, 140, 227-238.
62. Overbeek, J. T. G., Voorn, M. J. *Journal of Cellular Comparative Physiology* **1957**, 49, 7-22.
63. Tainaka, K. *Journal of the Physical Society Japan* **1979**, 46, 1899-1906.
64. Veis, A., Aranyi, C. *Journal of Physical Chemistry* **1960**, 64, 1203-1210.
65. Cockbain, E. G. *Transactions of the Faraday Society* **1953**, 49, 104-111.
66. Knox, W. J., Parshall, T. O. *Journal of Colloid and Interface Science* **1970**, 33, 16-23.
67. Cabane, B., Duplessix, R. *Colloids and Surfaces* **1985**, 13, 19-33.
68. Chu, D., Thomas, J. K. *Journal of the American Chemical Society* **1986**, 108, 6270-6276.
69. Laschewsky, A. *Advances in Polymer Science* **1995**, 124, 1-86.
70. Takisawa, N., Brown, P., Bloor, D., Hall, D. G., Wyn-Jones, E. *Journal of the Chemical Society Faraday Transactions* **1989**, 85, 2099-2112.
71. Triener, C., Nguyen, D. *Journal of Physical Chemistry* **1990**, 94, 2021.

72. Ohbu, K., Hiraishi, O., Kashiwa, I. *Journal of the American Oil Chemists Society* **1982**, 59, 108-112.
73. Yamato, N. K., R.; Lochhead, R. Y. In *Photophysical study of the interactive behavior between sodium N-acyl-L-glutamate and cationic cellulose*, Proceedings of the International Conference on Colloid and Surface Science, Tokyo, Japan, November 5-8, 2000; Tokyo, Japan, 2000.
74. Netz, R. R., Joanny, J-F. *Macromolecules* **1999**, 32, 9026-9040.
75. Dubin, P. L., Chew, C. H., Gan, L.-M. *Journal of Colloid and Interface Science* **1989**, 128, 566-576.
76. Choi, L., Kim, O. *Langmuir* **1994**, 10, 57-60.
77. Dubin, P. L., The, S. S., McQuigg, D. W., Chew, C. H., Gan, L.-M. *Langmuir* **1989**, 5, 89-95.
78. Guillot, S., Delsanti, M., Desert, S., Langevin, D. *Langmuir* **2003**, 19, 230-237.
79. Xia, J., Zhang, H., Rigsbee, D. R., Dubin, P. L., Shaikh, T. *Macromolecules* **1993**, 26, 2759-2766.
80. Zhang, H., Ohbu, K., Dubin, P. L. *Langmuir* **2000**, 16, 9082-9086.
81. Chen, J., Heitmann, J. A., Hubbe, M. A. *Colloids and Surfaces A* **2003**, 223, 215-230.
82. Guillemet, F., Piculell, L. *Journal of Physical Chemistry* **1995**, 99, 9201-9209.
83. Meier, M. A. R., Hoogenboom, R., Schubert, U. S. *Macromol. Rapid Commun.* **2004**, 25, 21-33.
84. Cabral, J. In *Discrete Combinatorial Phase Behavior Mapping*, NCMC-6: Advanced Materials Forum, Gaithersburg, MD, November 8-9, 2004; Gaithersburg, MD, 2004.

85. Cabral, J., Hudson, S. D., Wu, T., Beers, K. L., Douglas, J. F., Karim, A., Amis, E. J. *Polymeric Materials Science & Engineering* **2004**, 90, 337-338.
86. Meredith, J. C., Karim, A., Amis, E. J. *MRS Bulletin* **2002**, 330-335.
87. Wu, T., Mei, Y., Cabral, J. T., Xu, C., Beers, K. L. *Journal of the American Chemical Society* **2004**, 126, 9880-9881.
88. Mao, H., Li, C., Zhang, Y., Furyk, S., Cremer, P. S., Bergbreiter, D. E. *Macromolecules* **2004**, 37, 1031-1036.
89. de Gans, B.-J., Schubert, U. S. *Macromolecular Rapid Communications* **2003**, 24, 659-666.
90. de Gans, B.-J., Kazancioglu, E., Meyer, W., Schubert, U. S. *Macromolecular Rapid Communications* **2004**, 25, 292-296.
91. de Gans, B.-J., Schubert, U. S. *Langmuir* **2004**, 20, 7789-7793.
92. Gottschalck, T. E., McEwen, G. N. Jr., *International Cosmetic Ingredient Dictionary and Handbook*. 10th ed.; The Cosmetic, Toiletry, and Fragrance Association: Washington, D.C., 2004; Vol. 2, p 1447.
93. *Cationic conditioners that revitalize hair and skin at www.dow.com/PublishedLiterature* **2002**.
94. Mark, H. F., Gaylord, N. G., Bikales, N. M., *Encyclopedia of Polymer Science: Cellulose Ethers*. 1965; Vol. 3.
95. Zhou, S., Xu, C., Wang, J., Golas, P., Batteas, J., Kreeger, L. *Langmuir* **2004**, 20, 8482-8489.
96. Kreeger, R. L., Zhou, S. *Cellulose Ethers*. 2005.
97. *SoftCAT SL Conditioning Polymers at www.dow.com/PublishedLiterature* **2004**.

98. Gottschalck, T. E. a. M., G. N. Jr., *International Cosmetic Ingredient Dictionary and Handbook*. 10th ed.; The Cosmetic, Toiletry, and Fragrance Association: Washington, D.C., 2004; Vol. 1, p 767.
99. DeMartino, R. N., Conciatori, A. B. Cationic polygalactomannan compositions. 4,031,307, 1977.
100. *Jaguar Cationic Guar Derivatives: Natural Conditioning Technologies at www.rhodia-hpcii.com* 2004.
101. Gunn, E., In Personal communication on polymer molecular weight and degree of substitution; Rhodia Inc.: 2005.
102. Convertine, A. J., Sumerlin, B. S., Thomas, D. B., Lowe, A. B., McCormick, C. L. *Macromolecules* 2003, 36, 4679-4681.
103. Tar, O. R., Apparent pKa Values of Poly (vinyl pyridines). In 2006.
104. Albert, A., Serjeant, E. P., *The Determination of Ionization Constants*. Chapman and Hall: New York, NY, 1984; p 203.
105. Dahanayake, M., Cohen, A. W., Rosen, M. *Journal of Physical Chemistry* 1986, 90, 2413.
106. Rosen, M. J., *Surfactants and Interfacial Phenomena*. John Wiley & Sons: New York, NY, 1978.
107. *POLYSTEP B-330A Product Bulletin*; Stepan Company: Northfield, IL, 2004.
108. *POLYSTEP B-22 Product Bulletin*; Stepan Company: Northfield, IL, 2004.
109. *POLYSTEP B-20 Product Bulletin*; Stepan Company: Northfield, IL, 2004.
110. *BIO-TERGE PAS-8S Product Bulletin*; Stepan Company: Northfield, IL, 2002.
111. Fevola, M. J., Bridges, J. K., Kellum, M. G., Hester, R. D., McCormick, C. L. *Journal of Applied Polymer Science* 2004, 94, (1), 24-39.

112. Regalado, E. J., Selb, J., Candau, F. *Macromolecules* **1999**, 32, 8580-8588.
113. *Malvern Instruments On-Demand Presentation: Dynamic Light Scattering Data Interpretation* (<http://www.malvern.co.uk/malvern/ondemand.nsf/id/73504>), accessed 9/28/06.
114. Instruments, M. *On-Demand Presentation: Dynamic Light Scattering Data Interpretation* (<http://www.malvern.co.uk/malvern/ondemand.nsf/id/73504>), accessed 9/28/06.
115. zimm plots. In *Zimm Plot/Second Virial Coefficient*; www.wyatt.com, Wyatt Technology Corporation, 2006.
116. Rosen, S. L., *Fundamental Principles of Polymeric Materials*. John Wiley & Sons: New York, NY, 1971.
117. Sjostrom, J., Piculell, L. *Colloids and Surfaces A* **2001**, 183-185, 429-448.
118. Kiemele, M. J., *Understanding Industrial Designed Experiments*. Fourth ed.; Air Academy Press: Colorado Springs, CO, 2000.
119. Li, Y., Dubin, P. L., Havel, H. A., Edwards, S. L., Duatzenberg, H. *Macromolecules* **1995**, 28, 3098-3102.
120. Ekwall, P., Mandell, L., Fontell, K. *Acta Chemica Scandinavica* **1968**, 22, (2), 697-699.
121. Fontell, K., Ekwall, P., Mandell, L., Danielsson, I. *Acta Chemica Scandinavica* **1962**, 16, 2894-2898.
122. Fontell, K., Mandell, L., Ekwall, P. *Acta Chemica Scandinavica* **1968**, 22, (10), 3209-3223.
123. Friberg, S., Mandell, L., Fontell, K. *Acta Chemica Scandinavica* **1969**, 23, (3), 1055-1057.
124. Morgan, S., In Personal Communication on High-Throughput Screening Reproducibility at The University of Southern Mississippi: May 2006.

125. Rosen, M. J., *Structure/Performance Relationships in Surfactants*. American Chemical Society: Washington, D. C., 1984.
126. Flory, P. J. *J. Chem. Phys.* **1942**, 10, 51.
127. Barton, A. F. M., *Handbook of Solubility Parameters and Other Cohesion Parameters*. CRC Press: Boca Raton, FL, 1983.
128. Patterson, D. *Macromolecules* **1969**, 2, 672.
129. Kujawa, P., Audibert-Hayet, A., Selb, J., Candau, F. *J. Poly. Sci. B* **2004**, 42, 1640-1655.
130. Guillot, S., McLoughlin, D., Jain, N., Delsanti, M., Langevin, D. *Journal of Physics: Condensed Matter* **2003**, 15, S219-S224.
131. Tanford, C. *J. Mol. Biol.* **1972**, 67, 59-74.
132. Sedláč, M. *Langmuir* **1999**, 15, 4045-4051.
133. Tanford, C. *Journal of Molecular Biology* **1972**, 67, 59-74.
134. Davidson, R. L., *Handbook of Water-Soluble Gums and Resins*. McGraw-Hill Book Co.: New York, NY, 1980; p 6.3-10.
135. Dubin, P. L., Oteri, R. *Journal of Colloid and Interface Science* **1983**, 95, 453-461.
136. Zhang, Y., Furyk, S., Bergbreiter, D. E., Cramer, P.S. *J. Amer. Chem. Soc.* **2005**, 127, 14505.
137. Hofmeister, F. *Arch. Exp. Pathol. Phamakol.* **1888**, 24, 247.
138. Tanford, C., *Physical Chemistry of Macromolecules*. John Wiley & Sons, Inc.: New York, NY, 1961.

139. Förster, S., Schmidt, M., Antonetti, M. *Polymer* **1990**, 31, 781.
140. Inoue, H. *Coll. Poly. Sci.* **1964**, 195, 1435-1536.
141. Cragg, L. H., Sones, R. H. *J. Poly. Sci.* **1952**, 9, 585.
142. Cragg, L. H., Bigelow, C. C. *J. Poly. Sci.* **1955**, 16, 177.
143. Yamakawa, H. *J. Chem. Phys.* **1961**, 34, 1360.
144. Lia, L.-S., Chian, H-F. *Food Hydrocolloids* **2002**, 16, 427-440.
145. Hall, D. G. *Journal of the Chemical Society Faraday Transactions 2* **1981**, 77, 1973-2006.
146. Holm, C., Joanny, J. F., Kremer, K., Netz, R. R., Reineker, P., Seidel, C., Vilgis, T. A., Winkler, R. G. *Adv Polym Sci* **2004**, 166, 67-111.
147. Xia, J., Dubin, P. L., Izumi, T., Hirata, M., Kokufuta, E. *J. Poly. Sci. B* **1996**, 34, 497-503.